



**UNIVERSIDADE DE LISBOA**  
**INSTITUTO SUPERIOR TÉCNICO**

**Molecular mechanisms of bile-acid induced  
apoptosis and cytoprotection**

Tânia Patrícia Marques de Sousa

***Supervisor:***      *Doctor Fábio Monteiro Fernandes*

***Co-Supervisor:***    *Doctor Manuel José Estevez Prieto*

***Thesis approved in public session to obtain the PhD Degree in Chemistry***

***Jury final classification: Pass with Distinction and Honour***

**2018**









**TÉCNICO**  
LISBOA

**UNIVERSIDADE DE LISBOA**

**INSTITUTO SUPERIOR TÉCNICO**

# **Molecular mechanisms of bile-acid induced apoptosis and cytoprotection**

Tânia Patrícia Marques de Sousa

Supervisor: Doctor Fábio Monteiro Fernandes

Co-Supervisor: Doctor Manuel José Estevez Prieto

**Thesis approved in public session to obtain the PhD Degree in Chemistry**

**Jury final classification: Pass with Distinction and Honour**

## **Jury**

**Chairperson:** Doctor Mário Nuno de Matos Sequeira Berberan e Santos, Instituto Superior Técnico, Universidade de Lisboa

### **Members of the Committee:**

**Doctor** Martin Hof, J. Heyrovský Institute of Physical Chemistry, Academy of Sciences of the Czech Republic

**Doctor** Cecília Maria Pereira Rodrigues, Faculdade Farmácia, Universidade de Lisboa

**Doctor** Luís Miguel Santos Loura, Faculdade Farmácia, Universidade de Coimbra

**Doctor** Fábio Monteiro Fernandes, Instituto Superior Técnico, University of Lisbon

**Funding Institution:** Fundação para a Ciência e a Tecnologia

**2018**







## Acknowledgements

During these last 4 years of my academic life I had the pleasure to work with splendid people that were an essential help and support in my scientific progress by passing on their knowledge and experience, making sure that I would be prepared for overcome any stone in my way to success. I am particularly grateful to:

My supervisors, Dr. Fábio Fernandes and Dr. Manuel Prieto, for receiving me with open arms and dedicating their time to teach me how to become a very good researcher. Also, for allowing me to learn how to use such a variety of spectroscopic and microscopic tools in my project. Specially I would like to thank Dr. Fábio for all the support he has shown in such a challenging project, never giving up on finding innovative ideas to overcome any obstacle in our scientific way. Definitely, he had an essential role in my personal and professional growing, turning me into a more autonomous, responsible and self-taught person and researcher.

Professor Ana Coutinho, for the dedication and constant interest in my work and for being always prepared for helping me with any question or problem encountered on my journey.

All the elements of the collaborations that were made to execute this project and without which it would be impossible to realize such a good work, specifically, the members of iMed.Ulisboa Research institute for Medicines, Rui E. Castro and Cecília M. P. Rodrigues, S.D Lucas and R. Moreira, For providing the biological material for my experiments and for carrying out the viability and cell death assays. To Professor Richard Youle (NIH, USA) for receiving me in his lab and Dr. Soojay Banerjee for passing to me the knowledge about Bax purification and also for providing us with biological material essential for the execution of my project. To Professor Martin Hof from the J. Heyrovský Institute of Physical Chemistry, for the support, Šárka Pokorná for the execution of the leakage assays and Professor Gerhard Gröbner from Umeå university for providing the protein for these experiments. To Samuel Jacob for the execution of the Zeta-Potential and partition experiments with K $\phi$ -bimane for Deoxycholic acid (DCA). To professor Arsénio Fialho, Dr. Nuno Bernardes and Dr. Dalila Mil-Homens from IBB, Institute for Bioengineering and Biosciences, for allowing me to perform all the protein purification process in their lab. I would like to give special acknowledgement to Dr. Nuno Bernardes for being like a second supervisor to me. Thank you for all the patience, dedication and friendship.

## Acknowledgements

---

I would like to express my gratitude to Centro de Química-Física Molecular, for receiving me and providing me everything that I needed to carry out this project.

I thank Fundação para a Ciência e Tecnologia (FCT) for the financial support of my research work (PhD fellowship SFRH/BD/92398/2013). Also, I express my gratitude to Biophysical Society, the European Biophysical Societies' Association (EBSA) and Federation of European Biochemical Societies (FEBS) for sponsoring my participations in several scientific meetings.

I would like to thank to all my past and present colleagues at the Biological Fluorescence group for the good and funny work environment, friendship and for all the knowledge that I obtained from all of them in a particular way. Specially, I would like to thank to my office colleagues that were always there for me, in the good and bad moments, between smiles, laughs and tears but always with encouraging words.

A super special acknowledgement to my colleague and best friend, Joana Ricardo, for all the support and patience for my craziness. Without her these 4 years would be much more difficult. Thank you for being there every time I fell, to help me to rise again. Never give up and "stay with the fight" - You are my president!

Switching to portuguese,

Finalmente, gostaria de dedicar algumas palavras especiais e de agradecimento aos meus amigos e familiares.

Gostaria de agradecer a todos aqueles que passaram pela minha vida nestes últimos 4 anos, estando ainda presentes ou não, contribuíram para o meu crescimento pessoal e profissional e ensinaram-me a ver que a vida é feita de alegrias, tristezas e também desilusões, mas que tudo é passageiro quando acreditamos que somos capazes.

Gostaria também de agradecer aos meus amigos mais próximos por todo o apoio e paciência nesta fase tão importante, mas também stressante da minha vida. Obrigada por todas as palavras amigas, por todo o apoio e puxões de orelhas quando mais necessitei. Obrigada por estarem lá, por não desistirem de mim e por sempre acreditarem que seria capaz de cumprir com sucesso este desafio.

À minha família, um muito obrigada por estarem presentes e me apoiarem com palavras amigas e motivadoras durante todo este longo caminho. Obrigada por se interessarem e por nunca vacilarem quando mais precisei de ajuda.

Agora um agradecimento super especial aos meus pais, Lurdes e Manuel, o vosso papel nesta etapa da minha vida foi essencial, sei que sem o vosso apoio tudo seria muito mais difícil ou quase impossível. Obrigada por acreditarem sempre que eu era capaz, por terem orgulho em mim e por estarem presentes em todos os momentos, por terem sido o meu porto de abrigo quando mais precisei e por sempre me incentivarem a nunca desistir, pelo amor incondicional e pela paciência para me aturar. Garanto que me sinto uma pessoa abençoada por poder ter-vos aos dois na minha vida. São os melhores pais do Mundo!



---

# Contents

<b>Acknowledgements</b> .....	i
<b>Abbreviations</b> .....	vii
<b>Resumo</b> .....	xi
<b>Abstract</b> .....	xiii
<b>Outline</b> .....	xv
<b>Chapter I</b> .....	1
<b>1. Biomembranes</b> .....	3
<b>1.1. Current view of biomembranes</b> .....	3
<b>1.2. Plasma Membrane</b> .....	5
<b>1.3. Mitochondrial Membranes</b> .....	7
<b>2. Apoptosis – Programmed cell death</b> .....	8
<b>2.1. The events of apoptosis</b> .....	8
<b>2.2. The apoptotic pathways</b> .....	9
2.2.1. <i>The extrinsic or death receptor pathway</i> .....	10
2.2.2. <i>The intrinsic or mitochondrial pathway</i> .....	10
<b>3. Bile Acid function, synthesis and chemistry</b> .....	20
<b>3.1. Physiological functions</b> .....	20
<b>3.2. Synthesis</b> .....	22
<b>3.3. Chemistry</b> .....	22
<b>3.4. Bile acids and apoptosis</b> .....	24
3.4.1 <i>Hydrophobicity / Cytotoxicity</i> .....	24
3.4.2 <i>Bile-acid-induced cell death pathways</i> .....	24
3.4.3. <i>Bile-acid-induced cell protection</i> .....	26
<b>3.5. Interaction of bile acids with lipid membranes</b> .....	29
<b>4. References</b> .....	31

<b>Chapter II</b> .....	43
Measuring membrane order in primary hepatocytes and isolated mitochondria by fluorescence imaging and spectroscopy .....	43
<b>Chapter III</b> .....	73
Deoxycholic acid modulates cell death signaling through changes in mitochondrial membrane properties .....	73
<b>Chapter IV</b> .....	111
Bile acids inhibit Bax-dependent membrane permeabilization .....	111
<b>Chapter V</b> .....	161
DCA-induced apoptosis and UDCA-mediated cytoprotection are independent of Bax in HCT116 cells .....	161
<b>Chapter VI</b> .....	197
The mitochondrial affinity of a charge sensor peptide is modified by the presence of bile acids .....	197
<b>Chapter VII</b> .....	235
Conclusions and future perspectives .....	235
<b>Conclusions</b> .....	237
<b>Future perspectives</b> .....	240

## Abbreviations

A594-WGA	Alexa Fluor 594 Conjugate of wheat germ agglutinin
Act D	Actinomycin D
Alexa 488	Alexa Fluor 488 SE (carboxylic acid, succinimidyl ester)
AMCA	7-Amino-4-methyl-3-coumarinylacetic acid
AP-1	Transcription factor activator protein
Apaf-1	Apoptotic protease activating factor 1
APD	Avalanche photodiode
BAs	Bile acids
Bax	Bcl-2 associated X protein
Bak	Bcl-2 homologous antagonist/killer
Bcl-2	B-cell lymphoma 2
Biotinylated DOPE	1,2-dioleoyl- <i>sn</i> -glycero-3-phosphoethanolamine-N-(cap biotinyl)
BOP	BH3-only protein
BSA	Bovine serum albumin
CA	Cholic acid
CD	Methyl- $\beta$ -cyclodextrin
CDCA	Chenodeoxycholic acid
CF	5(6)-carboxyfluorescein
Chol	Cholesterol
CL	Cardiolipin (1,3-bis( <i>sn</i> -3'-phosphatidyl)- <i>sn</i> -glycerol)
CMC	Critical micellar concentration
CMX	MitoTracker™ Red CMXRos
Cyt c	Cytochrome c
DCA	Deoxycholic acid
$\Delta\psi_m$	Mitochondrial membrane potential
DHE	Dehydroergosterol
Di-4-ANEPPDHQ	1-[2-Hydroxy-3-(N,N-di-methyl-N-hydroxyethyl)ammoniopropyl]-4-[ $\beta$ -[2-(di-n-butylamino)-6-naphthyl] vinyl]pyridinium dibromide
DiD	DiI18(5)
DISC	Death-inducing signaling complex
DKO	Double knockout

## Abbreviations

---

DMEM	Dulbecco's Modified Eagle Medium
DMSO	Dimethyl sulfoxide
DOPC	1,2-Dioleoyl- <i>sn</i> -glycero-3-phosphocholine
DOPE	1,2-Dioleoyl- <i>sn</i> -glycero-3-phosphoethanolamine
DOPE-Rho	1,2-Dioleoyl- <i>sn</i> -glycero-3-phosphoethanolamine-N-(lissamine rhodamineB sulfonyl)
DPH	1,6-Diphenyl-1,3,5-hexatriene
DTT	Dithiothreitol
EF2-1	Elongation factor 2-1
ER	Endoplasmic reticulum
FADD	Fas-associated death domain
Fas	First apoptosis signal
FBS	Fetal bovine serum
FCS	Fluorescence correlation spectroscopy
FFS	Fluorescence fluctuation spectroscopy
FLIM	Fluorescence lifetime imaging microscopy
FRET	Förster resonance energy transfer
GCDCA	Glycochenodeoxycholic acids
GFP	Green fluorescent protein
GP	Generalized polarization
GPMV	Giant plasma membrane vesicle
GUV	Giant unilamellar vesicle
IPTG	Isopropyl $\beta$ -D-1-thiogalactopyranoside
IRF	Instrument response function
$K_d$	Dissociation constant
$K_p$	Partition coefficient
Laurdan	6-Dodecanoyl-2-dimethylaminonaphthalene
LCA	Lithocholic acid
LDH	Lactate dehydrogenase
$I_o$	Liquid ordered phase
LUV	Large unilamellar vesicle
MAPK	<i>Mitogen-activated protein kinases</i>
mGSH	<i>mitochondrial glutathione</i>
MIM	Mitochondrial inner membrane
MOM	Mitochondrial outer membrane
MOMP	Mitochondrial outer membrane permeability

---

MMP	Mitochondrial membrane potential
MPT	Mitochondrial membrane permeability transition
MPTP	Mitochondrial permeability transition pore
NaCl	Sodium chloride
NBD	<i>n</i> -(7-nitrobenz-2-oxa-1,3-diazol-4yl)
NF- $\kappa$ B	Nuclear factor kappaB
NSR	Nuclear steroid receptor
OM	<i>n</i> -Octyl $\beta$ -D-maltoside
PC	Phosphatidylcholine
PCH	Photon counting histogram
PDM	Product from the difference from the mean
PE	Phosphatidylethanolamine
PI	L- $\alpha$ -Phosphatidylinositol
PI3K	Phosphatidylinositol 3-kinase
PL	Phospholipid
POPC	1-Palmitoyl-2-oleoyl- <i>sn</i> -glycero-3-phosphocholine
POPS	1-palmitoyl-2-oleoyl- <i>sn</i> -glycero-3-phospho-L-serine
PSM	<i>N</i> -palmitoyl- <i>D</i> -erythrosphingosylphosphorylcholine
PS	phosphatidylserine
RFP	Red fluorescent protein
Rho-123	[6-amino-9-(2-methoxycarbonylphenyl)xanthen-3-ylidene]azanium;
ROI	Region of interest
ROS	Reactive oxygen species
R <sub>r</sub>	Pearson's correlation coefficient
SEC	Size exclusion chromatography
SLO	Streptolysin O
$\tau$	Fluorescence lifetime
tBid	Truncated Bid
TAMRA	5-Carboxytetramethylrhodamine
TCEP	Tris(2-carboxyethyl)phosphine hydrochloride
TCSPT	Time-correlated single-photon timing
T <sub>m</sub>	Main transition temperature
TNF	Tumor necrosis factor
TOCL	1,1',2,2'-tetraoleoyl-cardiolipin
TRAIL	TNF-related apoptosis inducing ligand

## Abbreviations

---

TRADD	TNFR1-associated death domain protein
TUDCA	Tauroursodeoxycholic acid
UDCA	Ursodeoxycholic acid
$\zeta$ -potential	Zeta potential

## Resumo

Certos ácidos biliares são conhecidos pela sua capacidade de modular o processo apoptótico em células hepáticas e não hepáticas. O ácido deoxicólico (DCA) é um conhecido indutor de apoptose, enquanto que os ácidos ursodeoxicólico (UDCA) e tauroursodeoxicólico (TUDCA) apresentam propriedades citoprotetoras. Embora os efeitos opostos destas moléculas estejam fortemente associados à sua hidrofobicidade, o mecanismo exato através do qual estes efeitos são desencadeados é ainda desconhecido. Neste trabalho utilizámos uma combinação de técnicas espectroscópicas e microscópicas para estudar o possível mecanismo de ação tanto dos ácidos biliares apoptóticos como citoprotetores. Estes estudos foram realizados em sistemas modelo de membranas, em mitocôndrios isolados, linhas celulares humanas e hepatócitos de rato, seguindo uma aproximação de crescente complexidade. Os nossos resultados demonstram que a indução de apoptose pelo DCA está muito provavelmente associada a alterações nas propriedades das membranas mitocondriais. De facto, usando sondas sensíveis à fluidez membranar em mitocôndrios isolados, foi confirmado que as alterações na estrutura da membrana mitocondrial externa após exposição a concentrações apoptóticas de DCA, precedem o início do processo de transição de permeabilidade mitocondrial (MPT). No entanto, em sistemas modelo de membranas tal não é observado, sugerindo que outras características das membranas mitocondriais, que não o ambiente lipídico, são responsáveis pela indução da apoptose pelo DCA, possivelmente através de proteínas mitocondriais. Considerando a Bax, uma das proteínas mais importantes na via intrínseca da apoptose, como um possível alvo da ação dos ácidos biliares citoprotetores, mostrámos que estas moléculas interatuam com a Bax, têm a capacidade de inibir a interação desta proteína com um péptido ativador, interferem com a integração da Bax em membranas lipídicas e também com a sua atividade formadora de poros em membranas. Ainda assim, em células HCT116 deficientes em Bax, observou-se que a apoptose induzida pelo DCA e a citoproteção pelo UDCA não são completamente dependentes da presença da Bax. Enquanto que para o DCA tal observação era esperada, considerando a sua capacidade de permeabilização de mitocôndrios isolados, estes resultados sugerem que para os ácidos biliares citoprotetores o alvo molecular não é exclusivamente a Bax. Uma vez que alterações na carga superficial das membranas mitocondriais intervêm no recrutamento de moléculas sinalizadoras durante a apoptose, também foi avaliado o impacto dos ácidos biliares na carga superficial dos mitocôndrios e membrana plasmática. Medições de potencial zeta em lipossomas de composição mimética destes organelos confirmam que o DCA induz de facto um aumento no carácter aniónico destas membranas. A interação de um sensor de carga peptídico, designado  $K\phi$ , com lipossomas miméticos do folheto interno da membrana

plasmática e membrana mitocondrial externa, foi caracterizada na presença de ácidos biliares citoprotetores e apoptóticos, bem como a sua distribuição entre os dois organelos em células HEK293T, também na presença destas moléculas. Os resultados mostram que concentrações fisiologicamente ativas de DCA induzem um aumento dramático da partição do  $K\phi$  para membranas modelo. Surpreendentemente, o UDCA, que como consequência da sua baixa associação com membranas lipídicas não tem impacto na afinidade de  $K\phi$  para lipossomas artificiais, induz uma considerável inibição da interação do  $K\phi$  com a membrana mitocondrial externa em células HEK293T. É proposto que este efeito esteja, tal como observado para a Bax, associado à interação do péptido com ácidos biliares em solução.

De forma relevante, os resultados incluídos nesta tese demonstram que o mecanismo de ação dos ácidos biliares com atividade moduladora da morte celular, não se encontram unicamente associados às consequências da sua interação com ambientes lipídicos na célula e que fatores adicionais serão necessários à regulação da apoptose.

Em suma, estes resultados sugerem que enquanto é esperado que o mecanismo de ação de ácidos biliares apoptóticos seja ditado maioritariamente pela permeabilização da membrana mitocondrial externa, os eventos associados com o efeito citoprotector dos ácidos biliares são provavelmente muito mais complexos. Possivelmente, a acumulação de ácidos biliares no ambiente intracelular levará a alterações extremamente complexas na distribuição subcelular de diferentes proteínas de relevância na via de sinalização apoptótica, contribuindo dessa maneira para a ativação de maquinaria molecular apoptótica ou citoprotetora.

**Palavras-chave:** Ácidos biliares, Apoptose, Biofísica de membranas, Mitocôndrios, Bax

---

## Abstract

Certain bile acids are known for their ability to modulate the apoptotic process in liver and non-liver cells. Deoxycholic acid (DCA) is a known inducer of apoptosis whereas ursodeoxycholic (UDCA) and tauroursodeoxycholic acids (TUDCA) have cytoprotective properties. Although the opposing effects of these molecules are strongly associated with their hydrophobicity, the exact mechanism by which these effects are triggered is still unknown. In this work, we used a combination of spectroscopic and microscopic techniques to study the possible mechanism of action of both apoptotic and cytoprotective bile acids. These studies were performed on model membrane systems, isolated mitochondria, human cell lines and rat hepatocytes, following a bottom-up approach. Our results demonstrate that the induction of apoptosis by DCA is most likely associated with changes in the properties of mitochondrial membranes. In fact, using membrane-sensitive probes in isolated mitochondria, it was confirmed that changes in the structure of the outer mitochondrial membrane after exposure to apoptotic concentrations of DCA, precede the onset of the mitochondrial permeability transition (MPT) process. However, in model membrane systems, extensive DCA-dependent permeabilization it is not observed, suggesting that other characteristics of mitochondrial membranes, not associated with the lipid environment, are responsible for the induction of apoptosis by DCA, possibly mitochondrial proteins. Considering Bax, one of the most important proteins in the intrinsic pathway of apoptosis, as a possible target for the activity of cytoprotective bile acids, we have shown that these molecules interact with Bax, have the ability to inhibit the interaction of this protein both with an activator peptide and with lipid membranes, and also inhibit its pore forming activity in membranes. However, in Bax-deficient HCT116 cells, it has been observed that DCA-induced apoptosis and UDCA cytoprotection are not strictly dependent on the presence of Bax. While for DCA such observation is not surprising, considering its permeabilization of isolated mitochondria, these results also suggest that for cytoprotective bile acids the molecular target is not exclusively Bax. Since changes in the surface charge of mitochondrial membranes intervene in the recruitment of signaling molecules during apoptosis, the impact of bile acids on the surface charge of the mitochondria and plasma membrane was also evaluated. Measurements of zeta potential in liposomes mimicking the lipid composition of these organelles confirm that DCA does indeed induce an increase in the anionic character of these membranes. The interaction of a charge sensing cationic peptide, K $\phi$ , with mimetic liposomes from the inner leaflet of the plasma membrane and outer mitochondrial membrane, was characterized in the presence of cytoprotective and apoptotic bile acids, as was its distribution between the two organelles in HEK293T cells, also in the presence of bile acids. The results show that physiologically active concentrations of

DCA induce a dramatic increase of  $K_{\phi}$  partition for model membranes. Surprisingly, UDCA, which as a consequence of its low association with lipid membranes has no impact on the affinity of  $K_{\phi}$  for artificial liposomes, induces a considerable inhibition of the interaction of  $K_{\phi}$  with the outer mitochondrial membrane in HEK293T cells. It is proposed that this effect, as observed for Bax, is associated with the interaction of the peptide with bile acids in solution.

Importantly, the results included in this thesis demonstrate that the mechanism of action of bile acids with cell death modulating activity are not solely associated with the consequences of their interaction with lipid environments in the cell and that additional factors will be required to regulate apoptosis.

In summary, these results suggest that while the mechanism of action of apoptotic bile acids is predicted to be largely dictated by the permeabilization of the outer mitochondrial membrane, the events associated with the cytoprotective effect of bile acids are likely to be much more complex. Possibly, the accumulation of bile acids in the intracellular environment will lead to extremely complex changes in the subcellular distribution of different proteins of relevance in the apoptotic signaling pathway, thus contributing to the activation of apoptotic or cytoprotective molecular machineries.

**Key-words:** Bile acids, Apoptosis, Membrane biophysics, Mitochondria, Bax

---

## Outline

Cell death by apoptosis is a crucial physiological process in all multicellular events, and its deregulation can lead to serious pathophysiological conditions. Cellular membranes play a central role in apoptosis. These structures are responsible for maintaining concentration gradients of ions and proteins across the membrane of different organelles, which when perturbed, act as triggers for apoptosis. Bile acids have been shown to interfere with the apoptotic machinery, contributing to the development of a large number of digestive tract diseases, including colon cancer and cholestasis.

The present work aimed at the study of the effect of apoptotic and cytoprotective bile acids on cell membranes and also on the apoptotic Bax protein activity. In fact, bile acids are known to be able to induce apoptosis or cytoprotection of hepatic and nonhepatic cells, depending on their structure and hydrophobicity. Nevertheless, the exact mechanism by which different bile acids exert opposite effects on the modulation of cell death remains a mystery. The main goal of this work was to identify the possible molecular targets of bile acids and elucidate the specific mechanisms behind their effects through the use of membrane model systems, isolated mitochondria and living cells, in a bottom-up approach.

This dissertation is divided in 7 chapters. The first chapter is further divided in three parts. The first part includes an overview of the properties of biological membranes, namely their structure, composition and typical characteristics. The second part of this chapter describes programmed cell death or apoptosis, in detail. Particular emphasis is given to the intrinsic pathway of apoptosis and to the Bcl-2 proteins, that are essential regulators of the apoptotic process. The third part of this chapter is dedicated to bile acids, their properties and biological relevance, while focusing on their effects over cellular membranes and the apoptotic process.

Chapter II concerns a methodologic approach to the determination of membrane order of primary hepatocytes and isolated mitochondria by fluorescence imaging and spectroscopy. This chapter is an invited contribution to be included in an upcoming edition of a book that will be published in the renowned series "Methods in Molecular Biology" from Springer and is based on published work.

Chapter III is a detailed characterization of the impact of bile acids on the membrane properties of the most likely targets for modulation of cell death by bile acids, the plasma membrane and the mitochondrial membranes of hepatocytes. This work was published in the *Journal of Lipid Research*.

The work described in chapters IV and V was carried out in response to the conclusions obtained in the previous chapter. Given that the permeabilization of isolated mitochondria by

apoptotic bile acids depend on features of mitochondrial membranes other than lipid composition, the work here focused on a particularly important protein for mitochondria permeabilization, the pore-forming Bax protein. Chapter IV describe the study of the impact of physiologically active concentrations of apoptotic and cytoprotective bile acids on Bax activity, oligomerization and mitochondrial membrane affinity. Chapter V focused on clarifying the relevance of Bax for bile-acid induced apoptosis and cytoprotection in colon cancer cells, as well as the impact of these molecules to the subcellular distribution of this apoptotic protein.

Chapter VI addresses the role of membrane charge in the mechanism of action of bile acids. The different studies carried out in the context of this thesis and presented in Chapters II-VI have either been published in the form of peer-reviewed scientific papers in international journals or are under preparation for that effect.

In the final chapter, an overall consideration of the developed work is presented, together with some future perspectives regarding control of cell fate by bile acids.

# Chapter I

---

Introduction



## 1. Biomembranes

The structure and function of cells are critically dependent on the existence of biomembranes, which not only function as structural barriers, separating the interior of the cell from its environment, but also define the internal compartmentalization of eukaryotic cells by the presence of several inner membranes, defining specific compartments with distinct compositions and functions. The separation between the intracellular space and its surroundings is the foundation for cell maintenance and homeostasis<sup>1</sup>.

Biomembranes possess dynamic biochemical and biophysical properties that allow to regulate traffic and communication across the membrane, orchestrate reaction sequences and promote cellular processes. The formation of biological membranes is based on the properties of its major components, the lipids. In cells, membranes share a common structural organization composed of bilayers of phospholipids with associated proteins<sup>2</sup>. Membrane lipids are responsible for fundamental processes such as energy transduction, cell-to-cell communication and cell division<sup>3</sup>. Membrane proteins are in control of several specialized functions, such as acting as receptors that allow the cell to respond to external signals, carrying out selective transport of molecules across the membrane, or participate in the electron transport and oxidative phosphorylation<sup>2</sup>. The common structural organization of membranes thus underlies a variety of biological processes and specialized membrane functions.

### 1.1. Current view of biomembranes

Cells present a wide variety of membranes and among cell types, the variability of these membranes is even larger. In any way, a common feature is shared between them: they all contain a phospholipid bilayer as a template. The evolution in spectroscopy and microscopy through the years allowed for a constant update of our understanding of the composition and organization of biomembranes, which is summarized in different models.

The first description of the biological membrane as a lipid bilayer was proposed by Gorter and Grendel in 1925<sup>4</sup>. While studying lipid extracts of human erythrocytes and depositing them in a Langmuir-Blodgett trough as lipid monolayers, they observed that the monolayers occupied twice the space that was occupied by the erythrocyte surface area which could only be explained by the presence of a lipid bilayer structure.

A decade later, Danielli and Davson proposed a modification of this concept by introducing proteins adsorbed to the surface of either side of the membrane as a component with such importance as the lipid bilayer for the constitutions of the biological membranes<sup>5</sup>.

The two models described above, together with several studies of permeability and diffusion of lipids and proteins within membranes, were the basis for the development of the most notable biomembrane model, the fluid-mosaic model, proposed by Singer and Nicolson in 1972<sup>6</sup> (Fig. 1.1A). According to the authors, the proteins are a heterogeneous set of globular molecules, each arranged in an amphipathic structure, meaning that the ionic and highly polar groups are protruding from the membrane into the aqueous phase, while the nonpolar groups are largely buried in the hydrophobic interior of the membrane<sup>6</sup>. These globular molecules are partially embedded in a viscous matrix of phospholipid that is organized as a discontinuous fluid bilayer. Resemblance with a mosaic is associated with the arbitrary feature of the protein-lipid interactions. The most important considerations that were introduced in this model and that were not taken into account by Danielli and Davson model were: i) the lateral diffusion of both lipids and proteins within membrane; ii) the lipid motion in the plane of the membrane at different space and time scales, together with limited transverse mobility; iii) the presence of proteins with different nature; iv) the lipid phase transitions and v) the observation that some enzyme's activity requires lipids<sup>7,8</sup>. Although the basic premises of the fluid mosaic model are still used to explain biomembranes, over the following years it was found that it did not provide adequate explanations for the great diversity of lipids that is maintained by the cell at each time or the dynamics of every membrane structure<sup>9</sup>.

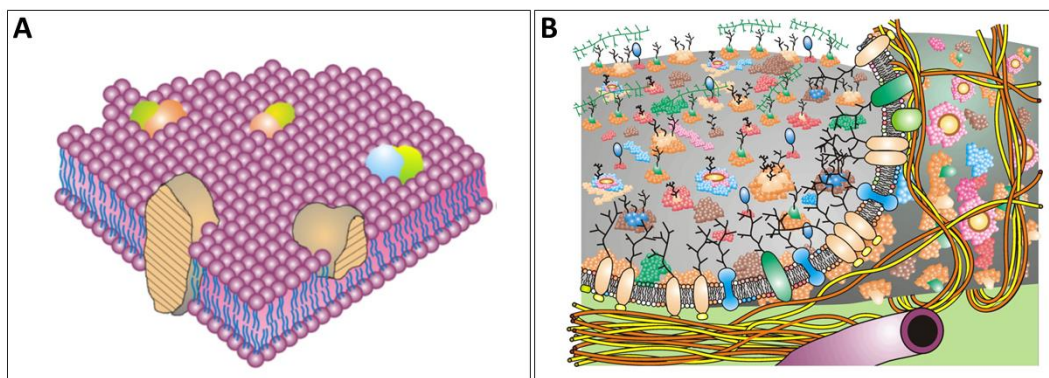


**Figure 1.1.** The Fluid-mosaic membrane model of biological membrane structure. (A) Original model proposed in 1972 by Singer and Nicolson<sup>6</sup>. Integral proteins are shown in a completely fluid bilayer lipid phase, and it does not contain other membrane-associated structures or membrane domains of different compositions. (B) An updated view of the Fluid-mosaic model that contains information on membrane domain structures and membrane-associated cytoskeletal and extracellular structures. Adapted from<sup>9</sup>.

Along the years, the fluid mosaic model had to be updated to take into account new findings that arose from the implementation of newly developed techniques (Fig. 1.1B). In updated versions of the model, more emphasis is given to the mosaic nature of the macrostructure of cellular membranes, where many protein and lipid components are limited in their rotational and lateral motilities in the membrane plane, especially in their natural states where lipid–lipid, protein–protein and lipid–protein interactions, as well as cell–matrix, cell–cell and intracellular membrane-associated protein and cytoskeletal interactions are important in restraining the lateral motility and range of motion of particular membrane components<sup>9</sup>. The formation of specialized membrane domains and the presence of tightly packed integral membrane protein complexes due to membrane associated barriers are considered very important in describing membrane dynamics and architecture<sup>9</sup>. These structures along with membrane-associated cytoskeletal and extracellular structures maintain the long-range, non-random mosaic macro-organization of membranes, while smaller membrane nano- and micro-sized domains, such as lipid rafts and protein complexes, are important in maintaining specialized membrane structures that are in cooperative dynamic flux in a crowded membrane plane<sup>9</sup>. The lipid raft concept was introduced in 1997 by Simons and Ikonen to explain the generation of the glycolipid-rich apical membrane of epithelial cells<sup>10</sup>. The raft hypothesis predicts the existence of small (10-200 nm), highly dynamic, sterol/sphingolipid enriched domains that are able to compartmentalize cellular processes<sup>11</sup>. It is thought that lipids present in these domains are enriched in saturated and longer hydrocarbon chains<sup>12</sup>. This model postulates that certain lipids and proteins, transiently segregate into highly concentrated nanodomains with specific cell functions<sup>13–15</sup>. The stabilization of these nanodomains is driven by specific lipid-lipid, protein-protein and protein-lipid interactions<sup>11</sup>.

The randomness implied in the fluid mosaic model is not feasible, and the presence of structured lipid domains is essential to organize and order many different molecular species through specific interactions, creating membrane compartments that support many aspects of membrane and cellular function. The realization that lipid-lipid interactions may play, as do proteins, a key role in cell signaling and functionality justify the need to comprehend how each individual lipid interacts with the remaining membrane components.

## **1.2. Plasma Membrane**

The plasma membrane in eukaryotic cells is the first barrier that separates the internal contents of the cell from the environment. Like all the other cellular membranes, the plasma membrane is composed by lipids and proteins. The proteins that are embedded within the bilayer carry out specific functions of the plasma membrane that include cell to cell recognition and transport of molecules<sup>2</sup>.

One of the main components of the plasma membrane in animal cells are phospholipids. These lipid molecules are composed of glycerol, two acyl chains and a phosphate head group. Plasma membrane contains four major phospholipids, namely, phosphatidylcholine (PC), phosphatidylethanolamine (PE), phosphatidylserine (PS) and sphingomyelin (SM)<sup>1</sup>. Phospholipids are asymmetrically distributed between the two leaflets of the plasma membrane, with PC and SM mainly found in the outer leaflet of the plasma membrane, and PE and PS in the inner leaflet of these membranes<sup>16</sup>. Another phospholipid that is present in the inner leaflet of plasma membrane is phosphatidylinositol (PI), representing only 1-2% of total phospholipids in living cells<sup>17</sup>, but playing a key role in cell signaling. Other molecules that compose the plasma membrane are glycolipids and cholesterol. Glycolipids are also a minor component of these membranes, exclusively found on the outer leaflet of the plasma membrane and result from the attachment of carbohydrate groups to lipids<sup>18</sup>. Sterols, such as cholesterol, are ubiquitous and apolar membrane components that in general rigidify fluid membranes by reducing the flexibility of adjacent unsaturated acyl chains, increasing in this way membrane thickness and playing an important role in membrane organization and stability<sup>7,19</sup>.

The plasma membrane-associated proteins are divided in two groups, according to Singer and Nicolson<sup>6</sup>, the peripheral and integral membrane proteins. Peripheral proteins are found both on the inside and outside surfaces of the plasma membrane, attached more loosely either to phospholipids or to integral proteins. Integral proteins have at least one hydrophobic region that anchors them to the hydrophobic core of the phospholipid bilayer.

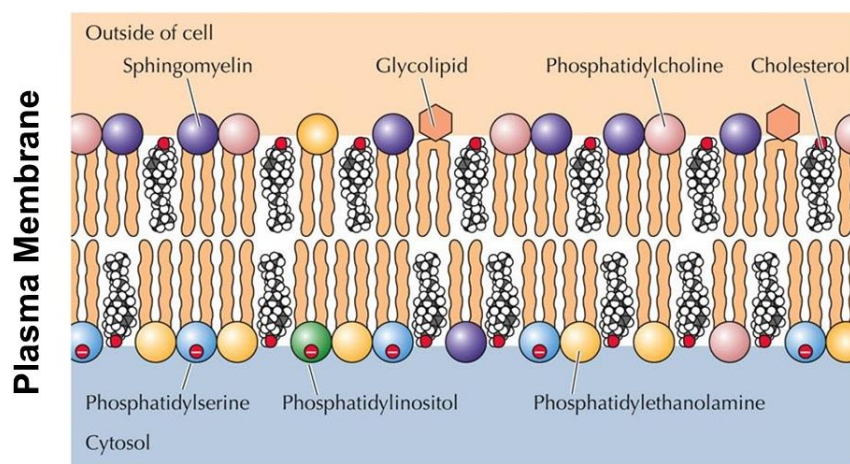


**Figure 1. 2.** Representation of the lipid components of the plasma membrane. On the outer leaflet of the plasma membrane we observe the presence of sphingomyelin (SM), phosphatidylcholine (PC) and glycolipids, whereas on the inner leaflet of the plasma membrane we observe the presence of

phosphatidylethanolamine (PE), phosphatidylserine (PS) and phosphatidylinositol (PI). Cholesterols is found in both leaflets. The net negative charge of PS and PI headgroups are shown. Adapted from<sup>2</sup>.

### 1.3. Mitochondrial Membranes

Mitochondria plays a vital role in the generation of metabolic energy in eukaryotic cells, being responsible for conversion of energy derived from the breakdown of carbohydrates and fatty acids to ATP by oxidative phosphorylation. These organelles are composed of a double-membrane system, consisting of the mitochondrial inner and outer membrane (MIM and MOM, respectively) separated by an intermembrane space. The MIM forms a series of folds (cristae), which extend into the matrix of the organelle. Each of these components play distinct functional roles, with the MIM and the matrix representing the major working compartments in energy generation<sup>2</sup>.

Both mitochondrial membranes are composed of a phospholipid bilayer, but they are distinct in appearance and in physicochemical properties, thus determining the biochemical function of each membrane. The inner and outer membranes are characterized by different phospholipid compositions and protein-to-lipid ratio is found to be much higher for MIM due to the presence of all the enzymatic machinery of oxidative phosphorylation<sup>20</sup>. In mitochondria, the major phospholipids are PC and phosphatidylethanolamine PE, which account together for about 80% of total phospholipids. Cardiolipin CL, an anionic lipid, is present in the range of 10-20% of total mitochondrial phospholipids<sup>21</sup>. Lipid composition can differ considerably between the two monolayers that constitute a defined membrane bilayer and the resulting asymmetry can induce membrane curvature and impose a transmembrane electrostatic potential difference<sup>22</sup>. CL is involved on this lipid asymmetry, in mitochondria, being mainly found in the MIM and in the inner leaflet of MOM<sup>23</sup>.

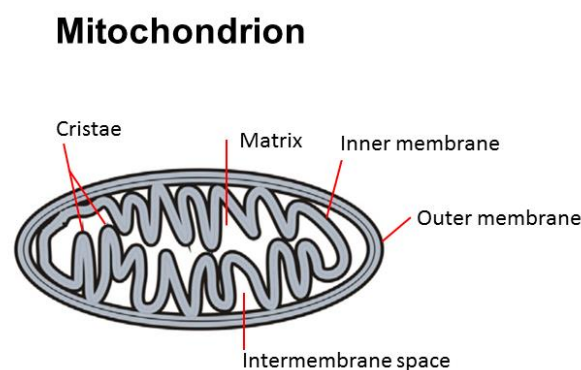


**Figure 1.3.** Representation of the major components of mitochondria. Mitochondria are bounded by a double-membrane system, consisting of inner and outer membranes. Folds in the inner membrane (cristae) extent into the matrix. Adapted from<sup>24</sup>.

## 2. Apoptosis – Programmed cell death

Apoptosis is a highly regulated process of programmed cell death that is vital for a wide variety of biological processes, like normal embryonic development and tissue homeostasis during adulthood. Apoptosis provides a defense mechanism by which damaged and potentially dangerous cells can be eliminated for the benefit of the organism as a whole<sup>2</sup>.

### 2.1. The events of apoptosis

Programmed cell death was first described in 1972 by Kerr *et al.*<sup>25</sup> and consists in a sequence of events, often initially visible through chromatin condensation and fragmentation as a result of cleavage between nucleosomes, resulting in the fragmentation of the nucleus. The cell then suffers a shrinkage process and breaks up into apoptotic bodies that correspond to membrane enclosed fragments of the cell<sup>26</sup>. These fragments are rapidly identified and phagocytosed by macrophages and neighboring cells, being readily removed from tissues and degraded. No inflammatory response occurs since no cellular content is released into the environment<sup>26</sup>.

As apoptosis corresponds to a controlled process, necrosis is a toxic and out of control process of cell death. During the necrotic process, the morphology of the cell is completely altered, a generalized swelling of the cell and all the organelles is observed, with consequent rupture of all of these structures as well as disruption of the plasma membrane. This results in the release of the cellular content to the environment, sending chemotatic signals with eventual recruitment of inflammatory cells<sup>27</sup>.

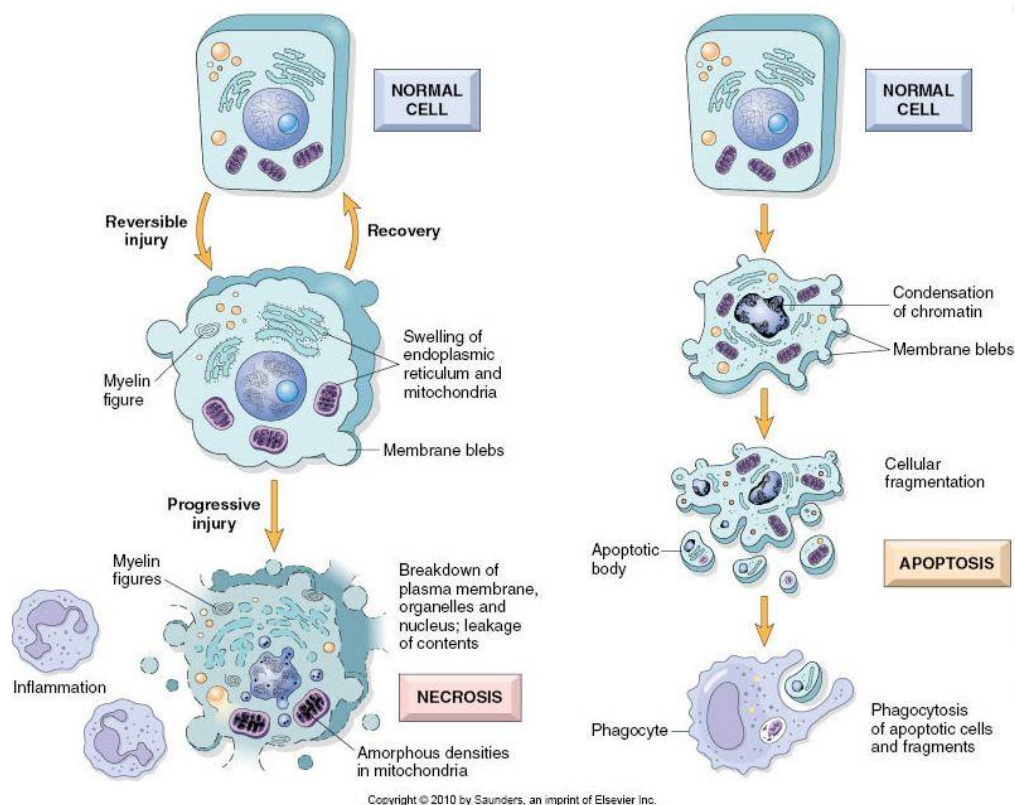


**Figure 1.4.** Representation of the morphological alterations that normal cells suffer after induction of necrosis and apoptosis. Necrosis is a toxic process where all the cell and cell components suffer swelling, leading to the rupture of cell organelles and even disruption of plasma membrane. Release of cellular content to the environment results in the activation of the inflammatory process. Apoptosis is a vital process in healthy cells. This process is characterized by a condensation of the chromatin and formation of membrane blebs. The cell then suffers a shrinkage and breaks up into apoptotic bodies, that correspond to membrane enclosed fragments of the cell that rapidly suffer phagocytosis and are degraded without triggering the inflammatory process. Taken from <sup>28</sup>.

## 2.2. The apoptotic pathways

The mechanisms of apoptosis are highly complex involving an energy dependent cascade of molecular events. There are two main apoptotic pathways: the extrinsic or death receptor pathway and the intrinsic or mitochondrial pathway. Both of these pathways converge at execution pathway. This pathway is initiated by the cleavage of caspase-3 resulting in DNA fragmentation, degradation of cytoskeletal and nuclear proteins, crosslinking of proteins, formation of apoptotic bodies, expression of ligands for phagocytic cell receptors and finally uptake by phagocytic cells<sup>29,30</sup>.

### 2.2.1. The extrinsic or death receptor pathway

The extrinsic pathway is initiated by ligand-induced activation of death receptors at the cell surface, triggering the recruitment and oligomerization of intracellular adaptor molecules (Figure 1.5). Death receptors are type 1 transmembrane proteins, belonging to the tumor necrosis factor (TNF) receptor superfamily. This includes TNF receptor-1, CD95/Fas, and TRAIL (TNF-related apoptosis inducing ligand)<sup>31-33</sup>. In the case of FasL/FasR and TNF- $\alpha$ /TNFR1 models, there is a clustering of receptors and binding with the homologous trimeric ligand. Upon ligand binding, cytoplasmic adapter proteins are recruited. The binding of Fas ligand to FasR results in the binding of the adapter protein FADD, and the binding of TNF ligand to TNFR results in the binding of the adapter protein TRADD with recruitment of FADD<sup>34,35</sup>. Consequently, FADD associates with procaspase-8 by dimerization of the death effector domain. Formation of the death-inducing signaling complex (DISC) is achieved, resulting in the activation of procaspase-8. As soon as caspase-8 is activated, the execution phase of apoptosis is triggered<sup>26,36</sup>.

### 2.2.2. The intrinsic or mitochondrial pathway

The intrinsic pathway of apoptosis is triggered by intracellular stresses that converge on mitochondria, leading to membrane permeabilization, consequently resulting in the release of apoptogenic proteins, and disruption of the mitochondrial membrane potential (Figure 1.5). These changes are the driving force for activation of caspases and finally cell death. Mitochondrial membrane permeabilization may be related with the opening of the mitochondrial permeability transition pore (MPTP) or the formation of specific release channels in the outer membrane, that are promoted by pro-apoptotic members of the Bcl-2 protein family, such as Bax (Bcl-2 associated X protein) or Bak (Bcl-2 homologous antagonist/killer). The Bcl-2 family is composed by different members that regulate the mitochondrial pathway in both a positive and negative way through a pro- or anti-apoptotic effect<sup>30</sup>. Following the induction of apoptosis, Bax and Bak undergo conformational changes, leading to oligomerization, and translocation from the cytosol to the mitochondria (or vice-versa), where they give rise to membrane pores for the release of apoptogenic factors such as cytochrome c<sup>30,37</sup>. Once in the cytosol, cytochrome c will oligomerize with Apaf-1 (Apoptotic protease activating factor 1), recruiting procaspase-9 to form the apoptosome (Figure 1.5). This results in cleavage and activation of caspase-9, which then cleaves and activates downstream caspases that function as effectors molecules of the apoptotic process<sup>30</sup>.

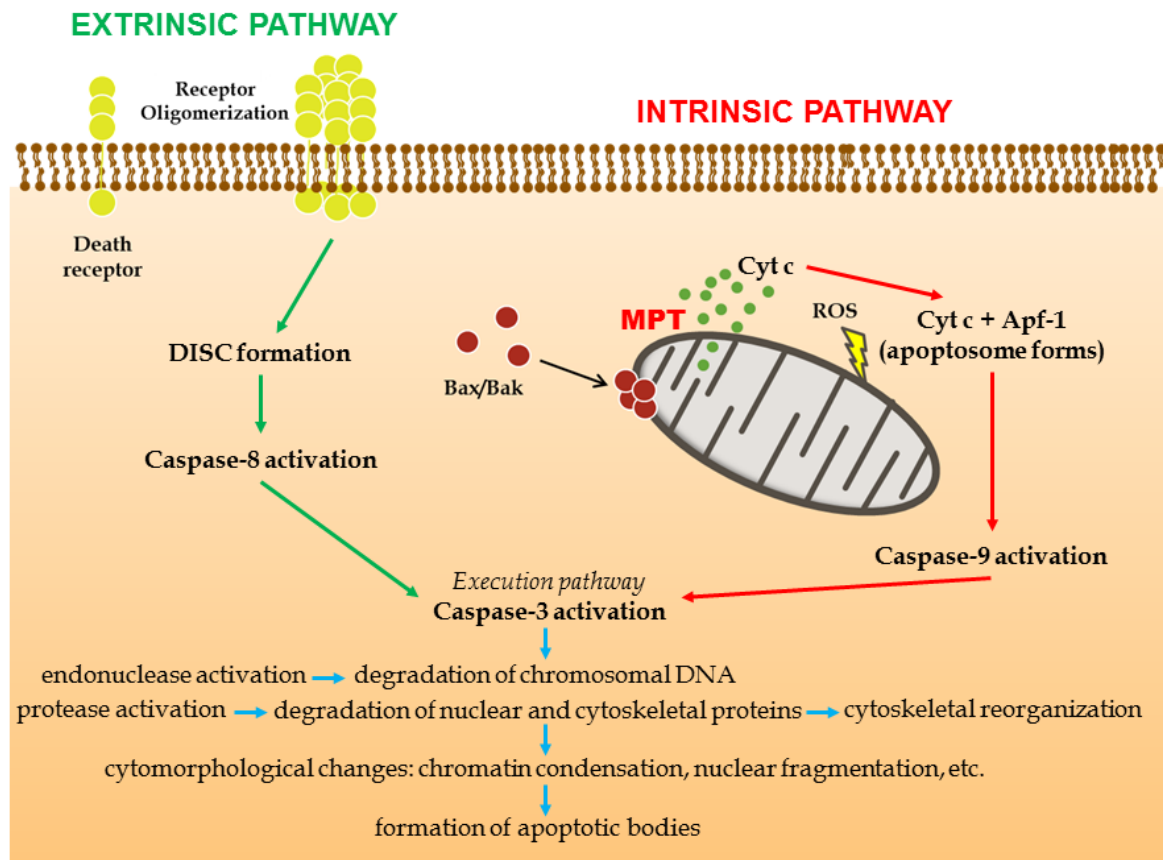


**Figure 1.5.** Schematic representation of apoptotic events. The two main apoptotic pathways, extrinsic and intrinsic pathways are shown. Each of them requires specific triggering signals. Each pathway leads to the activation of its initiator caspase (8 and 9, respectively) which in turn will activate the executioner caspase-3. The execution phase results in DNA fragmentation, degradation of cytoskeletal and nuclear proteins, crosslinking of proteins, formation of apoptotic bodies, expression of ligands for phagocytic cell receptors and finally uptake by phagocytic cells. Adapted from<sup>26</sup>.

### 2.2.2.1. Bcl-2 family of proteins – apoptosis regulators

Bcl-2 is a protein family that is involved in the regulation of the intrinsic apoptotic process. This protein family presents amino acid sequence homology within four Bcl-2 homology domains (Fig. 1.6A) (BH1-BH4)<sup>38</sup>. The members of this family are divided in three major groups according to their cytoprotective or cytotoxic effect: anti-apoptotic Bcl-2-like proteins, the pro-apoptotic multi-domain proteins, such as Bax or Bak, and finally the pro-apoptotic BH3-only proteins (BOPs)<sup>39–41</sup>. However, until now, the precise features that determine the behavior of each subtype of Bcl-2 proteins remained unclear<sup>41</sup>. Moreover, BOPs and anti-apoptotic proteins exert antagonizing effects over the regulation of multi-domain proteins activation and

their oligomerization in the mitochondrial outer membrane (MOM). Oligomerization of apoptotic multi-domain proteins ultimately leads to apoptotic mitochondrial permeabilization (Figure 1.6B)<sup>37</sup>.

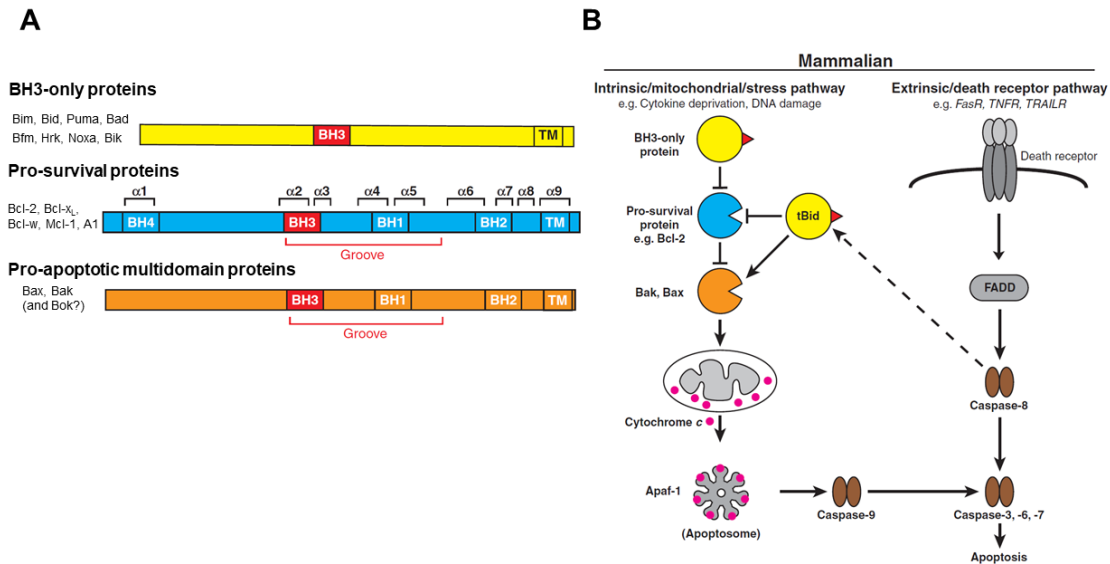


**Figure 1.6.** Bcl-2 protein family and their role in the regulation of apoptotic pathways. (A) Bcl-2 family members are divided in three major groups based on their function and their homologous domains (BH): pro-survival Bcl-2-like proteins, the pro-apoptotic multi-domain proteins such as Bax or Bak, and the pro-apoptotic BH3-only proteins. Many members also possess a C-terminal hydrophobic transmembrane (TM) domain that can anchor proteins in the MOM. Interactions between different family members can occur via binding of the BH3 domain to the hydrophobic surface groove. (B) Both intrinsic and extrinsic pathways culminate in the activation of the proteolytic caspases, but only the intrinsic pathway is associated with regulation by Bcl-2 proteins. Adapted from<sup>38</sup>.

BH3-only proteins, which are induced transcriptionally or post-translationally by cytotoxic stress signals<sup>42</sup>, carry out their pro-apoptotic function by two processes: neutralization of the prosurvival Bcl-2 family proteins and direct activation of the pro-apoptotic effectors Bax and Bak. To understand the consequence of the interactions among the three subgroups, several models have been proposed.

In the direct activation model, the different BH3 proteins are divided by qualitative differences in function<sup>43</sup> (Figure 1.7A). Here, the BH3 proteins with high affinity for binding and activating Bax and Bak, such as the truncated form of Bid (tBid), Bim and possibly PUMA, are termed “activators”<sup>44</sup>, whereas those that only bind the antiapoptotic proteins, such as Bad, are termed “sensitizers”<sup>45</sup>. The activator BH3 proteins directly interact with and activate Bax and Bak to promote mitochondrial outer membrane permeabilization (MOMP). The antiapoptotic proteins inhibit MOMP by specifically sequestering the BH3 activators. The BH3

sensitizer proteins can compete for binding with the antiapoptotic proteins, thus releasing the BH3 activator proteins to promote MOMP through activation and oligomerization of Bax and Bak<sup>46</sup>. Notably, it has been difficult to identify the complex Bax-BH3-only, since there are some evidences that point to a transient and quick interaction between these molecules<sup>47,48</sup>. This type of model is called “hit and run” and is based on the fact that when a BH3-only protein interacts with Bax or Bak it causes a conformational change in the last ones that leads to the detachment of the two types of proteins. Still, several studies have captured or implicated direct binding and activation of Bax and Bak by BH3-only proteins using biochemical, structural and genetic approaches<sup>48–50</sup>.

According to the displacement model, BH3 proteins can be categorized exclusively based on their affinities of binding for the antiapoptotic proteins, not being recognized as activators (Figure 1.7B). In this model, Bax and Bak are constitutively active and oligomerize to induce MOMP unless they are regulated by the antiapoptotic proteins<sup>46,51</sup>.

The embedded together model introduces an active role for the membrane and combines the major aspects of the previous models (Figure 1.7C). The interactions between members of the Bcl-2 family are controlled by equilibria and therefore are dependent on the relative protein concentrations as well as their binding affinities<sup>52,53</sup>. The latter are determined by posttranslational modifications, fraction of protein bound to the membrane, and cellular physiology. In membranes, the activator BH3 proteins directly activate Bax and Bak, which then oligomerize, inducing MOMP. Both activator and sensitizer BH3 proteins can recruit and sequester antiapoptotic proteins in the membrane. The anti-apoptotic proteins inhibit apoptosis by sequestering the BH3 proteins and Bax and Bak in the membrane or by preventing their binding to membranes<sup>54</sup>. At different intracellular membranes, the local concentrations of specific subsets of Bcl-2 family members alter the binding of Bcl-2 proteins to the membrane and the binding equilibria between family members. As a result, Bcl-2 family proteins have distinct but overlapping functions at different cellular locations<sup>52,54,55</sup>.

Finally, the unified model (Figure 1.7D) considers two modes of action of antiapoptotic proteins that are based on the embedded together model: Mode 1 where the antiapoptotic proteins sequester the activator BH3 proteins, preventing Bax and Bak from being activated and mode 2 where they sequester Bax and Bak molecules that are already activated (Figure 6D). It differs in that in the unified model, inhibition of apoptosis through mode 1 is less effective and therefore easier to overcome by sensitizer BH3 proteins<sup>46,49,56</sup>. The transient character of the interaction between Bax and BH3-only proteins is still associated with some controversy and recent studies in fibroblasts<sup>57</sup> and epithelial cells<sup>58</sup> showed a dynamic equilibrium of Bax localization at cytosol and MOM, suggesting that Bax translocate continuously between the cytosol and the mitochondria, and that Bcl-XL is responsible for translocating it back to cytosol

in healthy cells. Also it was already observed that Bax spontaneously interacts with membranes even in the absence of activator proteins<sup>59</sup>.

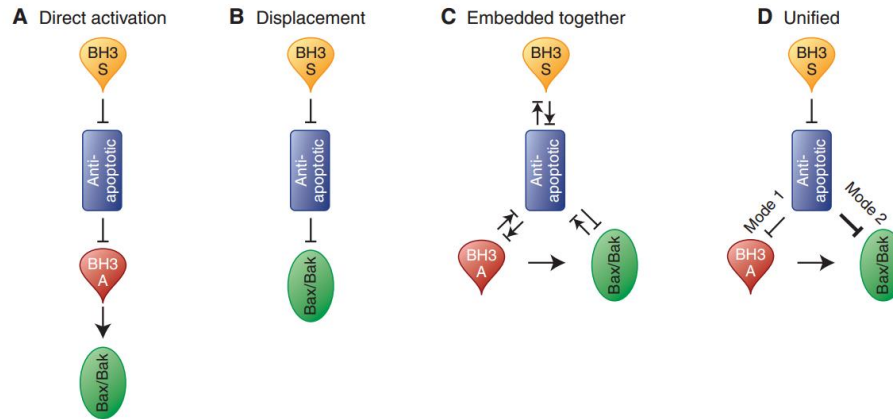


**Figure 1.7.** Models addressing how the interactions between members of the Bcl-2 family control the apoptotic switch. ( $\uparrow$ ) Activation; ( $\perp$ ) inhibition; ( $\perp\uparrow$ ) mutual recruitment/sequestration. Paired forward and reverse symbols indicate equilibria. (A) In the direct activation model, the different BH3 proteins divided by qualitative differences in function. The activator BH3 proteins directly interact with and activate Bax and Bak to promote MOMP. The antiapoptotic proteins inhibit MOMP by specifically sequestering the BH3 activators. The BH3 sensitizer proteins can compete for binding with the antiapoptotic proteins, thus releasing the BH3 activator proteins to promote MOMP through activation and oligomerization of Bax and Bak. (B) In the displacement model, BH3 proteins do not directly bind to Bax and Bak to cause their activation. Rather, Bax and Bak are constitutively active and therefore must be inhibited by the antiapoptotic proteins for the cell to survive. To initiate apoptosis, BH3 proteins displace Bax and Bak from the antiapoptotic proteins to promote Bax- or Bak-mediated MOMP. (C) In the embedded together model, the interactions between members of the Bcl-2 family are controlled by equilibria and therefore are dependent on the relative protein concentrations as well as their binding affinities. In membranes, the activator BH3 proteins activate Bax and Bak directly, which then oligomerize, inducing MOMP. Both activator and sensitizer BH3 proteins can recruit and sequester antiapoptotic proteins in the membrane. The anti-apoptotic proteins inhibit apoptosis by sequestering the BH3 proteins and Bax and Bak in the membrane or by preventing their binding to membranes. (D) The unified model is based on the embedded together model by proposing that the antiapoptotic proteins sequester the activator BH3 proteins (mode 1) and sequester Bax and Bak (mode 2). Adapted from<sup>46</sup>.

### 2.2.2.2. *Bax (Bcl-2 associated X protein)*

Human Bax is a 22 kDa (192 amino acids) globular protein composed of nine alpha helices (Figure 1.8). The  $\alpha 9$  helix is a transmembranar domain that is associated with regulation of Bax activity, since it is responsible for anchoring Bax to the MOM. On the cytosolic Bax, it resides in a hydrophobic groove preventing interactions between Bax and other molecules such as activator proteins or Bax itself. Thus, this helix provides a simultaneous control over its mitochondrial targeting and dimer formation<sup>60</sup>. The  $\alpha 5/\alpha 6$  helices represent the hydrophobic core of the protein and are essential to Bax insertion into MOM since they have been proposed to be pore-forming transmembrane domains. The  $\alpha 2$  helix contains the BH3 domain, which is crucial for Bax activation and oligomerization<sup>39,40,50,61</sup>.

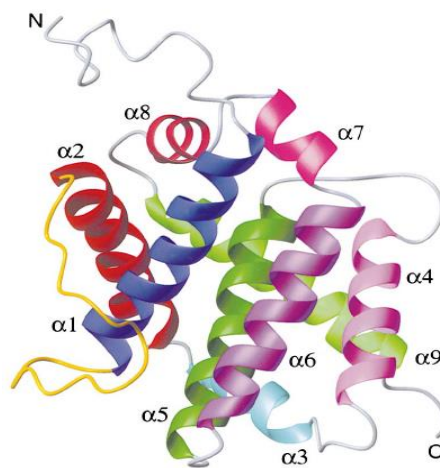


**Figure 1.8.** Ribbon representation of an average minimized NMR structure for Bax. The 9 alpha helices that compose Bax are distinguished by different colors. Adapted from <sup>38</sup>.

### 2.2.2.3. *Regulatory mechanisms of Bax activity*

Given their critical role in mediating mitochondrial apoptosis, Bax and Bak have to be firmly regulated by other members of the Bcl-2 family. At least five mammalian prosurvival proteins have been identified that can inhibit Bax and Bak via three distinct mechanisms: mode 0, mode 1 and mode 2 (Figure 1.9)<sup>62</sup>. Modes 1 and 2 describe the indirect and direct inhibition of Bax and Bak, where prosurvival proteins sequester BH3-only proteins to stop them activating Bax and Bak and bind to activated Bax and Bak to prevent their homo-

oligomerization, respectively<sup>45</sup>. Mode 0 is the newly described mechanism in healthy cells by which prosurvival proteins regulate Bax mitochondrial localization by binding of proteins such as Bcl-XL to peripheral Bax at mitochondria and retro-translocate it to cytosol<sup>57,62</sup>. Deregulated Bcl-2 proteins are associated with a series of diseases, making the Bcl-2 family members and their interactions a focus for novel therapeutics. BH3 mimetics such as ABT737<sup>63-65</sup>, its derivative ABT263<sup>66</sup>, and the newly developed ABT199<sup>67</sup>, which bind and inhibit prosurvival Bcl-2 proteins, provide information for the design of selective drugs that activate the apoptotic program in cancer cells and have encouraged the search for anti-cancer drugs that directly activate Bax and Bak<sup>68</sup>.

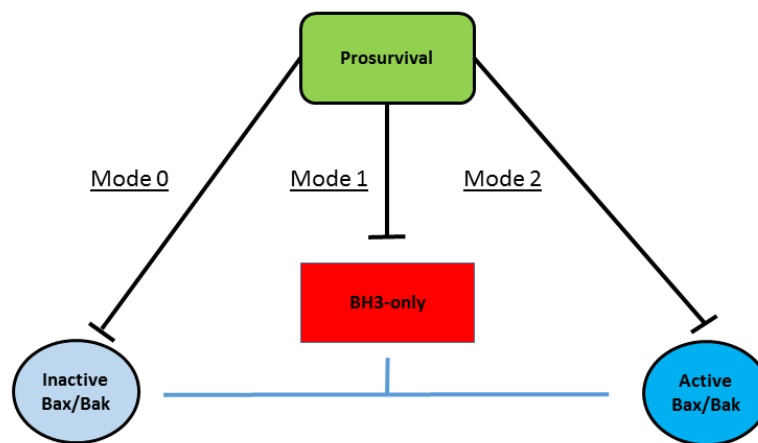


**Figure 1.9.** Schematic representation of the Bcl-2 family interaction network. Inhibition by prosurvival proteins may occur through 3 modes: In mode 0 prosurvival proteins such as Bcl-XL bind to Bax at mitochondria and retro-translocate it to cytosol. During mode 1 prosurvival proteins sequester BH3-only proteins in order prevent them from activating Bax and Bak. In mode 2 prosurvival proteins bind directly to activated Bax and Bak to prevent their homo-oligomerization. Note that blue lines show an activation process. Adapted from<sup>62</sup>.

#### 2.2.2.4. Bax activation mechanism, oligomerization and membrane insertion

The exact mechanism by which Bax is activated, oligomerize and exert its pore-forming activity is yet not clear. However, for Bax to be activated, and consequently exert its pore-forming action, an interaction with a BH3-only protein like truncated Bid (tBid) is needed<sup>38,47,69,70</sup>. During apoptosis, cleavage of Bid by caspase 8 produces p15 tBid, the active form of

Bid, which can rapidly translocate to mitochondria leading to destabilization of mitochondrial membrane structure and bioenergetics. This action is related with its ability to bind to cardiolipin that is a signature mitochondrial lipid involved in curvature stress<sup>23,71</sup>. Thus tBid may play a primary role on mitochondrial membrane destabilization, having a synergistic effect with Bax or Bak<sup>70</sup>. After interaction with BH3-only proteins, Bax undergoes multiple conformational changes in order to bind to membranes and oligomerize to form pores<sup>46</sup>.

Over the last few years several models of Bax oligomerization have been suggested<sup>55,72,73</sup>. For example, it was proposed that oligomerization could be explained by two different models (Figure 1.10): symmetrical dimers, where the BH3 domain of one Bax interacts with the BH3 binding groove of another<sup>38,39</sup>, or asymmetrical dimers<sup>46,55</sup>. In the case of symmetrical dimers, dimer formation causes a conformational change, which opens up a dimer interaction surface thereby permitting Bax dimers to join to each other and form higher order oligomers<sup>55</sup>. In the case of the asymmetrical dimers model, the BH3 domain of an activated Bax can interact with the “rear pocket” of another Bax<sup>73,74</sup>. This interaction causes allosteric conformational changes that displace helix 9, which allows Bax to target MOM<sup>47</sup>. Sequential oligomerization proceeds by the BH3 region of an activated Bax binding to the rear pocket of another Bax monomer, exposing its BH3 domain to further propagate oligomerization, finally culminate in MOMP. Note that in this type of mechanism, the BH3-only protein does not need to be dissociated from Bax since they bind in different grooves<sup>55</sup>.

These contrasting models propose different “units” that are joined to form the oligomer. However it is clear that in each model both hydrophobic pockets are important for the proapoptotic function of Bax<sup>46</sup>.

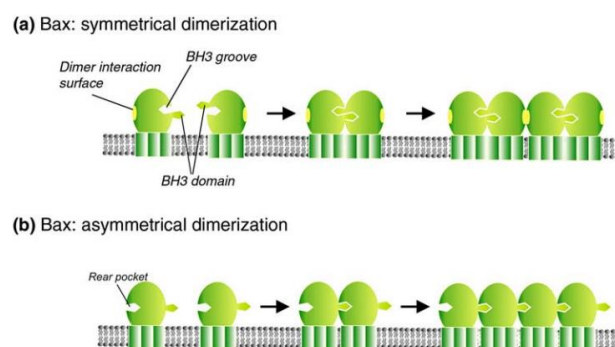


**Figure 1.10.** Models of Bax dimer formation: (a) Symmetrical dimers: The BH3 domain of one Bax interacts with the BH3 binding groove of another. Bax dimer formation causes a conformational alteration, permitting Bax dimers to join to each other and form higher order oligomers. (b) Asymmetrical dimers: The BH3 domain of an activated Bax can interact with the ‘rear pocket’ of another Bax. This interaction causes a conformational change in Bax allowing the BH3 domain to be exposed such that it binds to the ‘rear pocket’ of an adjacent Bax. This leads to oligomerization of Bax dimers and results in MOMP. Adapted from<sup>55</sup>.

Supporting the symmetrical dimer model, Czabotar *et al.* revealed through the resolution of truncated Bax (lacking  $\alpha 9$ ) crystallography structures that a BH3-only protein such as tBid, interacts with Bax causing it to undergo conformational changes where Bax exposes the  $\alpha 9$  helix for its anchoring into the MOM (Figure 1.11)<sup>39,50</sup>. Furthermore, the activator molecule also insert its BH3 domain into the hydrophobic groove of Bax, initiating the release of the core domain ( $\alpha 1$ - $\alpha 5$ ) from the latch domain ( $\alpha 6$ - $\alpha 9$ ) and displacement of the BH3 domain of Bax (Figure 1.11). Then this domain can compete with the BH3 domain of the activator molecule for the hydrophobic groove of another Bax molecule due to the increased stability of the BH3-in-groove symmetric dimer<sup>50,69</sup>. This dimer is able to nucleate oligomerization of the Bax core domain ultimately leading to MOM permeabilization<sup>38,50</sup>. Note that the authors do not discard the hypothesis of the existence of the asymmetrical dimers, however their studies do not address whether some alternative site contributes to earlier activation steps, such as release of  $\alpha 9$  from the groove. Moreover, they considered that BH3 interactions with two different sites on Bax may play sequential roles in activation, as some biochemical evidence suggests<sup>47</sup>.

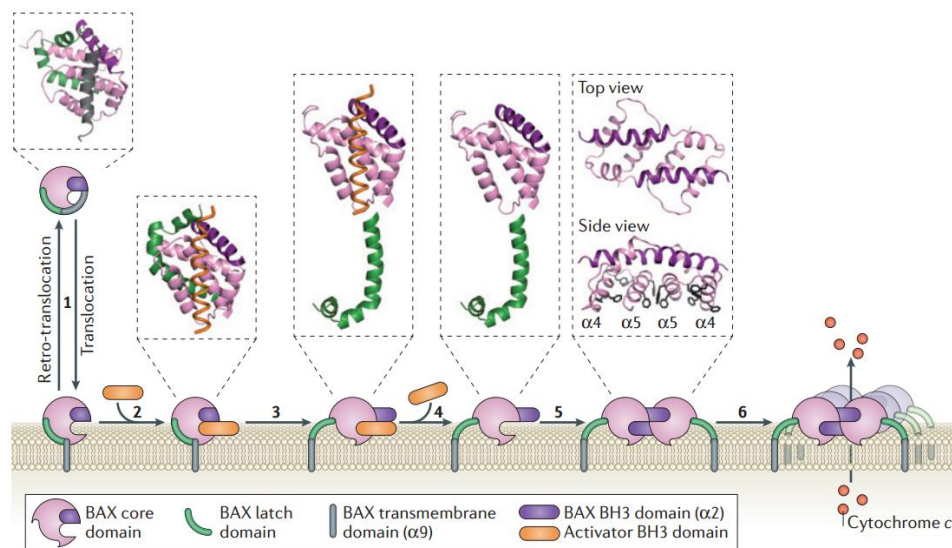


**Figure 1.11.** Model for the activation and oligomerization of Bax. Step 1 illustrates the proposed shuttling of Bax to the MOM and its retro-translocation to the cytosol<sup>57</sup>. The movement of Bax to the MOM may be triggered or increased by engagement of the rear pocket of the protein by a BH3-only protein. Consequently, the transmembrane domain, corresponding to helix 9, is now freed from the Bax surface groove and can be inserted across the MOM, generating the membrane-bound form of Bax. In step 2 and 3, an activator BH3 domain binds to Bax groove, promoting the release of the “latch” domain from the “core” domain of Bax and destabilizes the Bax BH3 domain,  $\alpha 2$ . The initiating activator BH3 domain then disengages (step 4) and consequently the exposure of the Bax BH3 domain allows for the interaction of two such molecules to form the BaxBH3-in-the-groove dimer (step 5). The structure of the BAX core ( $\alpha 2$ - $\alpha 5$ ) as a symmetrical dimer reveals a hydrophobic layer of two  $\alpha 4$  and two  $\alpha 5$  chains with

12 protruding aromatic residues (side view). Although it is unclear how the larger oligomers form (step 6), the core  $\alpha 4$ – $\alpha 5$  surface might engage the outer leaflet of the outer mitochondrial membrane, thereby inducing tension and contributing to membrane permeabilization<sup>50</sup>. Adapted from<sup>56</sup>.

Recent studies have given new insights over Bax integration and oligomerization in the membrane<sup>59,75–77</sup>. In healthy cells, Bax can translocate, alone, to the MOM and binds to the membrane as monomer, while a cytosolic dimeric form of the protein was shown to be in the inactivated state<sup>78</sup>. More recently, Subburaj *et al.* reported that Bax binds to the membrane in a monomeric state but quickly associate into dimers, being the unit for high-order oligomers<sup>75</sup>. In this way, Bax-induced MOM permeabilization would not be mediated by a unique, well-defined Bax pore structure, but rather by multiple Bax pores with different sizes, already reported to be of tunable size<sup>76</sup>, and stoichiometries that adapt to Bax density at the MOM. This report is in accordance with previous work that considers the dimer as the unit for further oligomerization<sup>50,73</sup>.

#### 2.2.2.5. *Bax interaction with membranes – effect of membrane lipid composition*

Mitochondrial lipids have an important role in mitochondrial regulation since they could be responsible for the specific recruitment of proteins of the Bcl-2 family, such as tBid, to mitochondria. They could also assist in regulating the conformational rearrangements of Bax and Bak and might contribute to their localization to specific regions of the MOM. More importantly, lipids could directly participate in the mechanism of MOM permeabilization<sup>79</sup>.

The plasma membrane is known to have lipid microdomains called lipid rafts mainly composed of sphingolipids and cholesterol that are considered an interface for specific regulatory mechanisms. It has recently been shown that mitochondria also possesses similar lipid domains which might serve as structural elements together with some of the mitochondrial permeability transition pore-forming proteins and with members of the Bcl-2 family<sup>80,81</sup>.

Ceramide, a pro-apoptotic sphingolipid is also present in these lipid microdomains. This molecule and Bax are able to induce MOM permeabilization synergistically, since the apparent affinity of activated Bax for ceramide increases with ceramide content, indicating that activated Bax shows enhanced capacity to permeabilize in the presence of ceramide. It has also been shown that ceramide is able to activate monomeric Bax in the presence of the MOM<sup>82</sup>.

On the other hand, lipids with negative intrinsic curvature, such as phosphatidylethanolamine (PE), were reported to inhibit Bax-induced release of fluorescent compounds trapped inside liposomes<sup>79</sup>.

Mitochondrial lipids were shown to suffer early modification following apoptosis induction. Cardiolipin (CL) rapidly undergoes hydrolysis and oxidation facilitating the redistribution of free cytochrome to the intermembrane space which could give signal to MOM permeabilization by Bax. It provides a docking site for the interaction and activation of pro-apoptotic Bcl-2 proteins, like tBid, in intact mitochondria<sup>79,83,84</sup>.

Mitochondrial membranes are much less enriched in cholesterol than the plasma membrane. However, this small pool of cholesterol plays a fundamental physiological role in the regulation of membrane organization, controlling membrane permeability and function of resident proteins. This molecule has the ability to inhibit Bax pore activation in mitochondria and liposomes through direct interaction with the protein<sup>85</sup>. Thus, it probably acts on the mitochondrial outer membrane environment to inhibit Bax integration into the membrane, possibly through a decrease in membrane fluidity that inhibits Bax oligomerization/association with the membrane<sup>83,86</sup>.

Taking all into account, the dependence of Bax activity on lipid composition suggests a potential mechanism for apoptotic regulation since it would be possible to control MOM permeabilization by molecules that affect the structure of the mitochondrial membrane.

### **3. Bile Acid function, synthesis and chemistry**

Bile acids (BAs) are cholesterol-derivative physiological detergents that generate bile flow and assist intestinal absorption and transport of lipids, nutrients, and vitamins<sup>87,88</sup>. BAs include molecular species with similar, but not identical, chemical structures that exhibit different physical properties and even more diverse biological features<sup>89</sup>.

After the discovery of the role of acidic steroids in many different physiological processes, the interest on bile acids has grown markedly. These discoveries had important implications from the point of view of liver and intestinal pathology and pharmacology. Furthermore, in recent years the application of bile acids in areas like supramolecular chemistry and nanotechnology has been the focus of intensive research<sup>30,90</sup>.

#### **3.1. Physiological functions**

BAs have diverse physiological functions, five of which are particularly important. The first of these is the route for cholesterol (Chol) elimination by conversion to bile acids and by micellar solubilization of Chol in bile, enabling it to move from the hepatocyte to the intestinal lumen, ultimately leading to elimination via the fecal route<sup>90</sup> (Figure 1.13).

Additionally, in the small intestine, bile acids promote dietary lipid absorption by solubilizing them as mixed micelles. The formation of these structures enhances the diffusion through the unstirred layer, increasing the rate of lipid absorption. If BAs were not present in this form it would not be possible to absorb fat-soluble vitamins like vitamin A, D, E and K<sub>1</sub>, leading to a deficiency in their physiological content<sup>90</sup>.

BAs are also able to stimulate bile flow and biliary phospholipid (PL) secretion. Bile acids are actively transported into the biliary canaliculi between hepatocytes, inducing bile flow by their osmotic properties and promoting the transfer of PL from the canalicular membrane into bile. The presence of these lipids in the bile results in a greater fraction of bile acids in the micellar form and a lower concentration in the monomeric form, which prevents them from damaging the bile duct epithelium<sup>90</sup>.

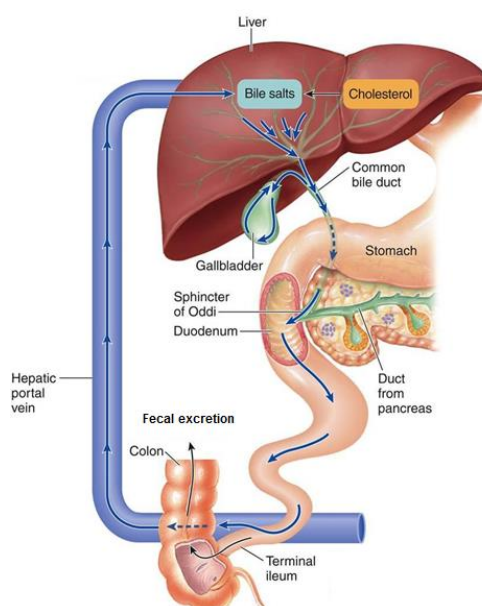


**Figure 1.12.** Enterohepatic circulation of bile acids. After excretion into bile, 95% of bile acids are reabsorbed in the intestine (mainly in the terminal ileum), returned to the liver, and then secreted again into bile in the enterohepatic circulation. In the gut, primary bile acids suffer bacterial transformation giving rise to secondary bile acids. Under normal circumstances, the majority of bile acids ( $\approx 95\%$ ) are conjugated and tightly bound to plasma and intracellular proteins; the free concentration is usually  $< 5\%$  of the total concentration, restricting their cytotoxic effect on healthy humans<sup>91</sup>. Adapted from<sup>92</sup>.

Finally, BAs exert a negative feedback regulation on Chol and their own biosynthesis. The concentration of BAs act as a signal: when a high concentration is achieved, the BAs synthesis is lowered; while with lower concentration, synthesis of Chol and BAs will increase. This type of response is transcriptional and mediated by members of the nuclear hormone

receptor family, acting on two genes that encode hydroxylase enzymes in the biosynthetic pathways<sup>29,88</sup>.

### 3.2. Synthesis

Primary BAs such as cholic acid (CA) and chenodeoxycholic acid (CDCA) (which are the most abundant in humans) are directly synthesized from cholesterol requiring a coordinated action of a dozen enzymes located in every major compartment of the hepatocyte. Thus, the addition of hydroxyl groups and the oxidation of its side chain occur to form a more water-soluble end product. Though the pattern of hydroxylation varies between BAs molecules, the hydroxylation is always on one side of the molecule, being the final product an amphipathic molecule (Figure 1.14B)<sup>93</sup>.

Within the intestines, C-7 dehydroxylation of the primary bile acids by bacterial transformation, produces secondary bile acids, known as deoxycholic acid (DCA; from CA) and lithocholic acid (LCA; from CDCA). The 7-hydroxy epimerization of CDCA gives rise to ursodeoxycholic acid (UDCA), currently used for cholesterol gallstone dissolution therapy and in the treatment of cholestatic liver diseases.

Within hepatocytes, all bile acids (primary or secondary) are conjugated at the terminal (C-24) carboxyl group mainly with glycine (75%) and to a less extent with taurine (25%). For example, UDCA can be conjugated with taurine resulting in the formation of tauroursodeoxycholic acid (TUDCA) that could be called a tertiary BA. This amidation increases aqueous solubility at acidic pH, increases resistance to precipitation by calcium and renders bile acids impermeable to cell membrane, which allows high concentrations of the molecule to persist in bile and intestinal content<sup>29,30</sup>.

### 3.3. Chemistry

The molecular structure of BAs is composed of a steroid nucleus, derived from the precursor Chol molecule, that consist of three six-member rings (A, B and C) and a five-member ring (D) (Figure 1.14A).

The presence in bile acid molecules of hydroxyl groups at different positions (in mammals, commonly at positions 3, 7 and/or 12) and of different side chain structures, results in different physical-chemical characteristics and variable degrees of hydrophobicity (Table 1)<sup>29</sup>. The hydroxyl groups, oriented towards the  $\alpha$ -side (with the exception of the naturally occurring

UDCA), and the carboxylic side chain, provides them their hydrophilic character. The hydrophobic methyl groups (at C-18 and C-19) are oriented towards the  $\beta$ -side (Figure 1.14B). As a consequence, they exhibit a great surface activity and in aqueous solutions they can form small aggregates or micelles. Micelles are formed when their concentrations are above a critical value, called the critical micellar concentration (CMC)<sup>89</sup>.

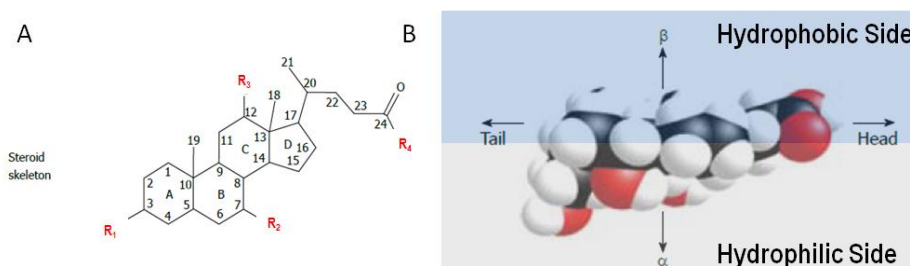


**Figure 1.13.** (A) Chemical structure of typical bile acids. Presence of a steroid nucleus that is composed by four rings (A to D). R<sub>1</sub>-R<sub>3</sub> can be either -H or -OH and R<sub>4</sub> can be a carboxyl acid, a taurine or glycine aminoacid. (B) Stereostructure of cholic acid - Space filling model to show the presence of an hydrophilic and an hydrophobic side of the molecule. Adapted from<sup>89</sup>.

**Table 1** – Chemical composition of most relevant bile acids according to the substitution positions shown on Figure 1.14.

Bile Acid	BA Type	R1	R2	R3	R4
Cholic acid (CA)	Primary	OH	OH	OH	OH
Chenodeoxycholic acid (CDCA)	Primary	OH ( $\alpha$ )	OH ( $\alpha$ )	H	OH
Deoxycholic acid (DCA)	Secondary	OH	H	OH	OH
Lithocholic acid (LCA)	Secondary	OH	H	H	OH
Ursodeoxycholic acid (UDCA)	Secondary	OH ( $\alpha$ )	OH ( $\beta$ )	H	OH
Tauroursodeoxycholic acid (TUDCA)	Tertiary (conjugated form)	OH ( $\alpha$ )	OH ( $\beta$ )	H	NHCH <sub>2</sub> CH <sub>2</sub> SO <sub>3</sub> H

### 3.4. Bile acids and apoptosis

#### 3.4.1 Hydrophobicity / Cytotoxicity

Bile acids are always cytotoxic when their concentrations increase to abnormally high levels, either intracellularly or extracellularly. BA cytotoxicity is strongly affected by its structure: a more hydrophobic molecule is associated with a greater cytotoxicity. BA hydrophobicity depends on the number, position and orientation of the hydroxyl groups, as well as amidation at the C-24 position. An hydrophobicity quantification can be obtained by performing reverse-phase High-Performance Liquid Chromatography (HPLC) and analyzing the BA partition between a hydrophobic stationary phase and an aqueous mobile phase<sup>94,95</sup>. Thus, concerning the magnitude of hydrophobicity of BAs the order would be TUDCA < UDCA < CA < CDCA < DCA < LCA. The conjugation reduces hydrophobicity when compared with unconjugated analogs<sup>93</sup>.

#### 3.4.2 Bile-acid-induced cell death pathways

Even at submicellar concentrations of BAs, these molecules can promote cell injury and death through two mechanisms dependent on the accumulated concentration: lower BA concentrations induce hepatocellular apoptosis while higher concentrations induce necrosis. Surprisingly, apoptosis induction is dependent on the BA, its concentration, and its conjugation state, instead of being solely correlated with hydrophobicity<sup>93</sup>.

Apoptosis is a highly regulated process of programmed cell death that is vital for a wide variety of biological processes like normal embryonic development and tissue homeostasis during adulthood. However, it may be also associated with pathology<sup>30</sup>. The onset of apoptosis in hepatocytes and bile duct epithelial cells has been implicated in the pathogenesis of many liver diseases. It is known that hydrophobic BAs can induce apoptosis through both the extrinsic and intrinsic apoptotic pathways<sup>29,30,90</sup>.

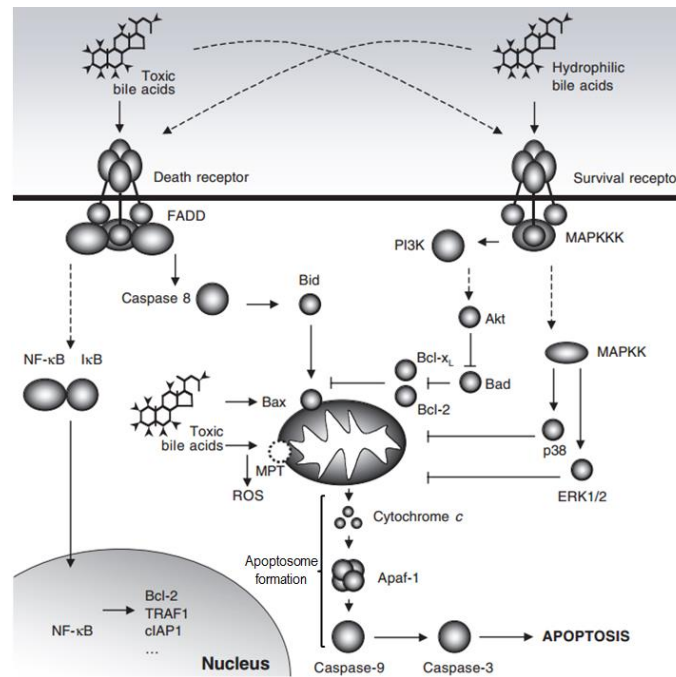


**Figure 1.14.** Death and survival transduction pathways that are modulated by bile acids. Hydrophobic bile acids induce apoptosis by activating both ligand-dependent and -independent death-receptor oligomerization. In cells such as hepatocytes, the progression of the apoptotic cascade depends on its amplification by mitochondria, that can be directly targeted through induction of the MPT (mitochondrial membrane permeability transition) and ROS (reactive oxygen species) formation, or activation of pro-apoptotic Bcl-2 members. On the other hand, hydrophilic bile acids activate survival signaling pathways, such as MAPK (*Mitogen-activated protein kinases*) and PI3K (*Phosphatidylinositol 3-kinase*), antagonizing Bcl-2 pro-apoptotic members and preventing mitochondrial dysfunction and apoptosis. Adapted from<sup>32</sup>.

The mechanism by which submicellar concentrations of BAs induce apoptosis in hepatocytes is not entirely clear. In fact, alternative mechanisms have been proposed for triggering of BA-induced apoptosis, including the activation of death receptors, like Fas, in a ligand independent oligomerization of Fas<sup>31</sup>, and cyclin D1-dependent Bax translocation through non-transcriptional p53-dependent mechanisms<sup>96–98</sup>. Importantly, mitochondrial perturbation with decreased  $\Delta\psi_m$  (mitochondrial membrane potential) and enhanced ROS (reactive oxygen species) generation is involved in cell death induced by hydrophobic bile acids, either directly participating in cell death or occurring concomitantly with other mitochondrial dysfunctions such as MPT (mitochondrial membrane permeability transition)<sup>99</sup>.

More recently, it has been demonstrated that hydrophobic BAs can also induce apoptosis in hepatocytes by endoplasmic reticulum (ER) stress<sup>93,100</sup>. GCDCA induces ER stress which, in turn, induces apoptotic signaling, in a time-dependent manner in isolated rat hepatocytes. This BA was responsible for the release of calcium that was followed by the activation of calpain and caspase-12, suggesting that GCDCA-induced ER stress might trigger the activation of both ER-mediated and mitochondria-mediated apoptosis in isolated rat hepatocytes by cross-talk between ER and mitochondria, using calcium ions as signal molecules<sup>101</sup>.

### 3.4.3. Bile-acid-induced cell protection

Hydrophilic BAs such as UDCA and TUDCA have become extremely popular because they are associated with low toxicity and have already demonstrated high efficiency in the treatment of diverse cholestatic liver diseases<sup>93</sup>. Moreover, it has become evident by now that these bile acids at submicellar concentrations are able to exert direct protective effects at a cellular and molecular level, through the stabilization of hepatocytes, the enhancement of the protection against oxidative stress and the inhibition of apoptosis induced by several agents, including hydrophobic BAs (Figure 1.16)<sup>102,103</sup>.

UDCA has the ability to stimulate bile flow and detoxification of cholephilic compounds preventing the accumulation of potentially toxic BAs in the liver. Otherwise these compounds would lead to necrosis, apoptosis, fibrosis, and ultimately liver cirrhosis. This protective function of UDCA can occur at normal secretion conditions and even in situations of impaired bile secretion<sup>104</sup>. UDCA action has been reported to be at least partially related to the potentiation of gene expression of carrier proteins and with the stimulation of murine renal and intestinal efflux transport proteins<sup>93</sup>.

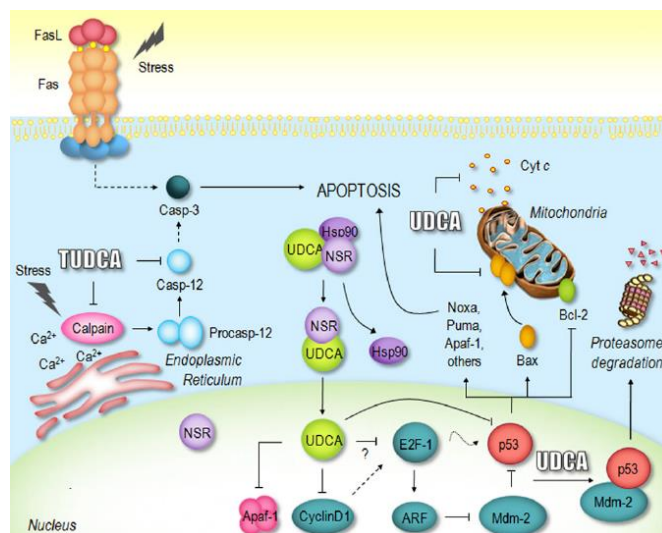


**Figure 1.15.** Proposed mechanism by which UDCA and TUDCA exert their anti-apoptotic effect. These bile acids are able to inhibit mitochondrial membrane damage, reducing BA-induced disruption of the mitochondrial membrane potential, ROS production, and Bax protein concentration in mitochondria. Moreover, UDCA prevents the release of cytochrome c and the subsequent cytosolic caspase activation, reduces the levels of cyclin D1, and specifically modulate the E2F-1/p53/Bax cell death pathway. TUDCA is able to abolish the typical morphological changes of ER stress preceding apoptosis by blocking the calcium-mediated apoptotic pathways and by inhibiting the caspase-12 activation. Adapted from<sup>30</sup>.

### 3.4.3.1. Inhibition of apoptosis

One of the most important protective actions of hydrophilic bile acids, such as UDCA and TUDCA, is the ability to inhibit hepatic and non-hepatic cellular apoptosis induced by certain agents like hydrophobic bile acids<sup>103</sup>.

The UDCA and TUDCA effect seems to be related with the blockage of mitochondrial membrane damage, reducing BA-induced disruption of the mitochondrial membrane potential, ROS production, and Bax protein concentration in mitochondria. They can also prevent the release of cytochrome c from mitochondria to the cytoplasm after mitochondrial injury and the subsequent cytosolic caspase activation and cleavage of the nuclear enzyme poly(ADP-ribose) polymerase<sup>105</sup>.

BA's have been detected within the nucleus in rat hepatocytes and it has been shown that the nuclear translocation is mediated by nuclear steroid receptors (NSRs), more specifically the glucocorticoid receptor (GR) which means that they can play an important role as an hepatic anti-inflammatory<sup>106</sup>. It has been proposed that UDCA plays a role in the

regulation of gene expression, being most of these genes related with apoptosis and cell cycle regulation<sup>107</sup>. For example, UDCA- reduces cyclin D1 expression , specifically modulate the E2F-1/p53/Bax cell death pathway and abolishes E2F-1-induced p53 and p53-associated Bax expression. The modulation of gene expression by UDCA is independent of its effect on mitochondria and/or caspases<sup>96,108</sup>.

Besides the inhibition of apoptotic signal pathways, the activation of survival pathways may be an additional and important mechanism by which UDCA exerts its anti-apoptotic action. For example, UDCA can stimulate the, NF- $\kappa$ B (nuclear factor kappaB), PI3K (phosphatidylinositol 3-kinase) and MAPK (mitogen-activated protein kinases) survival pathways through the activation of the epidermal growth factor receptor (EGFR)<sup>109</sup>.

TUDCA has similar physiological effects to the ones exerted by UDCA. This BA modulates apoptosis by blocking mitochondrial membrane perturbation by a mechanism that is independent of the MPT and is associated to the inhibition of Bax-mediated structural changes in the lipid and protein environment of the mitochondrial membrane. Thus, TUDCA prevents the binding of Bax to the mitochondria and inhibits oxidative lipid injury<sup>32,110</sup>. TUDCA is also able to abolish the typical morphological changes of ER stress preceding apoptosis by blocking the calcium-mediated apoptotic pathways<sup>111</sup>. This bile acid also exerts a regulatory effect over gene expression by the inhibition of the human transcription factor activating protein (AP-1) and has a stimulatory effect over survival pathways like p38/ERK/MAPK and PI3K, upon activation of cytotoxicity by hydrophobic bile acids. This protective effect of TUDCA is independent of caspases inhibition, NF- $\kappa$ B activation, and competition at the cell membrane with toxic bile acids<sup>32,112</sup>.

In summary, bile acids can be separated in two different classes, with cytoprotective or cytotoxic physiological properties depending on their hydrophobicity. However, several questions associated with the mechanisms by which bile acids exert their effects remain to be revealed. Mainly, how can BAs have so many different effects? More specifically, how can bile acids affect both apoptotic pathways? Is this associated with intercorrelation between those pathways or could it be related with some type of basic interaction with lipid membranes? Since some BAs are able to regulate Bax-mediated apoptosis, could these molecules directly induce protein activation/inhibition? These are some of the many questions that remain to be answered.

### 3.5. Interaction of bile acids with lipid membranes

Bile acids have long been known to partition to lipid membranes, even at submicellar concentrations, being able to affect cell integrity by modifying its properties such as membrane permeability<sup>113–115</sup>. More hydrophobic/cytotoxic bile acids have been suggested to be both intercalated with the acyl-chains in membranes, like cholesterol (Chol), or adsorbed to the membrane surface<sup>115</sup>. Recent studies have shown that both hydrophobic and hydrophilic/cytoprotective BAs present a very limited insertion into the membrane, being expected to have an interfacial location upon binding to lipid membranes. Cytotoxic bile acids present a higher partition to membranes that is dependent on membrane order, and it is expected that the plasma membrane of living cells would present a higher affinity for the cytotoxic bile acids DCA or CDCA than for the cytoprotective BAs UDCA or TUDCA<sup>116</sup>.

Cytotoxic bile acids such as DCA or CDCA have the ability to disrupt to some extent the membrane ordering effect induced by Chol<sup>116</sup>. This effect was shown to be more pronounced for lower Chol concentrations, for which the membrane is mainly found in the liquid disordered phase ( $l_o$ ). In fact, this disordering effect of cytotoxic bile acids in the presence of cholesterol is significantly reduced for membranes containing very high Chol content. This is probably related with an absence of efficient membrane binding by BAs to membranes in the liquid ordered phase ( $l_o$ ). In this way, the apoptotic effect of BAs could also be related with changes in membrane structure or modulation of membrane composition, since lipid rafts are crucial for apoptotic signaling and its homeostasis disruption could lead to apoptosis<sup>117,118</sup>.

Co-incubation of liposomes containing cholesterol with cytotoxic and cytoprotective BAs, does not result in an inhibition of the effect of cytotoxic BAs on lipid membrane order, and in fact, a cumulative disordering effect on the membrane order is observed<sup>116</sup>. It was also proved that the cytotoxic BA-dependent disruption of the membrane ordering effect induced by Chol, is not a result of cholesterol removal from the membrane, since its fluorescent analog dehydroergosterol (DHE) is not affected by the presence of physiologically active concentrations of cytotoxic bile acids<sup>116,119</sup>.

For GPMVs (giant plasma membrane vesicles), bile acids were also shown to disrupt to some extent the order of membranes and induce domain immiscibility, possibly due to intercalation into plasma membrane and alteration of plasma membrane proteolipid domains, leading to modulation of protein-protein interactions and consequent signal propagation<sup>120</sup>. However, the impact of apoptotic bile acids on membrane structure was not fully reproducible on plasma membranes, suggesting strong cellular compensatory mechanisms for regulation of membrane order<sup>116</sup>.

Recent work characterized the effect of physiologically active concentrations of cytotoxic and cytoprotective bile acids on the membrane properties of the most likely targets for modulation of cell death by bile acids, the mitochondrial and plasma membranes<sup>119</sup>. It was shown that even very high concentrations of both cytotoxic and cytoprotective bile acids, only increase plasma membrane fluidity of hepatocytes to a minor extent, and that this effect is not correlated with the onset of apoptosis. Additionally, the plasma membrane fluidity recovers to normal (untreated) values during long incubations, confirming the presence of cellular compensatory mechanisms to maintain plasma membrane integrity. The impact of cytotoxic and cytoprotective bile acids on the average intracellular membrane fluidity is comparable, although for longer incubation times, a dramatic decrease in membrane fluidity is only observed for the cytotoxic DCA. The latter effect is preceded by apoptosis and it is likely a consequence of the apoptotic process itself. On the other hand, only cytotoxic bile acids had an impact on isolated mitochondrial outer membrane order, and this effect preceded the onset of mitochondria permeabilization. In addition, DCA mediated changes in mitochondrial membrane organization are not observed in protein-free liposomes mimicking mitochondrial membrane lipid composition. These findings identify mitochondrial membranes as a likely target of the cytotoxic bile acid DCA, and suggest that the mechanism of action of DCA is associated to changes in mitochondrial membrane features which are absent from protein-free mimetic liposomes, such as the double membrane structure, lipid asymmetry or the mitochondrial protein environment<sup>119</sup>.

---

## 4. References

1. Cox, M. M. & Nelson, D. L. *Lehninger Principles of Biochemistry*. (W. H. Freeman and Company, 2008).
2. Cooper, G. M. & Hausman, R. E. *The cell: A Molecular Approach*. (ASM Press, 2007).
3. Dowhan, W. & Bogdanov, M. Chapter 1 Functional roles of lipids in membranes. *New Compr. Biochem.* **36**, 1–35 (2002).
4. Gorter, B. E. & Grendel, F. On bimolecular layers of lipoids on the chromocytes of the blood. *J. Exp. Med.* **41**, 439–43 (1925).
5. Danielli, J. F. & Davson, H. A contribution to the theory of permeability of thin films. *J. Cell. Comp. Physiol.* **5**, 495–508 (1935).
6. Singer, S. J. & Nicolson, G. L. The fluid mosaic model of the structure of cell membranes. *Science* **175**, 720–31 (1972).
7. Mouritsen, O. G. *Life - as a matter of fat: the emerging science of lipidomics*. (Springer, 2005).
8. Edidin, M. Lipids on the frontier: a century of cell-membrane bilayers. *Nat. Rev. Mol. Cell Biol.* **4**, 414–418 (2003).
9. Nicolson, G. L. The Fluid - Mosaic Model of Membrane Structure: Still relevant to understanding the structure, function and dynamics of biological membranes after more than 40 years. *Biochim. Biophys. Acta - Biomembr.* **1838**, 1451–1466 (2014).
10. Simons, K. & Van Meer, G. Lipid sorting in epithelial cells. *Biochemistry* **27**, 6197–6202 (1988).
11. Pike, L. J. Rafts defined: a report on the Keystone symposium on lipid rafts and cell function. *J. Lipid Res.* **47**, 1597–1598 (2006).
12. Lingwood, D. & Simons, K. Lipid Rafts As a Membrane-Organizing Principle. *Science (80- )*. **327**, 46–50 (2010).
13. Kusumi, A. & Suzuki, K. Toward understanding the dynamics of membrane-raft-based molecular interactions. *Biochim. Biophys. Acta - Mol. Cell Res.* **1746**, 234–251 (2005).
14. Sezgin, E., Levental, I., Grzybek, M., Schwarzmann, G., Mueller, V., Honigsmann, A., Belov, V. N., Eggeling, C., Coskun, Ü., Simons, K. & Schwille, P. Partitioning, diffusion, and ligand binding of raft lipid analogs in model and cellular plasma membranes.

- Biochim. Biophys. Acta - Biomembr.* **1818**, 1777–1784 (2012).
15. Simons, K. & Gerl, M. J. Revitalizing membrane rafts: new tools and insights. *Nat. Rev. Mol. Cell Biol.* **11**, 688–699 (2010).
  16. Devaux, P. F. Lipid transmembrane asymmetry and flip-flop in biological membranes and in lipid bilayers: Current Opinion in Structural Biology 1993, 3:489–494. *Curr. Opin. Struct. Biol.* **3**, 489–494 (1993).
  17. Balla, T. Phosphoinositides: Tiny Lipids With Giant Impact on Cell Regulation. *Physiol. Rev.* **93**, 1019–1137 (2013).
  18. Holthuis, J. C. M. & Menon, A. K. Lipid landscapes and pipelines in membrane homeostasis. *Nature* **510**, 48–57 (2014).
  19. Mouritsen, O. G. & Zuckermann, M. J. What's so special about cholesterol? *Lipids* **39**, 1101–13 (2004).
  20. Krauss, S., Israel, B. & Medical, D. Mitochondria : Structure and Role in Respiration. 1–6 (2001).
  21. Daum, G. & Graz, T. U. Lipids of mitochondria. *Biochim. Biophys. Acta* **822**, 1–42 (1985).
  22. Leventis, P. a. & Grinstein, S. The Distribution and Function of Phosphatidylserine in Cellular Membranes. *Annu. Rev. Biophys.* **39**, 407–427 (2010).
  23. Schug, Z. T. & Gottlieb, E. Cardiolipin acts as a mitochondrial signalling platform to launch apoptosis. *Biochim. Biophys. Acta* **1788**, 2022–31 (2009).
  24. Cosentino, K. & García-Sáez, A. J. Mitochondrial alterations in apoptosis. *Chem. Phys. Lipids* **181**, 62–75 (2014).
  25. Kerr, J. F., Wyllie, A. H. & Currie, A. R. Apoptosis: a basic biological phenomenon with wide-ranging implications in tissue kinetics. *Br. J. Cancer* **26**, 239–57 (1972).
  26. Elmore, S. Apoptosis: A Review of Programmed Cell Death. *Toxicol Pathol.* **35**, 495–516 (2007).
  27. Syntichaki, P. & Tavernarakis, N. Death by necrosis. Uncontrollable catastrophe, or is there order behind the chaos? *EMBO Rep.* **3**, 604–9 (2002).
  28. Kumar, V., Abbas, A. K., Aster, J. C. & Perkins, J. A. *Robbins and Cotran pathologic basis of disease.*

29. Palmeira, C. M. & Rolo, A. P. Mitochondrially-mediated toxicity of bile acids. *Toxicology* **203**, 1–15 (2004).
30. Amaral, J. D., Viana, R. J. S., Ramalho, R. M., Steer, C. J. & Rodrigues, C. M. P. Bile acids: regulation of apoptosis by ursodeoxycholic acid. *J. Lipid Res.* **50**, 1721–34 (2009).
31. Sodeman, T., Bronk, S. F., Roberts, P. J., Miyoshi, H., Gregory, J., Gores, G. J. & Rob, P. J. Bile salts mediate hepatocyte apoptosis by increasing cell surface trafficking of Fas. *Physiol, Am J Liver, Gastrointest Liver* (2012).
32. Castro, R. E. & Solá, S., Steer, C. J. and R. C. M. P. in *Hepatotoxicity: From Genomics to in vitro and in vivo Models* (ed. John Wiley & Sons, L.) (2007).
33. Ashkenazi, A. & Dixit, V. M. Death receptors: signaling and modulation. *Science* **281**, 1305–8 (1998).
34. Hsu, H., Xiong, J. & Goeddel, D. V. The TNF receptor 1-associated protein TRADD signals cell death and NF-kappa B activation. *Cell* **81**, 495–504 (1995).
35. Wajant, H. The Fas Signaling Pathway: More Than a Paradigm. *Science (80-. )*. **296**, 1635–1636 (2002).
36. Chang, D. W., Xing, Z., Capacio, V. L., Peter, M. E. & Yang, X. Interdimer processing mechanism of procaspase-8 activation. *EMBO J.* **22**, 4132–42 (2003).
37. Lalier, L., Cartron, P.-F., Juin, P., Nedelkina, S., Manon, S., Bechinger, B. & Vallette, F. M. Bax activation and mitochondrial insertion during apoptosis. *Apoptosis* **12**, 887–96 (2007).
38. Dewson, G. & Kluck, R. M. Mechanisms by which Bak and Bax permeabilise mitochondria during apoptosis. *J. Cell Sci.* **122**, 2801–2808 (2009).
39. Bleicken, S., Classen, M., Padmavathi, P. V. L., Ishikawa, T., Zeth, K., Steinhoff, H.-J. & Bordignon, E. Molecular details of Bax activation, oligomerization, and membrane insertion. *J. Biol. Chem.* **285**, 6636–47 (2010).
40. Bleicken, S. & Zeth, K. Conformational changes and protein stability of the pro-apoptotic protein Bax. *J. Bioenerg. Biomembr.* **41**, 29–40 (2009).
41. García-Sáez, A. J. The secrets of the Bcl-2 family. *Cell Death Differ.* **19**, 1733–1740 (2012).
42. Adams, J. M. & Cory, S. The Bcl-2 apoptotic switch in cancer development and therapy.

- Oncogene* **26**, 1324–37 (2007).
43. Letai, A., Bassik, M. C., Walensky, L. D., Sorcinelli, M. D., Weiler, S. & Korsmeyer, S. J. Distinct BH3 domains either sensitize or activate mitochondrial apoptosis, serving as prototype cancer therapeutics. *Cancer Cell* **2**, 183–192 (2002).
  44. Kim, H., Rafiuddin-Shah, M., Tu, H.-C., Jeffers, J. R., Zambetti, G. P., Hsieh, J. J.-D. & Cheng, E. H.-Y. Hierarchical regulation of mitochondrion-dependent apoptosis by BCL-2 subfamilies. *Nat. Cell Biol.* **8**, 1348–58 (2006).
  45. Peng, R., Tong, J.-S., Li, H., Yue, B., Zou, F., Yu, J. & Zhang, L. Targeting Bax interaction sites reveals that only homo-oligomerization sites are essential for its activation. *Cell Death Differ.* **20**, 744–54 (2013).
  46. Shamas-Din, A., Kale, J., Leber, B. & Andrews, D. W. Mechanisms of action of Bcl-2 family proteins. *Cold Spring Harb. Perspect. Biol.* **5**, 1–21 (2013).
  47. Kim, H., Tu, H.-C., Ren, D., Takeuchi, O., Jeffers, J. R., Zambetti, G. P., Hsieh, J. J.-D. & Cheng, E. H.-Y. Stepwise activation of BAX and BAK by tBID, BIM, and PUMA initiates mitochondrial apoptosis. *Mol. Cell* **36**, 487–99 (2009).
  48. Dai, H., Smith, A., Meng, X. W., Schneider, P. A., Pang, Y.-P. & Kaufmann, S. H. Transient binding of an activator BH3 domain to the Bak BH3-binding groove initiates Bak oligomerization. *J. Cell Biol.* **194**, 39–48 (2011).
  49. Llambi, F., Moldoveanu, T., Tait, S. W. G., Bouchier-Hayes, L., Temirov, J., McCormick, L. L., Dillon, C. P. & Green, D. R. A unified model of mammalian BCL-2 protein family interactions at the mitochondria. *Mol. Cell* **44**, 517–31 (2011).
  50. Czabotar, P. E., Westphal, D., Dewson, G., Ma, S., Hockings, C., Fairlie, W. D., Lee, E. F., Yao, S., Robin, A. Y., Smith, B. J., Huang, D. C. S., Kluck, R. M., Adams, J. M. & Colman, P. M. Bax Crystal Structures Reveal How BH3 Domains Activate Bax and Nucleate Its Oligomerization to Induce Apoptosis. *Cell* **152**, 519–531 (2013).
  51. Lomonosova, E. & Chinnadurai, G. *BH3-only proteins in apoptosis and beyond: an overview.* *Oncogene* **27 (Suppl)**, (2008).
  52. Leber, B., Lin, J. & Andrews, D. W. Still Embedded Together Binding to Membranes Regulates Bcl-2 Protein Interactions. *Oncogene* **29**, 5221–5230 (2010).
  53. García-Sáez, A. J., Ries, J., Orzáez, M., Pérez-Payà, E. & Schwille, P. Membrane promotes tBID interaction with BCL(XL). *Nat. Struct. Mol. Biol.* **16**, 1178–85 (2009).

- 
54. Leber, B., Lin, J. & Andrews, D. W. Embedded Together: The Life and Death Consequences of Interaction of the Bcl-2 Family with Membranes. **12**, 897–911 (2007).
  55. Bogner, C., Leber, B. & Andrews, D. W. Apoptosis: Embedded in membranes. *Curr. Opin. Cell Biol.* **22**, 845–851 (2010).
  56. Czabotar, P. E., Lessene, G., Strasser, A. & Adams, J. M. Control of apoptosis by the BCL-2 protein family: implications for physiology and therapy. *Nat. Rev. Mol. Cell Biol.* **15**, 49–63 (2014).
  57. Edlich, F., Banerjee, S., Suzuki, M., Cleland, M. M., Arnoult, D., Wang, C., Neutzner, A., Tjandra, N. & Youle, R. J. Bcl-x(L) retrotranslocates Bax from the mitochondria into the cytosol. *Cell* **145**, 104–116 (2011).
  58. Schellenberg, B., Wang, P., Keeble, J. A., Rodriguez-Enriquez, R., Walker, S., Owens, T. W., Foster, F., Tanianis-Hughes, J., Brennan, K., Streuli, C. H. & Gilmore, A. P. Bax exists in a dynamic equilibrium between the cytosol and mitochondria to control apoptotic priming. *Mol. Cell* **49**, 959–71 (2013).
  59. Luo, L., Yang, J. & Liu, D. Integration and Oligomerization of Bax Protein in Lipid Bilayers Characterized by Single Molecule Fluorescence Study. *J. Biol. Chem.* **289**, 31708–31718 (2014).
  60. Suzuki, M., Youle, R. J. & Tjandra, N. Structure of Bax: coregulation of dimer formation and intracellular localization. *Cell* **103**, 645–54 (2000).
  61. Annis, M. G., Soucie, E. L., Dlugosz, P. J., Cruz-Aguado, J. a, Penn, L. Z., Leber, B. & Andrews, D. W. Bax forms multispinning monomers that oligomerize to permeabilize membranes during apoptosis. *EMBO J.* **24**, 2096–103 (2005).
  62. Westphal, D., Kluck, R. M. & Dewson, G. Building blocks of the apoptotic pore: how Bax and Bak are activated and oligomerize during apoptosis. *Cell Death Differ.* **21**, 196–205 (2014).
  63. Czabotar, P. E., Lee, E. F., Thompson, G. V, Wardak, A. Z., Fairlie, W. D. & Colman, P. M. Mutation to Bax beyond the BH3 domain disrupts interactions with pro-survival proteins and promotes apoptosis. *J. Biol. Chem.* **286**, 7123–31 (2011).
  64. Wang, C. & Youle, R. J. Predominant requirement of Bax for apoptosis in HCT116 cells is determined by Mcl-1's inhibitory effect on Bak. *Oncogene* **31**, 3177–89 (2012).
  65. Gahl, R. F., He, Y., Yu, S. & Tjandra, N. Conformational Rearrangements in the Pro-apoptotic Protein, Bax, as It Inserts into Mitochondria: A CELLULAR DEATH SWITCH.

- J. Biol. Chem.* **289**, 32871–32882 (2014).
66. Barrasa, J. I., Santiago-Gómez, A., Olmo, N., Lizarbe, M. A. & Turnay, J. Resistance to butyrate impairs bile acid-induced apoptosis in human colon adenocarcinoma cells via up-regulation of Bcl-2 and inactivation of Bax. *Biochim. Biophys. Acta - Mol. Cell Res.* **1823**, 2201-09 (2012).
67. Vaillant, F., Merino, D., Lee, L., Breslin, K., Pal, B., Ritchie, M. E., Smyth, G. K., Christie, M., Phillipson, L. J., Burns, C. J., Mann, G. B., Visvader, J. E. & Lindeman, G. J. Targeting BCL-2 with the BH3 Mimetic ABT-199 in Estrogen Receptor-Positive Breast Cancer. *Cancer Cell* **24**, 120–9 (2013).
68. Adams, J. M. & Cory, S. The Bcl-2 apoptotic switch in cancer development and therapy. *Oncogene* **26**, 1324–1337 (2010).
69. Lovell, J. F., Billen, L. P., Bindner, S., Shamas-din, A., Fradin, C. & Leber, B. Supplemental Data Membrane Binding by tBid Initiates an Ordered Series of Events Culminating in Membrane Permeabilization by Bax. **135**, 1–12
70. Gonzalez, F., Pariselli, F., Dupaigne, P., Budihardjo, I., Lutter, M., Antonsson, B., Diolez, P., Manon, S., Martinou, J.-C., Gubern, M., Wang, X., Bernard, S. & Petit, P. X. tBid interaction with cardiolipin primarily orchestrates mitochondrial dysfunctions and subsequently activates Bax and Bak. *Cell Death Differ.* **12**, 614–26 (2005).
71. Kuwana, T., Mackey, M. R., Perkins, G., Ellisman, M. H., Latterich, M., Schneider, R., Green, D. R. & Newmeyer, D. D. Bid, Bax, and lipids cooperate to form supramolecular openings in the outer mitochondrial membrane. *Cell* **111**, 331–42 (2002).
72. Pang, Y.-P., Dai, H., Smith, A., Meng, X. W., Schneider, P. a. & Kaufmann, S. H. Bak Conformational Changes Induced by Ligand Binding: Insight into BH3 Domain Binding and Bak Homo-Oligomerization. *Sci. Rep.* **2**, (2012).
73. Westphal, D., Dewson, G., Czabotar, P. E. & Kluck, R. M. Molecular biology of Bax and Bak activation and action. *Biochim. Biophys. Acta* **1813**, 521–31 (2011).
74. Czabotar, P. E., Westphal, D., Dewson, G., Ma, S., Hockings, C., Fairlie, W. D., Lee, E. F., Yao, S., Robin, A. Y., Smith, B. J., Huang, D. C. S., Kluck, R. M., Adams, J. M. & Colman, P. M. Bax Crystal Structures Reveal How BH3 Domains Activate Bax and Nucleate Its Oligomerization to Induce Apoptosis. *Cell* **152**, 519–531 (2013).
75. Subburaj, Y., Cosentino, K., Axmann, M., Pedrueza-Villalmanzo, E., Hermann, E., Bleicken, S., Spatz, J. & García-Sáez, A. J. Bax monomers form dimer units in the

- membrane that further self-assemble into multiple oligomeric species. *Nat. Commun.* **6**, 8042 (2015).
76. Bleicken, S., Landeta, O., Landajuela, A., Basañez, G. & García-Sáez, A. J. Proapoptotic Bax and Bak proteins form stable protein-permeable pores of tunable size. *J. Biol. Chem.* **288**, 33241–52 (2013).
  77. Sung, T.-C., Li, C.-Y., Lai, Y.-C., Hung, C.-L., Shih, O., Yeh, Y.-Q., Jeng, U.-S. & Chiang, Y.-W. Solution Structure of Apoptotic BAX Oligomer: Oligomerization Likely Precedes Membrane Insertion. *Structure* **23**, 1878–88 (2015).
  78. Garner, T. P., Reyna, D. E., Priyadarshi, A., Chen, H.-C., Li, S., Wu, Y., Ganesan, Y. T., Malashkevich, V. N., Cheng, E. H. & Gavathiotis, E. An Autoinhibited Dimeric Form of BAX Regulates the BAX Activation Pathway. *Mol. Cell* **63**, 485–497 (2016).
  79. Lucken-Ardjomande, S., Montessuit, S. & Martinou, J.-C. Contributions to Bax insertion and oligomerization of lipids of the mitochondrial outer membrane. *Cell Death Differ.* **15**, 929–37 (2008).
  80. Martínez-Abundis, E., García, N., Correa, F., Franco, M. & Zazueta, C. Changes in specific lipids regulate BAX-induced mitochondrial permeability transition. *FEBS J.* **274**, 6500–10 (2007).
  81. Martínez-Abundis, E., Correa, F., Pavón, N. & Zazueta, C. Bax distribution into mitochondrial detergent-resistant microdomains is related to ceramide and cholesterol content in postischemic hearts. *FEBS J.* **276**, 5579–88 (2009).
  82. Ganesan, V., Perera, M. N., Colombini, D., Datskovskiy, D., Chadha, K. & Colombini, M. Ceramide and activated Bax act synergistically to permeabilize the mitochondrial outer membrane. *Apoptosis* **15**, 553–62 (2010).
  83. Montero, J., Mari, M., Colell, A., Morales, A., Basañez, G., Garcia-Ruiz, C. & Fernández-Checa, J. C. Cholesterol and peroxidized cardiolipin in mitochondrial membrane properties, permeabilization and cell death. *Biochim. Biophys. Acta* **1797**, 1217–1224 (2010).
  84. Mignard, V., Lalier, L., Paris, F. & Vallette, F. M. Bioactive lipids and the control of Bax pro-apoptotic activity. *Cell Death Dis.* **5**, e1266 (2014).
  85. Christenson, E., Merlin, S., Saito, M. & Schlesinger, P. Cholesterol effects on BAX pore activation. *J. Mol. Biol.* **381**, 1168–83 (2008).
  86. Lucken-Ardjomande, S., Montessuit, S. & Martinou, J.-C. Bax activation and stress-

- induced apoptosis delayed by the accumulation of cholesterol in mitochondrial membranes. *Cell Death Differ.* **15**, 484–93 (2008).
87. Zhou, Y., Doyen, R. & Lichtenberger, L. M. The role of membrane cholesterol in determining bile acid cytotoxicity and cytoprotection of ursodeoxycholic acid. *Biochim. Biophys. Acta* **1788**, 507–13 (2009).
88. Chiang, J. Y. L. Bile acids: regulation of synthesis. *J. Lipid Res.* **50**, 1955–66 (2009).
89. Monte, M.-J. Bile acids: Chemistry, physiology, and pathophysiology. *World J. Gastroenterol.* **15**, 804 (2009).
90. Hofmann, A. F. The continuing importance of bile acids in liver and intestinal disease. *Arch. Intern. Med.* **159**, 2647–58 (1999).
91. Trauner, M. & Graziadei, I. W. Review article: mechanisms of action and therapeutic applications of ursodeoxycholic acid in chronic liver diseases. *Aliment. Pharmacol. Ther.* **13**, 979–96 (1999).
92. Clarissa Williams. Food Nutrition And Dietetics. *StudyBlue* (2012). at <<http://www.studyblue.com/notes/note/n/liver-and-accessory-organs/deck/4044148>>
93. Perez, M. J. Bile-acid-induced cell injury and protection. *World J. Gastroenterol.* **15**, 1677 (2009).
94. Powell, A. a, Rue, J. M. L. a, Batta, a K. & Martinez, J. D. Bile acid hydrophobicity is correlated with induction of apoptosis and/or growth arrest in HCT116 cells. **486**, 481–486 (2001).
95. Heuman, D. M. Quantitative estimation of the hydrophilic-hydrophobic balance of mixed bile salt solutions. *J. Lipid Res.* **30**, 719–30 (1989).
96. Castro, R. E., Amaral, J. D., Solá, S., Kren, B. T., Steer, C. J. & Rodrigues, C. M. P. Differential regulation of cyclin D1 and cell death by bile acids in primary rat hepatocytes. *Am. J. Physiol. Gastrointest. Liver Physiol.* **293**, G327-34 (2007).
97. Amaral, J. D., Castro, R. E., Solá, S., Steer, C. J. & Rodrigues, C. M. P. Ursodeoxycholic acid modulates the ubiquitin-proteasome degradation pathway of p53. *Biochem. Biophys. Res. Commun.* **400**, 649–54 (2010).
98. Ferreira, D. M. S., Afonso, M. B., Rodrigues, P. M., Simão, A. L., Pereira, D. M., Borralho, P. M., Rodrigues, C. M. P. & Castro, R. E. c-Jun N-Terminal Kinase 1/c-Jun Activation of the p53/MicroRNA 34a/Sirtuin 1 Pathway Contributes to Apoptosis Induced by Deoxycholic Acid in Rat Liver. *Mol. Cell. Biol.* **34**, 1100–20 (2014).

99. Rodrigues, C. M., Fan, G., Wong, P. Y., Kren, B. T. & Steer, C. J. Ursodeoxycholic acid may inhibit deoxycholic acid-induced apoptosis by modulating mitochondrial transmembrane potential and reactive oxygen species production. *Mol. Med.* **4**, 165–78 (1998).
100. Pusl, T., Wild, N., Vennegeerts, T., Wimmer, R., Göke, B., Brand, S. & Rust, C. Free fatty acids sensitize hepatocytes to bile acid-induced apoptosis. *Biochem. Biophys. Res. Commun.* **371**, 441–5 (2008).
101. Tsuchiya, S., Tsuji, M., Morio, Y. & Oguchi, K. Involvement of endoplasmic reticulum in glycochenodeoxycholic acid-induced apoptosis in rat hepatocytes. *Toxicol. Lett.* **166**, 140–9 (2006).
102. Paumgartner, G. & Beuers, U. Ursodeoxycholic acid in cholestatic liver disease: mechanisms of action and therapeutic use revisited. *Hepatology* **36**, 525–31 (2002).
103. Rodrigues, C. M., Fan, G., Ma, X., Kren, B. T. & Steer, C. J. A novel role for ursodeoxycholic acid in inhibiting apoptosis by modulating mitochondrial membrane perturbation. *J. Clin. Invest.* **101**, 2790–9 (1998).
104. Pusl, T. & Beuers, U. Ursodeoxycholic acid treatment of vanishing bile duct syndromes. *World J. Gastroenterol.* **12**, 3487–95 (2006).
105. Rodrigues, C. M., Ma, X., Linehan-Stieers, C., Fan, G., Kren, B. T. & Steer, C. J. Ursodeoxycholic acid prevents cytochrome c release in apoptosis by inhibiting mitochondrial membrane depolarization and channel formation. *Cell Death Differ.* **6**, 842–54 (1999).
106. Sharma, R., Prichard, D., Majer, F., Byrne, A.-M., Kelleher, D., Long, A. & Gilmer, J. F. Ursodeoxycholic Acid Amides As Novel Glucocorticoid Receptor Modulators. *J. Med. Chem.* 122–130 (2010). doi:10.1021/jm100860s
107. Solá, S., Amaral, J. D., Castro, R. E., Ramalho, R. M., Borralho, P. M., Kren, B. T., Tanaka, H., Steer, C. J. & Rodrigues, C. M. P. Nuclear translocation of UDCA by the glucocorticoid receptor is required to reduce TGF-beta1-induced apoptosis in rat hepatocytes. *Hepatology* **42**, 925–34 (2005).
108. Castro, R. E., Solá, S., Ma, X., Ramalho, R. M., Kren, B. T., Steer, C. J. & Rodrigues, C. M. P. A distinct microarray gene expression profile in primary rat hepatocytes incubated with ursodeoxycholic acid. *J. Hepatol.* **42**, 897–906 (2005).
109. Qiao, L., Yacoub, A., Studer, E., Gupta, S., Pei, X. Y., Grant, S., Hylemon, P. B. & Dent,

- P. Inhibition of the MAPK and PI3K pathways enhances UDCA-induced apoptosis in primary rodent hepatocytes. *Hepatology* **35**, 779–89 (2002).
110. Rodrigues, C. M. P., Solá, S., Sharpe, J. C., Moura, J. J. G. & Steer, C. J. Tauroursodeoxycholic acid prevents Bax-induced membrane perturbation and cytochrome C release in isolated mitochondria. *Biochemistry* **42**, 3070–80 (2003).
111. Xie, Q., Khaoustov, V. I., Chung, C. C., Sohn, J., Krishnan, B., Lewis, D. E. & Yoffe, B. Effect of tauroursodeoxycholic acid on endoplasmic reticulum stress-induced caspase-12 activation. *Hepatology* **36**, 592–601 (2002).
112. Schoemaker, M. H., Conde de la Rosa, L., Buist-Homan, M., Vrenken, T. E., Havinga, R., Poelstra, K., Haisma, H. J., Jansen, P. L. M. & Moshage, H. Tauroursodeoxycholic acid protects rat hepatocytes from bile acid-induced apoptosis via activation of survival pathways. *Hepatology* **39**, 1563–73 (2004).
113. Halin, J. & Mattjus, P. Effects of bile salts on glucosylceramide containing membranes. *Biochim. Biophys. Acta* **1808**, 2886–93 (2011).
114. Ben Mouaz A, Lindheimer, M., Montet, J., Zajac, J. & Lagerge, S. A study of the adsorption of bile salts onto model lecithin membranes. *Colloids Surf. B. Biointerfaces* **20**, 119–127 (2001).
115. Ollila, F. & Slotte, J. P. A Thermodynamic Study of Bile Salt Interactions with Phosphatidylcholine and Sphingomyelin Unilamellar Vesicles. *Sci. York* 2835–2840 (2001).
116. Mello-Vieira, J., Sousa, T., Coutinho, A., Fedorov, A., Lucas, S. D., Moreira, R., Castro, R. E., Rodrigues, C. M. P., Prieto, M. & Fernandes, F. Cytotoxic bile acids, but not cytoprotective species, inhibit the ordering effect of cholesterol in model membranes at physiologically active concentrations. *Biochim. Biophys. Acta* **1828**, 2152–2163 (2013).
117. Mollinedo, F. & Gajate, C. Fas/CD95 death receptor and lipid rafts: new targets for apoptosis-directed cancer therapy. *Drug Resist. Updat.* **9**, 51–73 (2006).
118. Gniadecki, R. Depletion of membrane cholesterol causes ligand-independent activation of Fas and apoptosis. *Biochem. Biophys. Res. Commun.* **320**, 165–9 (2004).
119. Sousa, T., Castro, R. E., Pinto, S. N., Coutinho, A., Lucas, S. D., Moreira, R., Rodrigues, C. M. P., Prieto, M. & Fernandes, F. Deoxycholic acid modulates cell death signaling through changes in mitochondrial membrane properties. *J. Lipid Res.* (2015). doi:10.1194/jlr.M062653

120. Zhou, Y., Maxwell, K. N., Sezgin, E., Lu, M., Liang, H., Hancock, J. F., Dial, E. J., Lichtenberger, L. M. & Levental, I. Bile acids modulate signaling by functional perturbation of plasma membrane domains. *J. Biol. Chem.* **288**, 35660–70 (2013).



## Chapter II

---

Measuring membrane order in primary hepatocytes and isolated mitochondria by fluorescence imaging and spectroscopy



## **MEASURING MEMBRANE ORDER IN PRIMARY HEPATOCYTES AND ISOLATED MITOCHONDRIA BY FLUORESCENCE IMAGING AND SPECTROSCOPY**

Tânia Sousa<sup>1,2</sup>, Rui E. Castro<sup>3</sup>, Ana Coutinho<sup>1,2,4</sup>, Cecília M.P. Rodrigues<sup>3</sup>, Manuel Prieto<sup>1,2</sup>, Fábio Fernandes<sup>1,2\*</sup>

<sup>1</sup>Centro de Química-Física Molecular and Institute of Nanoscience and Nanotechnology, Instituto Superior Técnico, University of Lisbon, Lisbon, Portugal

<sup>2</sup>iBB-Institute for Bioengineering and Biosciences, Biological Sciences Research Group, Av. Rovisco Pais 1, 1049-001 Lisbon, Portugal

<sup>3</sup>Research Institute for Medicines (iMed.Ulisboa), Faculty of Pharmacy, University of Lisbon, Lisbon, Portugal

<sup>4</sup>Departamento de Química e Bioquímica, Faculty of Sciences, University of Lisbon, Lisbon, Portugal



## **Abstract**

Cholestasis is characterized by impaired secretion of bile flow, that can result in the accumulation of highly abnormal levels of bile acids causing hepatocyte and biliary injury. As amphipathic molecules, bile acids can intercalate in lipid membranes, and pathophysiologic concentrations of bile acids have the potential to induce marked changes in the biophysical properties of biomembranes, including membrane ordering. These effects, particularly on the mitochondrial and plasma membranes, have been proposed to trigger toxicity of bile acids. The present chapter details different fluorescence-based methods (fluorescence polarization, and spectroscopy/imaging of solvatochromic dyes) to evaluate the impact of different bile acids on membrane order. Protocols are described for the application of these methods to biomimetic vesicles, isolated mitochondria and hepatocytes, following a bottom-up approach.



## 1. Introduction

Cholestasis is characterized by the decrease in bile flow due to impaired secretion by hepatocytes or by obstruction of bile ducts<sup>1</sup>. This impairment results in the accumulation of bile acids (BAs) in the liver to abnormally high levels intracellularly and extracellularly, causing hepatocyte and biliary injury and inflammation<sup>2</sup>. Submicellar concentrations of more hydrophobic BAs can induce hepatocellular apoptosis or necrosis, depending on BA levels<sup>3</sup>. Surprisingly, apoptosis induction is dependent on the bile acid, its concentration, and its conjugation state, instead of being solely correlated with hydrophobicity<sup>4</sup>. Nevertheless, more hydrophilic bile acids such as ursodeoxycholic acid (UDCA) and tauroursodeoxycholic acid (TUDCA) have been shown to have cytoprotective properties, inhibiting apoptosis in both hepatic and nonhepatic cells<sup>5,6</sup>.

The mechanism by which submicellar concentrations of cytotoxic bile acids induce apoptosis in hepatocytes is not entirely clear<sup>6-8</sup>. However, it has been suggested that hydrophobic bile acids such as LCA (lithocholic acid), DCA (deoxycholic acid) or GCDCA (glycochenodeoxycholic acid) induce apoptosis by directly activating death receptors, like Fas, in a ligand independent oligomerization of Fas<sup>9</sup>. On the other hand, cell death induced by hydrophobic bile acids is associated with mitochondrial perturbation with decreased  $\Delta\psi_m$  (mitochondrial membrane potential) and enhanced ROS (reactive oxygen species) generation<sup>10</sup>. DCA-dependent Bax translocation to the mitochondrial membrane has also been shown to occur<sup>11</sup>.

BAs are amphipathic molecules known to intercalate in lipid membranes. At their pathophysiological concentrations ( $>50 \mu\text{M}$ )<sup>12,13</sup> BAs induce changes in the biophysical properties of biomembranes. In this regard, it was shown that while apoptotic bile acids, such as deoxycholic acid (DCA) and chenodeoxycholic acid (CDCA), promote disordering of the lipid membrane on both large unilamellar vesicles<sup>12</sup> (LUVs) and giant plasma membrane vesicles<sup>14</sup> (GPMVs), cytoprotective bile acids failed to induce significant changes in membrane structure<sup>12</sup>. These differences are very likely the result of dramatically different partition behavior of these bile acids, as the more hydrophobic DCA and CDCA exhibit considerably larger preference for incorporation in lipid bilayers<sup>12</sup>. Experiments with active isolated mitochondria also revealed that physiologically active concentrations of DCA change mitochondria outer membrane (MOM) order in a concentration- and time-dependent manner, and that these changes preceded the MPT (mitochondrial membrane permeability transition)

<sup>15</sup>.

Several biological functions, including cell death, are intrinsically dependent on the physicochemical properties of lipid membranes<sup>15–18</sup>. In this way, the ability of hydrophobic bile acids to modulate membrane ordering is likely to play a key role in the toxicity of these molecules under cholestatic conditions. The current chapter describes different fluorescence-based methods (fluorescence polarization, and spectroscopy/imaging of solvatochromic dyes) to determine the impact of bile acids on membrane order.

Fluorescence-based methods offer several advantages over other biophysical techniques sensitive to membrane order, particularly concerning its sensitivity and applicability to live cells and tissue.

The techniques presented here rely on the use of different fluorescent membrane probes, sensitive to either membrane microviscosity and polarity, both of which are affected upon changes in membrane order. Membrane microviscosity is typically evaluated through fluorescence depolarization measurements using long and rigid hydrophobic fluorophores (such as diphenylhexatriene – DPH<sup>19</sup>), that intercalate between acyl-chains. The fluorescence depolarization of these molecules is directly dependent on their tumbling within the membrane environment and can be quantified through fluorescence anisotropy measurements (Fig. 1A), which are ideal to monitor changes in the membrane order of biomimetic vesicles or isolated mitochondria.

Polarity sensitive fluorescent probes such as di-4-ANEPPDHQ and Laurdan<sup>20</sup> are also able to sense changes in lipid packing. In Laurdan's case, its fluorescence emission spectra exhibit extensive shifts due to dipolar relaxation processes, which are known to be dependent on membrane ordering<sup>21</sup>. These shifts can be quantified in a convenient manner in cell imaging applications through a ratiometric measurement of the fluorescence intensity recorded in two spectral channels, known as a generalized polarization (GP) value<sup>20,22</sup> (Fig. 1B). Di-4-ANEPPDHQ is also sensitive to lipid packing and can be used in an identical way to detect changes in membrane order, although the photophysical properties responsible for this sensitivity are significantly more complex<sup>21</sup>.



and temperature. Disordered membranes typically display Laurdan GP values (obtained through microscopy) below 0.3, while ordered membranes present GP values between 0.3-0.6<sup>23</sup>.

Due to the intrinsic complexity of biological membranes, they are often studied at a basic level through the use of model lipid vesicles, which through the judicious choice of lipid composition, can be used as biomimetic membranes. In these systems, variables such as chemical composition and structure can be controlled with great precision, allowing for access to information regarding the relevance of particular membrane components on biomembrane properties<sup>24</sup>, protein-lipid interactions<sup>25</sup>, membrane topology<sup>26</sup> or membrane/water partition coefficients of relevant molecules<sup>27</sup>. While the use of biomimetic vesicles has greatly contributed to our current understanding of membrane-dependent physiological mechanisms, these systems are still limited to a small number of membrane components, far from reflecting the massive complexity of cellular membranes. Additionally, model membranes lack bilayer asymmetry and protein components. This is an even larger problem in the case of mitochondrial membranes, given the high level of protein content found there. For these reasons, the methods presented here are applied to different membranes following a bottom-up rationale of increasing complexity. In this way, methods are included for measurement of the impact of bile acids on the membrane order of biomimetic vesicles<sup>12</sup>, isolated mitochondria and primary hepatocytes<sup>15</sup>.

## 2. Materials

1. Bile acid solutions (DCA, CDCA, UDCA and TUDCA) were prepared in the appropriate buffer for each experiment. These were kept at 4°C until shortly before use (see **Note 1**).
2. Buffers (see **Note 2**):

Buffer I: 10 mM HEPES, 150 mM NaCl, pH 7.4

Buffer II: 10mM HEPES, 10 mM succinate, 215 mM mannitol, 71 mM sucrose, pH 7.4

## 2.1 Impact of physiologically active concentrations of bile acids on biomimetic vesicles

Membrane model systems such as large unilamellar vesicles (LUVs) can be prepared with different lipid mixtures, according to the desired type of membrane under study.

1. For the examples described below, the lipids 1-palmitoyl-2-oleoyl-sn-glicero-3-phosphocholine (POPC) and Cholesterol (Chol) were used. Prepare stock solutions in Uvasol grade chloroform and store at -20°C (see **Note 3** and **Note 4**).
2. 1,6-Diphenyl-1,3,5-hexatriene (DPH) dissolved in Uvasol grade DMSO (see **Note 5**).
3. Buffer I.
4. DCA and CDCA stock solutions prepared in buffer I.
5. Polycarbonate membranes of 100 nm pore diameter.
6. Lipid extruder (see **Note 6**).
7. 0.5 cm x 0.5 cm path length quartz cuvettes.
8. Magnetic stirring bars Micro 2 mm x 2 mm.
9. Time-Related Single-Photon Timing setup (TCSPT) with polarizers.

## 2.2 Impact of physiologically active concentrations of bile acids on rat isolated mitochondria

1. Fresh rat liver mitochondria isolated by density gradient centrifugation<sup>28,29</sup>.
2. 1-[2-Hydroxy-3-(*N,N*-di-methyl-*N*-hydroxyethyl)ammoniopropyl]-4-[ $\beta$ -[2-(*di-n*-butylamino)-6-naphthyl] vinyl]pyridinium dibromide (Di-4-ANEPPDHQ) dissolved in Uvasol grade DMSO (see **Note 5**).

3. Buffer II.
4. DCA and TUDCA prepared in buffer II.
5. Centrifuge with temperature control.
6. 0.5 cm x 0.5 cm path length quartz cuvettes.
7. Magnetic stirring bars Micro 2 mm x 2 mm.
8. Spectrofluorimeter with polarizers.

### **2.3 Impact of physiologically active concentrations of bile acids on rat primary hepatocytes**

1. Rat primary hepatocytes seeded into 8-well chamber slides.
2. 6-dodecanoyl- 2–dimethylaminonaphthalene (Laurdan) dissolved in Uvasol grade DMSO (see **Note 5**).
3. Medium I: Complete William's E medium.
4. DCA, UDCA and TUDCA solutions prepared in medium I.
5. CO<sub>2</sub> Incubator (37°C, 5% CO<sub>2</sub>).
6. Laminar air flow cabinet.
7. Two-photon excitation fluorescence microscope or a widefield/confocal microscope with UV- excitation (see **Note 7**).

### 3. Methods

#### 3.1 Impact of physiologically active concentrations of bile acids on biomembranes mimetic systems

##### 3.1.1 Liposome preparation

1. Prepare the desired lipid mixture to a final lipid concentration of 5 mM by mixing the adequate volumes of each stock solution of lipid and DPH to a lipid/probe ratio of 1/200.
2. Dry the solvent out, gently, under a N<sub>2</sub> flux and leave the samples overnight in vacuum, using an oil pump, to remove any residual chloroform (see **Note 8**).
3. Hydrate the mixtures with buffer I for 30 minutes and resuspend the lipid films by vortexing until everything is removed from the recipient wall (see **Note 9**).
4. Perform six freeze-thaw cycles using liquid nitrogen and a water bath at 50°C (see **Note 9**), to re-equilibrate and homogenize the samples.
5. Extrude the lipid suspension at least 21 times using 100 nm pore size polycarbonate membranes (see **Note 10**).
6. The resulting stock solution is stored at 4°C, in the dark, until being used, at most for 48h after being prepared.
7. Incubate LUVs to a final lipid concentration of 200 μM with apoptotic bile acids (DCA and CDCA) at 500 μM overnight

### 3.1.2 Transient-state fluorescence anisotropy measurements.

The fluorescence anisotropy,  $r$ , is related to the intensities ( $I$ ) of the horizontal (H) and vertical (V) planes of polarization, defined as (Eq.1,<sup>30</sup>):

$$\langle r \rangle = \frac{I_{VV} - G \cdot I_{VH}}{I_{VV} + 2 G \cdot I_{VH}}; \quad G = \frac{I_{HV}}{I_{HH}} \quad (1), (2)$$

where  $I_V$  represents the steady-state vertical (parallel,  $I_{VV}$ ) and horizontal (perpendicular,  $I_{VH}$ ) components of the fluorescence emission with excitation polarized vertically.  $G$  is a correction factor for different sensitivity of the optics in the spectrofluorimeter to polarized light.  $G$  can be obtained by the ratio of vertical ( $I_{HV}$ ) and horizontal ( $I_{HH}$ ) components of the emission with the excitation polarized horizontally<sup>30</sup>.

Anisotropy values can either be calculated in the steady-state ( $\langle r \rangle$ ), or in the transient state ( $r(t)$ ), that is, the values of  $r$  at time  $t$  following pulsed excitation at time 0. Although fluorescence anisotropy measurements of DPH can be carried out in steady-state using a common spectrofluorimeter with polarizers, additional information is available from measurements of the time-dependent anisotropy, namely regarding the presence of heterogeneity in DPH environment, and the presence of hindered rotation within the membrane. Additionally, measurements of anisotropy decays are less sensitive to artifacts than  $\langle r \rangle$  (see **Note 11**). In this section, instructions are included for measuring the fluorescence anisotropy decays of DPH through Time-Correlated Single-Photon Timing technique (TCSPT), using a pulsed laser excitation.

1. DPH excitation is achieved by excitation pulses at 340 nm.
2. Anisotropy decays can be obtained by alternating the emission polarizer between 0° (vertical) and 90° (horizontal) degrees, keeping the excitation polarizer in the vertical position (see **Note 12**).
3. The fluorescence must be detected with a microchannel plate photomultiplier at the desired wavelength (430 nm for DPH). Select 430 nm as the emission wavelength with a monochromator in combination with an adequate cut-off filter to avoid interference from Rayleigh-scattered light.
4. Determine the instrument response function (IRF) with a Ludox solution (see **Note 13**).

- Collect the data in a multichannel analyzer with a time window of 1024 channels, at typically 4 - 20 ps/channel and up to 50 000 and 20 000 counts in the peak channel of the IRF and decay curves, respectively (see **Note 14**).
- Data analysis must be carried out using a nonlinear, least-square iterative convolution method based on the Marquardt algorithm<sup>31</sup> (see **Note 15**).

On the example described below we were interested on evaluating the effect of apoptotic bile acids DCA and CDCA (500  $\mu$ M) on Chol-containing membranes, mimicking the plasma membrane. For that we made use of transient-state fluorescence anisotropy measurements with 200  $\mu$ M LUVs containing POPC:Chol mixtures with variable fractions of Chol (0, 20 and 40%), co-solubilized with DPH in a probe/lipid ratio of 1/200 (Figure 2)<sup>12</sup>.

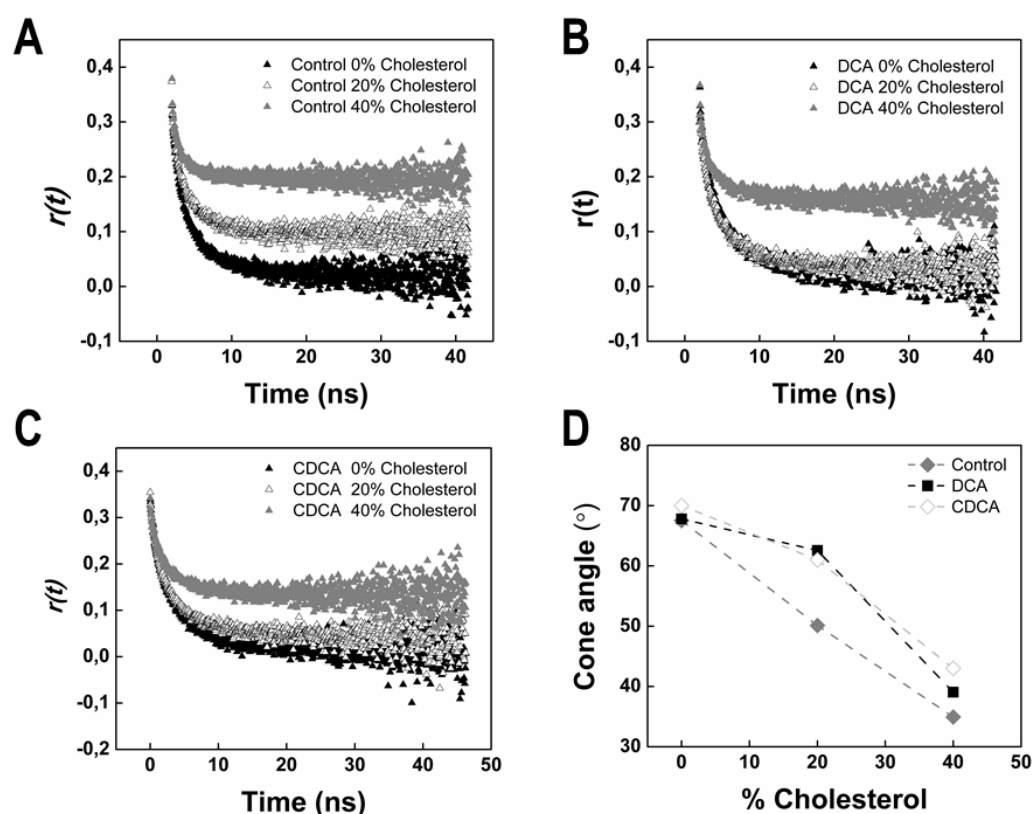


**Figure 2. Cytotoxic BAs inhibit the ordering effect of cholesterol in cholesterol containing membranes.** Fluorescence anisotropy decays of DPH in POPC:Chol liposomes with different Chol concentrations in the absence (A), or presence of 500  $\mu$ M of DCA (B) or CDCA (C), following an overnight incubation with the cytotoxic BAs. (D) Semiangles of DPH mobility cone according to the wobbling-in-cone model (see **Note 16**)<sup>32</sup>. Lines are drawn as guides. Adapted from<sup>12</sup>.

### 3.2 Impact of physiologically active concentrations of bile acids on rat isolated mitochondria

#### 3.2.1 Isolation of rat hepatocytes mitochondria

1. Low calcium liver mitochondria were isolated from male 200–250 g Sprague-Dawley rats by density gradient centrifugation, as previously published<sup>28,29</sup>.

#### 3.2.2 Sample preparation

1. Add Di-4-ANEPPDHQ or Laurdan to the mitochondria suspension to a final concentration of 5  $\mu\text{M}$  (see **Note 17**).
2. Incubate the mixture for 1h at room temperature.
3. Centrifuge the mixture at 7000g for 10 minutes at 4°C to remove the unbound probe.
4. Discard the supernatant carefully and resuspend labeled mitochondria in buffer II.
5. Dilute the stock suspension of labeled isolated mitochondria in buffer II to a final concentration of 0.5 mg/mL of protein.
6. Incubate labeled mitochondria with bile acids at a final concentration of 100 or 500  $\mu\text{M}$  for 15 minutes at room temperature.

#### 3.2.3 Steady-state fluorescence anisotropy measurements

1. Select the excitation and emission wavelengths that are more appropriate for the fluorescence probe in use (for Di-4-ANEPPDHQ,  $\lambda_{\text{ex}} = 460 \text{ nm}$  and  $\lambda_{\text{em}} = 590 \text{ nm}$ ) (see **Note 18**).
2. The steady state anisotropies,  $\langle r \rangle$ , can be determined by measurement of the steady-state vertical ( $I_{\text{V}}$ ) and horizontal ( $I_{\text{H}}$ ) components of the fluorescence emission with excitation polarized vertically<sup>33</sup>.

- In each measurement, the correction factor  $G$  is also determined for differences in the sensitivity to polarized light of the optics in the spectrofluorimeter.  $G$  can be obtained by the ratio of vertical ( $I_{HV}$ ) and horizontal ( $I_{HH}$ ) components of the emission with the excitation polarized horizontally<sup>30</sup>.
- The steady-state fluorescence anisotropy,  $\langle r \rangle$ , can be calculated using the values of the components of the fluorescence intensity with the expression  $\langle r \rangle = (I_{VV} - G \cdot I_{VH}) / (I_{VV} + 2G \cdot I_{VH})$  (see **Note 19**)<sup>30</sup>.

We were interested on studying the impact of cytotoxic and cytoprotective bile acids on isolated mitochondria, more specifically on their membranes by the determination of the steady-state fluorescence anisotropy, as a measure of the effect of bile acids over membrane order. Measurements were performed using isolated mitochondria labeled with Di-4-ANEPPDHQ after incubation with DCA, UDCA and TUDCA at physiologically active concentrations (100 and 500  $\mu\text{M}$ ) (Figure 3)<sup>15</sup>.

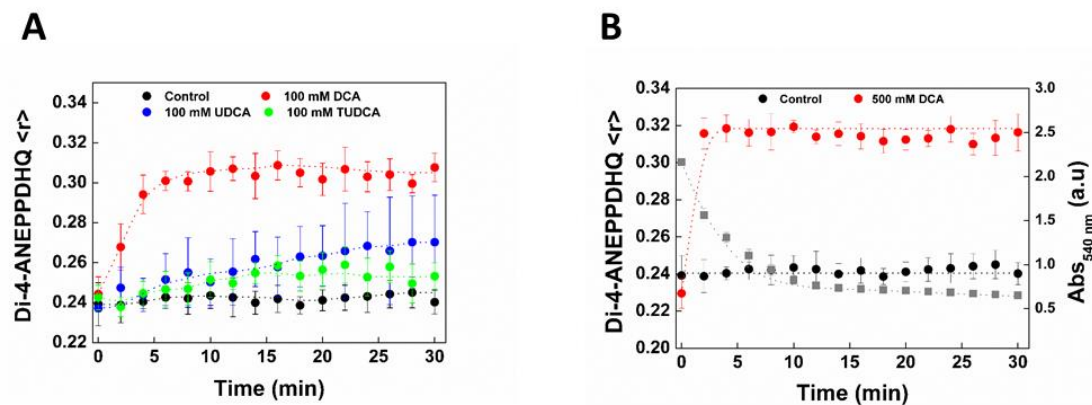


**Figure 3. DCA induces changes in MOM structure, which precede the onset of MPT.** Comparison between changes in membrane order of freshly isolated rat liver mitochondria over time after exposure to DCA (red), UDCA (blue), and TUDCA (green) at 100  $\mu\text{M}$  (A). Mitochondrial membrane order in freshly isolated rat liver mitochondria was monitored through steady-state fluorescence anisotropy measurements of di-4-ANEPPDHQ. Changes in the fluorescence anisotropy of di-4-ANEPPDHQ (red) and mitochondrial swelling (gray) for isolated mitochondria in the presence of 500  $\mu\text{M}$  DCA (B). Control values for di-4-ANEPPDHQ fluorescence anisotropy are shown in black (see **Note 20** and **Note 21**) Adapted from<sup>15</sup>.

### 3.3 Impact of physiologically active concentrations of bile acids on rat primary hepatocytes

#### 3.3.1 Cell culture of rat primary hepatocytes

1. Primary rat hepatocytes were isolated from the liver of male rats (100-150 g) by collagenase perfusion as previously described<sup>34,35</sup>.
2. After isolation, hepatocytes were resuspended in Complete William's E medium (Sigma-Aldrich Co., St Louis, MO, USA)<sup>36</sup> and plated on Primaria™ tissue culture dishes (BD Biosciences, San Jose, CA, USA) at  $5 \times 10^4$  cells/ cm<sup>2</sup>.
3. Cells were maintained at 37°C in a humidified atmosphere of 5% CO<sub>2</sub> for 6 hours, to allow attachment.
4. Plates were then washed with medium to remove dead cells and incubated in Complete William's E medium.

#### 3.3.2 Sample preparation (see **Note 22**)

1. Dilute the stock solutions of bile acids in medium I, to a final concentration of 100 or 500 μM per well (200 μL).
2. Incubate the hepatocytes with bile acid solution for 30 min, 1h or 16h at 37°C.
3. Dilute the stock solution of Laurdan to a final concentration of 5 μM in Complete William's E medium per well (200 μL).
4. Incubate the hepatocytes with Laurdan solution for 15 minutes at 37°C.
5. Replace the incubation medium with fresh medium.

### 3.3.3 Two-photon excitation microscopy measurements (see **Note 23**)

1. Select an appropriate wavelength for two-photon excitation of Laurdan (760-800 nm).
2. Fluorescence emission of Laurdan must be collected at 400–460 nm ( $I_{400-460}$ ) and 470–530 nm ( $I_{470-530}$ ) to determine the GP value (see **Note 24**).
3. For each measurement, two images are recovered that correspond to the intensities of Laurdan in each channel.
4. Conditions for acquisition should be chosen so that signal to noise error is minimized while maintaining detection intensities far from saturating values, as this would skew recovered GP data.
5. Generalized Polarization (GP) is defined by  $GP = (I_{400-460} - G \cdot I_{470-530}) / (I_{400-460} + G \cdot I_{470-530})$ , where  $I$  represents the intensity in each pixel in the image acquired in the indicated spectral channel and  $G$  is a calibration factor (see **Note 25** and **Note 26**).
6. A Laurdan GP image can be determined by using a script, for example in Matlab (MathWorks, Natick, MA) environment, that allows for the conversion of the Laurdan fluorescence intensity of each pixel in the two detection channels into a GP value by applying the previous equation (see **Note 27**).
7. Average Laurdan GP values per cell in the plasma membrane or intracellular regions can be determined by careful selection of regions of interest corresponding to each of areas.

For studying the impact of cytotoxic and cytoprotective bile acids on hepatocytes, more specifically on their membranes, we followed Laurdan fluorescence emission spectral shifts, quantified by the Generalized Polarization (GP) function, as an estimation of the effect of bile acids over membrane order at shorter and longer incubation times<sup>20</sup>. Measurements were performed using rat primary hepatocytes labeled with 5 $\mu$ M of Laurdan after incubation with DCA, UDCA and TUDCA at 100  $\mu$ M (Figure 4)<sup>15</sup>.

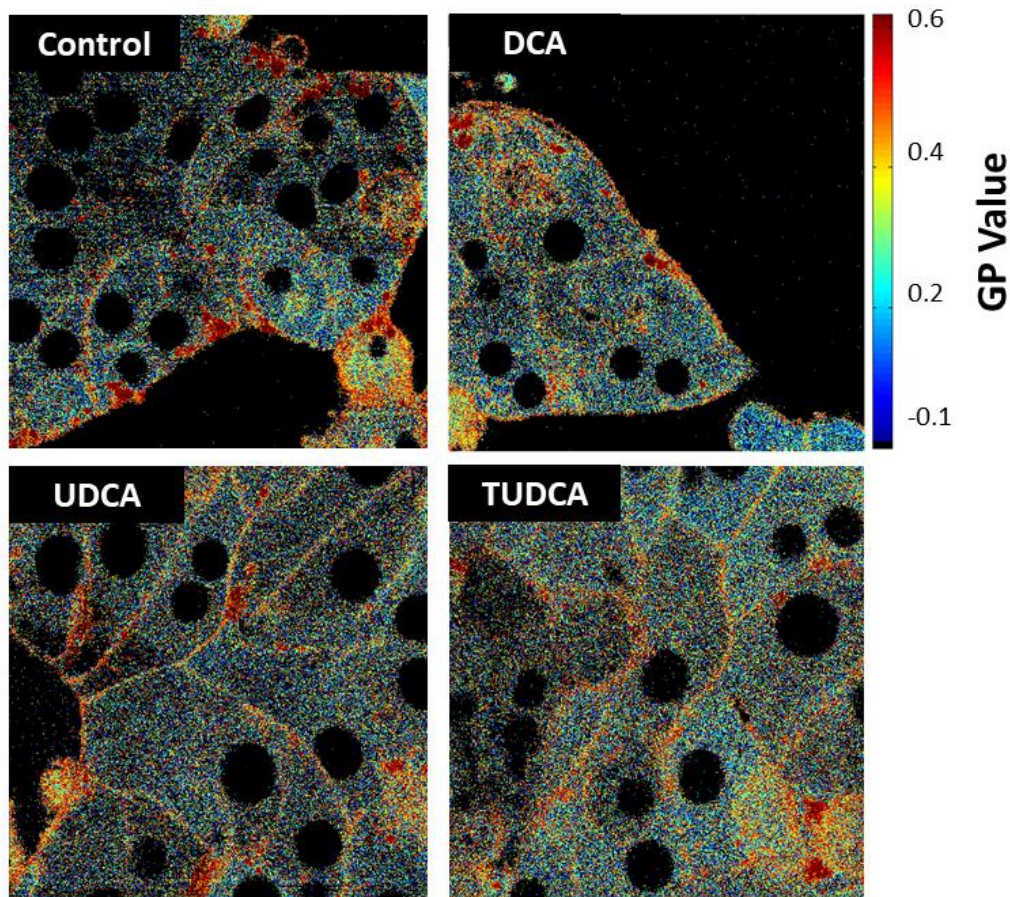


**Figure 4. Changes in Laurdan GP values in membranes of rat hepatocytes in the presence of DCA and the cytoprotective UDCA/TUDCA bile acids.** Laurdan GP values were calculated as described in Materials and Methods sections. GP images of hepatocytes after 30 min incubation with 100  $\mu$ M of bile acids. Plasma membrane shows a high order (higher GP value) than intracellular membranes that translates into red-orange color, while intracellular membranes are visible in blue (less ordered membranes). Adapted from<sup>15</sup>.

## 4. Notes

1. Bile acids in the sodium salt form are preferable due to the higher solubility in water/buffer. These bile acids were selected since their physiological apoptotic or cytoprotective effects are well characterized<sup>6,37</sup>.
2. All buffer solutions must be prepared using ultrapure water, produced by a system such as a Milly-Q system (specific resistance >18 MΩ cm). Buffers must be kept at 4°C shortly until use.
3. Concentrations of lipid stock solutions in organic solvents can change during storage due to solvent evaporation. In this way, concentration should be frequently confirmed using phosphate determination<sup>38</sup>. Stock solutions were kept in organic solvents at -26°C.
4. Cholesterol concentration in stock solution was determined gravimetrically with a high-precision scale. The empty vials were weighted and then filled with a certain volume of cholesterol stock solution. Then the solvent was evaporated using a nitrogen (N<sub>2</sub>) flux and kept in the vacuum overnight to ensure complete chloroform evaporation. Vials were weighted, and cholesterol mass was determined by the difference between the weight of empty vials and vials containing cholesterol.
5. Concentration of probes was determined spectrophotometrically with absorbance data and using absorption coefficients obtained from literature<sup>20,39,40</sup>. Stock solutions were kept in organic solvents at -20°C.
6. The liposomes must be unilamellar in order that the available lipid for interaction with bile acids is maximized and precisely defined in each experiment.

7. Two-photon excitation microscopy is often used for imaging of Laurdan GP values, since one-photon excitation induces more severe photobleaching of the probe<sup>41</sup>.
8. Both the solutions of fluorescent probes as well as the suspensions of lipid vesicles and isolated mitochondria loaded with these molecules should be kept always protected from light, as both DPH and Laurdan are sensitive to photobleaching.
9. During lipid film hydration, thawing (in freeze-thaw cycles) and extrusion, the sample should be kept at a temperature above the main transition temperature ( $T_m$ ) of the lipid specie within the lipid mixture with the highest  $T_m$ , to ensure homogeneity of lipid composition between vesicles.
10. The number of extrusion cycles must be an odd number to ensure that all lipid vesicles within the sample were extruded through the membrane.
11. Steady-state fluorescence anisotropy values ( $\langle r \rangle$ ) are dependent on the average fluorescence lifetime ( $\langle \tau \rangle$ ) of DPH, and changes in  $\langle r \rangle$  due to differences in  $\langle \tau \rangle$  can be erroneously interpreted as changes in membrane order. Additionally, the presence of significant light scattering can induce a decrease in  $\langle r \rangle$  values which can also lead to incorrect interpretations of DPH fluorescence data, while being readily identified in anisotropy decays.
12. Light was completely depolarized after passing through the polarizers meaning that a correction factor (instrumental G factor is expected to be 1) is not necessary, and the detected light for each polarization was proportional to the emitted one.
13. Measurement of the excitation light scattered by a Ludox solution allows for the correction of the measurements for the instrument response. The fluorescence decays must then be deconvoluted with this function.
14. Photon count rates in detection must be kept low to avoid pile-up effects which would bias fluorescence decays to shorter lifetimes.

15. For more complex decays (multi-exponential), the intensity is assumed to decay as the sum of individual single exponentials (Eq. 1,<sup>33</sup>):

$$I(t) = \sum_{i=1}^n \alpha_i \times e^{\frac{-t}{\tau_i}} \quad (1)$$

In this expression,  $\tau_i$  are the decay times,  $\alpha_i$  represent the amplitudes of the components at  $t=0$  and  $n$  is the number of decay times.

The fluorescence anisotropy decay can be described by a sum of exponentials, as shown in the next equation (Eq. 2,<sup>33</sup>):

$$r(t) = \sum_{i=1}^n \beta_i e^{\frac{-t}{\theta_i}} + r_\infty \quad (2)$$

Where  $\beta_i$  and  $\theta_i$  represent the initial anisotropy and rotational diffusion coefficient of the  $i^{\text{th}}$  component of the decay.  $r_\infty$  represents the limiting anisotropy of the sample, which can be a sign of restricted depolarization in ordered membranes.

The anisotropy decays were also analyzed through the commercial software package TRFA data processor (SSTC, Minsk), by solving the next system of equations (Eq.3,<sup>33</sup>):

$$\begin{cases} I_{VV}^{\text{exp}}(t) = \frac{I_{\text{exp}}(t)}{3} [1 + 2 \cdot r_{\text{exp}}(t)] \\ I_{VH}^{\text{exp}}(t) = \frac{I_{\text{exp}}(t)}{3} [1 - r_{\text{exp}}(t)] \end{cases} \quad (3)$$

The values of  $\alpha_i$  and  $\tau_i$  were recovered from the fitted global intensity decays  $I_{\text{exp}}(t)$  curves as described above. A  $r_{\text{theoretical}}(t)$  curve was fitted to the  $r_{\text{exp}}(t)$  curve by optimization of  $\alpha_i$ ,  $\beta_i$  and  $\theta_i$  parameters while maintaining the  $\tau_i$  values obtained from the first fit. Fits were accepted when the  $\chi_2$  value was lower than 1.2 and weighted residuals plots were randomly distributed around 0.

16. When  $r_\infty > 0$ , the wobbling-in-cone model developed by Kinosita<sup>32</sup> was used to quantify the extent of restricted motion. In this model, the rotation of the fluorophore is assumed to be restricted to the volume of a given cone. The opening or semiangle of that cone is related to  $r_\infty$  by the next equation (Eq. 4,<sup>32</sup>):

$$\frac{r_\infty}{r_0} = \left[ \frac{1}{2} \cos \theta_c (1 + \cos \theta_c) \right]^2 \quad (4)$$

where  $r_\infty$  is the limiting anisotropy value,  $r_0$  is the fundamental anisotropy  $r(t=0)$  and  $\theta_c$  the value of the cone semiangle. Values vary between  $0^\circ$  ( $r_\infty = r_0$ , no rotation during the excited state) to  $90^\circ$  ( $r_\infty = 0$ , complete depolarization during the excited state).

17. DMSO concentration should be kept below 1%, to prevent changes in lipid packing due to interaction with organic solvents.
18. Di-4-ANEPPDHQ fluorescence data should be interpreted with caution when analyzing mitochondrial membrane properties during mitochondrial depolarization, since it is also a voltage sensitive dye, and its quantum yield is moderately sensitive to changes in membrane potential. Additionally, the photophysical processes responsible for Di-4-ANEPPDHQ spectral shifts in lipid membranes are more complex than the ones observed for Laurdan<sup>21</sup>. When analyzing fluorescence anisotropies of these probes, fluorescence lifetimes should also be monitored to confirm that changes in fluorescence anisotropy values are not influenced by differences in  $\langle \tau \rangle$ , as predicted by the Perrin Equation<sup>33</sup>:

$$\langle r \rangle = \frac{r_0}{1 + \frac{\langle \tau \rangle}{\theta}} \quad (5)$$

where  $r_0$  corresponds to the fundamental anisotropy of the fluorophore,  $\langle \tau \rangle$  is the average lifetime that the fluorophore stays in the excited state and  $\theta$  is the rotational correlation time.

19. Since anisotropies are the result of a ratio of intensities, the uncertainty associated with the measurements is much higher. So, for accurate determination of  $\langle r \rangle$  for each

sample at least 8 measurements of the fluorescence intensity components should be performed, reducing the associated error.

20. Background contribution is always subtracted for all samples.
21. Mitochondrial swelling was detected through changes in optical density (OD) at 540 nm according to the literature<sup>15</sup>.
22. Every step of cell manipulation should be performed inside the laminar air flow cabinet and the incubation at 37°C inside the incubator.
23. Alternatively, Laurdan can also be imaged with UV single-photon excitation. However, two-photon excitation has several advantages over UV illumination, namely lower phototoxicity and lower extent of photobleaching above and below the focal plane.
24. Recovered GP values depend strongly on the exact choice of excitation wavelength and detection windows. Since Laurdan GP values obtained from microscopy are often determined using different detection and excitation conditions, these values are not always comparable between different studies.
25. G calibration factor is required for comparison with GPs measured in different conditions (different setups, PMTs, PMT gains and detection windows)<sup>20</sup>. G can be obtained with a homogeneous solution of Laurdan in DMSO, as the GP value of Laurdan in DMSO (as measured in a calibrated spectrofluorimeter) is 0.035<sup>23</sup>. Through the use of  $GP = (I_{400-460} - G \cdot I_{470-530}) / (I_{400-460} + G \cdot I_{470-530})$ , values of G that reproduce calibrated GP values of Laurdan in DMSO are estimated. By calculating G values on a pixel by pixel basis using a MATLAB script, a G image is recovered. This can be used to evaluate homogeneity of calibration for the whole field of view.
26. Theoretically, the values for the GP function range from -1 to +1. Disordered membranes typically display Laurdan GP values (obtained through microscopy) below 0.3, while ordered membranes present GP values between 0.3-0.6<sup>23</sup>. For the plasma membrane, values of Laurdan GP obtained by microscopy are commonly found between 0.4 and 0.6.

27. Both channel intensities are corrected for background contributions. These are determined by measuring the average intensity in unlabeled cells imaged at the same conditions<sup>15,20</sup>.

## 5. References

1. Woolbright, B. L. & Jaeschke, H. Novel insight into mechanisms of cholestatic liver injury. *World J. Gastroenterol.* **18**, 4985–93 (2012).
2. Li, T., Apte, U. & City, K. Bile acid metabolism and signaling in cholestasis, inflammation and cancer. (2016). doi:10.1016/bs.apha.2015.04.003.Bile
3. Gumprich, E., Devereaux, M. W., Dahl, R. H. & Sokol, R. J. Glutathione status of isolated rat hepatocytes affects bile acid-induced cellular necrosis but not apoptosis. *Toxicol. Appl. Pharmacol.* **164**, 102–111 (2000).
4. Perez, M. J. Bile-acid-induced cell injury and protection. *World J. Gastroenterol.* **15**, 1677 (2009).
5. Rodrigues, C. M., Fan, G., Ma, X., Kren, B. T. & Steer, C. J. A novel role for ursodeoxycholic acid in inhibiting apoptosis by modulating mitochondrial membrane perturbation. *J. Clin. Invest.* **101**, 2790–9 (1998).
6. Amaral, J. D., Viana, R. J. S., Ramalho, R. M., Steer, C. J. & Rodrigues, C. M. P. Bile acids: regulation of apoptosis by ursodeoxycholic acid. *J. Lipid Res.* **50**, 1721–34 (2009).
7. Palmeira, C. M. & Rolo, A. P. Mitochondrially-mediated toxicity of bile acids. *Toxicology* **203**, 1–15 (2004).
8. Hofmann, A. F. The continuing importance of bile acids in liver and intestinal disease. *Arch. Intern. Med.* **159**, 2647–58 (1999).
9. Sodeman, T., Bronk, S. F., Roberts, P. J., Miyoshi, H., Gregory, J., Gores, G. J. & Rob, P. J. Bile salts mediate hepatocyte apoptosis by increasing cell surface trafficking of Fas. *Physiol, Am J Liver, Gastrointest Liver* (2012).

10. Rodrigues, C. M., Fan, G., Wong, P. Y., Kren, B. T. & Steer, C. J. Ursodeoxycholic acid may inhibit deoxycholic acid-induced apoptosis by modulating mitochondrial transmembrane potential and reactive oxygen species production. *Mol. Med.* **4**, 165–78 (1998).
11. Castro, R. E., Amaral, J. D., Solá, S., Kren, B. T., Steer, C. J. & Rodrigues, C. M. P. Differential regulation of cyclin D1 and cell death by bile acids in primary rat hepatocytes. *Am. J. Physiol. Gastrointest. Liver Physiol.* **293**, G327-34 (2007).
12. Mello-Vieira, J., Sousa, T., Coutinho, A., Fedorov, A., Lucas, S. D., Moreira, R., Castro, R. E., Rodrigues, C. M. P., Prieto, M. & Fernandes, F. Cytotoxic bile acids, but not cytoprotective species, inhibit the ordering effect of cholesterol in model membranes at physiologically active concentrations. *Biochim. Biophys. Acta* **1828**, 2152–2163 (2013).
13. Benz, C., Angermüller, S., Otto, G., Sauer, P., Stremmel, W. & Stiehl, a. Effect of tauroursodeoxycholic acid on bile acid-induced apoptosis in primary human hepatocytes. *Eur. J. Clin. Invest.* **30**, 203–9 (2000).
14. Zhou, Y., Maxwell, K. N., Sezgin, E., Lu, M., Liang, H., Hancock, J. F., Dial, E. J., Lichtenberger, L. M. & Levental, I. Bile acids modulate signaling by functional perturbation of plasma membrane domains. *J. Biol. Chem.* **288**, 35660–70 (2013).
15. Sousa, T., Castro, R. E., Pinto, S. N., Coutinho, A., Lucas, S. D., Moreira, R., Rodrigues, C. M. P., Prieto, M. & Fernandes, F. Deoxycholic acid modulates cell death signaling through changes in mitochondrial membrane properties. *J. Lipid Res.* (2015). doi:10.1194/jlr.M062653
16. Bogner, C., Leber, B. & Andrews, D. W. Apoptosis: Embedded in membranes. *Curr. Opin. Cell Biol.* **22**, 845–851 (2010).
17. Schug, Z. T. & Gottlieb, E. Cardiolipin acts as a mitochondrial signalling platform to launch apoptosis. *Biochim. Biophys. Acta* **1788**, 2022–31 (2009).
18. Yeung, T., Gilbert, G. E., Shi, J., Silvius, J., Kapus, A. & Grinstein, S. Membrane phosphatidylserine regulates surface charge and protein localization. *Science* (80-. ). **319**, 210–213 (2008).
19. Lentz, B. R. Membrane “fluidity” as detected by diphenylhexatriene probes. *Chem. Phys. Lipids* **50**, 171–190 (1989).
20. Owen, D. M., Rentero, C., Magenau, A., Abu-Siniyeh, A. & Gaus, K. Quantitative imaging of membrane lipid order in cells and organisms. *Nat. Protoc.* **7**, 24–35 (2012).

21. Amaro, M., Reina, F., Hof, M., Eggeling, C. & Sezgin, E. Laurdan and Di-4-ANEPPDHQ probe different properties of the membrane. *J. Phys. D. Appl. Phys.* **50**, 134004 (2017).
22. Parasassi, T., Gratton, E., Yu, W. M., Wilson, P. & Levi, M. Two-photon fluorescence microscopy of laurdan generalized polarization domains in model and natural membranes. *Biophys. J.* **72**, 2413–2429 (1997).
23. Sanchez, S. A., Tricerri, M. A., Gunther, G. & Gratton, E. Laurdan Generalized Polarization : from cuvette to microscope. *Mod. Res. Educ. Top. Microsc.* 1007–1014 (2007).
24. Chan, Y.-H. M. & Boxer, S. G. Model membrane systems and their applications. *Curr. Opin. Chem. Biol.* **11**, 581–587 (2007).
25. Loura, L. M. S., Prieto, M. & Fernandes, F. Quantification of protein-lipid selectivity using FRET. *Eur. Biophys. J.* **39**, 565–578 (2010).
26. Dietrich, C., Bagatolli, L. A., Volovyk, Z. N., Thompson, N. L., Levi, M., Jacobson, K. & Gratton, E. Lipid rafts reconstituted in model membranes. *Biophys. J.* **80**, 1417–28 (2001).
27. Sarmiento, M. J., Pinto, S. N., Coutinho, A., Prieto, M. & Fernandes, F. Accurate quantification of inter-domain partition coefficients in GUVs exhibiting lipid phase coexistence. *RSC Adv.* **6**, 66641–66649 (2016).
28. Botla, R., Spivey, J., Aguilar, H., Bronk, S. & Gores, G. Ursodeoxycholate (UDCA) inhibits the mitochondrial membrane permeability transition induced by glycochenodeoxycholate: a mechanism of UDCA cytoprotection. *J. Pharmacol. Exp. Ther.* **272**, 930–938 (1995).
29. Walajtys-Rhode, E., Zapatero, J., Moehren, G. & Hoek, J. B. The role of the matrix calcium level in the enhancement of mitochondrial pyruvate carboxylation by glucagon pretreatment. *J. Biol. Chem.* **267**, 370–9 (1992).
30. J.R Lakowicz. *Principles of Fluorescence Spectroscopy*. (2006). doi:10.1007/3-540-29623-9\_7040
31. Marquardt, D. W. An Algorithm for Least-Squares Estimation of Nonlinear Parameters. *J. Soc. Ind. Appl. Math.* **11**, 431–441 (1963).
32. Kinosita, K., Ikegami, A. & Kawato, S. On the wobbling-in-cone analysis of fluorescence anisotropy decay. *Biophys. J.* **37**, 461–4 (1982).

33. Lakowicz, J. R. *Principles of Fluorescence Spectroscopy*. (2006).
34. Mariash, C. N., Seelig, S., Schwartz, H. L. & Oppenheimer, J. H. Rapid synergistic interaction between thyroid hormone and carbohydrate on mRNAS14 induction. *J. Biol. Chem.* **261**, 9583–6 (1986).
35. Castro, R. E., Ferreira, D. M. S., Zhang, X., Borralho, P. M., Sarver, A. L., Zeng, Y., Steer, C. J., Kren, B. T. & Rodrigues, C. M. P. Identification of microRNAs during rat liver regeneration after partial hepatectomy and modulation by ursodeoxycholic acid. *Am. J. Physiol. Gastrointest. Liver Physiol.* **299**, G887-97 (2010).
36. Castro, R. E., Ferreira, D. M. S., Afonso, M. B., Borralho, P. M., Machado, M. V, Cortez-Pinto, H. & Rodrigues, C. M. P. miR-34a/SIRT1/p53 is suppressed by ursodeoxycholic acid in the rat liver and activated by disease severity in human non-alcoholic fatty liver disease. *J. Hepatol.* **58**, 119–25 (2013).
37. Monte, M.-J. Bile acids: Chemistry, physiology, and pathophysiology. *World J. Gastroenterol.* **15**, 804 (2009).
38. McClare, C. W. An accurate and convenient organic phosphorus assay. *Anal. Biochem.* **39**, 527–30 (1971).
39. Pinto, S. N., Silva, L. C., de Almeida, R. F. M. & Prieto, M. Membrane domain formation, interdigitation, and morphological alterations induced by the very long chain asymmetric C24:1 ceramide. *Biophys. J.* **95**, 2867–79 (2008).
40. Parasassi, T. & Gratton, E. Membrane Lipid Domains and Dynamics as Detected by Laurdan Fluorescence. *J. Fluoresc.* **5**, 59–69 (1995).
41. Bagatolli, L. A., Sanchez, S. A., Hazlett, T. & Gratton, E. Giant vesicles, Laurdan, and two-photon fluorescence microscopy: evidence of lipid lateral separation in bilayers. *Methods Enzymol.* **360**, 481–500 (2003).



## **Chapter III**

---

Deoxycholic acid modulates cell death signaling through changes in mitochondrial membrane properties





## Deoxycholic acid modulates cell death signaling through changes in mitochondrial membrane properties<sup>§</sup>

Tânia Sousa,\* Rui E. Castro,<sup>†</sup> Sandra N. Pinto,\* Ana Coutinho,\*<sup>§</sup> Susana D. Lucas,<sup>†</sup> Rui Moreira,<sup>†</sup> Cecília M. P. Rodrigues,<sup>†</sup> Manuel Prieto,\* and Fábio Fernandes<sup>1,\*</sup>

Centro de Química-Física Molecular and Institute of Nanoscience and Nanotechnology, Instituto Superior Técnico,\* Research Institute for Medicines (iMed.Ulisboa), Faculty of Pharmacy,<sup>†</sup> and Departamento de Química e Bioquímica, Faculty of Sciences,<sup>§</sup> University of Lisbon, Lisbon, Portugal

### Abstract

Cytotoxic bile acids, such as DCA, are responsible for hepatocyte cell death during intrahepatic cholestasis. The mechanisms responsible for this effect are still unclear, and recent studies are conflicting, pointing to either a modulation of plasma membrane structure or to mitochondrial-mediated toxicity through perturbation of mitochondrial outer membranes (MOM) properties. Here, we carried out a comprehensive comparative study of the impact of cytotoxic and cytoprotective bile acids on the membrane structure of different cellular compartments. We show that DCA increases the plasma membrane fluidity of hepatocytes only to a minor extent, and that this effect is not correlated with the incidence of apoptosis. Additionally, plasma membrane fluidity recovers to normal values overtime suggesting the presence of cellular compensatory mechanisms for this perturbation. Colocalization experiments in living cells confirmed the presence of bile acids within mitochondrial membranes. Experiments with active isolated mitochondria, revealed that physiologically active concentrations of DCA changes mitochondrial outer membrane order in a concentration- and time-dependent manner, and that these changes preceded the mitochondrial permeability transition (MPT). Importantly, these effects are not observed on liposomes mimicking MOM lipid composition, suggesting that DCA apoptotic activity depends on features of mitochondrial membranes which are absent from protein-free mimetic liposomes, such as the double membrane structure, lipid asymmetry or the mitochondrial protein environment. In contrast, the mechanism of action of cytoprotective bile acids is likely not associated with changes in cellular membrane structure.



## 1. Introduction

Intrahepatic cholestasis is associated with the accumulation of abnormally high levels of hydrophobic bile acids in the liver, with elevated cytotoxic effects in hepatocytes and bile duct cells<sup>1</sup>. Ultimately, bile acid toxicity can result in organ failure<sup>2</sup>. Hydrophobic bile acids, such as deoxycholic acid (DCA; Supplemental Figure 1), have been reported to induce apoptosis in hepatocytes at low concentrations ( $\leq 100 \mu\text{M}$ ) well below their critical micellar concentration<sup>3</sup>, while higher concentrations ( $\geq 250 \mu\text{M}$ ) induce cell death by necrosis<sup>4</sup>. At submicellar extracellular concentrations (50-100  $\mu\text{M}$ ), these molecules have been proposed to activate cell death receptors in a ligand independent manner<sup>5</sup>, induce JNK1-mediated activation of p53, EF2-1 and cyclin D1 expression<sup>3,6,7</sup>, induce oxidative damage<sup>8</sup>, promote both Bcl-2 associated protein X (Bax) translocation to mitochondria<sup>9</sup> and induce mitochondrial dysfunction<sup>8,10</sup>. Any of these modifications alone are sufficient for caspase activation and initiation of apoptosis<sup>3,11</sup>. However, the precise triggering mechanism responsible for the activation of these apoptotic signaling events is still unknown.

On the other hand, submicellar extracellular concentrations (50-100  $\mu\text{M}$ ) of the more hydrophilic bile acids such as ursodeoxycholic acid (UDCA) and tauroursodeoxycholic acid (TUDCA) (Supplemental Figure 1) have the ability to inhibit apoptosis induced by certain agents in both hepatic and non-hepatic cells<sup>10,12</sup>. The UDCA and TUDCA effect seems to be related with the blockage of mitochondrial membrane damage<sup>8</sup>, inhibiting disruption of the mitochondrial membrane potential by hydrophobic bile acids, ROS production<sup>10</sup>, and Bax protein translocation to mitochondria<sup>13</sup>.

Activity of both cytotoxic and cytoprotective bile acids is likely to be triggered through two main mechanisms: *i*) death receptor modulation through changes in plasma membrane organization (extrinsic pathway of apoptosis), and/or *ii*) induction/inhibition of the membrane permeability transition in mitochondria (intrinsic pathway of apoptosis).

In support of the hypothesis that the plasma membrane is the target of cytotoxic bile acids, a recent study showed that cytotoxic bile acids such as DCA or chenodeoxycholic acid have the ability to disrupt to some extent the membrane ordering effect induced by cholesterol (Chol)<sup>14</sup>. Interestingly, this effect was much less efficient in the cholesterol rich liquid ordered phase ( $l_o$ ), possibly as a consequence of a lower affinity of the bile acids toward more ordered membranes<sup>14-16</sup>. This was also recently confirmed in giant plasma membrane vesicles (GPMV's) isolated from rat tumor mast cells<sup>17</sup>. The authors have suggested that DCA might interfere with the organization of signaling proteins due to its membrane disordering effect.

In support of a classical intrinsic apoptotic pathway target, cytoprotective UDCA and TUDCA increased the threshold for apoptosis through inhibition of the mitochondrial

membrane permeability transition (MPT) in hepatocytes<sup>10,13,18</sup>. It is possible that DCA and other cytotoxic bile acids act through activation of intrinsic pathways as well. This hypothesis is supported by evidence showing that hepatocytes deficient in Fas-receptor still undergo cell death after bile duct ligation or in culture after exposure to bile acids, indicating that the extrinsic apoptotic pathway is not essential for cytotoxic action<sup>19</sup>. In this case, cytotoxic bile acids could act directly on mitochondrial membranes, either through a change of mitochondrial membrane properties or through a direct increase in the permeability of mitochondrial membranes. A recent study put forward compelling evidence suggesting that cytotoxic bile acids detach the inner boundary membrane from the mitochondrial outer membrane (MOM), and finally induce MPT, likely at the remaining contact sites<sup>20</sup>.

In this work, we aimed to carry out for the first time a comprehensive characterization of the effect of physiologically active concentrations of cytotoxic and cytoprotective bile acids on the membrane properties of the most likely targets for modulation of cell death by bile acids, the plasma membrane and the mitochondrial membranes. We show that even very high concentrations of both cytotoxic and cytoprotective bile acids, only increase plasma membrane fluidity of hepatocytes to a minor extent, and that this effect is not correlated with apoptosis. Additionally, the plasma membrane fluidity recovers to normal (untreated) values during long incubations, suggesting the presence of cellular compensatory mechanisms to maintain plasma membrane integrity. The impact of cytotoxic and cytoprotective bile acids on the average intracellular membrane fluidity is comparable, although for longer incubation times, a dramatic decrease in membrane fluidity is only observed for the cytotoxic DCA. The latter effect is preceded by apoptosis and it is likely a consequence of the apoptotic process itself. On the other hand, only cytotoxic bile acids had an impact on isolated mitochondrial outer membrane order, and this effect preceded the onset of mitochondria permeabilization. In addition, we showed that DCA mediated changes in mitochondrial membrane organization are not observed in protein-free liposomes mimicking mitochondrial membrane lipid composition. These findings identify mitochondrial membranes as a likely target of the cytotoxic bile acid DCA and suggest that the mechanism of action of DCA is associated to changes in mitochondrial membrane features which are absent from protein-free mimetic liposomes.

## 2. Materials and methods

### 2.1 Chemicals and Reagents

1,2-dioleoyl-*sn*-glycero-3-phosphocholine (DOPC), 1,2-dioleoyl-*sn*-glycero-3-phosphoethanolamine (DOPE), L- $\alpha$ -Phosphatidylinositol sodium salt (PI), 1-palmitoyl-2-oleoyl-*sn*-glycero-3-phosphocholine (POPC); *N*-palmitoyl-*D*-erythrospingosylphosphorylcholine (PSM) and 1,3-bis(*sn*-3'-phosphatidyl)-*sn*-glycerol (cardiolipin, CL), were purchased from Avanti Polar Lipids (Alabaster, AL, USA). Chol was obtained from Sigma-Aldrich (St. Louis MO, USA). Stock solutions of all lipids were prepared with Uvasol grade chloroform with the exception of CL that was prepared in chloroform/methanol (2:1). Both solvents were obtained from Sigma-Aldrich. DCA and TUDCA in sodium salt form, methyl- $\beta$ -cyclodextrin (CD), NaCl, succinate and sucrose were purchased from Sigma-Aldrich. UDCA sodium salt was purchased from Santa Cruz Biotechnologies (Santa Cruz, CA) and Tris from Merck (Darmstadt, Germany).

1-[2-hydroxy-3-(*N,N*-di-methyl-*N*-hydroxyethyl)ammoniopropyl]-4-[ $\beta$ -[2-(*di-n*-butylamino)-6-naphthyl] vinyl]pyridinium dibromide (Di-4-ANEPPDHQ), 6-dodecanoyl-2-dimethylaminonaphthalene (Laurdan), [6-amino-9-(2-methoxycarbonylphenyl)xanthen-3-ylidene]azanium (Rho-123) and Wheat germ agglutinin (WGA) conjugated with Alexa Fluor 594 were purchased from Invitrogen (Carlsbad, CA, USA). 5(6)-carboxyfluorescein (CF) was obtained from Sigma-Aldrich. Fluorescently labeled bile acid derivatives were obtained as previously described<sup>14</sup>.

### 2.2 Cell culture, isolation of rat primary hepatocytes and rat liver mitochondria

Primary rat hepatocytes were isolated from the liver of male rats (100-150 g) by collagenase perfusion as previously described<sup>21,22</sup>. After isolation, hepatocytes were resuspended in Complete William's E medium (Sigma-Aldrich Co., St Louis, MO, USA)<sup>23</sup> and plated on Primaria™ tissue culture dishes (BD Biosciences, San Jose, CA, USA) at  $5 \times 10^4$  cells/cm<sup>2</sup>. Cells were maintained at 37°C in a humidified atmosphere of 5% CO<sub>2</sub> for 6 hours, to allow attachment. Plates were then washed with medium to remove dead cells and incubated in Complete William's E medium. Experiments with hepatocytes were carried out 24h after plating. HEK 293 cells were cultured and maintained in DMEM with 10% FBS and 1% of penicillin-streptomycin (Sigma Chemical Co., St. Louis, MO) at the incubator with controlled temperature (37°C), humidity and CO<sub>2</sub> levels (5%). Low calcium liver mitochondria

were isolated from male 200–250 g Sprague-Dawley rats by density gradient centrifugation, as previously published<sup>18,24</sup>. All experiments involving animals were performed by an investigator accredited for directing animal experiments (FELASA level C), in conformity with the Public Health Service (PHS) Policy on Humane Care and Use of Laboratory Animals, incorporated in the Institute for Laboratory Animal Research (ILAR) Guide for Care and Use of Laboratory Animals. Experiments received prior approval from the Portuguese National Authority for Animal Health (DGAV).

### **2.3 Cell viability and caspase-3/7 activity measurements**

Rat primary hepatocytes were cultured in 96-well assay plates, and the The ApoTox-Glo triplex assay (Promega Corp., Madison, WI) was used according to the manufacturer's protocol. Cell death was also evaluated by the LDH assay kit (Sigma) and LDH activity was evaluated in cell culture media. Fluorescence measurements were carried out using a Bio-Rad microplate reader model 680 (Bio-Rad, Hercules, CA).

### **2.4 Confocal and two-photon fluorescence microscopy**

All measurements were performed on a Leica TCS SP5 (Leica Microsystems CMS GmbH, Mannheim, Germany) inverted confocal microscope (DMI600). Excitation lines were provided by an Argon laser that was focused into the sample by an apochromatic water immersion objective (63x, NA 1.2; Zeiss, Jena Germany). A 111.4  $\mu\text{m}$  diameter pinhole positioned in front of the image plane blocked out-of-focus signals.

Two photon excitation measurements of Laurdan were obtained using the same set-up coupled to a Ti:sapphire laser (Mai Tai, Spectra-Physics, Darmstadt, Germany) as the excitation source. The excitation wavelength was set to 780 nm and the fluorescence emission of Laurdan was collected at 400–460 nm ( $I_{400-460}$ ) and 470–530 nm ( $I_{470-530}$ ). Following incubation with bile acids, rat primary hepatocytes and HEK293T cells were incubated with 5  $\mu\text{M}$  of Laurdan for 15 minutes. Generalized Polarization (GP) images were obtained using homemade software developed in a MATLAB environment, with the GP value defined as  $GP = (I_{400-460} - G \cdot I_{470-530}) / (I_{400-460} + G \cdot I_{470-530})$ . Both channel intensities are corrected for background contributions and the calibration factor  $G$  was obtained from imaging Laurdan in DMSO using the same experimental conditions as those set for the samples under study<sup>25</sup>.

Colocalization studies with Alexa 594-WGA were performed with 633 nm excitation and detection of emission at  $695 \pm 55$  nm. For the colocalization studies between bile acid analogues and the mitochondrial marker, Rho-123, spectral imaging was performed in combination with linear unmixing<sup>26</sup>, since the NBD and Rho-123 spectra display partial overlapping. Briefly, fluorescence from cells labeled with bile acid analogues and Rho-123 was acquired at different wavelengths for excitation at 458 and 514 nm, and images were computationally processed by a linear unmixing algorithm using the distinct reference spectrum of NBD and Rho-123, which were obtained independently. This procedure was carried out using homemade software created in a MATLAB environment (Mathworks, Natick, MA). The product from the difference from the mean (PDM) and Pearson's correlation coefficient ( $R_r$ )<sup>27</sup> parameters were obtained through WCIF ImageJ (<http://www.uhnresearch.ca/facilities/wcif/imagej/>).

## **2.5 Fluorescence lifetime imaging (FLIM)**

FLIM of di-4-ANEPPDHQ in HEK293T cells was performed using a Becker & Hickl setup (Berlin, Germany). 800 nm two-photon excitation was used to excite di-4-ANEPPDHQ. Two-photon excitation pulses were generated by an Ti:sapphire laser with a pulse frequency of 80 MHz. Emission light was selected with a dichroic beam splitter with an excitation SP700 short pass filter and an emission 535/85 band-pass filter inserted in front of the photomultiplier and was recorded using a PMC-100-4 cooled high speed PMT detection head (Becker & Hickl). Images were acquired using a Becker & Hickl SPC 830 module.

The analysis of fluorescence decays was carried out using a nonlinear, least-squares iterative convolution method based on the Marquardt algorithm<sup>28</sup> through the use of the software SPCImage software (Beker & Hickl, Berlin, Germany).

## **2.6 Mitochondria permeability transition (MPT) detection**

MPT was measured spectrophotometrically during 30-min incubations at 37°C using mitochondria (1 mg of protein/ml) suspended in 3 ml of a Chelex-100–treated buffer containing 0.1 M NaCl, 10 mM MOPS, pH 7.4<sup>10</sup>. Mitochondrial swelling was monitored at 540 nm in a Beckman DU 64 spectrophotometer. Basal values of mitochondria absorbance were measured for 5 min.

## **2.7 Lipid vesicle preparation**

100 nm large unilamellar vesicles (LUVs) were prepared through extrusion as previously described<sup>29</sup>. Vesicles were suspended in Tris buffer (10 mM Tris, 150 mM NaCl at pH 8.0, prepared in Milli-Q water) followed by freeze–thaw cycles and extrusion through polycarbonate filters (100 nm pore size). Liposomes with encapsulated dye were prepared in 10 mM Tris, 150 mM NaCl, 90 mM 5(6)-carboxyfluorescein (CF) at pH 8.0. Non-encapsulated CF was separated from the liposomes by gel filtration chromatography on a Sephadex G-50 column.

All LUVs were kept at room temperature and in the dark until being used, at most for 48 h after being prepared. Lipid concentrations were determined by phosphorous analysis<sup>30</sup> and Chol concentration was determined gravimetrically.

## **2.8 Membrane fluidity measurements in isolated mitochondria and protein-free liposomes**

Fluorescence steady-state measurements of di-4-ANEPPDHQ were performed as previously described<sup>14</sup>. The fluorescence intensities were calculated through integration of the emission spectra obtained, and background fluorescence intensity was always subtracted. For measurement of mitochondrial membrane fluidity, isolated rat liver mitochondria were incubated with 5  $\mu$ M di-4-ANEPPDHQ for 1h. Unbound probe was removed through a 10-minute centrifugation (7000 g) at 4°C. Fluorescence anisotropy values of di-4-ANEPPDHQ ( $\lambda_{exc} = 460$  nm;  $\lambda_{em} = 590$  nm) were determined after incubating these samples with bile acids at 37°C. Di-4-ANEPPDHQ were incorporated in LUVs mimicking mitochondrial membranes at a probe to lipid ratio of 1/200.

## 2.9 Leakage assays in protein free liposomes

In the 5(6)-carboxyfluorescein (CF) leakage assay ( $\lambda_{\text{exc}} = 492 \text{ nm}$ ;  $\lambda_{\text{em}} = 517 \text{ nm}$ ), LUVs encapsulating CF in suspensions containing  $200 \mu\text{M}$  of lipids were incubated with  $100\text{-}500 \mu\text{M}$  of bile acids. Complete (100%) permeabilization was achieved via the addition of Triton X-100 to a final concentration of 1%. Spontaneous leakage was always measured in the absence of bile acids, and experiments were conducted at  $25^\circ\text{C}$ . The percentage of CF leakage induced by bile acids was calculated as:  $\text{Leakage (\%)} = 100 \times [(F - F_0) - (F_c - F_0)] / (F_t - F_0)$ , in which  $F$  and  $F_t$  are the fluorescence intensity prior to and after the addition of the Triton X-100 (after incubation with bile acids), respectively, and  $F_0$  and  $F_c$  are the fluorescence of intact vesicles before and after the same incubation time. In this way, leakage values were corrected for any intrinsic leakage observed in the absence of bile acids.

## 3. Results

### ***Concentration and time-dependent effect of cytotoxic and cytoprotective bile acids on hepatocyte viability and apoptosis***

In order to investigate a possible correlation between programmed cell death and changes in hepatocyte membrane order after treatment with bile acids, we first studied the concentration and time-dependent effect of the cytotoxic and cytoprotective bile acids on cell viability and on the triggering of apoptosis (Figure 1). Results clearly show that at the lower concentrations used ( $100 \mu\text{M}$ ), only cells treated with DCA have significantly lower viability and highly upregulated apoptosis overtime (Fig. 1A,C). Increased levels of apoptosis during DCA treatment are only detected after an incubation of 4h (Fig. 1C), and cell viability starts to decrease after this time (Fig. 1A). For a necrosis-inducing concentration of DCA ( $500 \mu\text{M}$ ), a significant decline in cellular viability and drastically higher apoptosis levels are already detected 2h hours after the start of the treatment (Fig.1B,D). Lower levels of apoptosis were detected for longer incubation times, probably as a result of necrosis. At this higher concentration, UDCA is no longer cytoprotective and an up-regulation of apoptosis is detected as well as a significant decrease in cell viability. TUDCA, on the other hand, did not demonstrate significant toxicity even after 24h of hepatocyte treatment at  $500 \mu\text{M}$  of the bile acid.

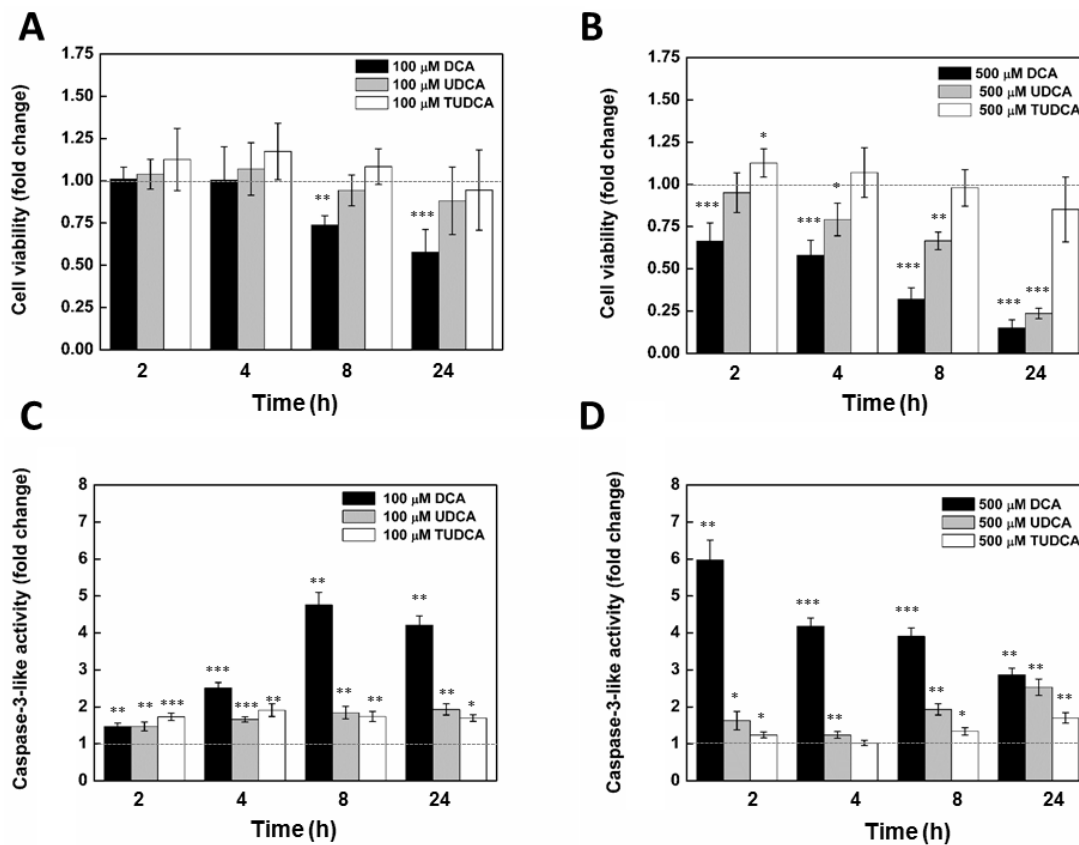


**Figure 1. Concentration and time dependency of cellular viability and caspase-3-like activity of primary rat hepatocytes in the presence of cytotoxic and cytoprotective bile acids.** Cells were isolated as described in Material and Methods and treated with 100 (A,C) or 500  $\mu\text{M}$  (B,D) of DCA (black), or the cytoprotective UDCA (gray)/TUDCA (white) bile acids. Both cellular viability (A,B) and caspase-3-like activity (C,D) in hepatocytes were measured with the ApoTox-Glo triplex assay. Values for both cellular viability and caspase-3-like activity are normalized to control samples from respective time point. Results are expressed as mean  $\pm$  SEM fold change of at least 3 independent experiments. \*  $p < 0.05$ , \*\*  $p < 0.01$ , and \*\*\*  $p < 0.001$  from respective time point control.

### ***Impact of cytotoxic and cytoprotective bile acids on plasma membrane and intracellular membrane fluidity***

Recent results on the interaction of cytotoxic bile acids such as DCA with membrane model systems and on GPMVs<sup>14,17</sup> have confirmed that apoptosis-inducing bile acids are able to modulate lipid membrane fluidity, suggesting that their physiological activity could be associated with this effect. Different organelles have been anticipated as targets for cytotoxic bile acids, namely the plasma membrane<sup>17</sup> and the mitochondria<sup>20</sup>. Our approach to elucidate

this issue was to carry out a quantitative evaluation of the impact of physiologically active DCA concentrations on the membrane order of both these organelles.

Confocal microscopy measurements on rat hepatocytes were carried out using fluorescent probes sensitive to membrane order. Both di-4-ANEPPDHQ<sup>31,32</sup> and Laurdan<sup>33,34</sup> have proven to be extremely sensitive to changes in membrane order through changes in their fluorescence emission spectra or lifetimes. Both molecules sense the reorientation of solvent dipoles, whose strength is directly dependent on membrane fluidity, this being related to water penetration within membranes<sup>31,33</sup>. The measurement of shifts in Laurdan emission spectra through ratiometric imaging<sup>25</sup> and changes of di-4-ANEPPDHQ fluorescence lifetime through FLIM<sup>32</sup>, are widely used methodologies that allow for a quantitative assessment of membrane order in living cells.

The membrane probe di-4-ANEPPDHQ failed to incorporate in hepatocytes so that only Laurdan was used to detect bile acid induced changes in the membrane order of these cells. Laurdan fluorescence emission spectral shifts were quantified through the generalized polarization (GP) function, and higher GP values are associated with higher membrane ordering. In agreement, higher GP values were measured for the plasma membrane, than in intracellular membranes (Fig. 2A, Supplemental Figure 2). This was expected since cholesterol concentration is much higher in the plasma membrane. The membrane order of untreated hepatocytes changed overtime in a reproducible way (Supplemental Figure 2), probably due to the adaptation of cells to the culture environment. From this experiment, control values are obtained ( $GP_{\text{control}}$ ), this allowing to determine the relative GP variations ( $\Delta GP = GP_{\text{bile acid}} - GP_{\text{control}}$ ), for each bile acid and incubation time. These values are shown in Fig. 2B-F. Results are presented for both the average  $\Delta GP$  of intracellular membranes (Fig. 2B-D), and for the plasma membrane (Fig. 2E-F) of bile-acid treated hepatocytes compared to untreated cells.

After incubation of hepatocytes with 100  $\mu\text{M}$  of DCA during 4h, only a moderate decrease of GP values in intracellular membranes was observed (Fig 2 B), and longer exposures lead to an increase in intracellular membrane order. Exposure to higher (necrosis inducing) concentrations of DCA (500  $\mu\text{M}$ ) virtually eliminated the early decrease in GP values for intracellular membranes, while potentiated the late increase in membrane ordering. Incubations of hepatocytes with UDCA and TUDCA at 100  $\mu\text{M}$  had no impact on intracellular membrane fluidity (Fig. 2 C,D), although higher concentrations of these bile acids also lead to an early decrease in the average intracellular membrane order. However, for both bile acids, Laurdan GP values recovered to control values overtime. This recovery is highly indicative of the presence of cellular compensatory mechanisms such as membrane traffic, lipid synthesis or bile acid efflux, which might contribute to reduce bile acid dependent membrane damage. In light of these results, the late increases in GP values observed after long incubations with DCA, are likely associated with membrane composition changes resulting from cell death,

since they are not detected for cytoprotective bile acids, and that for 100  $\mu$ M DCA, it only occurs after the onset of apoptosis (Fig. 1C) and cell death (Fig. 2G).

The impact on hepatocyte plasma membrane order was moderate for all bile acids studied, even at high concentrations and short (Fig. 2E) or long (Fig. 2F) incubation times. Lower hepatocyte plasma membrane order was detected 1h after incubation with DCA, UDCA, and TUDCA (Fig. 2E), and as observed for intracellular membranes, Laurdan GP recovered over time to values closer to control values (Fig. 2F). Unlike in intracellular membranes, no significant late changes in membrane order were detected for the plasma membrane after DCA treatment, even at necrosis inducing concentrations (Fig.2F).

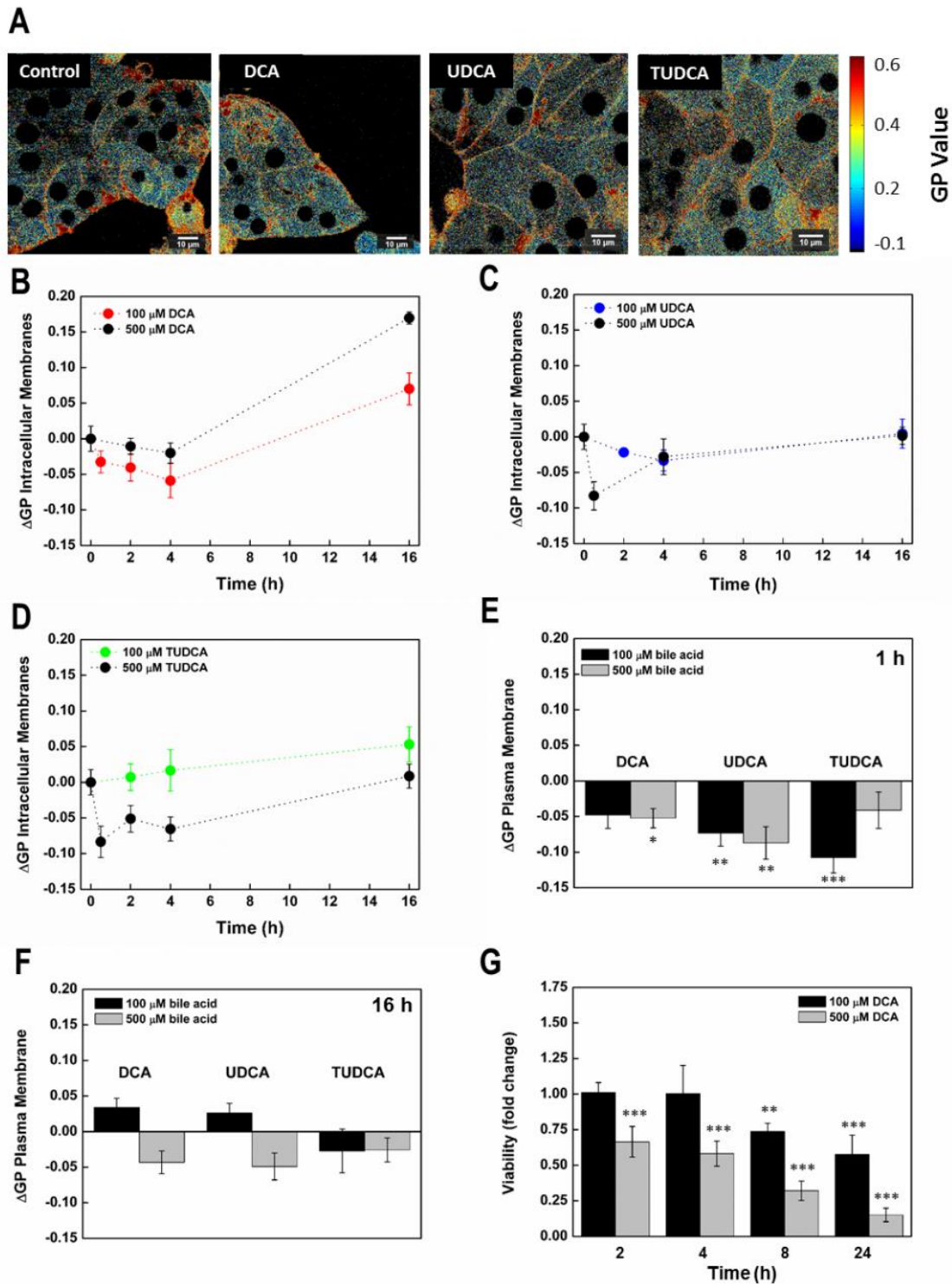


**Figure 2. Changes in Laurdan generalized polarization (GP) values in membranes of rat hepatocytes in the presence of DCA, and the cytoprotective UDCA/TUDCA bile acids.** Laurdan GP values were calculated as described in Material and Methods. GP images of hepatocytes after 30 min incubation with 100  $\mu\text{M}$  of bile acids (A). Relative changes ( $\Delta\text{GP}$ ) between treated and untreated cultures of hepatocytes at different incubation times are shown (B-G). The impact of exposure to bile acids on GP values overtime is shown for hepatocyte intracellular membranes in the presence of DCA (B), UDCA (C), and TUDCA (D) at both 100 and 500  $\mu\text{M}$ . The impact of exposure to bile acids on

hepatocyte plasma membrane GP values is shown both for 1h (E) and 16h (F) incubation. Time-dependency of DCA toxicity on isolated hepatocytes at 100 (black) and 500  $\mu$ M (gray) is also shown for comparison (G). Results are expressed as mean  $\pm$  SEM fold change of at least 12 cells (B-F) or as mean  $\pm$  SEM fold change of at least 3 independent experiments (G). \*  $p < 0.05$ , \*\*  $p < 0.01$ , and \*\*\*  $p < 0.001$  from respective time point control.

The impact of cytotoxic and cytoprotective bile acids on plasma and intracellular membrane structure was also assessed in HEK293T cells. A much lower intracellular bile acid influx is anticipated for the non-hepatic HEK293T cells, given the absence of the bile acid transporters present in hepatocytes<sup>35</sup>, so only the outer leaflet of the plasma membrane is expected to be in contact with a significant concentration of these molecules, eliminating a possible influence of bile acids on mitochondrial membrane properties and on intrinsic apoptotic pathways. In fact, cytotoxicity studies confirmed that this cell line had very low susceptibility for cell death induced by DCA (Supplemental Figure 3). Laurdan GP values in both intracellular and plasma membranes of HEK293T cells after exposure to DCA, UDCA and TUDCA are shown on Figs. 3A-C. In the absence of significant intracellular influx, no changes in intracellular membrane fluidity are also observed (Fig. 3B) and Laurdan GP values for the plasma membrane, which is exposed to bile acids, are largely insensitive to the presence of cytotoxic and cytoprotective bile acids (Fig. 3C).

The alternative sensor for membrane order, di-4-ANEPPDHQ, efficiently incorporated in the plasma membrane of HEK293T cells and was also used to probe for bile acid-induced changes in plasma membrane properties (Fig. 3D-F). Decreases in membrane ordering are expected to induce a significant decrease in fluorescence lifetime of di-4-ANEPPDHQ in living cells<sup>32</sup>, and FLIM measurements were carried out in HEK293T cells before and after a 30 min exposure to bile acids (Fig. 3D). A minor decrease in plasma membrane order after exposure to physiologically active concentrations of bile acids was detectable through di-4-ANEPPDHQ fluorescence lifetimes, since incubation of HEK293T cells with DCA, UDCA and TUDCA, induced a small decrease in the fluorescence lifetime of di-4-ANEPPDHQ (Fig. 3E). As previously observed in hepatocytes with Laurdan, after long incubations with bile acids, membrane fluidity returned to control levels (Fig. 3F). The fact that no significant changes in HEK293T plasma membrane fluidity were observed with Laurdan after exposure to bile acids, but some decrease in membrane order is still observed with di-4-ANEPPDHQ, suggest that the impact of bile acids on the plasma membrane is much higher in the bile acid-exposed outer leaflet, as the translocation of the cationic di-4-ANEPPDHQ across the membrane is very slow, while Laurdan easily flip-flops due to the absence of charge. This is consistent with the

absence of bile acid internalization, when only the outer leaflet of the plasma membrane remains exposed to bile acids.

Since cholesterol was recently shown to modulate the membrane affinity of bile acids<sup>14</sup>, the impact of DCA on plasma membrane order was also evaluated after partial cholesterol depletion with 10 mM cyclodextrin (CD). This concentration of CD has been reported to remove 30-60 % of cellular cholesterol, depending on cell type, and to disrupt membrane rafts<sup>36</sup>. CD treatment reduced plasma membrane order considerably, as reported by the considerable decrease in di-4-ANEPPDHQ fluorescence lifetime, but even after cholesterol depletion, 100  $\mu$ M DCA had no major impact on plasma membrane order (Fig. 3E).

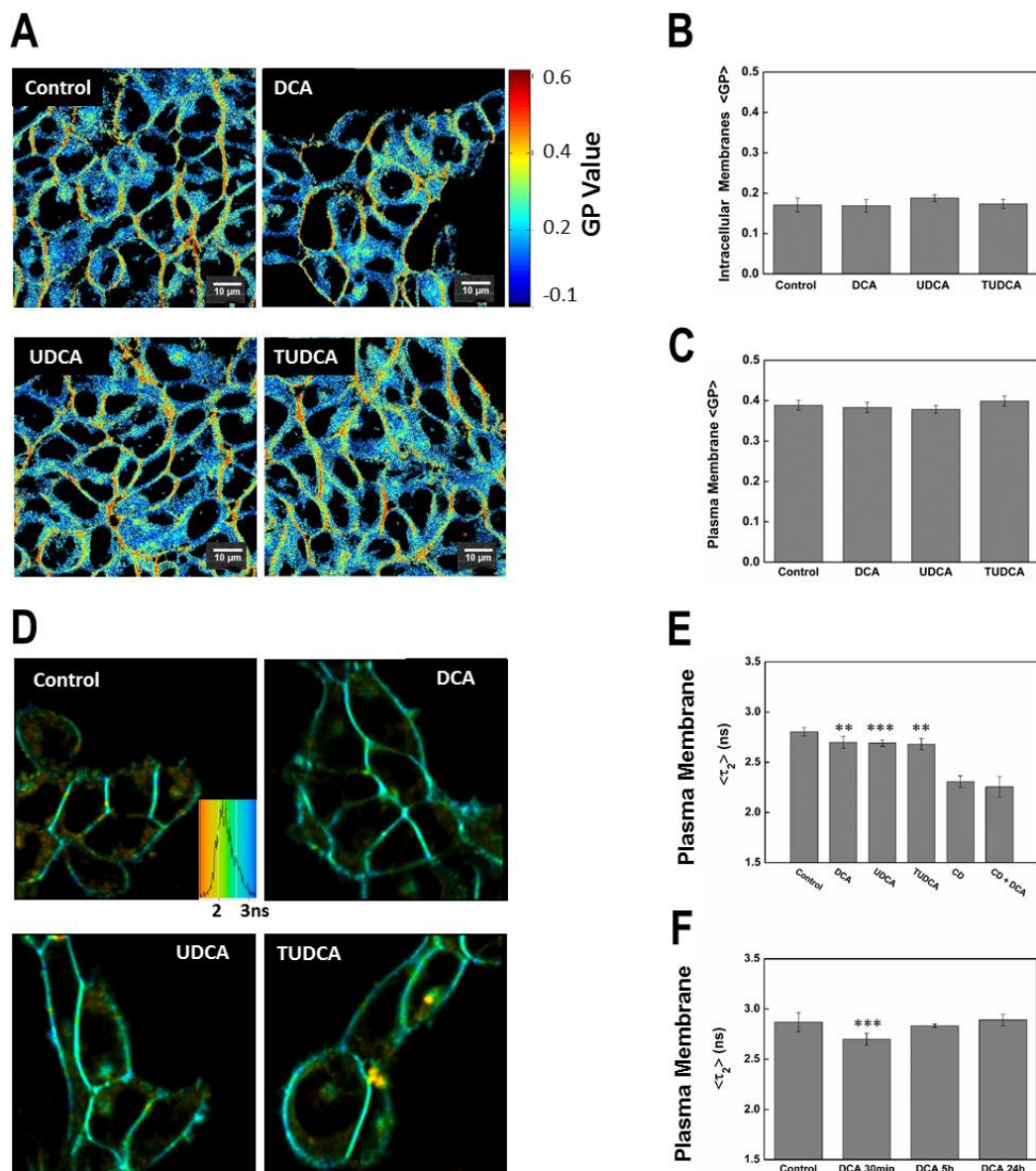


**Figure 3. Impact of DCA and cytoprotective bile acids UDCA/TUDCA on the membrane fluidity of HEK293T cells.** HEK293T cells were loaded either with 5  $\mu$ M of Laurdan (A) or 5  $\mu$ M of di-4-ANEPPDHQ (D) after incubation with 100  $\mu$ M of bile acids for 30 minutes at 37°C. Representative Laurdan GP (A)

and di-4-ANEPPDHQ fluorescence lifetime ( $\tau$ ) (D) images are shown. Laurdan GP values, di-4-ANEPPDHQ fluorescence lifetimes and the respective images were obtained as described in the Materials and Methods section. Average Laurdan GP values after incubation with bile acids are shown for both intracellular (B) and the plasma membranes (C). Average di-4-ANEPPDHQ fluorescence lifetimes are shown for the plasma membrane of HEK293T cells after treatment with bile acids for 30 min. (E). The impact of DCA on the plasma membrane fluidity on HEK293T cells is shown to be time-dependent, as fluorescence lifetimes of di-4-ANEPPDHQ return to control values for incubations longer than 5h (F). Only the value for the longer lifetime component ( $\tau$ ) of di-4-ANEPPDHQ fluorescence decay is shown (E,F), since this component corresponds to  $\sim 97\%$  total fluorescence intensity. Partial cholesterol extraction from the plasma membrane with 10mM CD reduced the order of the plasma membrane as expected (CD), but the plasma membrane order remained insensitive to the presence of DCA, even after cholesterol extraction (CD + DCA). Average GP values are expressed as mean  $\pm$  SEM from an average of 12 individual cells, while average di-4-ANEPPDHQ fluorescence lifetimes are the average of 50-100 cells.

The absence of considerable and non-transient modulation of plasma membrane order by DCA is surprising, given the ability of this bile acid to inhibit cholesterol ordering in membrane model systems<sup>14</sup>. Clearly, the minor changes in plasma membrane properties detected upon DCA treatment of hepatocytes are not responsible for its apoptosis/necrosis promoting effect, since identical relative changes are observed in both DCA-responsive (hepatocytes) and -nonresponsive cells (HEK293T), as well as for noncytotoxic bile acids. These results strongly suggest that changes in plasma membrane order are not the mechanism through which DCA induces apoptosis.

Similarly, the changes detected in intracellular membrane order in hepatocytes after a short incubation period with bile acids were common to all bile acids tested (Figure 2), and only the onset of apoptosis gave rise to considerable hepatocyte intracellular membrane modifications as revealed by their biophysical parameters. In the absence of apoptosis, both hepatocytes and a non-hepatic cell line were shown to have compensatory mechanisms which lead to full abolition of bile acid perturbation of cellular membrane order after long incubations. Thus, it seems evident that the apoptotic modulatory effect of cytoprotective UDCA/TUDCA and cytotoxic DCA is also not the result of indiscriminate changes in the structure of cellular membranes, and more specific mechanisms must account for these effects.

### Subcellular distribution of bile acid derivatives

In order to determine if bile acids have the potential to incorporate in mitochondrial membranes, the distribution of the fluorescent conjugates, DCA-NBD and UDCA-NBD, in living cells was followed through confocal microscopy, both in hepatocytes (Figure 4) and in HEK293T cells (Figure 5). Similar fluorescent conjugates of bile acids have been extensively employed to study the mechanisms of uptake and excretion of bile acids by hepatocytes<sup>37–40</sup>. These bile acid fluorescent analogues were characterized in a previous study, where DCA-NBD and UDCA-NBD were shown to have a superficial location in lipid membranes and to interact preferentially with less ordered liposomes, in agreement with results obtained with unmodified bile acids<sup>14</sup>. Thus, the labeled bile acids are expected to be adequate reporters for the intracellular distribution of unmodified bile acids. However, some important differences between the modified and unmodified molecules are still present, namely, since the fluorescent analogues are uncharged, cellular uptake does not require membrane transporters and uptake by both hepatic and non-hepatic cells (HEK293T) is passive and fast (Figures 4,5).

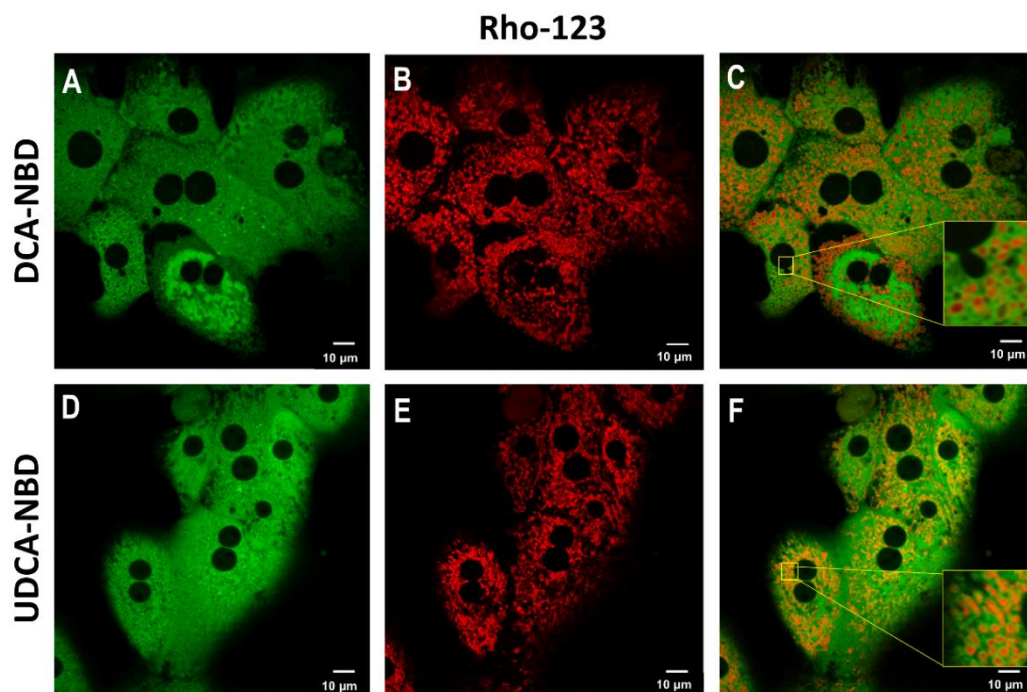


**Figure 4. Subcellular distribution of bile acid fluorescent analogues in hepatocytes.** Representative confocal microscopy analysis of the subcellular distribution of DCA-NBD (A) and UDCA-NBD (D) in hepatocytes after internalization. Rat liver hepatocytes were incubated with 20  $\mu$ M of bile acid analogues during 30 min at 37°C. Mitochondria were fluorescently stained with 5  $\mu$ M Rho-123 for 15 minutes at 37°C (B, E). Overlay images are shown (C, F). Inset images show the presence of bile acid analogues in the outer mitochondrial membrane (OMM).

Rho-123 is a non-cytotoxic, cell-permeant, cationic dye, that is rapidly sequestered in the matrix space of polarized mitochondria<sup>41</sup>. Hepatocytes were incubated with Rho-123 and either DCA-NBD or UDCA-NBD, and the respective fluorescence confocal microscopy images are shown in Figure 4. Efficient mitochondria labeling by Rho-123 on hepatocytes was observed (Fig. 4B,E), while DCA-NBD and UDCA-NBD are found to incorporate non-specifically in intracellular membranes. The bile acid analogues exhibit a very limited insertion in the plasma membrane, suggesting a low affinity for this environment. The concentrations of the bile acid analogues in the cytosol are also relatively low. Both bile acid analogues are also clearly shown to insert in the mitochondrial membranes of hepatocytes (Fig. 4C, F - insets). Full overlap of Rho-123 and bile acid-NBD fluorescence is not observed, since Rho-123 is found within the matrix space of mitochondria and the bile acid analogues insert mostly in the outer mitochondrial membranes (Supplemental Figure 4).

Interaction of bile acid analogues with mitochondria is not specific to hepatocytes, as it is also observed in HEK293T cells. In these cells, DCA-NBD fluorescence is also found in mitochondria as evidenced by partial colocalization of Rho-123 marker and DCA-NBD (Fig. 5C). This partial colocalization is confirmed and quantified through calculation of products of the difference from the mean (PDM) (Fig. 5D) and of the Pearson's correlation coefficient ( $\langle R_p \rangle$ ) of the two signals (Fig. 5H). Although this colocalization is clear, DCA-NBD fluorescence is again observed throughout different intracellular compartments, revealing no apparent specific enrichment (Fig. 5B,F). As in hepatocytes, very little DCA-NBD fluorescence is detected in the plasma membrane (Fig. 5E-H).

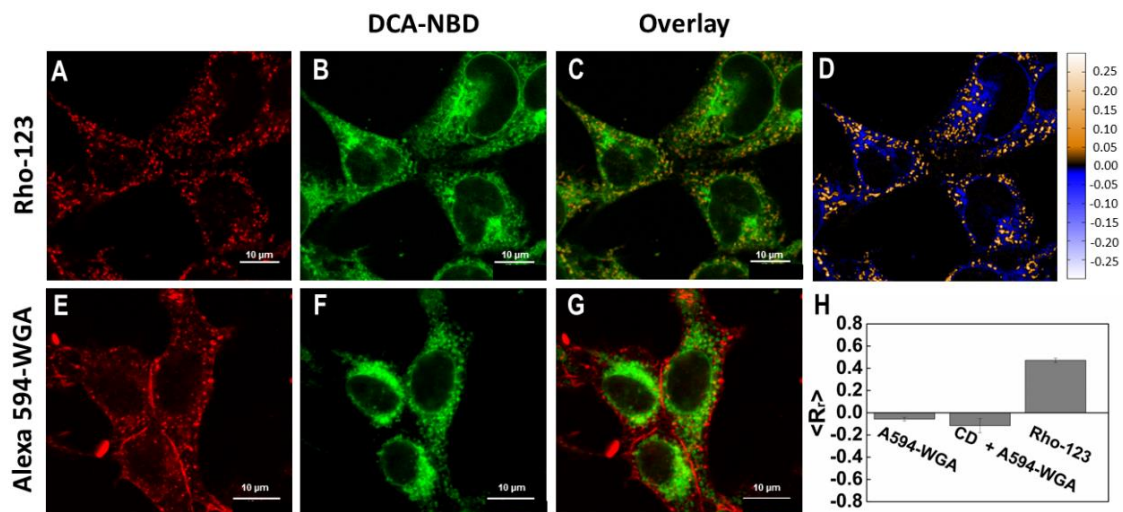


**Figure 5. Subcellular distribution of DCA-NBD in HEK293T cells.** Mitochondria or plasma membrane of HEK293T cells were fluorescently stained with 5  $\mu$ M Rho-123 (mitochondrial marker) (A) and 130 nM Alexa 594-WGA (plasma membrane marker) (E), respectively. The subcellular distribution of 20  $\mu$ M of DCA-NBD (B, F) in these cells after internalization is also shown by colocalization analysis. Overlay

images for DCA-NBD fluorescence and mitochondria (C) or plasma membrane staining (G) are also shown. DCA-NBD distributes through different organelles, including mitochondria, showing clear insertion of DCA-NBD in mitochondria (C, Inset). As a result, positive products of the differences from the mean (PDM, <sup>27</sup>) values are obtained within the mitochondria, while other intracellular organelles loaded with DCA-NBD present negative PDM values (D). Pearson correlation coefficients ( $R_r$ ) <sup>27</sup> confirm partial colocalization between DCA-NBD and Rho-123 signals as well as poor colocalization of DCA-NBD with the plasma membrane marker A594-WGA (H). Partial cholesterol extraction with 10mM CD did not increase incorporation of DCA-NBD in the plasma membrane (CD + A594-WGA) (H). Results are expressed as mean  $\pm$  SEM of 50-60 cells.

Previous work with model membranes showed that membrane ordering and cholesterol concentration dramatically influenced the partition of both cytotoxic and cytoprotective bile acids to lipid membranes<sup>14</sup>. The preference of DCA-NBD for intracellular membranes, which present significantly lower cholesterol concentration compared to the plasma membrane, suggested that this property could contribute to define the preferential sites for accumulation of bile acids intracellularly. However, cholesterol depletion and membrane raft disruption with 10 mM CD had no impact on the concentration of DCA-NBD in the plasma membrane (Fig. 5H). Thus, it is unlikely that exclusion of bile acids from the plasma membrane is solely dictated by differences in cholesterol concentration and other unknown factors are expected to be responsible for this effect.

The results for the subcellular distribution of UDCA-NBD after uptake in HEK293T cells are largely analogous to those obtained with DCA-NBD (Supplemental Figure 5). Cytoprotective UDCA-NBD is also found in mitochondrial membranes, while very little UDCA-NBD is detected at the plasma membrane. These results reinforce the notion that apoptosis modulation by bile acids is likely not the result of changes in plasma membrane organization.

### ***Impact of cytotoxic and cytoprotective bile acids on mitochondrial membranes***

The ability of bile acid conjugates to bind to mitochondria was also confirmed through steady-state fluorescence intensity measurements of bile acid fluorescent analogues. Incubation of both DCA-NBD and UDCA-NBD with freshly isolated liver mitochondria resulted in an increase in fluorescence intensity of the labeled bile acids, which is a clear evidence of interaction (Supplemental Figure 6).

Given the presence of both classes of bile acids in the mitochondrial membrane during incubation of living cells, there is a strong potential for modulation of mitochondrial membrane properties. Since the integrity of mitochondrial membranes is essential for cellular survival, these changes might also potentially lead to an activation/inhibition of MPT. Importantly,

changes in mitochondrial membrane fluidity have been correlated with differential Bax activation and apoptosis<sup>42</sup>, and import of glutathione into the mitochondria (mGSH)<sup>43</sup>. Recently, it was demonstrated through electron microscopy of isolated mitochondria, that after exposure to toxic concentrations of bile acids, mitochondria undergo a dramatic reorganization of the MOM before the onset of MPT, suggesting that the MOM is the major target site for cytotoxic bile acids within mitochondria<sup>20</sup>. Previous studies had also identified changes in average membrane fluidity of isolated mitochondria after exposure to toxic bile acids<sup>44</sup>. Here, we aimed to follow in real time the changes in MOM properties and correlate these changes with the onset of MPT. Although during *in vivo* cholestasis, the total intracellular concentrations of bile acids in hepatocytes are reported to be ~800  $\mu\text{M}$ <sup>45,46</sup>, it is difficult to estimate the intracellular concentration of free bile acids as a significant population is expected to be complexed with membranes and proteins. For this reason, we choose to carry out measurements with isolated mitochondria at identical concentrations than used in the other experiments, so that direct comparisons for membrane sensitivity to DCA insertion can be established.

Measurements of MOM fluidity in functional freshly isolated mitochondria were carried out using di-4-ANEPPDHQ (Figure 6), whose fluorescence properties have been shown to be extremely sensitive to membrane composition and order<sup>25</sup>. Although the MOM is permeable to small hydrophilic molecules due to the presence of mitochondrial porins<sup>47</sup>, di-4-ANEPPDHQ is expected to selectively stain the MOM, as a result of the presence of two cationic groups and a large hydrophobic moiety in this molecule, which drastically minimize flip-flop across membranes<sup>31</sup> and porin transport<sup>47</sup>, respectively. The fluorescent membrane probe readily incorporated in isolated mitochondria and unbound di-4-ANEPPDHQ was removed through centrifugation. Fluorescence anisotropy of membrane inserted probes such as di-4-ANEPPDHQ, is ideally suited to follow changes in membrane structure/dynamics. In fact, since rotation of these molecules is hindered within membranes, any structural or dynamical change in membrane properties will affect the rotational freedom of the molecule, and this is easily detected through steady-state fluorescence anisotropy ( $\langle r \rangle$ ) measurements. The fluorescence anisotropy of di-4-ANEPPDHQ within isolated mitochondria was measured to be  $\langle r \rangle \sim 0.24$  (Figure 6).

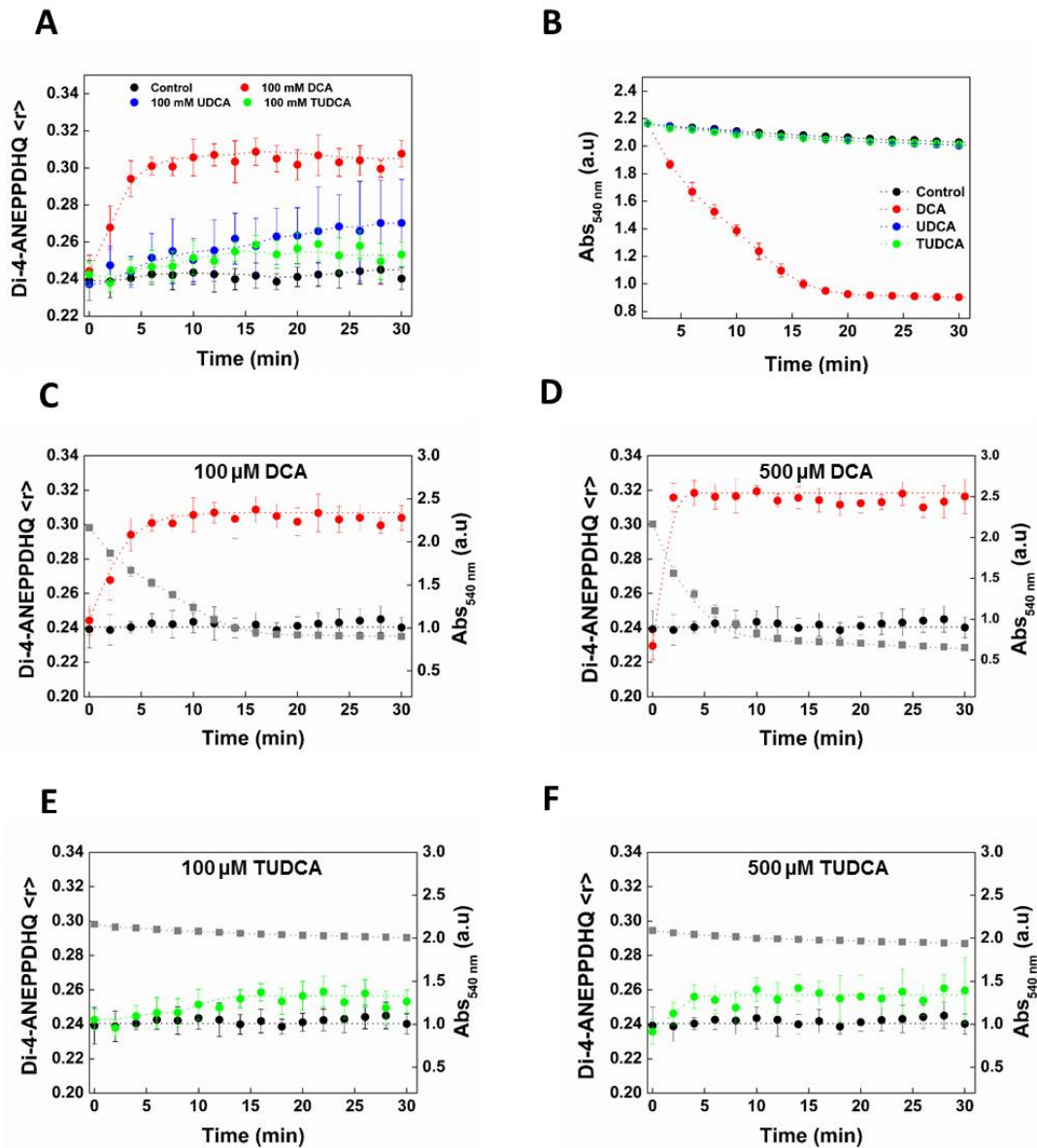


**Figure 6. DCA induces changes in MOM structure which precede the onset of MPT.** Comparison between changes in membrane order of freshly isolated rat liver mitochondria overtime after exposure to DCA (red), UDCA (blue) and TUDCA (green) at 100  $\mu$ M (A). Mitochondrial membrane order in freshly isolated rat liver mitochondria was monitored through fluorescence anisotropy measurements of di-4-ANEPPDHQ after removal of unbound membrane probe by centrifugation. Control values (untreated samples) are shown in black. Detection of mitochondrial swelling after exposure of isolated rat liver mitochondria to DCA (red), UDCA (blue) and TUDCA (green) at 100  $\mu$ M (B). Control values are shown in black. Mitochondrial swelling was detected through changes in O.D. at 540 nm. Changes in the fluorescence anisotropy of di-4-ANEPPDHQ (red) and mitochondrial swelling (gray) for isolated mitochondria in the presence of 100  $\mu$ M DCA (C) and 500  $\mu$ M DCA (D). Results for mitochondrial membrane order (green) and mitochondrial swelling (gray) for isolated mitochondria in the presence of 100  $\mu$ M TUDCA (E) and 500  $\mu$ M TUDCA (F). Control values for di-4-ANEPPDHQ fluorescence anisotropy are shown in black.

The fluorescence anisotropy ( $\langle r \rangle$ ) of di-4-ANEPPDHQ within MOM increased immediately after exposure of isolated mitochondria to DCA, in a concentration dependent manner. At lower concentrations of DCA (100  $\mu\text{M}$ ), the fluorescence anisotropy of di-4-ANEPPDHQ stabilized at  $\langle r \rangle \sim 0.30$ , 10 min. after the start of the incubation, while for necrosis-inducing concentrations (500  $\mu\text{M}$ ), the fluorescence anisotropy reached  $\langle r \rangle \sim 0.32$ , just 2 min. after the start of the incubation (Fig. 6 C,D). The fluorescence anisotropy is dependent on both rotational motions and on the fluorescence lifetime of the fluorophore, as described by Perrin's equation<sup>48</sup>, but although a minor fluorescence quenching of di-4-ANEPPDHQ is observed in the presence of DCA (5-10%, depending on [DCA]), this is outright insufficient to produce the observed changes in fluorescence anisotropy (50-62 % fluorescence quenching would be necessary to induce the observed increases in  $\langle r \rangle$  as dictated by Perrin's equation<sup>48</sup>). Therefore, the increase in fluorescence anisotropy of di-4-ANEPPDHQ within the MOM observed after exposure to DCA is a result of decreased anisotropic rotational motions within the membrane and reflects considerable changes in MOM structure and dynamics. A shift of di-4-ANEPPDHQ fluorescence emission spectra to shorter wavelengths is also observed after exposure to DCA, which is consistent with a less polar environment (Supplemental Figure 7).

The increase in di-4-ANEPPDHQ fluorescence anisotropy in the presence of DCA is considerably faster than the swelling of mitochondria, as detected by changes in O.D. at 540 nm (Fig. 6B-D), suggesting that the structural changes observed in the MOM precede activation of MPT. On the other hand, UDCA and TUDCA only induced minor increases in the fluorescence anisotropy of di-4-ANEPPDHQ (Fig. 6A,E,F), and did not lead to activation of MPT, as no swelling was detected (Fig. 6B).

For comparison purposes, protein-free liposomes mimetic of MOM were also prepared with a lipid composition of PC:PE:PI:Cl:Chol 48:25:12:6:9<sup>49-53</sup>. Mitochondrial phospholipid composition varies little among different cells, and although the concentration of cardiolipin at the MOM is still a controversial subject<sup>51,53</sup>, the presence of significant concentrations of this lipid at mitochondrial contact sites (MCSs) has been extensively confirmed<sup>50,53</sup>. The fluorescence anisotropy of di-4-ANEPPDHQ within MOM mimetic liposomes is significantly higher ( $\langle r \rangle \sim 0.30$ ) than the value obtained for di-4-ANEPPDHQ within isolated mitochondria (Figure 7). Since the fluorescence anisotropy of di-4-ANEPPDHQ exhibited very little sensitivity to small changes in the proportion of the lipid components of liposomes mimetic of MOM (results not shown), the observed differences cannot be attributed to the uncertainty in mitochondrial membrane lipid composition and must be associated either with differences in structure (absence of mitochondrial double membrane structure in protein-free liposomes

mimetic of MOM), with the asymmetric distribution of lipids in mitochondrial membranes, or with the presence of proteins within the MOM<sup>53</sup>.

The specific nature of the structural changes detected in the MOM after exposure to DCA are unclear, since no alteration in di-4-ANEPPDHQ fluorescence anisotropy is observed in protein-free liposomes mimicking the MOM lipid composition after exposure to DCA, even at high concentrations (Fig.7A). No changes in di-4-ANEPPDHQ, fluorescence emission spectra after incubation with DCA were identified as well (results not shown). MOM mimetic liposomes were loaded with carboxyfluorescein (CF) under fluorescence self-quenching conditions and were exposed for 1h to 100  $\mu$ M of DCA, UDCA, and TUDCA. The increase in fluorescence intensity is proportional to the fraction of CF released and can be used to estimate liposome permeability to small molecules (% CF leakage). At apoptotic concentrations of DCA, the permeability of these protein-free liposomes mimicking MOM lipid composition was only marginally increased, without significant differences between cytotoxic and cytoprotective bile acids (Fig.7B, Supplemental Figure 8).

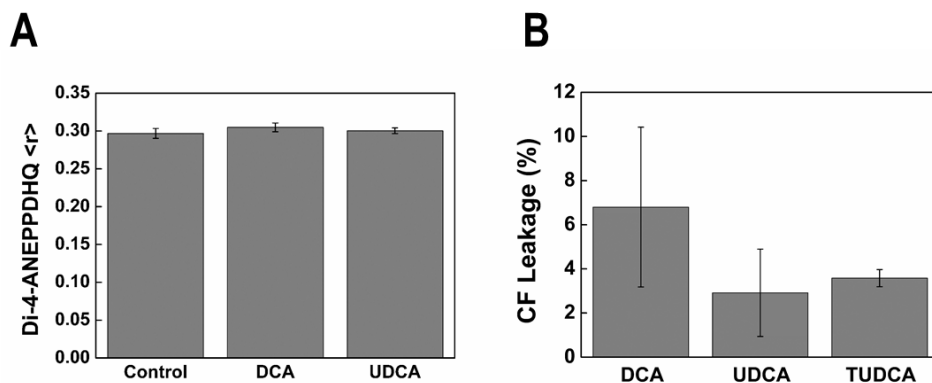


**Figure 7. Impact of bile acids on membrane fluidity and permeability of liposomes mimicking MOM composition.** Fluorescence anisotropy measurements of di-4-ANEPPDHQ within protein-free liposomes mimicking MOM lipid composition (PC:PE:PI:Cl:Chol 48:25:12:6:9) (A). Measurements in the presence of 500  $\mu$ M of DCA or UDCA were carried out after a 15 min. incubation with the bile acid. MOM biomimetic liposomes were loaded with 90 mM CF (under fluorescence self-quenching conditions) and exposed for 1 hour at room temperature to 100  $\mu$ M of DCA, UDCA, and TUDCA at room temperature (B). Results are shown for the increase in CF leakage from liposomes. The increase in CF fluorescence intensity is proportional to the fraction of CF released and can be used to evaluate liposome permeability as described in the Materials and Methods section.

These results are strongly supportive of the notion that DCA, in the range of concentrations where it is physiologically active, does not increase mitochondrial membrane permeability through direct modulation of the mitochondrial lipid structure, and DCA apoptotic activity depends on features of mitochondrial membranes that are absent from protein-free

mimetic liposomes, namely the mitochondrial double membrane structure, the asymmetric distribution of lipids or the mitochondrial protein environment.

## 4. Discussion

Cytotoxic bile acids have been shown to induce cell death through multiple pathways, depending on its concentration<sup>3,4</sup> but the corresponding mechanism of action of these molecules is still highly ambiguous and a matter of much debate, as the target of these molecules has recently been alternatively suggested to be the plasma membrane<sup>17</sup> or the mitochondrial outer membrane<sup>20</sup>. Our previous studies have demonstrated that at physiologically active concentrations, cytotoxic bile acids have the potential to modulate the structure of lipid membranes, but only for certain lipidic compositions, namely in the presence of low concentrations of cholesterol<sup>14</sup>. These results confirmed that the mechanism of action of cytotoxic bile acids could be associated with modulation of membrane properties but did not offer any information on the cellular target of these molecules. In order to address this issue, we aimed here to carry out a comprehensive study on the impact of physiologically active concentrations of the cytotoxic bile acid DCA on the membrane structure of both the plasma membrane and the MOM of isolated hepatocytes. Since the detection of membrane structural changes is not by itself evidence that the impacted organelle is the site of action of DCA, we also carried out time-dependent quantitative measurements of membrane fluidity (both on live cells and isolated organelles), cell death, apoptosis, and mitochondrial swelling, which allowed for correlations to be established. Both concentrations of DCA previously shown to induce apoptosis (100  $\mu\text{M}$ ) and necrosis (500  $\mu\text{M}$ ) were tested to probe for distinctive patterns of membrane perturbation associated with each of the cell death pathways. Experiments were also always carried out in parallel with cytoprotective bile acids for comparison.

Ours results clearly show that the fluidity of the plasma membrane increases after exposure to DCA or to the cytoprotective UDCA or TUDCA, as evaluated from changes in Laurdan GP values (Fig. 2E). A similar effect is also observed for HEK293T cells (Fig. 3E), which are not susceptible to DCA-induced cell death and for which a much lower bile-acid influx is expected, given the absence of the bile acid transporters. As a result of the lower intracellular concentrations of bile acids within these cells, the membrane order of the outer leaflet of the plasma membrane seems to be more sensitive to the presence of bile acids than the inner leaflet. However, plasma membrane fluidity for both cell types quickly recovered to control values after < 5h of incubation (Fig. 2F, Fig. 3F), suggesting that efficient cellular

mechanisms are present to compensate for this effect. Such compensatory mechanisms had also been previously observed when cytotoxic bile acids induced a much larger impact on isolated giant plasma membrane vesicles (GPMVs) than on the plasma membrane of living cells<sup>17</sup>. Although we cannot totally exclude an effect of bile acids on very specific plasma membrane components, these results strongly suggest that nonspecific changes in plasma membrane biophysical properties are not the mechanism through which DCA induces apoptosis in healthy hepatocytes. These results were further supported by the detection through confocal microscopy of very low levels of bile acid fluorescent analogues in the plasma membrane of hepatocytes (Figure 4).

For hepatocyte intracellular membranes, the average membrane fluidity also increases initially (Laurdan  $\Delta GP$  decreases) after incubation with both cytoprotective and cytotoxic bile acids (Fig. 2 B-D). As in the plasma membrane, membrane fluidity recovers to control values for cytoprotective bile acids, suggesting similar compensatory effects. However, only for the cytotoxic DCA, a late decrease in membrane fluidity (Laurdan  $\Delta GP$  increases) is observed (Fig. 2B). This is associated with compositional changes in intracellular membranes of dead/dying cells, since they only occur after the onset of apoptosis and cell death (Fig. 1C, Fig. 2G). Again, the impact of DCA and the non-toxic bile acid TUDCA on the average intracellular membrane fluidity (before the onset of apoptosis and cell-death), suggests that the overall decrease in membrane fluidity detected shortly after incubation with DCA is not responsible for the activation of cell death pathways.

Since neither changes in plasma membrane structure or generalized changes in intracellular membrane fluidity are responsible for the physiological impact of DCA, activation of cell death must be associated with an alternative target. Confocal microscopy measurements with both bile acid fluorescent analogues studied (DCA-NBD and UDCA-NBD) showed no evidence of enrichment in specific organelles. However, mitochondria were shown here to incorporate significant levels of these molecules. Given that resistance to cytotoxic bile acids by specific cell types have been associated with both up-regulation of Bcl-2 proteins<sup>54,55</sup>, as well as changes in mitochondria membrane composition<sup>56</sup>, and that cytotoxic bile acids have been shown to induce MPT, cytochrome *c* release from isolated mitochondria and changes in MOM morphology<sup>20,57</sup>, it is reasonable to assume that mitochondrial membranes are a likely target for these molecules.

After incubation of isolated mitochondria with DCA, both time- and concentration dependent perturbations of MOM structure were detected, as revealed by fluorescence anisotropy measurements of di-4-ANEPPDHQ (Figure 6). These membrane changes preceded the MPT, and are likely related to the previously observed morphological changes in

MOM morphology during incubation of isolated mitochondria with toxic bile acids<sup>20</sup>. Importantly, cytoprotective bile acids were not able to alter mitochondrial membrane structure, unlike previously observed for other organelles (Figure 2). Thus, our results strongly suggest that unlike the plasma membrane, the MOM structure is specifically modified by cytotoxic bile acids. The protein and lipid makeup of these two compartments is drastically different<sup>52,58</sup>, which could justify the much greater affinity of bile acid analogues for the mitochondrial membranes (Figures 4,5). These results are consistent with a mechanism of action involving triggering of cell death through a mitochondria-dependent pathway. This would be in agreement with reports showing that changes in mitochondrial membrane properties are correlated with differential Bax activation and apoptosis<sup>42</sup>, and import of glutathione into the mitochondria (mGSH)<sup>43</sup>. Such modulation of cell death by modification of mitochondria outer membrane structure could also help explain why cytotoxic bile acids induce the mitochondrial translocation of Bcl-2 proteins<sup>3,7,59,60</sup>. In this case, the extent of mitochondria membrane perturbation by cytotoxic bile acids could contribute for the definition of cell death pathway, as apoptotic and necrotic-inducing concentrations of DCA perturbed the MOM to different degrees (Figure 7). Our data also shows that the changes in mitochondrial membrane fluidity and permeability induced by DCA were not reproduced in protein-free liposomes with a lipidic composition mimetic of the MOM. These results indicate that the DCA apoptotic activity depends on features of mitochondrial membranes which are absent from protein-free mimetic liposomes, such as the double membrane structure, lipid asymmetry or the mitochondrial protein environment. It is also relevant that both cytoprotective bile acids used in this work did not induce significant non-transient changes in any of the cellular membranes studied. Therefore, their mechanism of action is likely not associated with direct perturbation of the membrane fluidity of neither the plasma membrane or the mitochondria.

In this report, we aimed to clarify the current ambiguity on the possible cellular targets of cytotoxic bile acids. The application in this study of a reductionist approach relying on the use of cell cultures, isolated mitochondria and protein-free liposomes has its limitations because, *in vivo*, the membranes of the different cellular organelles will be exposed to a considerably more complex mixture of bile acids, as well as to a much greater heterogeneity in both protein-bile acid and lipid-bile acid complexes. However, the results presented here, strongly suggest that mitochondrial membranes are more susceptible to DCA-induced structural changes than the plasma membrane and support a model of mitochondria-dependent pathway for cell death modulation by DCA, induced by perturbation of the mitochondrial membrane environment.

We show that while both toxic (DCA) and non-toxic bile acids (UDCA, TUDCA) induce an increase in the average membrane fluidity of hepatocytes, these effects are transient and not correlated with apoptosis. Importantly, the plasma membrane is only moderately affected

by both classes of bile acids, including in non-hepatic cells which are not susceptible to apoptosis by DCA. On the other hand, mitochondrial outer membrane structure is shown to be heavily perturbed in the presence of DCA, while only marginally sensitive to the presence of nontoxic concentrations of UDCA/TUDCA. MOM perturbation by DCA also precedes the onset of MPT, suggesting a possible link between the two processes.

### **Acknowledgements/Grant Support**

Authors acknowledge funding by FCT project references RECI/CTM-POL/0342/2012, PTDC/QUI-BIO/119494/2010. T.S, S.N.P. and F.F are the recipients of fellowships from FCT (SFRH/BD/92398/2013, SFRH/BPD/92409/2013 and SFRH/BPD/64320/2009, respectively).

## **5. References**

1. Schmucker DL, Ohta M, Kanai S, Sato Y, K. K. Hepatic injury induced by bile salts: correlation between biochemical and morphological events. *Hepatology* **12**, 1216–21 (1990).
2. Yamazaki, M., Miyake, M., Sato, H., Masutomi, N., Tsutsui, N., Adam, K.-P., Alexander, D. C., Lawton, K. a, Milburn, M. V, Ryals, J. a, Wulff, J. E. & Guo, L. Perturbation of bile acid homeostasis is an early pathogenesis event of drug induced liver injury in rats. *Toxicol. Appl. Pharmacol.* **268**, 79–89 (2013).
3. Castro, R. E., Amaral, J. D., Solá, S., Kren, B. T., Steer, C. J. & Rodrigues, C. M. P. Differential regulation of cyclin D1 and cell death by bile acids in primary rat hepatocytes. *Am. J. Physiol. Gastrointest. Liver Physiol.* **293**, G327-34 (2007).
4. Gumprich, E., Devereaux, M. W., Dahl, R. H. & Sokol, R. J. Glutathione status of isolated rat hepatocytes affects bile acid-induced cellular necrosis but not apoptosis. *Toxicol. Appl. Pharmacol.* **164**, 102–111 (2000).
5. Faubion, W. A., Guicciardi, M. E., Miyoshi, H., Bronk, S. F., Roberts, P. J., Svingen, P. A., Kaufmann, S. H. & Gores, G. J. Toxic bile salts induce rodent hepatocyte apoptosis via direct activation of Fas. *J. Clin. Invest.* **103**, 137–45 (1999).
6. Ferreira, D. M. S., Afonso, M. B., Rodrigues, P. M., Simão, A. L., Pereira, D. M., Borralho, P. M., Rodrigues, C. M. P. & Castro, R. E. c-Jun N-Terminal Kinase 1/c-Jun

- Activation of the p53/MicroRNA 34a/Sirtuin 1 Pathway Contributes to Apoptosis Induced by Deoxycholic Acid in Rat Liver. *Mol. Cell. Biol.* **34**, 1100–20 (2014).
7. Webster, C. R. L., Johnston, A. N. & Anwer, M. S. Protein kinase C delta protects against bile acid apoptosis by suppressing proapoptotic JNK and BIM pathways in human and rat hepatocytes. *Am. J. Physiol. Gastrointest. Liver Physiol.* **307**, G1207-1215 (2014).
  8. Rodrigues, C. M., Fan, G., Wong, P. Y., Kren, B. T. & Steer, C. J. Ursodeoxycholic acid may inhibit deoxycholic acid-induced apoptosis by modulating mitochondrial transmembrane potential and reactive oxygen species production. *Mol. Med.* **4**, 165–78 (1998).
  9. Amaral, J. D., Castro, R. E., Solá, S., Steer, C. J. & Rodrigues, C. M. P. p53 is a key molecular target of ursodeoxycholic acid in regulating apoptosis. *J. Biol. Chem.* **282**, 34250–9 (2007).
  10. Rodrigues, C. M., Fan, G., Ma, X., Kren, B. T. & Steer, C. J. A novel role for ursodeoxycholic acid in inhibiting apoptosis by modulating mitochondrial membrane perturbation. *J. Clin. Invest.* **101**, 2790–9 (1998).
  11. Amaral, J. D., Castro, R. E., Steer, C. J. & Rodrigues, C. M. P. p53 and the regulation of hepatocyte apoptosis: implications for disease pathogenesis. *Trends Mol. Med.* **15**, 531–41 (2009).
  12. Amaral, J. D., Viana, R. J. S., Ramalho, R. M., Steer, C. J. & Rodrigues, C. M. P. Bile acids: regulation of apoptosis by ursodeoxycholic acid. *J. Lipid Res.* **50**, 1721–34 (2009).
  13. Rodrigues, C. M., Ma, X., Linehan-Stieers, C., Fan, G., Kren, B. T. & Steer, C. J. Ursodeoxycholic acid prevents cytochrome c release in apoptosis by inhibiting mitochondrial membrane depolarization and channel formation. *Cell Death Differ.* **6**, 842–54 (1999).
  14. Mello-Vieira, J., Sousa, T., Coutinho, A., Fedorov, A., Lucas, S. D., Moreira, R., Castro, R. E., Rodrigues, C. M. P., Prieto, M. & Fernandes, F. Cytotoxic bile acids, but not cytoprotective species, inhibit the ordering effect of cholesterol in model membranes at physiologically active concentrations. *Biochim. Biophys. Acta* **1828**, 2152–2163 (2013).
  15. Mohapatra, M. & Mishra, A. K. Effect of submicellar concentrations of conjugated and unconjugated bile salts on the lipid bilayer membrane. *Langmuir* **27**, 13461–7 (2011).
  16. Coreta-Gomes, F. M., Martins, P. T., Velázquez-Campoy, A., Vaz, W. L. C., Geraldés, C. F. G. C. & Moreno, M. J. Interaction of bile salts with model membranes mimicking the gastrointestinal epithelium: a study by isothermal titration calorimetry. *Langmuir*

- 150804122127008 (2015). doi:10.1021/acs.langmuir.5b01810
17. Zhou, Y., Maxwell, K. N., Sezgin, E., Lu, M., Liang, H., Hancock, J. F., Dial, E. J., Lichtenberger, L. M. & Levental, I. Bile acids modulate signaling by functional perturbation of plasma membrane domains. *J. Biol. Chem.* **288**, 35660–70 (2013).
  18. Botla, R., Spivey, J., Aguilar, H., Bronk, S. & Gores, G. Ursodeoxycholate (UDCA) inhibits the mitochondrial membrane permeability transition induced by glycochenodeoxycholate: a mechanism of UDCA cytoprotection. *J. Pharmacol. Exp. Ther.* **272**, 930–938 (1995).
  19. Nalapareddy, P. D., Schüngel, S., Hong, J.-Y., Manns, M. P., Jaeschke, H. & Vogel, A. The BH3-only protein bid does not mediate death-receptor-induced liver injury in obstructive cholestasis. *Am. J. Pathol.* **175**, 1077–85 (2009).
  20. Schulz, S., Schmitt, S., Wimmer, R., Aichler, M., Eisenhofer, S., Lichtmanegger, J., Eberhagen, C., Artmann, R., Tookos, F., Walch, A., Krappmann, D., Brenner, C., Rust, C. & Zischka, H. Progressive stages of mitochondrial destruction caused by cell toxic bile salts. *Biochim. Biophys. Acta* **1828**, 2121–33 (2013).
  21. Mariash, C. N., Seelig, S., Schwartz, H. L. & Oppenheimer, J. H. Rapid synergistic interaction between thyroid hormone and carbohydrate on mRNAS14 induction. *J. Biol. Chem.* **261**, 9583–6 (1986).
  22. Castro, R. E., Ferreira, D. M. S., Zhang, X., Borralho, P. M., Sarver, A. L., Zeng, Y., Steer, C. J., Kren, B. T. & Rodrigues, C. M. P. Identification of microRNAs during rat liver regeneration after partial hepatectomy and modulation by ursodeoxycholic acid. *Am. J. Physiol. Gastrointest. Liver Physiol.* **299**, G887-97 (2010).
  23. Castro, R. E., Ferreira, D. M. S., Afonso, M. B., Borralho, P. M., Machado, M. V., Cortez-Pinto, H. & Rodrigues, C. M. P. miR-34a/SIRT1/p53 is suppressed by ursodeoxycholic acid in the rat liver and activated by disease severity in human non-alcoholic fatty liver disease. *J. Hepatol.* **58**, 119–25 (2013).
  24. Walajtys-Rhode, E., Zapatero, J., Moehren, G. & Hoek, J. B. The role of the matrix calcium level in the enhancement of mitochondrial pyruvate carboxylation by glucagon pretreatment. *J. Biol. Chem.* **267**, 370–9 (1992).
  25. Owen, D. M., Rentero, C., Magenau, A., Abu-Siniyeh, A. & Gaus, K. Quantitative imaging of membrane lipid order in cells and organisms. *Nat. Protoc.* **7**, 24–35 (2012).
  26. Zimmermann, T., Rietdorf, J. & Pepperkok, R. Spectral imaging and its applications in live cell microscopy. *FEBS Lett.* **546**, 87–92 (2003).
  27. Wu, Y., Zinchuk, V., Grossenbacher-Zinchuk, O. & Stefani, E. Critical evaluation of

- quantitative colocalization analysis in confocal fluorescence microscopy. *Interdiscip. Sci.* **4**, 27–37 (2012).
28. Marquardt, D. W. An Algorithm for Least-Squares Estimation of Nonlinear Parameters. *J. Soc. Ind. Appl. Math.* **11**, 431–441 (1963).
29. Sarmiento, M. J., Coutinho, A., Fedorov, A., Prieto, M. & Fernandes, F. Ca<sup>2+</sup> induces PI(4,5)P<sub>2</sub> clusters on lipid bilayers at physiological PI(4,5)P<sub>2</sub> and Ca<sup>2+</sup> concentrations. *Biochim. Biophys. Acta* **1838**, 822–830 (2014).
30. McClare, C. W. An accurate and convenient organic phosphorus assay. *Anal. Biochem.* **39**, 527–30 (1971).
31. Jin, L., Millard, A. C., Wuskell, J. P., Dong, X., Wu, D., Clark, H. A. & Loew, L. M. Characterization and application of a new optical probe for membrane lipid domains. *Biophys. J.* **90**, 2563–75 (2006).
32. Owen, D. M., Lanigan, P. M. P., Dunsby, C., Munro, I., Grant, D., Neil, M. a a, French, P. M. W. & Magee, A. I. Fluorescence lifetime imaging provides enhanced contrast when imaging the phase-sensitive dye di-4-ANEPPDHQ in model membranes and live cells. *Biophys. J.* **90**, L80-2 (2006).
33. Parasassi, T. & Gratton, E. Membrane Lipid Domains and Dynamics as Detected by Laurdan Fluorescence. *J. Fluoresc.* **5**, 59–69 (1995).
34. Pinto, S. N., Fernandes, F., Fedorov, A., Futerman, A. H., Silva, L. C. & Prieto, M. A combined fluorescence spectroscopy, confocal and 2-photon microscopy approach to re-evaluate the properties of sphingolipid domains. *Biochim. Biophys. Acta* **1828**, 2099–110 (2013).
35. Dawson, P. a, Lan, T. & Rao, A. Bile acid transporters. *J. Lipid Res.* **50**, 2340–57 (2009).
36. Zidovetzki, R. & Levitan, I. Use of cyclodextrins to manipulate plasma membrane cholesterol content: evidence, misconceptions and control strategies. *Biochim Biophys Acta* **1768**, 1311–1324 (2007).
37. Holzinger, F., Scheingart, C. D., Ton-Nu, H. T., Cerrè, C., Steinbach, J. H., Yeh, H. Z. & Hofmann, a F. Transport of fluorescent bile acids by the isolated perfused rat liver: kinetics, sequestration, and mobilization. *Hepatology* **28**, 510–20 (1998).
38. Waart, D. R. De, Ha, S., Vlaming, M. L. H., Kunne, C., Ha, E., Gruss, H., Elferink, R. P. J. O. & Stieger, B. Hepatic Transport Mechanisms of Cholyl-L-Lysyl-Fluorescein. *J Pharmacol Exp* **334**, 78–86 (2010).

39. Bravo, P., Bender, V. & Cassio, D. Efficient in vitro vectorial transport of a fluorescent conjugated bile acid analogue by polarized hepatic hybrid WIF-B and WIF-B9 cells. *Hepatology* **27**, 576–83 (1998).
40. Kitamura, T., Gatmaitan, Z. & Arias, I. M. Serial quantitative image analysis and confocal microscopy of hepatic uptake, intracellular distribution and biliary secretion of a fluorescent bile acid analog in rat hepatocyte doublets. *Hepatology* **12**, 1358–64 (1990).
41. Kim, M., Cooper, D. D., Hayes, S. F. & Spangrude, G. J. Rhodamine-123 staining in hematopoietic stem cells of young mice indicates mitochondrial activation rather than dye efflux. *Blood* **91**, 4106–17 (1998).
42. Lucken-Ardjomande, S., Montessuit, S. & Martinou, J.-C. Bax activation and stress-induced apoptosis delayed by the accumulation of cholesterol in mitochondrial membranes. *Cell Death Differ.* **15**, 484–93 (2008).
43. Marí, M., Caballero, F., Colell, A., Morales, A., Caballeria, J., Fernandez, A., Enrich, C., Fernandez-Checa, J. C. & García-Ruiz, C. Mitochondrial free cholesterol loading sensitizes to TNF- and Fas-mediated steatohepatitis. *Cell Metab.* **4**, 185–98 (2006).
44. Solá, S., Brito, M. a, Brites, D., Moura, J. J. G. & Rodrigues, C. M. P. Membrane structural changes support the involvement of mitochondria in the bile salt-induced apoptosis of rat hepatocytes. *Clin. Sci. (London, England)* **103**, 475–85 (2002).
45. Benz, C., Angermüller, S., Otto, G., Sauer, P., Stremmel, W. & Stiehl, a. Effect of tauroursodeoxycholic acid on bile acid-induced apoptosis in primary human hepatocytes. *Eur. J. Clin. Invest.* **30**, 203–9 (2000).
46. Rolo, a P., Oliveira, P. J., Moreno, a J. & Palmeira, C. M. Bile acids affect liver mitochondrial bioenergetics: possible relevance for cholestasis therapy. *Toxicol. Sci.* **57**, 177–85 (2000).
47. Benz, R. Permeation of hydrophilic solutes through mitochondrial outer membranes: Review on mitochondrial porins. *Biochim. Biophys. Acta - Rev. Biomembr.* **1197**, 167–196 (1994).
48. Lakowicz, J. R. *Principles of Fluorescence Spectroscopy*. (Springer, 2006).
49. Lucken-Ardjomande, S., Montessuit, S. & Martinou, J.-C. Contributions to Bax insertion and oligomerization of lipids of the mitochondrial outer membrane. *Cell Death Differ.* **15**, 929–37 (2008).
50. Daum, G. & Graz, T. U. Lipids of mitochondria. *Biochim. Biophys. Acta* **822**, 1–42 (1985).

51. Gebert, N., Joshi, A. S., Kutik, S., Becker, T., Guan, X. L., Mooga, V. P., Stroud, D. A., Kulkarni, G., Wenk, R., Rehling, P., Meisinger, C., Ryan, M. T., Wiedemann, N., Greenberg, L. & Pfanner, N. Biogenesis : implications for Barth syndrome. *Curr. Biol.* **19**, 2133–2139 (2015).
52. Osman, C., Voelker, D. R. & Langer, T. Making heads or tails of phospholipids in mitochondria. *J. Cell Biol.* **192**, 7–16 (2011).
53. Ardail, D., Privat, J.-P., Egret-Charlier, M., Levrat, C., Lerne, F. & Louisot, P. Mitochondrial contact sites. *J. Biol. Chem.* **265**, 18797–18802 (1990).
54. Barrasa, J. I., Santiago-Gómez, A., Olmo, N., Lizarbe, M. A. & Turnay, J. Resistance to butyrate impairs bile acid-induced apoptosis in human colon adenocarcinoma cells via up-regulation of Bcl-2 and inactivation of Bax. *Biochim. Biophys. Acta - Mol. Cell Res.* **1823**, 2201-09 (2012).
55. Powell, A. a, Rue, J. M. L. a, Batta, a K. & Martinez, J. D. Bile acid hydrophobicity is correlated with induction of apoptosis and/or growth arrest in HCT116 cells. **486**, 481–486 (2001).
56. Gumprich, E., Devereaux, M. W., Dahl, R., Soden, J. S., Sparagna, G. C., Leonard, S. W., Traber, M. G. & Sokol, R. J. Resistance of Young Rat Hepatic Mitochondria to Bile Acid- Induced Permeability Transition: Potential Role of Alpha Tocopherol. *Physiology* **64**, 498–504 (2009).
57. Rolo, A. P., Oliveira, P. J., Moreno, A. J. & Palmeira, C. M. Chenodeoxycholate induction of mitochondrial permeability transition pore is associated with increased membrane fluidity and cytochrome c release: protective role of carvedilol. *Mitochondrion* **2**, 305–11 (2003).
58. van Meer, G., Voelker, D. R. & Feigenson, G. W. Membrane lipids: where they are and how they behave. *Nat. Rev. Mol. Cell Biol.* **9**, 112–24 (2008).
59. Webster, C. R. L., Usechak, P. & Anwer, M. S. cAMP inhibits bile acid-induced apoptosis by blocking caspase activation and cytochrome c release. *Am. J. Physiol. Gastrointest. Liver Physiol.* **283**, G727–G738 (2002).
60. Denk, G. U., Kleiss, C. P., Wimmer, R., Vennegeerts, T., Reiter, F. P., Schulz, S., Zischka, H. & Rust, C. Tauro-beta-muricholic acid restricts bile acid-induced hepatocellular apoptosis by preserving the mitochondrial membrane potential. *Biochem. Biophys. Res. Commun.* **424**, 758–764 (2012).

## 6. Supplementary Materials

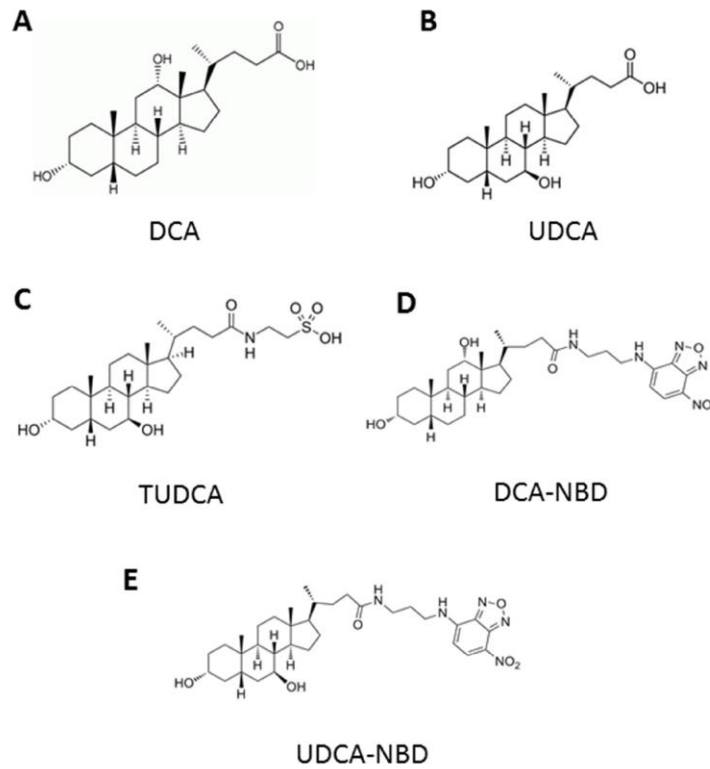


**Figure S1. Chemical Structures of DCA (A), UDCA (B), TUDCA (C), and of the NBD fluorescent analogues of DCA (D) and UDCA (E).**

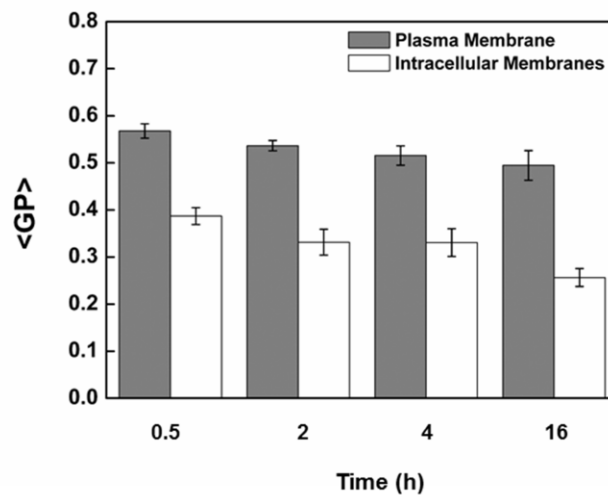


**Figure S2. Membrane order of untreated hepatocytes changed overtime during cell culture.** Control values of absolute Laurdan generalized polarization (GP) in membranes of untreated cultured rat hepatocytes during the duration of bile acid incubations, initiated 24h after plating (Experimental

conditions of Figure 2). The membrane order of untreated hepatocytes changed overtime during in vitro culture in a reproducible manner. Results are expressed as mean  $\pm$  SEM fold change of at least 12 cells (B-F) or as mean  $\pm$  SEM fold change of at least 3 independent experiments (G). \*  $p < 0.05$ , \*\*  $p < 0.01$ , and \*\*\*  $p < 0.001$  from respective time point control.

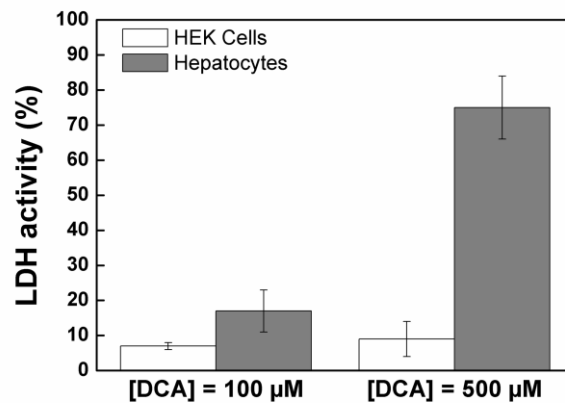


**Figure S3. Hepatocyte and HEK293T cellular death in the presence of DCA.** Cellular death of HEK293T cells and rat hepatocytes in the presence of apoptotic (100  $\mu$ M) and necrotic (500  $\mu$ M) concentrations of DCA after a 3h incubation was estimated through measurement of LDH activity in cell culture media, as described in the Materials and Methods section. Leakage of LDH into the cell culture media is associated with cellular death. Results are expressed as mean  $\pm$  SEM fold change of at least 3 independent experiments.

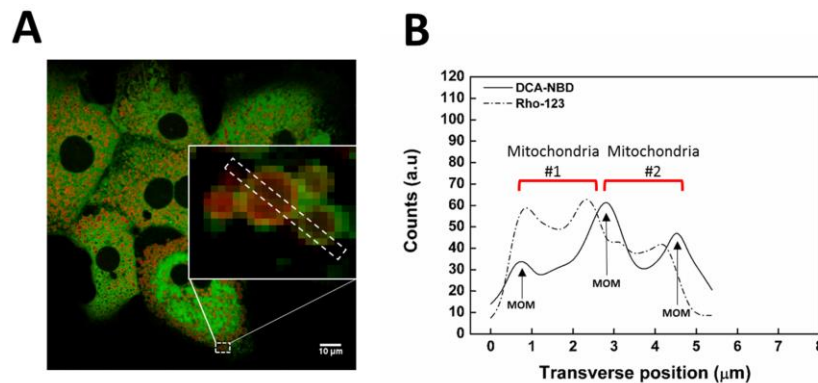


**Figure S4. Distribution of DCA-NBD in cultured rat hepatocytes labeled with the mitochondrial matrix marker Rho-123.** DCA-NBD distributes through different organelles, including mitochondria. Insertion in mitochondrial membranes is mainly observed on the mitochondrial outer membrane (MOM) as evidenced by the transverse profile correspondence to boxed region in (A), where DCA-NBD is shown to accumulate in the limits of Rho-123 enrichment (B).

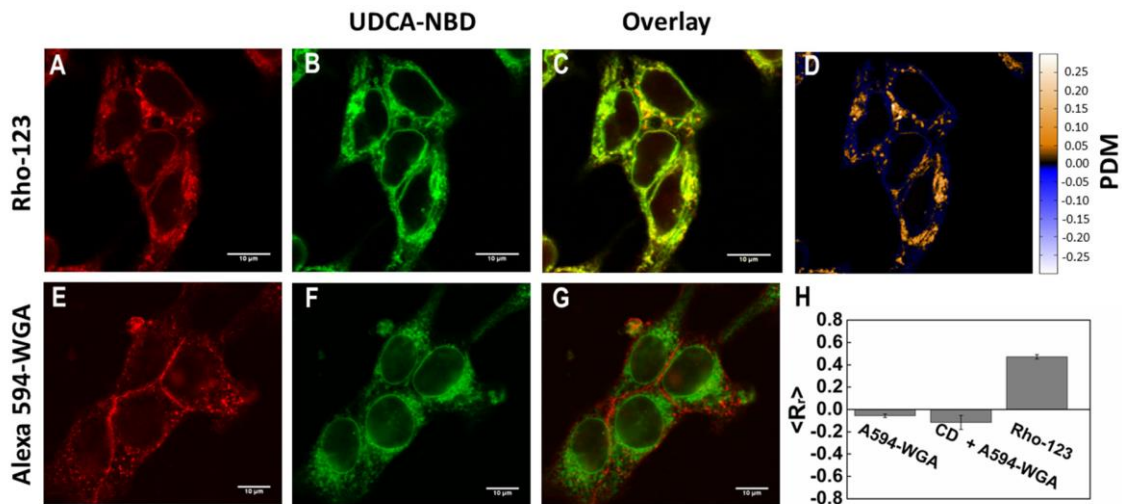


**Figure S5. Subcellular distribution of UDCA-NBD in HEK293T cells.** Mitochondria or plasma membrane were fluorescently stained with 5  $\mu\text{M}$  Rho-123 (mitochondrial marker) (A) and 130 nM Alexa 594-WGA (plasma membrane marker) (E), respectively. The subcellular distribution of 20  $\mu\text{M}$  of UDCA-NBD (B, F) in these cells after internalization is also shown by colocalization analysis. Overlay images for UDCA-NBD fluorescence and mitochondria (C) or plasma membrane staining (G) are also shown. UDCA-NBD distributes through different organelles, including mitochondria. Positive products of the differences from the mean (PDM, (26)) values are obtained within the mitochondria, while other intracellular organelles loaded with DCA-NBD present negative PDM values (D). Pearson correlation coefficients ( $R_r$ ) (26) confirm partial colocalization between UDCA-NBD and Rho-123 signals as well as poor colocalization of DCA-NBD with the plasma membrane marker. Results are expressed as mean  $\pm$  SEM of 50-60 cells.

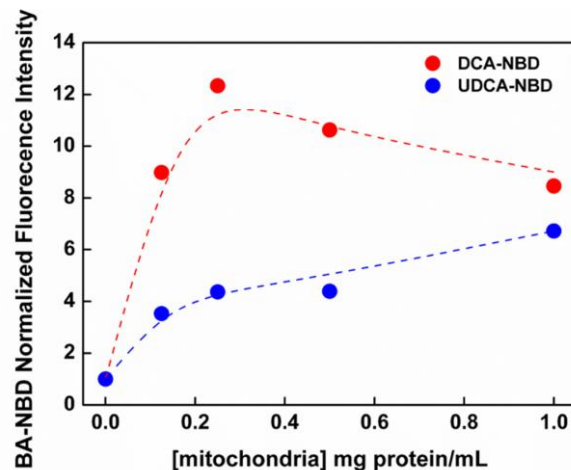


**Figure S6. Binding of bile acid fluorescent analogues to isolated mitochondria.** Both DCA-NBD and UDCA-NBD fluorescent analogues at 4  $\mu\text{M}$  bind with high affinity to isolated mitochondria as evidenced by increases in fluorescence intensity of these molecules after incubation with freshly isolated rat liver mitochondria.

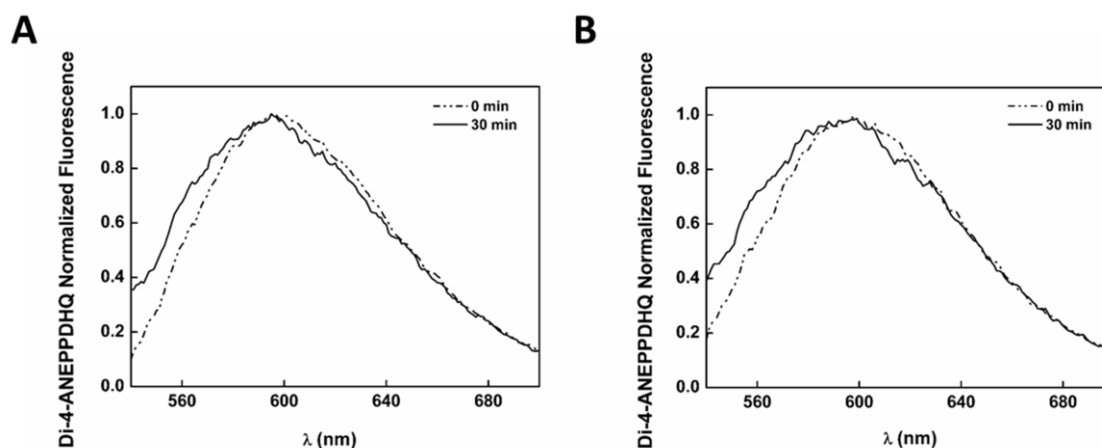


**Figure S7.** The fluorescence emission spectra of Di-4-ANEPPDHQ shifts to shorter wavelengths after incubation of freshly isolated mitochondria with 100 $\mu$ M (A) or 500  $\mu$ M (B) DCA. This spectral shift is consistent with a less polar environment for the membrane probe in the presence of bile acids.

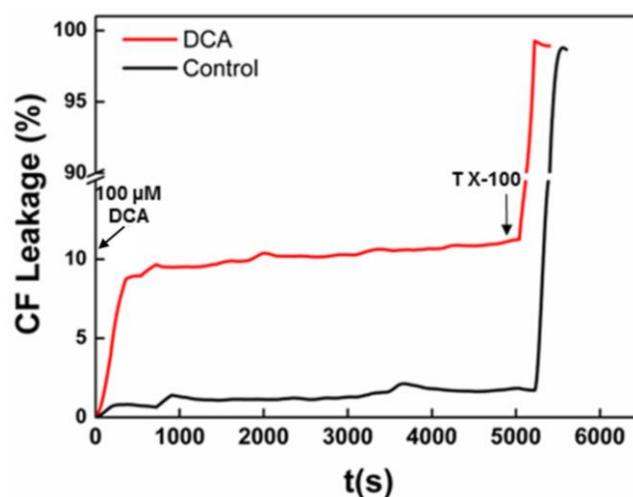


**Figure S8.** CF leakage curve of MOM biomimetic liposomes in the presence of DCA. MOM biomimetic liposomes composed of PC:PE:PI:Cl:Chol (48:25:12:6:9) were loaded with 90 mM CF (under fluorescence self-quenching conditions) and incubated with 100  $\mu$ M of DCA at room temperature. The release kinetics of carboxyfluorescein can be followed through the increase in fluorescence intensity which is proportional to the fraction of CF released. Significant permeation by DCA (in red) was only observed in a limited time-scale, possibly due to transbilayer movement (flip-flop) of DCA until equal concentrations of the bile acid are found in the opposing bilayer leaflets. Leakage in the absence of DCA is shown in black. Total lipid concentration was 200  $\mu$ M. Triton X-100 disruption of vesicles and subsequent leakage was used as a positive control. The percentage of CF leakage induced by DCA was calculated as:  $\text{CF Leakage (\%)} = 100 \times [(F - F_0) - (F_c - F_0)] / (F_1 - F_0)$ , in which  $F$  and  $F_1$  are the fluorescence intensity prior to and after the addition of the Triton X-100 (after incubation with bile acids), respectively, and  $F_0$  and  $F_c$  are the fluorescence of intact vesicles before and after the same incubation time.

## **Chapter IV**

---

Bile acids inhibit Bax-dependent membrane permeabilization



## **BILE ACIDS INHIBIT BAX-DEPENDENT MEMBRANE PERMEABILIZATION**

Tânia Sousa<sup>1,2</sup>, Šárka Pokorná<sup>3</sup>, Rui E. Castro<sup>4</sup>, Nuno Bernardes<sup>2</sup>, Soojay Banerjee<sup>7</sup>,  
Gerhard Gröbner<sup>8</sup>, Richard J. Youle<sup>7</sup>, Ana Coutinho<sup>1,2,9</sup>, Cecília M.P. Rodrigues<sup>4</sup>, Martin Hof<sup>6</sup>,  
Manuel Prieto<sup>1,2</sup>, Fábio Fernandes<sup>1,2</sup>

<sup>1</sup>Centro de Química-Física Molecular and Institute of Nanoscience and Nanotechnology, Instituto Superior Técnico, University of Lisbon, Lisbon, Portugal

<sup>2</sup>iBB-Institute for Bioengineering and Biosciences, Biological Sciences Research Group, Av. Rovisco Pais 1, 1049-001 Lisbon, Portugal

<sup>3</sup>J. Heyrovský Institute of Physical Chemistry, Academy of Sciences of the Czech Republic, v. v. i., Dolejškova 3, 182 23 Prague 8, Czech Republic; Department of Biochemistry, Charles University, Hlavova 8, 128 40 Prague 2, Czech Republic.

<sup>4</sup>Research Institute for Medicines (iMed.Ulisboa), Faculty of Pharmacy, University of Lisbon, Lisbon, Portugal

<sup>5</sup>Institute for Biotechnology & Bioengineering; Department of Bioengineering; Instituto Superior Técnico; Universidade de Lisboa; Lisbon, Portugal.

<sup>6</sup>J. Heyrovský Institute of Physical Chemistry, Academy of Sciences of the Czech Republic, v. v. i., Dolejškova 3, 182 23 Prague 8, Czech Republic.

<sup>7</sup>Surgical Neurology Branch, NINDS, NIH Bethesda, MD 20892, USA

<sup>8</sup>Department of Chemistry, University of Umeå, SE-901 87 Umeå, Sweden

<sup>9</sup>Departamento de Química e Bioquímica, Faculty of Sciences, University of Lisbon, Lisbon, Portugal



## Abstract

Cytoprotective bile acids such as ursodeoxycholic acid (UDCA) and tauroursodeoxycholic acid (TUDCA) are known for their ability to inhibit apoptosis at submicellar concentrations in both hepatic and nonhepatic cells. The exact mechanism by which they exert this cytoprotection is not yet entirely clear, but it is at least partially associated with the blockage of mitochondria membrane damage. It has already been shown that both UDCA and TUDCA are able to inhibit the translocation of Bcl-2-associated X protein (Bax) to the mitochondria. Bax plays a key role in apoptosis, which is achieved through translocation of the protein to the mitochondria from the cytosol after an apoptotic stimulus and formation of pores in mitochondrial membranes. Given the reported impact of cytoprotective bile acids on Bax mitochondrial translocation, this protein is a strong candidate as the crucial target for cytoprotective bile acids. This study aimed to characterize the impact of physiologically active concentrations of UDCA and TUDCA on recombinant Bax oligomerization, membrane affinity and activity. We show that both UDCA and TUDCA interact with soluble recombinant Bax, and that in the case of TUDCA, the complexes of Bax and bile acid molecules are large enough to exhibit significantly lower diffusion coefficients. Cytoprotective bile acids are also shown to inhibit the interaction of Bax with activator molecules such as the Bid-BH3 peptide and decrease the affinity of Bax for liposomes mimicking outer mitochondrial membrane composition. Importantly, UDCA and TUDCA are shown to dramatically inhibit Bax-induced permeabilization of model membranes. These effects are not specific to cytoprotective bile acids, as incubation of recombinant Bax with the apoptotic deoxycholic acid (DCA) produces similar results. The findings presented here clearly show that at physiologically active submicellar concentrations, bile acids have the ability to inhibit Bax pore-forming activity and suggest that the cytoprotective activity of UDCA and TUDCA could be the result of this process. On the other hand, for toxic bile acids, these cytoprotective effects are negated due to the intrinsic mitochondrial permeabilization properties of these molecules.



## 1. Introduction

The bile acids ursodeoxycholic acid (UDCA) and tauroursodeoxycholic acid (TUDCA), have been shown to inhibit apoptosis at low, submicellar concentrations in both hepatic and nonhepatic cells, against a long list of apoptosis-inducing agents<sup>1-4</sup>. In fact, UDCA has been used as therapeutic agent for several years, initially for gallstone dissolution and subsequently for the treatment of chronic cholestatic diseases<sup>3</sup>. There is also a growing area of research for both UDCA and TUDCA as potential therapeutic agents on a wide variety of non-liver diseases, such as neurodegenerative<sup>5-9</sup> and cardiovascular diseases<sup>10,11</sup>.

Given the amphipathic nature of UDCA and TUDCA, their presence at physiologically active concentrations (50-100  $\mu\text{M}$ )<sup>12,13</sup>, could induce changes in the biophysical properties of mitochondrial membranes. In this regard, it was recently shown by us and others that while apoptotic bile acids, such as deoxycholic acid (DCA) and chenodeoxycholic acid (CDCA), promoted disordering of the lipid membrane on both large unilamellar vesicles<sup>12</sup> (LUVs) and giant plasma membrane vesicles<sup>14</sup> (GPMVs), this effect was not observed in the presence of cytoprotective bile acids<sup>12</sup>. These differences are very likely the result of dramatically different partition behavior of these bile acids, as the more hydrophobic DCA and CDCA exhibit considerably larger preference for incorporation in lipid bilayers<sup>12</sup>. Additionally, we recently observed that in hepatocytes, bile acids produced only minor transient increases in fluidity of cellular membranes<sup>15</sup>. The transient nature of these changes is likely due to the presence of cellular compensatory mechanisms to maintain membrane integrity. Through confocal imaging of fluorescent analogues of bile acids it was also evident that these molecules had low preference for incorporation in the plasma membrane, exhibiting some incorporation in mitochondria<sup>15</sup>. Additionally, while cytotoxic bile acids have been shown to promote mitochondrial permeability transition (MPT), cytochrome c release, and changes in mitochondrial outer membrane (MOM) morphology<sup>16,17</sup>, UDCA and TUDCA have no effect on mitochondrial permeability of isolated mitochondria<sup>15,18</sup>. In this context, unlike apoptotic bile acids, the activity of cytoprotective UDCA and TUDCA is likely not dependent on direct modulation of mitochondrial membrane structure.

In fact, the exact mechanisms by which UDCA and TUDCA exert their cytoprotective effects are not entirely clear, but these are at least partially associated with a blockage of mitochondria membrane damage<sup>1,9,18-21</sup>. In this regard, prolonged incubation (several hours) with UDCA and TUDCA has been shown to inhibit the translocation of Bcl-2-associated X protein (Bax) to the mitochondria<sup>18,19,22,23</sup>. Moreover, it has been shown that in isolated mitochondria, TUDCA and UDCA prevent Bax-mediated release of cytochrome c<sup>18,19</sup>. On the other hand, these molecules have also been proposed to act through different upstream targets, including

nuclear receptors, transcriptional regulation or activation of signaling pathways<sup>5,23–26</sup>, as well as through modulation of mitophagy<sup>9</sup>.

In apoptosis, the key protein Bax promotes caspase activation through release of mitochondrial proteins after mitochondrial membrane permeabilization. Bax is a pore-forming protein that belongs to the pro-apoptotic multi-domain group of Bcl-2 proteins. In healthy cells, Bax resides largely on the cytosol as an inactive monomer that continuously binds to mitochondria and retrotranslocates back to the cytosol through interaction with Bcl-xL, an anti-apoptotic member of Bcl-2 family<sup>27–30</sup>. However, recently Bax was also shown to dimerize in a number of cell lines, forming inhibited dimers which dissociate to monomeric Bax before Bax activation<sup>31</sup>. The exact mechanism by which Bax is activated, oligomerize and exert its pore-forming activity is not yet entirely clear and is the subject of great controversy. In fact, elucidation of this issue has been termed the “holy grail” of apoptosis research<sup>32</sup>. For Bax to be activated, an interaction with a BH3-only protein like truncated Bid (tBid) is needed<sup>30,33–35</sup>. After this interaction Bax undergoes multiple conformational changes and domain rearrangements in order to bind to membranes and oligomerize to form pores. Recent reports show that Bax binds to the membrane in a monomeric state but quickly associate into dimers, the structural unit for further oligomerization<sup>36–38</sup>. In this way, Bax-induced MOM permeabilization would not be mediated by a unique, well-defined Bax pore structure, but rather by multiple Bax pores with different sizes, already reported to be of tunable size, and stoichiometries that adapt to Bax density at the MOM<sup>39</sup>.

Given the reported impact of cytoprotective bile acids on Bax mitochondrial translocation, this protein is a strong candidate as the crucial target for cytoprotective bile acids. Importantly, interaction with micelles of some nonionic detergents induce conformational changes in soluble Bax, including exposure of an N-terminal domain, which favors activation of the protein and translocation to the mitochondria<sup>40–42</sup>. Depending on the detergent, presence of activating peptides or use of different forms of Bax, this activated form of Bax was also found to correspond to monomeric or oligomeric forms of the protein<sup>31,42–44</sup>. Also, a specific form of Bax dimer obtained after treatment with detergents corresponds to an off-pathway inactive oligomer, and the formation of this specie might be promoted through the use of low detergent concentrations<sup>44,45</sup>. In light of these results, it is possible that submicellar concentrations of UDCA and TUDCA modulate Bax activity through direct interaction with the protein.

In this work, a detailed biophysical study was carried out to characterize the impact of physiologically active concentrations of UDCA and TUDCA on recombinant Bax oligomerization, membrane affinity, and activity. We show that both UDCA and TUDCA, interact with soluble recombinant Bax, and that complexes of Bax and TUDCA are large

enough to exhibit significantly lower diffusion coefficients. Cytoprotective bile acids are also shown to inhibit the interaction of Bax with activator molecules such as the Bid-BH3 peptide and decrease the affinity of Bax for liposomes mimicking outer mitochondrial membrane composition. Finally, UDCA and TUDCA are also shown to inhibit Bax-induced permeabilization of model membranes. These effects are not specific to cytoprotective bile acids, as incubation of recombinant Bax with DCA produces similar results.

The findings presented here clearly show that at submicellar concentrations, bile acids have the ability to inhibit Bax pore-forming activity and suggest that the cytoprotective activity of UDCA and TUDCA could be the result of this process. On the other hand, for toxic bile acids, these cytoprotective effects are negated due to the intrinsic mitochondrial permeabilization properties of these molecules.

## 2. Materials and methods

### 2.1. Chemicals and Reagents

1,2-dioleoyl-*sn*-glycero-3-phosphocholine (DOPC), 1,2-dioleoyl-*sn*-glycero-3-phosphoethanolamine (DOPE), *L*- $\alpha$ -Phosphatidylinositol sodium salt (PI), 1-palmitoyl-2-oleoyl-*sn*-glycero-3-phosphocholine (POPC); Bovine heart cardiolipin (CL), 1,1',2,2'-tetraoleoyl-cardiolipin (TOCL) and 1,2-dioleoyl-*sn*-glycero-3-phosphoethanolamine-N-(cap biotinyl) (biotinylated DOPE) were purchased from Avanti Polar Lipids (Alabaster, AL, USA). Chol was obtained from Sigma-Aldrich (St. Louis MO, USA). Stock solutions of all lipids were prepared with Uvasol grade chloroform with the exception of CL that was prepared in chloroform/methanol (2:1). Both solvents were obtained from Sigma-Aldrich. DCA and TUDCA in sodium salt form, Tris(2-carboxyethyl)phosphine hydrochloride (TCEP), NaCl, Trizma®, Glycerol, bovine serum albumin (BSA), biotinylated BSA, DL-Dithiothreitol (DTT) and Isopropyl  $\beta$ -D-1-thiogalactopyranoside (IPTG) were purchased from Sigma-Aldrich. UDCA sodium salt was purchased from Santa Cruz Biotechnologies (Santa Cruz, CA), Tris from Merck (Darmstadt, Germany) and streptavidin was obtained from IBA (Goettingen, Germany). BH3 and BH3 labeled with TAMRA (5-Carboxytetramethylrhodamine, BH3-TAMRA) peptide from Bid were purchased from Anaspec (Fremont, USA).

1,2-Dioleoyl-*sn*-glycero-3-phosphoethanolamine-N-(lissamine rhodamineB sulfonyl) (DOPE-Rho) was obtained from Avanti Polar Lipids. Alexa Fluor 488 SE (carboxylic acid,

succinimidyl ester, mixed isomers, dilithiumsalt) (Alexa 488) and rhodamine 110 (Rho110) were obtained from Molecular Probes, Invitrogen (Eugene,OR) and Calcein was purchased from Sigma Aldrich (St. Louis MO, USA). DiIC18(5) (DiD) and ATTO 488 were supplied by Life Technologies Corporation (Carlsbad, CA) and ATTO-TEC (Siegen, Germany).

## **2.2. Protein expression, purification and labeling**

Recombinant human Bax was expressed by transformation of the pTYB1 (New England BioLabs, Inc., Beverly, MA) vector containing the cDNA of human Bax into the BL21DE3 strain of *E. coli*, as previously described<sup>46</sup>. The expression of the Bax protein was induced with IPTG at 37°C. Recombinant proteins were isolated by a chitin affinity chromatography (New England BioLabs, Inc., Beverly, MA) and eluted using 40 mM dithiothreitol (DTT). Further purification was achieved through ion-exchange chromatography on a Mono-Q column (GE Healthcare). Pure protein was stored at -80 °C in 10 mM Tris-HCl (pH 8.0) supplemented with 150 mM of NaCl, 1mM of TCEP and 10% (v/v) glycerol. Protein to be used in leakage assays was stored in 10mM Hepes (pH 7.4), 100mM KCl and 20% (v/v) glycerol. Protein purity was assessed by SDS-PAGE and protein concentration was determined on the basis of the samples absorption at 280 nm.

Bax was labeled with Alexa Fluor® 488 NHS Ester (Succinimidyl Ester, Molecular Probes, Invitrogen (Eugene,OR)) or with NBD - X, NHS ester (Succinimidyl 6 - (N - (7 - nitrobenz - 2 - oxa - 1,3 - diazol - 4 - yl)amino)hexanoate, Anaspec Inc.) in 6-fold molar excess for 1h at room temperature. Unreacted dye was removed by dialysis.

## **2.3. Size exclusion chromatography**

Size exclusion chromatography (SEC) was performed to Alexa488-labeled Bax (Bax-A488) at 0.2 µM pre-incubated or not for 15 minutes with 100 µM of cytoprotective bile acids, using a Superdex 75 column (GE Healthcare). Prior, to Bax experiments, a volume calibration curve was determined by using a kit with standard proteins of known molecular weight (12-200 kDa, Sigma-Aldrich)<sup>47</sup>.

## 2.4. Vesicle preparation

LUV for partition or leakage studies were prepared by extrusion of multilamellar vesicles as previously described<sup>48</sup>. For the partition studies, liposomes mimetic of MOM were prepared with a lipid composition of PC:PE:PI:CL:Chol at molar ratios of 48:25:12:6:9. For the purpose of FRET experiments, DOPE-Rho was added to the lipid mixture at a molar ratio of 1:200. Adequate volumes of different lipid stock solutions were mixed, and the organic solvent was removed under a N<sub>2</sub> flux, followed by vacuum overnight. For membrane binding experiments, the resulting lipid film was re-suspended in 10 mM Tris-HCl, 150 mM NaCl at pH 7.4, followed by freeze–thaw cycles to homogenize liposome composition. LUVs were then obtained by extrusion of the solutions at room temperature with an Avanti Mini-Extruder (Alabaster, AL) using 100 nm pore size polycarbonate membranes. Probe concentrations were determined spectrophotometrically, using  $\epsilon(\text{DOPE-Rho}, 559 \text{ nm, chloroform}) = 95 \times 10^3 \text{ M}^{-1} \text{ cm}^{-1}$ , lipid concentrations by phosphorous analysis<sup>49</sup> and Chol concentration was determined gravimetrically.

For leakage assays, liposomes were prepared with a more stable lipid composition of PC:PE:TOCL at molar ratios of 43:36:21. Cholesterol was not included since it has been shown to inhibit Bax permeabilization activity<sup>50</sup>. Dried lipid films were rehydrated in 0.5 mL calcein containing phosphate buffer (35 mM calcein, 25 mM sodium phosphate, 20 mM KCl, 1 mM EDTA, pH 7.4 and 255 mOsm). LUVs were also obtained by extrusion as above and free calcein was removed by size exclusion chromatography.

GUVs were prepared with a lipid composition of POPC:POPE:TOCL at molar ratios of 54:36:10 by the electroformation method<sup>51,52</sup> in a 275 mOsm sucrose solution. In order to visualize the membrane and immobilize the vesicles DiD dye (protein-to-lipid ratio 1:2500) and biotinylated lipid DOPE (2 % of total lipid number) were used, respectively. Shortly, the lipid mixtures were spread on two hollow titanium plates, heated to approximately 40 °C to facilitate solvent evaporation and placed in vacuum. After 1 h, the lipid-coated plates were sealed with parafilm and filled with 275 mM sucrose solution. The formed chambers were then exposed to the following sequence of voltages and frequencies: First, the peak to peak voltage U was increased stepwise from 0.02 V to 1.1 V at 10 Hz for 45 min. Then, U was kept constant at 1.1 V and 10 Hz for 90 min, and finally the frequency was lowered to 4 Hz while U was increased to 1.3 V; these conditions were maintained for 30 min.

## 2.5. Steady-state fluorescence spectroscopy

Fluorescence measurements with Bax-Alexa Fluor 488 were carried out in a SLM-Aminco 8100 Series 2 spectrofluorimeter (Rochester, NY). The light source was a 450-W Xe arc lamp and a Rhodamine B quantum counter solution was used as reference. Fluorescence measurements for Bax-NBD required higher detection sensitivity and were carried out in a HORIBA Jobin Yvon Fluorolog-3-21 spectrofluorimeter (New Jersey, USA). This spectrofluorimeter has double excitation and single emission monochromators (IHR 320, New Jersey, USA). The light source was a 450-watt Xe lamp and the reference was a silicon diode. In both cases, 0.5 cm x 0.5 cm width quartz cuvettes were used, and measurements were carried out in a right-angle geometry and at room temperature. Bax-A488 and Bax-NBD fluorescence intensities were obtained by excitation at 480 nm and 460 nm, respectively. When required, fluorescence intensities were corrected for the inner filter effects as described elsewhere<sup>51</sup>. Bax-A488 steady-state anisotropy,  $\langle r \rangle$ , was measured with excitation at 480 nm and emission at 515 nm and is defined as<sup>52</sup>:

$$\langle r \rangle = \frac{I_{VV} - GI_{VH}}{I_{VV} + 2GI_{VH}} \quad (1)$$

where  $I_{VV}$  and  $I_{VH}$  are the steady-state vertical and horizontal components of fluorescence emission, respectively, with excitation accomplished with vertically polarized light. The G factor is calculated by considering the components with excitation horizontal to the emission axis,  $I_{HV}$  and  $I_{HH}$ <sup>52</sup>:

$$G = \frac{I_{HV}}{I_{HH}} \quad (2)$$

For the polarization of excitation and emission light, Glan-Thompson polarizers were used. Blank subtraction was taken into account in all the anisotropy components as well as in the other fluorescence measurements.

### FRET measurements

Förster resonance energy transfer (FRET) was applied to follow the interaction between Bax-A488 and activator peptide BH3 from Bid labeled with TAMRA (BH3-TAMRA,

AnaSpec) in the presence or absence of bile acids. FRET can be followed by loss of donor (Bax-A488) fluorescence, since the donor quantum yield decreases in the presence of the acceptor (BH3-TAMRA), which can be quantified by changes in the steady-state fluorescence intensity,  $I$ , as described below<sup>52</sup>:

$$E_{FRET} = 1 - \frac{I_{DA}}{I_D} \quad (3)$$

where the indexes refer to the fluorescence intensity of the donor in the absence (D) and the presence (DA) of the acceptor.

### Partition coefficient determination

Membrane/water partition coefficient ( $K_p$ ) values are a quantified measure of the affinity of a particular molecule for lipid membranes. In order to obtain  $K_p$ 's of Bax-A488 in the absence or presence of bile acids, the following equation was fitted to the FRET efficiency data<sup>53</sup>:

$$E = \frac{E_w + K_p \gamma_L [L] E_L}{1 + K_p \gamma_L [L]} \quad (4)$$

where  $E_w$  and  $E_L$  are the FRET efficiencies for the probe in solution or in the lipid membrane, respectively;  $K_p$  is the partition coefficient and  $\gamma_L$  is lipid molar volume. A  $\gamma_L = 0.78 \text{ dm}^3 \text{ mol}^{-1}$  was used<sup>54</sup>.  $E_w$  is assumed to be the FRET efficiency obtained in the absence of lipid.  $E_L$  and  $K_p$  were optimized using the least-square method with GraphPad Prism 5 (GraphPad Software, CA, USA).

## **2.6. Fluorescence fluctuation spectroscopy (FFS)**

FFS measurements were performed on a Leica TCS SP5 (Leica Microsystems CMS GmbH, Mannheim, Germany) inverted confocal microscope (DMI6000). The 488-nm line provided by an Argon laser was focused into the sample by an apochromatic water immersion objective (63x, NA 1.2; Zeiss, Jena, Germany). Fluorescence emission was confocally detected using avalanche photodiodes (APDs) after passing through a 500–550 band-pass filter. A 111.44  $\mu\text{m}$  diameter pinhole in the image plane blocked out-of-focus signals and defined the detection volume. FFS data for Bax-A488 was acquired in the presence and absence of bile acids. Protein concentration was kept at 10 nM, and bile acid concentration

was 100  $\mu\text{M}$ . Each measurement consisted of 5 to 8 FFS datasets acquired for 50s each, with a sampling frequency of 500 kHz. Measurements were carried out using 8-well chamber slides (Ibidi, Martinsried, Germany). To prevent nonspecific adsorption of Bax-A488, the chamber wells were precoated with a 10% bovine serum albumin (BSA) solution and the samples were loaded after extensive rinsing with buffer.

### Fluorescence Correlation Spectroscopy (FCS)

Considering the presence of single fluorescent particles, the autocorrelation curve for a fluorescence fluctuation experiment is given by:

$$G(\tau) = G_T(\tau) \cdot G_D(\tau) \quad (5)$$

where  $G_D(\tau)$  and  $G_T(\tau)$  represent the parts of the correlation function for translational diffusion and triplet-state formation, respectively. If  $N$  is the average number of fluorescent molecules in the detection volume, then  $G_D(\tau)$  is given by:

$$G_D(\tau) = \frac{1}{N} \cdot \left(1 + \frac{\tau}{\tau_D}\right)^{-1} \cdot \left(1 + \frac{\tau}{S^2\tau_D}\right)^{-1/2} \quad (6)$$

where  $\tau_D$  is the translational diffusion time of the particles. This correlation time is the characteristic average diffusional transit time during which a molecule resides in the observation volume with the axial ( $\omega_z$ ) to lateral ( $\omega_{xy}$ ) dimension ratio,  $S$ .

$$S = \frac{\omega_z}{\omega_{xy}}; \quad \tau_D = \frac{\omega_{xy}^2}{4D} \quad (7), (8)$$

where  $D$  is the diffusion coefficient. On the other hand,  $G_T(\tau)$  is given by:

$$G_T(\tau) = 1 + \frac{T}{1-T} \cdot \exp\left(-\frac{\tau}{\tau_T}\right) \quad (9)$$

where  $T$  and  $\tau_T$  are the fraction of fluorophores in the triplet state and their triplet lifetime, respectively.

For Bax-A488, a 3D Gaussian with triplet contribution model<sup>55-61</sup>, considering  $n$  diffusing species (Eq. 10) was globally fitted to the experimental data by linking the triplet and diffusing times ( $\tau_T$  and  $\tau_D$ , respectively) across all the curves obtained for each sample. Also, the structural parameter  $S$  obtained in the calibration procedure using 10 nM of rhodamine 110, was subsequently fixed for the other samples measured in the same chamber slide.

$$G(\tau) = 1 + \frac{1}{N} \cdot \left( \frac{1-T + T \cdot e^{-\frac{\tau}{\tau_T}}}{1-T} \right) \cdot \left\{ \sum_{i=1}^n \frac{f_i}{\left(1 + \frac{\tau}{\tau_D}\right) \sqrt{1 + \tau(S^{-2}\tau_D)}} \right\} \quad (10)$$

where,  $f_i$  is the fractional population, of  $n$  different diffusion species. The dimensions of the focal volume (0.24 fL) were determined by calibration with rhodamine 10 nM in milliQ water using the same optical setup as the samples. A rhodamine 110 diffusion coefficient ( $D$ ) of  $440 \mu\text{m}^2\text{s}^{-1}$  was considered<sup>62</sup>. The beam waist of the laser focus,  $\omega_0$ , was calculated and then fixed in all the subsequent analysis of samples measured in the same  $\mu$ -Slide. Analysis of FCS data was performed using the ISS Vista software through a nonlinear least-squares fitting routine.

#### Photon counting histogram (PCH) analysis

PCH is the probability distribution of photon counts in the detection volume during FFS acquisition. To carry out PCH analysis, 3D Gaussian approximation for one-photon excitation and confocal detection was used<sup>63</sup>. The analytical expression for the PCH integration in this case is given by  $p_G$ :

$$p_G(k; Q, \varepsilon) = \frac{1}{Q\pi^{1/2}k!} \int_0^\infty \gamma(k, \varepsilon e^{-2x^2}) dx \quad (11)$$

where  $k$  corresponds to the photons counts,  $Q$  is the ratio between the reference volume and the size of the observation volume as described elsewhere<sup>63,64</sup>,  $\varepsilon$  is the brightness of the

fluorescent specie, and  $\gamma$  is the incomplete Gamma function. A correction to Eq. 11 is available that takes into account out-of-focus emission, so that the probability of observing  $k$  photons of the fluorescent specie  $i$  is given by  $p^{(i)}$ <sup>64</sup>:

$$p^{(i)}(1; Q, \varepsilon) = \frac{1}{(1+F)^2} \left[ p_G^{(i)}(1; Q, \varepsilon) + \frac{\varepsilon F}{2\sqrt{2Q}} \right] \quad (12)$$

and:

$$p^{(i)}(k; Q, \varepsilon) = \frac{1}{(1+F)^2} p_G^{(i)}(k; Q, \varepsilon) \text{ for } k > 1 \quad (13)$$

where,  $F$  corresponds to the correction factor that is applied for a first-order correction of the 3D Gaussian approximation, indicating the fraction of detected photons from the non-Gaussian part of the observation volume profile. These equations are all derived by integrating over all space and are only applicable for  $k > 0$ . The probability of receiving no photon counts is given by the normalization condition of probability distribution, so that  $P(0; Q, \varepsilon) = 1 - \sum_k^\infty P(k; Q, \varepsilon)$ <sup>63</sup>.

In case two fluorescent species are present, the photon counting histogram can be obtained by convoluting the photon counting histograms of the individual species<sup>63</sup>:

$$P(k; \bar{N}_1, \varepsilon_1, \bar{N}_2, \varepsilon_2) = P(k; \bar{N}_1, \varepsilon_1) \otimes P(k; \bar{N}_2, \varepsilon_2) \quad (14)$$

where  $\bar{N}_i$  and  $\varepsilon_i$  are defined as the average number of particles and brightness of the respective specie  $i$  in the observation volume.

Data analysis was performed with homemade software in a Matlab environment (Mathworks, Natick, MA). This program uses a Marquardt–Levenberg nonlinear least-squares fitting routine and the goodness of the fittings can be judged by the recovered  $\chi^2$  and random distribution of the weighted residuals. The first-order correction factor,  $F$ , for the PCH model of a confocal microscope with one-photon excitation was determined by calibration with Rho110 at 10 nM in milliQ water, using the same optical setup as for the samples. For samples of Bax-A488, Eq. 14 was globally fitted to the experimental data by considering the presence of two populations with different brightness's,  $\varepsilon_1$  and  $\varepsilon_2$ , that correspond to the monomeric and oligomerized form of the protein, respectively. For this analysis, we consider that the monomer brightness does not change from sample to sample by linking  $\varepsilon_1$  across all the curves obtained.

## 2.7. Leakage assays

Measurements were carried out with calcein-loaded LUVs (0.075 mM total lipid concentration) in the presence or not of bile acids at 100  $\mu$ M. Fluorescence measurements were carried out overtime at 25°C, using a cuvette with a path length of 0.5 cm and a FluoroLog 3 steady-state fluorescence spectrometer (model FL3-11; Horiba Jobin Yvon Inc., Edison, USA NJ) with constant stirring. Calcein fluorescence was measured with an excitation wavelength of 492 nm and emission at 520 nm. Calcein within liposomes is at self-quenching concentrations and basal fluorescence intensities were measured for 10 min. before adding recombinant Bax at a protein to lipid ratio (P/L) of 1/100 or 1/200, and the fluorescence intensity was recorded for cca 45 min. Eventually, 50  $\mu$ L of 10% Triton-X was used to fully disrupt the vesicles ensuring the release of residual entrapped calcein. The recorded fluorescence intensity curves were normalized and fitted to the following equation which assumes a simple flux  $J$  across the lipid bilayer in the direction of the concentration gradient<sup>65</sup>:

$$F_n = F_n^0 \left( 1 - e^{-\frac{3J \cdot (t-t_0)}{r}} \right) \quad (15)$$

In this equation,  $F_n$  is the normalized fluorescent intensity,  $F_n^0$  denotes the extent of leakage,  $r$  is the vesicle radius,  $t$  the time and  $t_0$  is the time when the leakage starts.

Giant Unilamellar Vesicles (GUVs) were prepared by the electroformation method in a 275 mOsm sucrose solution, as described elsewhere<sup>66,67</sup>. Lower CL levels were chosen for GUV formation, since high concentrations of this lipid inhibited electroformation. DiD was added to the lipid mixture at a dye-to-lipid ratio of 1:2500, to allow for visualization of vesicles in the confocal microscope. Biotinylated DOPE was also included (2 % of total lipid number) for immobilization of GUVs in Lab-Tek® observation chambers, coated with biotinylated BSA – streptavidin linker. An ATTO 488 solution (in 25 mM sodium phosphate, 100 mM KCl, 1 mM EDTA, pH 7.4) was added to the vesicles in the observation chamber, to final concentration of 1 $\mu$ M. Osmolarity of this solution was controlled to prevent leakage induced by osmolarity differences. Subsequently, Bax was added at a 1/100 protein to lipid ratio. The sample was scanned before and 60 minutes after Bax addition. Around 30 images were acquired at different areas of the observation chamber during each scan. Between 300 and 1000 vesicles were analyzed per sample. The measurements were performed using a confocal microscope equipped with an UPLSAPO 60x W N.A. 1.20 objective. Influx of ATTO 488 into GUVs was monitored by fluorescence through excitation with 488 nm laser line, while DiD signal was

measured through 632 nm excitation with the FluoView 1000 software package (Olympus, Hamburg, Germany). The data was analyzed using home-written Matlab scripts. The extent of permeabilization of each individual GUV was calculated according to:

$$F(\%) = \frac{F_v - F_b}{F_{out} - F_b} \times 100 \quad (16)$$

where  $F_v$  is the average intensity per pixel inside a GUV,  $F_b$  is the average background intensity per pixel and  $F_{out}$  is the initial average fluorescence intensity per pixel outside the GUVs.

### 3. Results

#### ***Impact of UDCA and TUDCA on Bax-A488 oligomerization***

In order to identify a possible effect of the cytoprotective bile acids, UDCA and TUDCA, at submicellar and physiologically active concentrations, over the oligomerization of full-length recombinant Bax, we first characterized the oligomerization of Alexa488-labeled Bax (Bax-A488) by size exclusion chromatography (SEC). Oligomerization was evaluated in the presence and absence of 100  $\mu$ M of cytoprotective bile acids. Protein fractions were further characterized by measuring fluorescence anisotropies (Figure 1). Here we observed that the full-length recombinant protein is mainly found in the monomeric form, both in the absence (Fig. 1 A) or presence of the cytoprotective bile acid UDCA (Fig. 1 B), which can be seen by a well-defined peak of  $\sim$ 22 kDa, which is in accordance with the molecular weight of the Bax monomer<sup>68</sup>. For TUDCA, the position of the monomer peak is somewhat shifted for larger sizes (35 kDa). A minor contribution of Bax dimers (2-5%) is also always detected, independently of the presence of bile acids. Fluorescence anisotropies found for monomer fractions of Bax-A488 are similar for all the samples ( $\langle r \rangle \sim 0.12$ ) (Fig. 1 A-C). Fluorescence anisotropies for dimer fractions could not be accurately measured due to very low fluorescence signal.

*n*-Octyl  $\beta$ -D-maltoside (OM) is a non-ionic detergent whose micelles are known to induce the formation of Bax dimers and higher order oligomers<sup>44</sup>. For the Bax-A488 in the presence of OM, we detected a fraction of protein with higher molecular weight, likely resulting from the interaction with OM micelles, since the correspondent fluorescence anisotropy is significantly higher ( $\langle r \rangle = 0.15$ ) than the monomer, when a decrease would be expected due to HomoFRET<sup>69</sup>. The protein fraction corresponding to high order oligomers ( $\sim$ 330 KDa) exhibit

a fluorescence anisotropy close to 0, as a result of extensive homoFRET within very large oligomeric structures<sup>69</sup>.

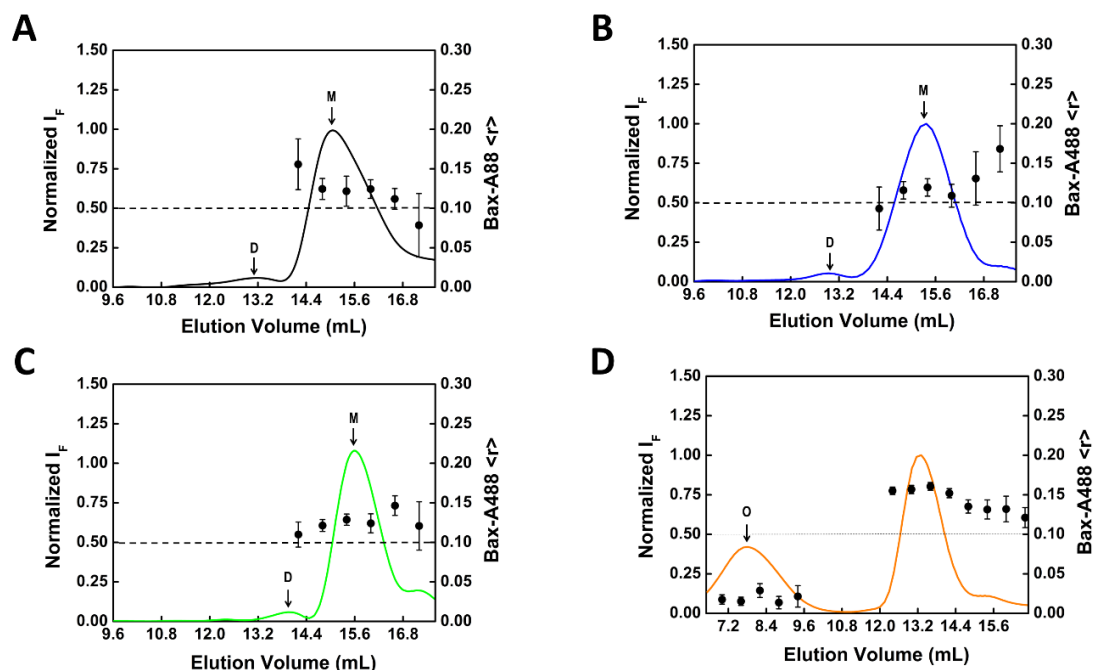


**Figure 5. Bax-A488 remains predominantly in the monomeric form even in the presence of cytoprotective bile acids** - Gel filtration profile (lines) and steady-state anisotropies (solid circles) of 200 nM Bax-A488 untreated (A) or treated with cytoprotective bile acids, UDCA (B) and TUDCA (C) at 100  $\mu$ M or treated with non-ionic detergent octyl-maltoside (D), OM, at 22 mM. For all the fractions collected, emission spectra and average steady-state anisotropies ( $\langle r \rangle$ ) were measured with excitation at 480 nm and emission at 515 nm. The error bars represent the standard deviation of 10 measurements each. Normalized  $I_F$  is given by performing integration between 500 and 600 nm of the fluorescence intensity already normalized for the maximum emission. All the elution profiles with the exception of OM show the presence of Bax-A488 mainly in the monomeric form (~22 kDa). Also, a minor contribution of dimeric Bax can be seen for lower elution volumes (~44 kDa). In the presence of OM, Bax also assembles into very large oligomers (~330 kDa). M, D and O stand for monomer, dimer and oligomer, respectively.

These results were further confirmed through FFS measurements and PCH analysis (Figure 2). Based on recovered chi-squares and distribution of residuals, a two-component model was chosen to fit the PCH data (Fig. 2 A-C). Due to the presence of 10 possible reaction sites for Alexa-488 on Bax, the labeling process is considered to be a random and independent process that assumes a Poisson distribution for the incorporation of the fluorophores, as

observed experimentally for other cases<sup>70–72</sup>. For monomeric proteins with low labeling efficiencies ( $<1$  dye/protein), the fraction of protein labeled with a single fluorophore is dominant and the brightness of this specie can be recovered through PCH analysis (for more detail see supplementary material). For the Bax-A488 used in PCH analysis, the labeling efficiency was 0.84, so that this criterion is met. In fact, the brightness of the dominant protein population, corresponding to the single-labeled Bax, was reliably and consistently recovered with an average value of  $0.069 \pm 0.004$  photon counts per bin time per molecule (cpbm) (Table S1). The second component is associated to the presence of a mixture of multi-labeled ( $\geq 2$  dyes per protein) Bax monomers and oligomers and presents a brightness of 3.4x that of the monomer (Table S1). The results of PCH analysis for Bax-A488 in the presence of UDCA and TUDCA (Fig. 2B and C) are shown in Table S1. The fraction of fluorescent species weighted by the brightness,  $F_1$  and  $F_2$  clearly show that the presence of UDCA and TUDCA has no impact whatsoever on Bax oligomerization (Fig. 2 D).

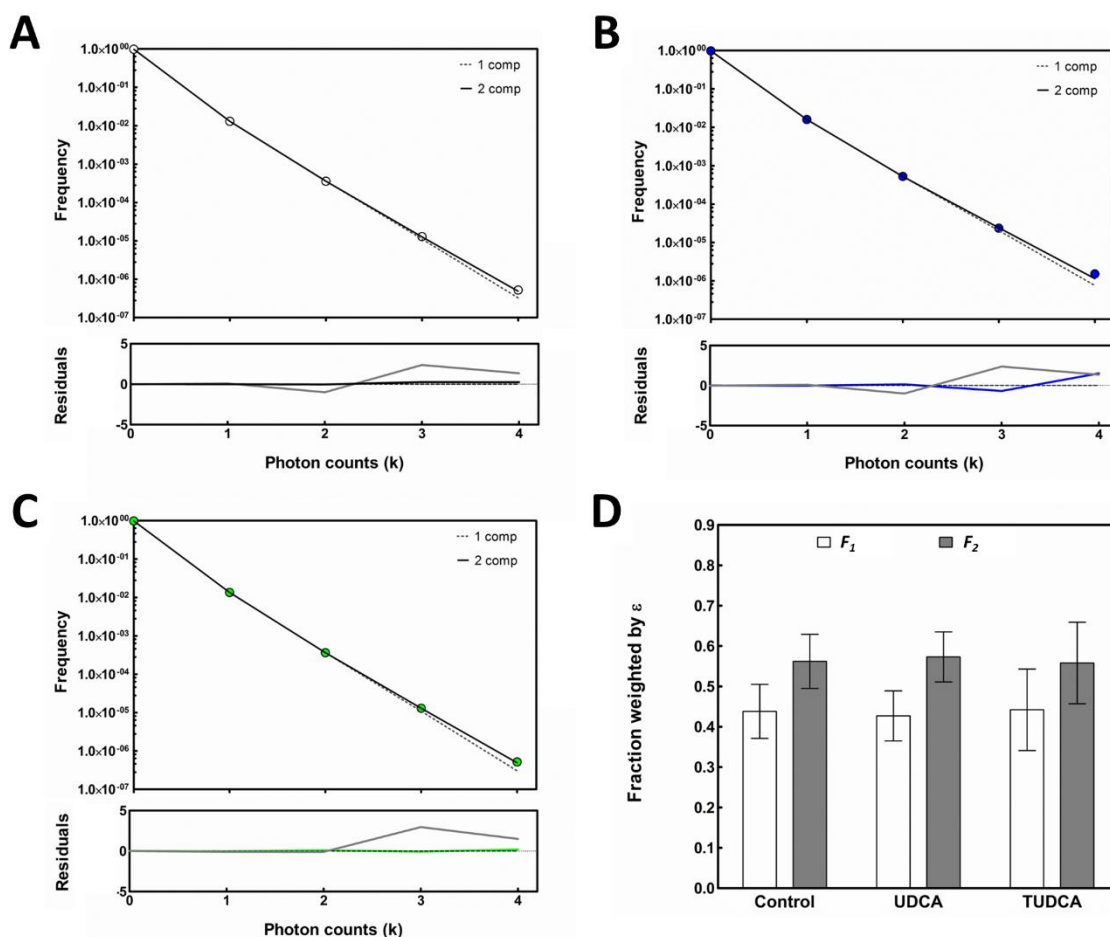


**Figure 6. The presence of cytoprotective bile acids has no impact on Bax-A488 oligomerization.** FFS measurements were carried out for 10 nM of Bax-A488 protein in solution after incubation with 100  $\mu$ M of bile acids. (A) Representative photon counting histograms of Bax-A488 alone and in the presence of UDCA (B) and TUDCA (C). PCH models considering only the presence of one protein

---

species (gray dashed line) or two different populations (black line) were fitted to the data. Residuals distribution clearly shows that the two-component model is most appropriate for the data analysis (black, blue and green lines). (D) The fractions of the first and second component weighted by the brightness,  $F_1$  and  $F_2$ , which give information about the contribution of each population to the total fluorescence, were calculated.  $F_i$  correspond to mean values  $\pm$  standard deviations of 5 to 8 measurements.

Fluorescence Correlation Spectroscopy (FCS) measurements were also performed for Bax-A488 in the presence of UDCA and TUDCA (Figure 3). We recovered a diffusion coefficient (D) for Bax-A488 alone of  $110 \pm 2 \mu\text{m}^2/\text{s}$  that is only slightly lower than the theoretical expectation for a monomeric protein of this size ( $D=117 \mu\text{m}^2/\text{s}$ )<sup>73</sup>. The diffusion coefficient recovered in the presence of UDCA and TUDCA was  $105 \pm 5$  and  $89 \pm 4 \mu\text{m}^2/\text{s}$ , respectively (Fig. 3 D). Both bile acids induce a decrease in diffusion coefficient, but the reduction is only significant for TUDCA (Fig. 3 C). Since we already ascertained through independent methodologies that TUDCA has not impact on Bax oligomerization, the decrease in diffusion coefficient of Bax-A488 is likely to report the formation of complexes between Bax and pre-micellar aggregates of TUDCA molecules, which are likely adsorbing to the protein surface. This is in agreement with the minor shift in monomer size observed in SEC experiments for Bax in the presence of TUDCA.

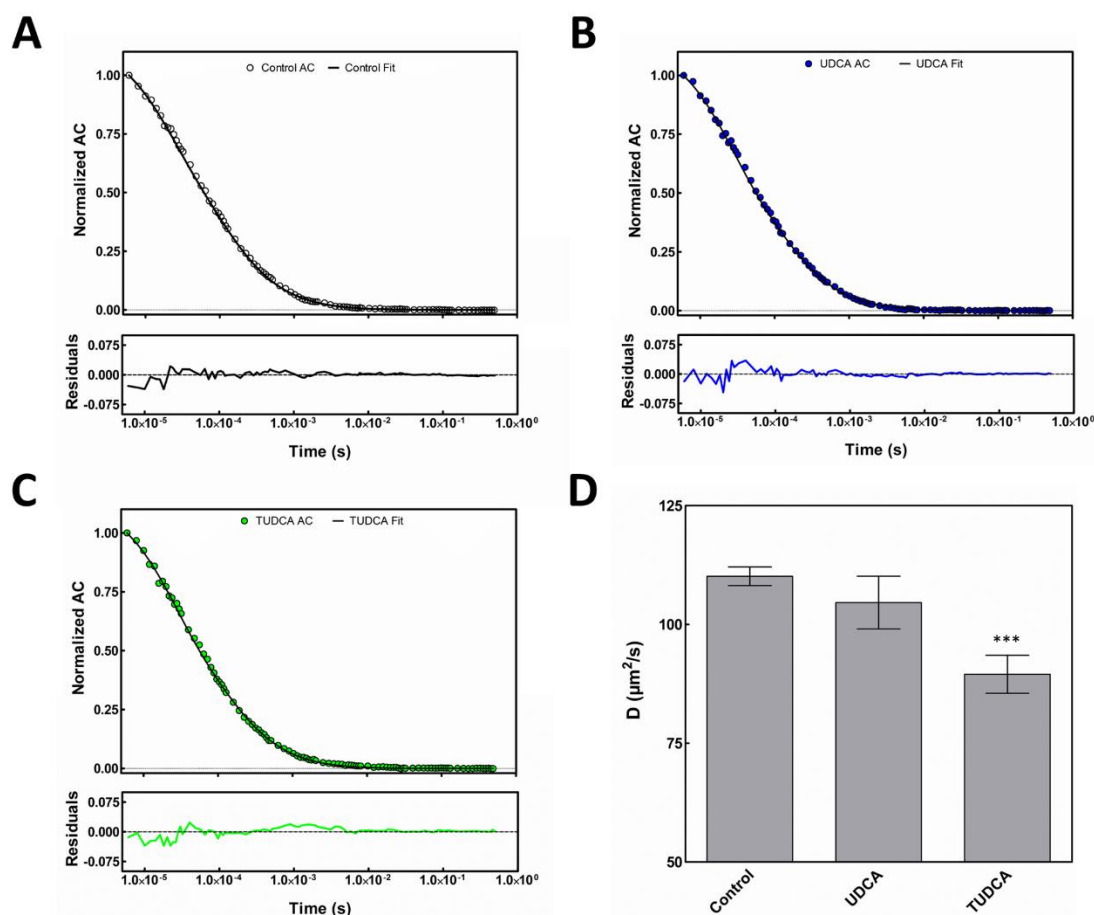


**Figure 7. The cytoprotective bile acid TUDCA induces a decrease in Bax-A488 diffusion coefficient, that results from the formation of complexes between Bax and pre-micellar aggregates of TUDCA molecules.** FFS measurements were carried out for 10 nM of Bax-A448 protein in solution after incubation with 100  $\mu\text{M}$  of bile acids. (A) Representative normalized autocorrelation curve (full line is a fitting of eq. 10) obtained for Bax-A488 alone in solution (A) or in the presence of UDCA (B), TUDCA (C). Fitting of Eq. 10 to experimental data (dots) is associated with residuals distribution around zero for all samples. (D) Diffusion coefficients of Bax-488 in the absence or presence of bile acids correspond to mean values  $\pm$  standard errors (\*\*\*) $p < 0.001$ ). Diffusion coefficient values for each condition are averages of at least 5 independent samples with 5 to 10 measurements each.

In order to confirm the interaction between bile acids and Bax, Bax was labeled with NBD, an amine-derivative fluorophore that possesses convenient photophysical properties, such as good fluorescence quantum yield and highly sensitivity to the environment<sup>74,75</sup>. Steady-state fluorescence measurements with Bax-NBD confirmed the interaction between the protein and both bile acids as a concentration-dependent increase in Bax-NBD fluorescence intensity is observed in the presence of UDCA or TUDCA (Figure S1).

### Impact of UDCA and TUDCA on the interaction between Bax-A488 and activator peptide BH3-TAMRA

One of the key steps in Bax activation is the interaction with a BH3-only protein, such as tBid, which induces conformational changes that allow for membrane-protein binding and pore formation<sup>30,33–35</sup>. BH3 peptides have been shown to mimic BH3-only protein activation of Bax<sup>76</sup> as they correspond to the domain that is inserted into Bax hydrophobic groove<sup>44</sup>. We performed a FRET-based interaction assay where we used Bax-A488 as a donor and the BH3 peptide from Bid, labeled with TAMRA, as the acceptor. The FRET efficiencies calculated according to Eq. 3 show that Bax-A488 binds to BH3-TAMRA, resulting in a peptide concentration-dependent increase in FRET efficiency. Both cytoprotective bile acids are shown to inhibit significantly the interaction between the protein and the activator peptide (Fig. 4A). Resulting dissociation constants ( $K_d$ ) are shown on Table S2. UDCA and TUDCA increase the recovered  $K_d$  by 4.8 and 3.2 times, respectively. This result suggests that the adsorption of premicellar aggregates of bile acids to Bax shields the protein from interaction and insertion of the Bid-BH3 peptide in the hydrophobic groove of the protein. On the other hand, the non-ionic detergent OM has no impact on Bax and activator peptide interaction (Fig. 4B), suggesting that the nature of interaction of UDCA and TUDCA is inherently different from that observed with activating detergents.

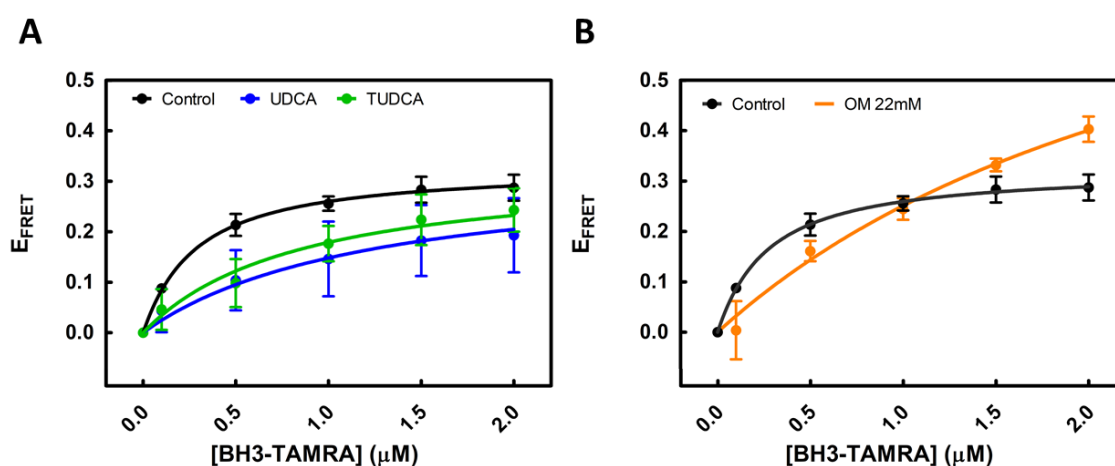


**Figure 8. Cytoprotective bile acids inhibit the interaction between Bax-A488 and activator peptide BH3-TAMRA.** 50 nM of Bax-A488 was previously incubated with 100  $\mu\text{M}$  of bile acids (A) or OM at 22 mM (B). Fluorescence emission of Bax-A488 was recovered between 500 and 530 nm ( $\lambda_{\text{exc}} = 480$  nm), and FRET efficiencies were calculated according to Eq. 3. Curves (solid lines) are fits of Eq. S6 to experimental data. The parameters  $K_d$  and  $E_{\text{bound}}$  were recovered through least-square regression of Eqs. S5 and S6 to the FRET data.

***Modulation of Bax-A488 partition to membranes by cytoprotective bile acids***

In order to identify a possible effect of cytoprotective bile acids on the affinity of Bax for membranes, a FRET experiment was designed to quantify membrane partition coefficients of Bax-A488 in the presence of both UDCA and TUDCA. LUVs with a lipid composition that mimics the mitochondrial outer membrane (MOM) and loaded with a labeled phospholipid (DOPE-Rho) were used. Association of Bax-A488 to the liposomes results in FRET between Bax-A488 and DOPE-Rho, that can be quantified through changes in fluorescence intensity of the labeled protein. Partition curves were obtained in the absence and presence of cytoprotective bile acids (Figure 5). Membrane/water partition coefficients ( $K_p$ ) of Bax-A488 are recovered through fitting of Eq. 4 to the experimental data and are shown on Table S3.  $K_p$  values do not change significantly in the absence or presence of either cytoprotective bile acid. In fact, the differences between partition curves are mainly found in the FRET efficiency measured for the protein after membrane insertion ( $E_L$ ). The recovered FRET efficiency values for the protein alone after incorporation in the membrane was 0.44, considerably higher than in the presence of UDCA or TUDCA (Fig. 4 A, B, respectively), for which the recovered  $E_L$  values were 0.29 and 0.26, respectively. These results imply that in the presence of bile acids and after membrane incorporation, the average position of A488 within Bax-A488 is considerably displaced from its position in the absence of bile acids, to a location farther away from the phospholipid headgroups (where the acceptor is present). In this way, after membrane interaction, the cytoprotective bile acids stabilize the protein in a more superficial conformation. This result suggests that cytoprotective bile acids could have the potential to interfere with the embedding of Bax in the membrane environment.

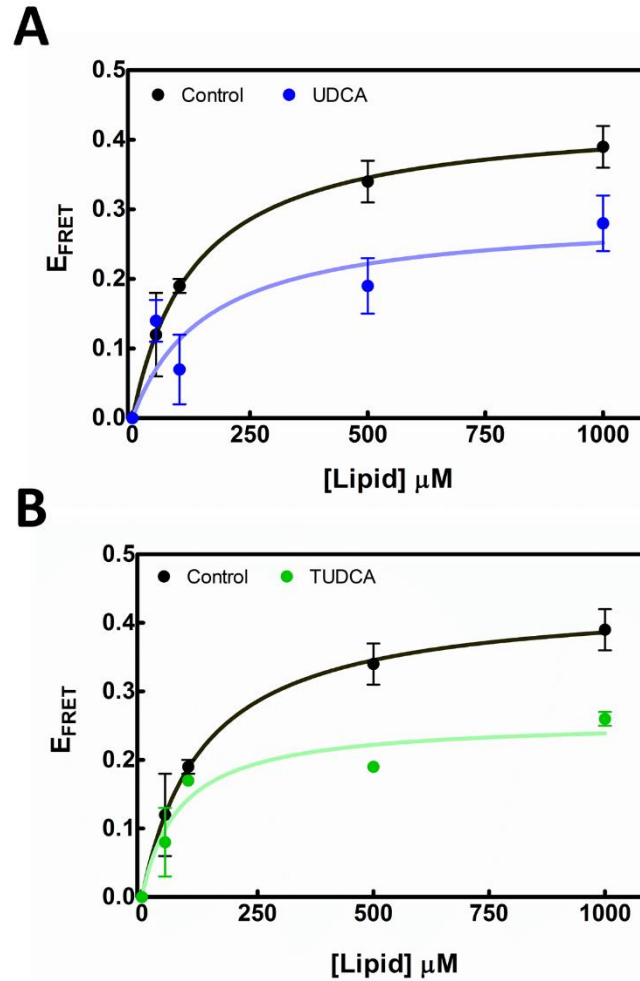


**Figure 9. Cytoprotective bile acids and BH3 are able to inhibit the partition of Bax-A488 to membranes mimicking the MOM.** Liposomes were composed of a lipid mixture that mimics MOM composition (PC/PE/PI/CL/Chol, 48:25:12:6:9 molar ratios)<sup>77</sup> and labeling was accomplished by the incorporation of Rho-DOPE into the lipid mixture at a labeled lipid to unlabeled lipid ratio of 1/200. Partition curves were obtained by incubation of 50 nM of Bax-A488 with increasing lipid concentration (0 to 1000  $\mu\text{M}$ ) in the absence (black) or presence of 100  $\mu\text{M}$  cytoprotective bile acids such as UDCA (A, Blue) and TUDCA (C, green). Fluorescence emission of Bax-A488 was recovered between 500 and 530 nm ( $\lambda_{\text{exc}} = 480$  nm), and FRET efficiencies were calculated according to Eq. 4. Curves (solid lines) are fits of Eq. 4 to experimental data. The  $K_p$  values recovered in the presence of bile acids do not differ significantly from the one found for the control. However, FRET efficiencies of the protein in the membrane ( $E_L$ ) decrease significantly in the presence of either UDCA or TUDCA.

### **Determination of cytoprotective bile acid effect on Bax pore-forming activity – leakage assays**

In order to evaluate the effect of bile acids over Bax pore-forming functionality on mitochondrial membranes, leakage studies were performed on LUVs and GUVs mimicking MOM lipid composition. In LUV experiments, calcein is encapsulated at self-quenching concentrations<sup>78</sup>, and leakage of calcein through the membrane is detected through an increase in fluorescence intensity of the dye. Here, we followed the leakage kinetics after incubation with 100  $\mu\text{M}$  of cytoprotective bile acids, UDCA and TUDCA, respectively (Figure 6). Applying Eq. 15, where we assume a simple flux across the lipid membrane in the direction of the concentration gradient, we can recover two parameters, the flux,  $J$ , that describes the speed by which molecules diffuse across the lipid bilayer and  $F_n^0$  that corresponds to the percentage of leaked dye<sup>79</sup>. Normalized fluorescence intensities measured overtime are shown in Figure 6 for a Bax-A488 to lipid ratio of 1/200 (Fig. 6A) and 1/100 (Fig. 6B), and the parameters obtained from fitting of the diffusion model to the data are presented in Table S4. Bax-induced leakage of LUVs is shown to be dependent on protein to lipid ratio (P/L), with significantly more leakage observed for higher P/L in all conditions. At a P/L of 1/200 and in the presence of UDCA and TUDCA, the rate of Bax-dependent leakage ( $J$ ) is markedly lower (Fig. 6A). The impact of bile acids on LUV permeabilization is decreased at higher P/L but is always significant (Fig. 6B).

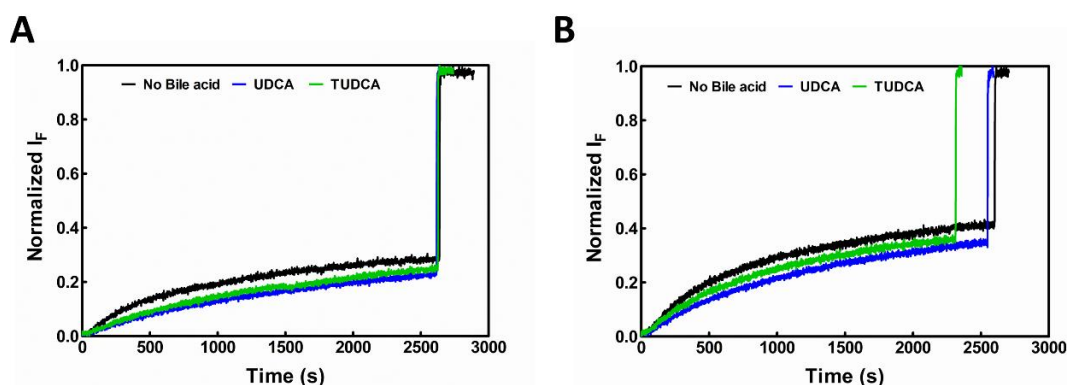


**Figure 10. Cytoprotective bile acids slow down the leakage induced by Bax and their efficiency is dependent on lipid concentration.** Leakage kinetics measured on LUVs composed of POPC: POPE: TOCL at molar ratios of 43:36:21 (mol:mol:mol) at a total lipid concentration of 0.15mM or 0.075mM (A and B, respectively) and loaded with calcein dye. LUVs were then incubated with 100  $\mu\text{M}$  UDCA (blue) or TUDCA (green), previous to measurement. Control sample (no bile acid - black) didn't contain any bile acid. Unlabeled Bax at 750 nM was added in  $t = 0$  s, in a final protein to lipid ratio of 1/200 (A) or 1/100 (B). After 45 minutes, finally, Triton X was added in order to disrupt the vesicles and release all the entrapped dye.

---

Since, GUVs are large enough to be visible under a conventional microscope, individual vesicles can be observed during the entire leakage process<sup>79</sup>. In this experiment, leakage is followed by an increase in the degree of GUV filling due to the influx of Atto-488 molecules that are present in the solution outside vesicles. The extent of permeabilization,  $F(\%)$  is given by Eq. 16 and vesicles with  $F(\%)$  values of 80-100% ( ) were considered to have leaked, those with values between 20 and 80% were considered partially leaked, and values of 0-20% were taken to indicate the absence of leakage. Results are shown in Figure 7 for GUVs before (0 min), 60 or 120 min after addition of Bax in the absence (Fig. 7A) or presence of cytoprotective bile acids, UDCA and TUDCA (Fig 7B, C, respectively). Control samples without Bax were only scanned after 120 minutes. In the absence of bile acids, and after the addition of Bax to the GUVs, 37% of these vesicles leaked and only 5% underwent partial leakage induced by Bax (Fig. 7A). The small fraction of partially permeabilized vesicles reflect an all-or-none leakage mechanism<sup>80</sup> which suggest long-lived pores as previously observed<sup>79</sup>.

Again, leakage is strongly inhibited by both UDCA and TUDCA (Fig. 7B, C), and in the presence of these bile acids, just 2 to 4% of the vesicles leaked after Bax addition, even for longer incubations (120 min). The inhibitory effect of cytoprotective bile acids over Bax pore-forming activity was much more pronounced for the case of the GUVs than for LUVs. This could be associated with a higher density of Bax in GUV assays, since for LUVs, UDCA and TUDCA inhibited Bax-dependent leakage more efficiently at lower protein densities. The dependence of Bax inhibition by bile acids on P/L ratios, could reflect an impact of bile acids on oligomerization of Bax within the membrane.

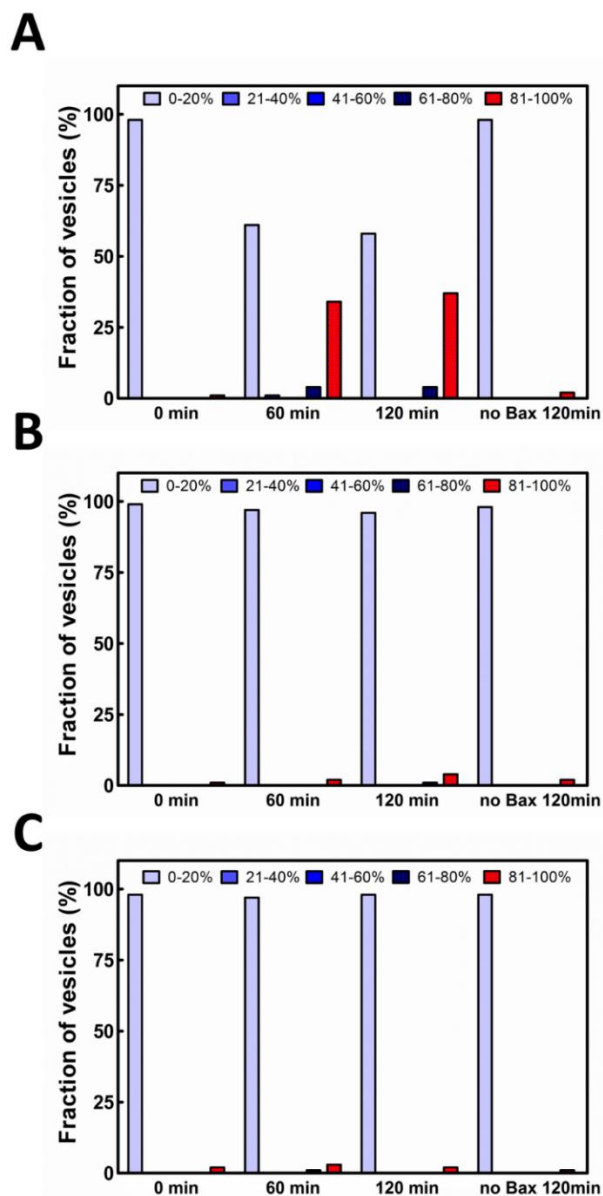


**Figure 11. Inhibition of GUV leakage is observed in the presence of cytoprotective bile acids.** After electroformation, the GUVs composed of POPC: POPE: TOCL at molar ratios of 54:36:10 (mol:mol:mol) were left in the Lab-Tek® chamber precoated, first with biotinylated albumin and then with streptavidin, in the presence of Atto488 dye and absence (A) or presence of cytoprotective bile acids, UDCA (B) and TUDCA (C), at a final concentration of 1  $\mu$ M and 100  $\mu$ M, respectively. After a 30-minute incubation, unlabeled Bax was added and sample was scanned before and 60/120 minutes after Bax addition. Control samples were prepared concurrently at the same conditions, Bax addition was skipped. During each scan around 30 pictures were taken and 500 to 1000 GUVs were analyzed. Histograms of GUV population describe the extent of permeabilization before (0 min) and 60/120 minutes after Bax addition. Control sample was scanned only after 120 minutes (no Bax 120min). Vesicles with fluorescence intensity losses between 0-20% were taken to indicate no leakage while percentages of 20-80% correspond to partial leakage and 80-100% to full leakage. Leakage inhibition by bile acids is much more pronounced for the assay with GUVs.

***Modulation of Bax activity by bile acids is not restricted to cytoprotective species***

Bile acids are always cytotoxic when their concentrations increase to abnormally high levels intracellularly and extracellularly<sup>81</sup>. Their cytotoxicity is strongly affected by its structure: hydrophobic bile acids, such as deoxycholic acid, DCA, have been reported to induce apoptosis in hepatocytes at low concentration ( $\leq 100 \mu\text{M}$ ), well below their critical micellar concentration<sup>24</sup>. At submicellar extracellular concentrations (50-100  $\mu\text{M}$ ), these molecules have been proposed to activate cell death receptors in a ligand-independent manner<sup>82</sup>; induce c-jun N-terminal kinase 1-mediated activation of p53, elongation factor 2-1, and cyclin D1 expression<sup>24,83,84</sup>; induce oxidative damage<sup>85</sup>; promote Bax translocation to mitochondria<sup>23</sup> and induce mitochondrial dysfunction<sup>1,85</sup>.

In order to evaluate if the impact of bile acids over Bax as described here, were exclusively observed for cytoprotective bile acids, experiments were also carried out using the apoptotic and more hydrophobic bile acid DCA (Figure S2). As observed for UDCA and TUDCA, DCA also inhibits interaction of Bax-A488 with the activating peptide Bid-BH3-TAMRA (Fig. S2A) and promotes a more superficial location for Bax in liposomes mimicking MOM lipid composition (Fig. S2B). As observed for TUDCA, the diffusion of Bax in the presence of DCA is also slowed down ( $D = 60 \pm 16 \mu\text{m}^2/\text{s}$ ) (Fig. S2C), possibly also due to the adsorption of a large number of DCA molecules to the surface of Bax. In fact, also as observed for TUDCA, this decrease in diffusion coefficient is not associated with protein oligomerization (Fig. S2D, E). Additionally, DCA is also shown to interact with Bax-NBD (Fig. S2F).

Importantly, Bax-induced leakage of LUVs and GUVs is also attenuated by DCA (Figure 8). For LUVs, DCA is even shown to inhibit Bax permeabilization more efficiently than UDCA or TUDCA ( $J$  is reduced by 66% for 1/200 P/L ratio) (Figure 8A, B and Table S4). Results for the leakage of GUVs with DCA are analogous to the results obtained with cytoprotective bile acids, showing almost full inhibition of Bax permeabilization activity (Fig. 8C). Unlike isolated mitochondria which are permeabilized by DCA at physiologically active apoptotic concentrations, liposomes mimicking mitochondrial membrane composition are not directly permeabilized by this bile acid<sup>15</sup>, and this result is again confirmed here.

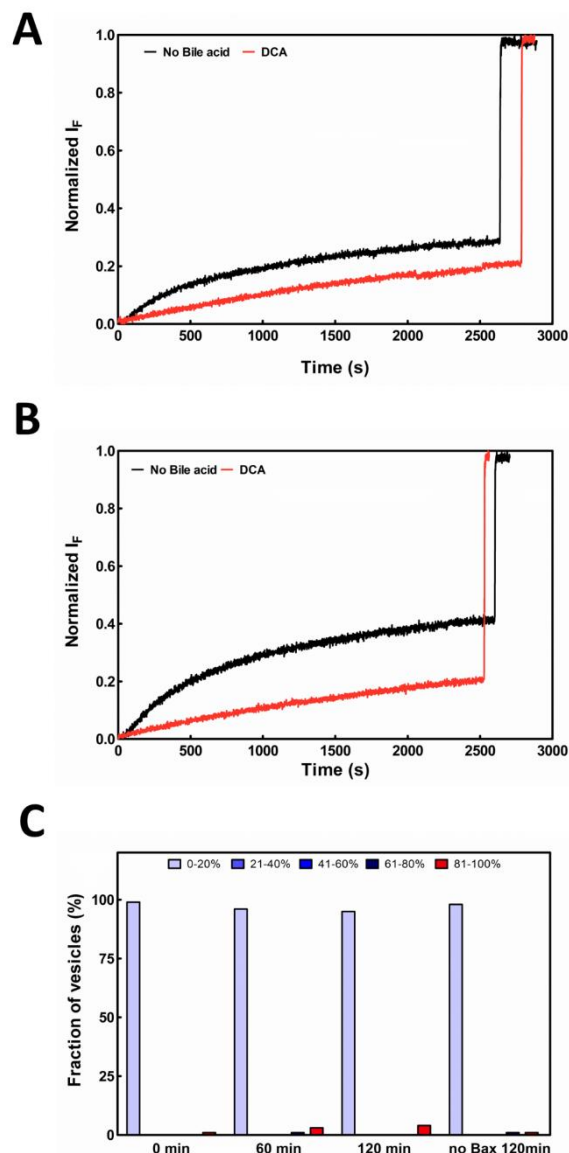


**Figure 12. Cytotoxic bile acid DCA inhibits the leakage induced by Bax on LUVs and GUVs.** Leakage kinetics measured on LUVs at a total lipid concentration of 0.15mM or 0.075mM (A and B, respectively) and loaded with calcein dye. LUVs were then incubated with 100  $\mu$ M DCA (red) previous to measurement. Control sample (No bile acid - black) didn't contain any bile acid. Unlabeled Bax was added in  $t = 0$  s, at a final protein to lipid ratio of 1/200 (A) or 1/100 (B). After 45 minutes, Triton X was added in order to disrupt the vesicles and release all the entrapped dye. (C) Inhibition of GUV leakage in the presence of DCA. After electroformation the GUVs were left in the Lab-Tek® chamber precoated, first with biotinylated albumin and then with streptavidin, in the presence of Atto488 dye and DCA, at a final concentration of 1  $\mu$ M and 100  $\mu$ M, respectively. After 30 minutes, unlabeled Bax was added (1/100 protein to lipid ratio). Sample was scanned before and 60/120 minutes after Bax addition. Control sample was prepared concurrently at the same conditions, Bax addition was skipped. During each scan, around 30 pictures were taken and 500 to 1000 GUVs were analyzed. Histograms of GUVs before (0 min) and

60 or 120 minutes after Bax addition. Control sample was scanned only after 120 minutes of incubation (no Bax 120min). Vesicles with fluorescence intensity losses between 0-20% were taken to indicate no leakage, while percentages of 20-80% correspond to partial leakage and 80-100% to full leakage. Leakage restriction is much more pronounced for GUVs assay, where only 4 % of GUVs leaked after 120 minutes in samples containing DCA.

Overall, these results show that interaction of UDCA and TUDCA with Bax is not the result of a specific interaction available solely for cytoprotective molecules, and likely results from non-specific adsorption of bile acids to the protein surface. The impact of bile acids on the membrane integration and permeabilization activity of Bax is a general effect and is not a feature of only cytoprotective molecules. It is possible that the difference between activation of cytoprotection or triggering of apoptosis by bile acids is just defined by the intrinsic ability of hydrophobic bile acids such as DCA for direct permeabilization of mitochondrial membranes, which is not observed for the more hydrophilic bile acids TUDCA and UDCA.

## 4. Discussion

The mechanism of Bax-mediated permeabilization of MOM is the subject of considerable controversy, and even the commonly shared view that the cytosolic protein is monomeric was recently challenged as for a number of cell lines, an inhibited dimeric form of soluble Bax was found<sup>31</sup>. Although the current assessment is that the monomer is the active protein form to insert into mitochondria<sup>29,31,36,86,87</sup>, studies on Bax activated by detergents have found the detergent-activated form of Bax to correspond to monomeric or oligomeric forms of the protein<sup>31,42-44</sup>.

While cytoprotective bile acids have been shown to inhibit apoptosis in both hepatic and nonhepatic cells<sup>1,2</sup>, the corresponding mechanism of action is still not understood. Nevertheless, the inhibitory effect of cytoprotective bile acids over Bax translocation to mitochondria after an apoptotic stimuli has been extensively reported<sup>18,19</sup>. Since cytoprotective bile acids exhibit very low partition to lipid membranes<sup>12</sup>, Bax in its cytosolic form seems to be a strong candidate as target for these molecules. This proposition is further supported by the activation and deactivation of Bax by different detergents, either priming it for activity or leading to the formation of non-functional dimers<sup>40-42</sup>. In order to address this hypothesis, we aimed here to carry out a comprehensive study of the impact of physiologically active concentrations of cytoprotective bile acids, UDCA and TUDCA, on Bax oligomerization, mitochondrial

membrane integration and pore-forming activity. Experiments were also carried out in parallel with the cytotoxic bile acid DCA for comparison.

Size exclusion chromatography (SEC) and PCH analysis of Bax-A488 samples after incubation with physiologically active concentrations of each of the cytoprotective bile acids in study, clearly show that although Bax is present in monomeric and dimeric forms, interaction with UDCA and TUDCA in this concentration range has no impact on protein oligomerization. These results differ from the observations with OM, which is known to activate Bax and induces considerable oligomerization of the protein. In this way, the nature of the interactions of cytoprotective bile acids or OM with Bax are shown to be distinct. The apoptotic bile acid DCA is also shown to have no impact on Bax oligomerization at physiologically active concentration. Nevertheless, the presence of both TUDCA and DCA, are shown to induce a considerable decrease in diffusion coefficients of Bax-A488, reflecting the increase in size of mixed Bax/bile acid complexes, as a great number of bile acid molecules adsorb to the protein surface. Interestingly, the mobility of Bax in the presence of UDCA is not significantly affected, likely reporting the formation of Bax/bile acid complexes of smaller dimensions. Interaction between bile acids and Bax is confirmed through the use of Bax labeled with an environment sensitive dye, NBD. Since interaction is observed for all bile acids, and in the case of TUDCA and DCA is actually detected through a decrease in protein diffusion, it is very likely that this interaction is non-specific and corresponds to adsorption of these molecules on the protein surface.

Bax complexed with bile acids is shown to have reduced affinity for Bid-BH3 activating peptide, as well as reduced membrane integration for all bile acids tested here. In fact, interestingly, FRET experiments showed that although the membrane affinity of Bax is not significantly affected by the presence of bile acids, the average distance of A488 fluorophores in the protein to the lipid membrane is greatly increased, suggesting a much more superficial location for Bax in the presence of bile acids. The results suggest that the partial solubilization of Bax with bile acids prevent both molecular recognition of binding partners as well as the complex Bax conformational rearrangements required for proper membrane embedding and oligomerization in lipid membranes. This is also evident from the lipid membrane permeabilization studies, where UDCA, TUDCA and DCA inhibited to different extents the pore-forming activity of Bax. As previously shown<sup>79</sup>, permeabilization by Bax follows an all-or-none mechanism, reflecting the long lifetime of these pores. Importantly, the inhibitory effect of bile acids on Bax pore formation is heavily dependent on Bax density. This suggests that the studied bile acids could interfere with protein oligomerization during pore formation, but further experiments are necessary to shed light on this issue.

Surprisingly, with this work, we showed that although UDCA/TUDCA and DCA have opposite effects on regulation of apoptosis, all the bile acids in study have comparable inhibitory effects over Bax membrane integration, interaction with activating Bid-BH3 peptide and pore formation. These results open the door to an interpretation regarding the differences in modulation of cell fate by bile acids, that considers that apoptosis or cytoprotection activities are defined by two competing mechanisms, direct permeabilization of mitochondrial membranes and inhibition of Bcl-2 proteins. In the case of cytoprotective bile acids, due to their hydrophilicity, limited interaction with membranes is observed<sup>12</sup>, and as such, do not promote mitochondrial permeabilization<sup>15</sup>. Simultaneously, as shown here, at least partially through interaction with either soluble or membrane-bound Bax, these bile acids could be able to promote cytoprotection. On the other hand, hydrophobic cytotoxic bile acids, exhibit considerable interaction with mitochondrial membranes<sup>12</sup>, and any possible inhibition of Bax activity is negated by direct permeabilization of the MOM<sup>15</sup>.

### **Acknowledgements/Grant Support**

Authors acknowledge funding by FCT project references RECI/CTM-POL/0342/2012, PTDC/QUI-BIO/119494/2010 and UID/NAN/50024/2013. T.S is the recipient of fellowship from FCT (SFRH/BD/92398/2013). F.F acknowledges FCT through Researcher Contract No. IF/00386/2015.

### **5. References**

1. Rodrigues, C. M., Fan, G., Ma, X., Kren, B. T. & Steer, C. J. A novel role for ursodeoxycholic acid in inhibiting apoptosis by modulating mitochondrial membrane perturbation. *J. Clin. Invest.* **101**, 2790–9 (1998).
2. Amaral, J. D., Viana, R. J. S., Ramalho, R. M., Steer, C. J. & Rodrigues, C. M. P. Bile acids: regulation of apoptosis by ursodeoxycholic acid. *J. Lipid Res.* **50**, 1721–34 (2009).
3. Paumgartner, G. & Beuers, U. Ursodeoxycholic acid in cholestatic liver disease: mechanisms of action and therapeutic use revisited. *Hepatology* **36**, 525–31 (2002).

4. Perez, M. J. Bile-acid-induced cell injury and protection. *World J. Gastroenterol.* **15**, 1677 (2009).
5. Ramalho, R. M., Borralho, P. M., Castro, R. E., Solá, S., Steer, C. J. & Rodrigues, C. M. P. Tauroursodeoxycholic acid modulates p53-mediated apoptosis in Alzheimer's disease mutant neuroblastoma cells. *J. Neurochem.* **98**, 1610–8 (2006).
6. Ramalho, R. M., Viana, R. J. S., Low, W. C., Steer, C. J. & Rodrigues, C. M. P. Bile acids and apoptosis modulation: an emerging role in experimental Alzheimer's disease. *Trends Mol. Med.* **14**, 54–62 (2008).
7. Mortiboys, H., Aasly, J. & Bandmann, O. Ursocholic acid rescues mitochondrial function in common forms of familial Parkinson's disease. *Brain* **136**, 3038–3050 (2013).
8. Keene, C. D., Rodrigues, C. M., Eich, T., Linehan-Stieers, C., Abt, a, Kren, B. T., Steer, C. J. & Low, W. C. A bile acid protects against motor and cognitive deficits and reduces striatal degeneration in the 3-nitropropionic acid model of Huntington's disease. *Exp. Neurol.* **171**, 351–60 (2001).
9. Fonseca, I., Gordino, G., Moreira, S., Nunes, M. J., Azevedo, C., Gama, M. J., Rodrigues, E., Rodrigues, C. M. P. & Castro-Caldas, M. Tauroursodeoxycholic Acid Protects Against Mitochondrial Dysfunction and Cell Death via Mitophagy in Human Neuroblastoma Cells. *Mol. Neurobiol.* **54**, 6107–6119 (2017).
10. Dromparis, P., Paulin, R., Stenson, T. H., Haromy, A., Sutendra, G. & Michelakis, E. D. Attenuating endoplasmic reticulum stress as a novel therapeutic strategy in pulmonary hypertension. *Circulation* **127**, 115–125 (2013).
11. Cai, Z., Li, F., Gong, W., Liu, W., Duan, Q., Chen, C., Ni, L., Xia, Y., Cianflone, K., Dong, N. & Wang, D. W. Endoplasmic reticulum stress participates in aortic valve calcification in hypercholesterolemic animals. *Arterioscler. Thromb. Vasc. Biol.* **33**, 2345–2354 (2013).
12. Mello-Vieira, J., Sousa, T., Coutinho, A., Fedorov, A., Lucas, S. D., Moreira, R., Castro, R. E., Rodrigues, C. M. P., Prieto, M. & Fernandes, F. Cytotoxic bile acids, but not cytoprotective species, inhibit the ordering effect of cholesterol in model membranes at physiologically active concentrations. *Biochim. Biophys. Acta* **1828**, 2152–2163 (2013).
13. Benz, C., Angermüller, S., Otto, G., Sauer, P., Stremmel, W. & Stiehl, a. Effect of tauroursodeoxycholic acid on bile acid-induced apoptosis in primary human hepatocytes. *Eur. J. Clin. Invest.* **30**, 203–9 (2000).
14. Zhou, Y., Maxwell, K. N., Sezgin, E., Lu, M., Liang, H., Hancock, J. F., Dial, E. J., Lichtenberger, L. M. & Levental, I. Bile acids modulate signaling by functional

- perturbation of plasma membrane domains. *J. Biol. Chem.* **288**, 35660–70 (2013).
15. Sousa, T., Castro, R. E., Pinto, S. N., Coutinho, A., Lucas, S. D., Moreira, R., Rodrigues, C. M. P., Prieto, M. & Fernandes, F. Deoxycholic acid modulates cell death signaling through changes in mitochondrial membrane properties. *J. Lipid Res.* (2015). doi:10.1194/jlr.M062653
  16. Schulz, S., Schmitt, S., Wimmer, R., Aichler, M., Eisenhofer, S., Lichtmanegger, J., Eberhagen, C., Artmann, R., Tookos, F., Walch, A., Krappmann, D., Brenner, C., Rust, C. & Zischka, H. Progressive stages of mitochondrial destruction caused by cell toxic bile salts. *Biochim. Biophys. Acta* **1828**, 2121–33 (2013).
  17. Rolo, A. P., Oliveira, P. J., Moreno, A. J. & Palmeira, C. M. Chenodeoxycholate induction of mitochondrial permeability transition pore is associated with increased membrane fluidity and cytochrome c release: protective role of carvedilol. *Mitochondrion* **2**, 305–11 (2003).
  18. Rodrigues, C. M. P., Solá, S., Sharpe, J. C., Moura, J. J. G. & Steer, C. J. Tauroursodeoxycholic acid prevents Bax-induced membrane perturbation and cytochrome C release in isolated mitochondria. *Biochemistry* **42**, 3070–80 (2003).
  19. Rodrigues, C. M., Ma, X., Linehan-Stieers, C., Fan, G., Kren, B. T. & Steer, C. J. Ursodeoxycholic acid prevents cytochrome c release in apoptosis by inhibiting mitochondrial membrane depolarization and channel formation. *Cell Death Differ.* **6**, 842–54 (1999).
  20. Amaral, J. D., Castro, R. E., Steer, C. J. & Rodrigues, C. M. P. p53 and the regulation of hepatocyte apoptosis: implications for disease pathogenesis. *Trends Mol. Med.* **15**, 531–41 (2009).
  21. Solá, S., Ribeiro, M. F., Genebra, T. & Rodrigues, C. M. P. in *Mitochondrial Biology and Experimental Therapeutics* (ed. Oliveira, P. J.) 407–421 (Springer International Publishing, 2018). doi:10.1007/978-3-319-73344-9
  22. Chun, H. S. & Low, W. C. Ursodeoxycholic acid suppresses mitochondria-dependent programmed cell death induced by sodium nitroprusside in SH-SY5Y cells. *Toxicology* **292**, 105–112 (2012).
  23. Amaral, J. D., Castro, R. E., Solá, S., Steer, C. J. & Rodrigues, C. M. P. p53 is a key molecular target of ursodeoxycholic acid in regulating apoptosis. *J. Biol. Chem.* **282**, 34250–9 (2007).
  24. Castro, R. E., Amaral, J. D., Solá, S., Kren, B. T., Steer, C. J. & Rodrigues, C. M. P. Differential regulation of cyclin D1 and cell death by bile acids in primary rat hepatocytes.

- Am. J. Physiol. Gastrointest. Liver Physiol.* **293**, G327-34 (2007).
25. Sola, S., Ma, X., Castro, R. E., Kren, B. T., Steer, C. J. & Rodrigues, C. M. P. Ursodeoxycholic acid modulates E2F-1 and p53 expression through a caspase-independent mechanism in transforming growth factor beta1-induced apoptosis of rat hepatocytes. *J. Biol. Chem.* **278**, 48831–8 (2003).
  26. Amaral, J. D., Castro, R. E., Solá, S., Steer, C. J. & Rodrigues, C. M. P. Ursodeoxycholic acid modulates the ubiquitin-proteasome degradation pathway of p53. *Biochem. Biophys. Res. Commun.* **400**, 649–54 (2010).
  27. Edlich, F., Banerjee, S., Suzuki, M., Cleland, M. M., Arnoult, D., Wang, C., Neutzner, A., Tjandra, N. & Youle, R. J. Bcl-x(L) retrotranslocates Bax from the mitochondria into the cytosol. *Cell* **145**, 104–16 (2011).
  28. Luo, L., Yang, J. & Liu, D. Integration and Oligomerization of Bax Protein in Lipid Bilayers Characterized by Single Molecule Fluorescence Study. *J. Biol. Chem.* **289**, 31708–31718 (2014).
  29. Schellenberg, B., Wang, P., Keeble, J. A., Rodriguez-Enriquez, R., Walker, S., Owens, T. W., Foster, F., Talianis-Hughes, J., Brennan, K., Streuli, C. H. & Gilmore, A. P. Bax exists in a dynamic equilibrium between the cytosol and mitochondria to control apoptotic priming. *Mol. Cell* **49**, 959–71 (2013).
  30. Kim, H., Tu, H.-C., Ren, D., Takeuchi, O., Jeffers, J. R., Zambetti, G. P., Hsieh, J. J.-D. & Cheng, E. H.-Y. Stepwise activation of BAX and BAK by tBID, BIM, and PUMA initiates mitochondrial apoptosis. *Mol. Cell* **36**, 487–99 (2009).
  31. Garner, T. P., Reyna, D. E., Priyadarshi, A., Chen, H. C., Li, S., Wu, Y., Ganesan, Y. T., Malashkevich, V. N., Almo, S. S., Cheng, E. H. & Gavathiotis, E. An Autoinhibited Dimeric Form of BAX Regulates the BAX Activation Pathway. *Mol. Cell* 1–13 (2015). doi:10.1016/j.molcel.2016.06.010
  32. Youle, R. J. & Strasser, A. The BCL-2 protein family: Opposing activities that mediate cell death. *Nat. Rev. Mol. Cell Biol.* **9**, 47–59 (2008).
  33. Lovell, J. F., Billen, L. P., Bindner, S., Shamas-din, A., Fradin, C. & Leber, B. Supplemental Data Membrane Binding by tBid Initiates an Ordered Series of Events Culminating in Membrane Permeabilization by Bax. **135**, 1–12
  34. Gonzalez, F., Pariselli, F., Dupaigne, P., Budihardjo, I., Lutter, M., Antonsson, B., Diolez, P., Manon, S., Martinou, J.-C., Gubern, M., Wang, X., Bernard, S. & Petit, P. X. tBid interaction with cardiolipin primarily orchestrates mitochondrial dysfunctions and subsequently activates Bax and Bak. *Cell Death Differ.* **12**, 614–26 (2005).

35. Dewson, G. & Kluck, R. M. Mechanisms by which Bak and Bax permeabilise mitochondria during apoptosis. *J. Cell Sci.* **122**, 2801–2808 (2009).
36. Subburaj, Y., Cosentino, K., Axmann, M., Pedrueza-Villalmanzo, E., Hermann, E., Bleicken, S., Spatz, J. & García-Sáez, A. J. Bax monomers form dimer units in the membrane that further self-assemble into multiple oligomeric species. *Nat. Commun.* **6**, 8042 (2015).
37. Czabotar, P. E., Westphal, D., Dewson, G., Ma, S., Hockings, C., Fairlie, W. D., Lee, E. F., Yao, S., Robin, A. Y., Smith, B. J., Huang, D. C. S., Kluck, R. M., Adams, J. M. & Colman, P. M. Bax Crystal Structures Reveal How BH3 Domains Activate Bax and Nucleate Its Oligomerization to Induce Apoptosis. *Cell* **152**, 519–531 (2013).
38. Westphal, D., Dewson, G., Czabotar, P. E. & Kluck, R. M. Molecular biology of Bax and Bak activation and action. *Biochim. Biophys. Acta* **1813**, 521–31 (2011).
39. Bleicken, S., Landeta, O., Landajuela, A., Basañez, G. & García-Sáez, A. J. Proapoptotic Bax and Bak proteins form stable protein-permeable pores of tunable size. *J. Biol. Chem.* **288**, 33241–52 (2013).
40. Hsu, Y. T. & Youle, R. J. Nonionic detergents induce dimerization among members of the Bcl-2 family. *J. Biol. Chem.* **272**, 13829–34 (1997).
41. Hsu, Y. T. & Youle, R. J. Bax in murine thymus is a soluble monomeric protein that displays differential detergent-induced conformations. *J. Biol. Chem.* **273**, 10777–83 (1998).
42. Ivashyna, O., García-Sáez, A. J., Ries, J., Christenson, E. T., Schwille, P. & Schlesinger, P. H. Detergent-activated BAX protein is a monomer. *J. Biol. Chem.* **284**, 23935–46 (2009).
43. Zhang, Z., Zhu, W., Lapolla, S. M., Miao, Y., Shao, Y., Falcone, M., Boreham, D., McFarlane, N., Ding, J., Johnson, A. E., Zhang, X. C., Andrews, D. W. & Lin, J. Bax forms an oligomer via separate, yet interdependent, surfaces. *J. Biol. Chem.* **285**, 17614–27 (2010).
44. Czabotar, P. E., Westphal, D., Dewson, G., Ma, S., Hockings, C., Fairlie, W. D., Lee, E. F., Yao, S., Robin, A. Y., Smith, B. J., Huang, D. C. S., Kluck, R. M., Adams, J. M. & Colman, P. M. Bax Crystal Structures Reveal How BH3 Domains Activate Bax and Nucleate Its Oligomerization to Induce Apoptosis. *Cell* **152**, 519–531 (2013).
45. Bleicken, S., Jeschke, G., Stegmüller, C., Salvador-Gallego, R., García-Sáez, A. J. & Bordignon, E. Structural Model of Active Bax at the Membrane. *Mol. Cell* **56**, 496–505 (2014).

46. Suzuki, M., Youle, R. J. & Tjandra, N. Structure of Bax: coregulation of dimer formation and intracellular localization. *Cell* **103**, 645–54 (2000).
47. Cox, M. M. & Nelson, D. L. *Lehninger Principles of Biochemistry*. (W. H. Freeman and Company, 2008).
48. Sarmiento, M. J., Coutinho, A., Fedorov, A., Prieto, M. & Fernandes, F. Ca<sup>2+</sup> induces PI(4,5)P<sub>2</sub> clusters on lipid bilayers at physiological PI(4,5)P<sub>2</sub> and Ca<sup>2+</sup> concentrations. *Biochim. Biophys. Acta* **1838**, 822–830 (2014).
49. McClare, C. W. An accurate and convenient organic phosphorus assay. *Anal. Biochem.* **39**, 527–30 (1971).
50. Christenson, E., Merlin, S., Saito, M. & Schlesinger, P. Cholesterol effects on BAX pore activation. *J. Mol. Biol.* **381**, 1168–83 (2008).
51. M. M. Puchalski, M. J. Morra, R. von W. Assessment of inner filter effect corrections in fluorimetry. *Fresenius J Anal Chem* 341–344 (1991).
52. Lakowicz, J. R. *Principles of Fluorescence Spectroscopy*. (2006).
53. Santos, N., Prieto, M. & Castanho, M. A. R. B. Quantifying molecular partition into model systems of biomembranes: an emphasis on optical spectroscopic methods. *Biochim. Biophys. Acta* **1612**, 123–135 (2003).
54. Greenwood A.I., Tristram-Nagle S., N. J. F. Partial molecular volumes of lipids and cholesterol. **100**, 130–134 (2012).
55. Aragon, S. R. & Pecora, R. Fluorescence correlation spectroscopy as a probe of molecular dynamics. *J. Chem. Phys.* **64**, 1791 (1976).
56. Rigler, R., Mets, Ü. ., Widengren, J. & Kask, P. Fluorescence correlation spectroscopy with high count rate and low background: analysis of translational diffusion. *Eur. Biophys. J.* **22**, 169–175 (1993).
57. Widengren, J., Rigler, R. & Mets, Ü. Triplet-state monitoring by fluorescence correlation spectroscopy. *J. Fluoresc.* **4**, 255–258 (1994).
58. Widengren, J., Mets, U. & Rigler, R. Fluorescence Correlation Spectroscopy of Triplet-States in Solution - a Theoretical and Experimental-Study. *J. Phys. Chem.* **99**, 13368–13379 (1995).
59. Werner, A. & Hahn, U. in *Nucleic Acid and Peptide Aptamers: Methods and Protocols* (ed. Mayer, G.) 107–114 (Humana Press, 2009). doi:10.1007/978-1-59745-557-2\_7
60. Majer, G. & Melchior, J. P. Characterization of the fluorescence correlation spectroscopy (FCS) standard Rhodamine 6G and calibration of its diffusion coefficient in aqueous

- solutions. *J. Chem. Phys.* **140**, (2014).
61. García-sáez, A. J., Carrer, D. C. & Schwille, P. in *Liposomes: Methods and Protocols* (ed. Weissig, V.) **Volume 2**, 493–508 (Humana Press, 2010).
  62. Gendron, P.-O., Avaltroni, F. & Wilkinson, K. J. Diffusion coefficients of several rhodamine derivatives as determined by pulsed field gradient-nuclear magnetic resonance and fluorescence correlation spectroscopy. *J. Fluoresc.* **18**, 1093–1101 (2008).
  63. Chen, Y., Müller, J. D., So, P. T. C. & Gratton, E. The Photon Counting Histogram in Fluorescence Fluctuation Spectroscopy. *Biophys. J.* **77**, 553–567 (1999).
  64. Huang, B., Perroud, T. D. & Zare, R. N. Photon counting histogram: One-photon excitation. *ChemPhysChem* **5**, 1523–1531 (2004).
  65. Schön, P., García-Sáez, A. J., Malovrh, P., Bacia, K., Anderluh, G. & Schwille, P. Equinatoxin II Permeabilizing Activity Depends on the Presence of Sphingomyelin and Lipid Phase Coexistence. *Biophys. J.* **95**, 691–698 (2008).
  66. Koukalová A, Pokorná Š, Fišer R, Kopecký V Jr, Humpolíčková J, Černý J, H. M. Membrane activity of the pentaene macrolide didehydroroflamycoin in model lipid bilayers. *Biochim. Biophys. Acta* **1848**, 444–452 (2015).
  67. Angelova, M., Soleau, S. & Méléard, P. Preparation of giant vesicles by external AC electric fields. Kinetics and applications. *Trends Colloid ...* **89**, 127–131 (1992).
  68. Satsoura, D., Kučerka, N., Shivakumar, S., Pencer, J., Griffiths, C., Leber, B., Andrews, D. W., Katsaras, J. & Fradin, C. Interaction of the full-length Bax protein with biomimetic mitochondrial liposomes: A small-angle neutron scattering and fluorescence study. *Biochim. Biophys. Acta* **1818**, 384–401 (2012).
  69. Runnels, L. W. & Scarlata, S. F. Theory and Application of Fluorescence Homotransfer to Melittin Oligomerization. *Biophys. J.* **69**, 1569–1583 (1995).
  70. Vira, S., Mekhedov, E., Humphrey, G. & Blank, P. S. Fluorescent-labeled antibodies: Balancing functionality and degree of labeling. *Anal. Biochem.* **402**, 146–50 (2010).
  71. Schnaible, V. & Przybylski, M. Identification of fluorescein-5'-isothiocyanate-modification sites in proteins by electrospray-ionization mass spectrometry. *Bioconjug. Chem.* **10**, 861–6
  72. Grunwaldt, G., Haebel, S., Spitz, C., Steup, M. & Menzel, R. Multiple binding sites of fluorescein isothiocyanate moieties on myoglobin: Photophysical heterogeneity as revealed by ground- and excited-state spectroscopy. *J. Photochem. Photobiol. B Biol.*

- 67**, 177–186 (2002).
73. Lakowicz, J. R. & Masters, B. R. Principles of Fluorescence Spectroscopy, Third Edition. *Journal of Biomedical Optics* **13**, 029901 (2008).
74. Loura, L. M. S., Fernandes, F., Fernandes, a C. & Ramalho, J. P. P. Effects of fluorescent probe NBD-PC on the structure, dynamics and phase transition of DPPC. A molecular dynamics and differential scanning calorimetry study. *Biochim. Biophys. Acta* **1778**, 491–501 (2008).
75. Lancet, D. & Pecht, I. Spectroscopic and immunochemical studies with nitrobenzoxadiazolealanine, a fluorescent dinitrophenyl analogue. *Biochemistry* **16**, 5150–7 (1977).
76. Letai, A., Bassik, M. C., Walensky, L. D., Sorcinelli, M. D., Weiler, S. & Korsmeyer, S. J. Distinct BH3 domains either sensitize or activate mitochondrial apoptosis, serving as prototype cancer therapeutics. *Cancer Cell* **2**, 183–192 (2002).
77. Lucken-Ardjomande, S., Montessuit, S. & Martinou, J.-C. Contributions to Bax insertion and oligomerization of lipids of the mitochondrial outer membrane. *Cell Death Differ.* **15**, 929–37 (2008).
78. Garg, P. pore formation by the carboxyl terminus of B. protein, Nemeč, K. N., Khaled, A. R. & Tatulian, S. a. Transmembrane pore formation by the carboxyl terminus of Bax protein. *Biochim. Biophys. Acta - Biomembr.* **1828**, 732–742 (2013).
79. Lidman M, Pokorná Š, Dingeldein AP, Sparrman T, Wallgren M, Šachl R, Hof M, G. G. The oxidized phospholipid PazePC promotes permeabilization of mitochondrial membranes by Bax. *Biochim. Biophys. Acta - Biomembr.* **1858**, 1288–1297 (2016).
80. Wimley, W. C., Selsted, M. E. & White, S. H. Interactions between human defensins and lipid bilayers: Evidence for formation of multimeric pores. *Protein Sci.* **3**, 1362–1373 (1994).
81. Schmucker DL, Ohta M, Kanai S, Sato Y, K. K. Hepatic injury induced by bile salts: correlation correlation between biochemical and morphological events. *Hepatology* **12**, 1216–21 (1990).
82. Faubion, W. A., Guicciardi, M. E., Miyoshi, H., Bronk, S. F., Roberts, P. J., Svingen, P. A., Kaufmann, S. H. & Gores, G. J. Toxic bile salts induce rodent hepatocyte apoptosis via direct activation of Fas. *J. Clin. Invest.* **103**, 137–45 (1999).
83. Ferreira, D. M. S., Afonso, M. B., Rodrigues, P. M., Simão, A. L., Pereira, D. M., Borralho, P. M., Rodrigues, C. M. P. & Castro, R. E. c-Jun N-Terminal Kinase 1/c-Jun Activation of the p53/MicroRNA 34a/Sirtuin 1 Pathway Contributes to Apoptosis Induced

- by Deoxycholic Acid in Rat Liver. *Mol. Cell. Biol.* **34**, 1100–20 (2014).
84. Webster, C. R. L., Johnston, A. N. & Anwer, M. S. Protein kinase C protects against bile acid apoptosis by suppressing proapoptotic JNK and BIM pathways in human and rat hepatocytes. *AJP Gastrointest. Liver Physiol.* **307**, G1207–G1215 (2014).
85. Rodrigues, C. M., Fan, G., Wong, P. Y., Kren, B. T. & Steer, C. J. Ursodeoxycholic acid may inhibit deoxycholic acid-induced apoptosis by modulating mitochondrial transmembrane potential and reactive oxygen species production. *Mol. Med.* **4**, 165–78 (1998).
86. Annis, M. G., Soucie, E. L., Dlugosz, P. J., Cruz-Aguado, J. a, Penn, L. Z., Leber, B. & Andrews, D. W. Bax forms multispinning monomers that oligomerize to permeabilize membranes during apoptosis. *EMBO J.* **24**, 2096–103 (2005).
87. Dlugosz, P. J., Billen, L. P., Annis, M. G., Zhu, W., Zhang, Z., Lin, J., Leber, B. & Andrews, D. W. Bcl-2 changes conformation to inhibit Bax oligomerization. *EMBO J.* **25**, 2287–2296 (2006).



## **BILE ACIDS INHIBIT BAX-DEPENDENT MEMBRANE PERMEABILIZATION**

Tânia Sousa<sup>1,2</sup>, Šárka Pokorná<sup>3</sup>, Rui E. Castro<sup>4</sup>, Nuno Bernardes<sup>2</sup>, Soojay Banerjee<sup>7</sup>, Gerhard Gröbner<sup>8</sup>, Richard J. Youle<sup>7</sup>, Ana Coutinho<sup>1,2,9</sup>, Cecília M.P. Rodrigues<sup>4</sup>, Martin Hof<sup>6</sup>, Manuel Prieto<sup>1,2</sup>,  
Fábio Fernandes<sup>1,2</sup>

<sup>1</sup>Centro de Química-Física Molecular and Institute of Nanoscience and Nanotechnology, Instituto Superior Técnico, University of Lisbon, Lisbon, Portugal

<sup>2</sup>iBB-Institute for Bioengineering and Biosciences, Biological Sciences Research Group, Av. Rovisco Pais 1, 1049-001 Lisbon, Portugal

<sup>3</sup>J. Heyrovský Institute of Physical Chemistry, Academy of Sciences of the Czech Republic, v. v. i., Dolejškova 3, 182 23 Prague 8, Czech Republic; Department of Biochemistry, Charles University, Hlavova 8, 128 40 Prague 2, Czech Republic.

<sup>4</sup>Research Institute for Medicines (iMed.Ulisboa), Faculty of Pharmacy, University of Lisbon, Lisbon, Portugal

<sup>5</sup>Institute for Biotechnology & Bioengineering; Department of Bioengineering; Instituto Superior Técnico; Universidade de Lisboa; Lisbon, Portugal.

<sup>6</sup>J. Heyrovský Institute of Physical Chemistry, Academy of Sciences of the Czech Republic, v. v. i., Dolejškova 3, 182 23 Prague 8, Czech Republic.

<sup>7</sup>Surgical Neurology Branch, NINDS, NIH Bethesda, MD 20892, USA

<sup>8</sup>Department of Chemistry, University of Umeå, SE-901 87 Umeå, Sweden

<sup>9</sup>Departamento de Química e Bioquímica, Faculty of Sciences, University of Lisbon, Lisbon, Portugal

### **Supplementary material**

### Definition of PCH parameters

The labeling stoichiometry ( $\lambda$ ) Alexa-488/Bax was determined spectroscopically to be  $\lambda = 0.84$  mol/mol. Since labeling was carried out with an amine-reactive probe, and Bax possesses 10 potential labeling sites we considered that the incorporation of fluorophores in the protein during labeling is a random, independent process, and the number of fluorophores per protein ( $N_F$ ) will follow Poisson statistics, as observed experimentally for other cases<sup>70-72</sup>. A Poisson distribution was considered, and  $N_F$  is given by:

$$f(N_F) = \frac{\lambda^{N_F} e^{-\lambda}}{N_F!} \quad (\text{S1})$$

where  $f(N_F)$  is the fraction of Bax labeled with  $N_F$  fluorophores. The fraction of protein with  $f(0)$  must be subtracted to the total protein content, as it will not be detected in the PCH experiment, so that the fraction of detected Bax labeled with  $N_F$  fluorophores,  $f(N_F)^*$  is given by:

$$f(N_F > 0)^* = \frac{f(N_F)}{\sum_{i=1} f(i)} \quad (\text{S2})$$

To calculate  $f(N_F)^*$  for populations of oligomers, we consider the oligomer as an individual protein unity and one has just to use the labeling stoichiometry of the oligomer ( $\lambda_o = N_o \lambda$ ), where  $N_o$  is the oligomerization number.

The fraction of total fluorescence intensity from each  $N_F$  population ( $F_i$ ) is the fraction weighted by the brightness and is given by:

$$F_{(i)} = \frac{f(i)^* \varepsilon_i}{\sum_{i=1} f(i)^* \varepsilon_i} \quad (\text{S3})$$

where  $\varepsilon_i$  is the brightness of the protein labeled with  $N_F=i$  fluorophores and equals to  $\varepsilon_1 \cdot N_F$ .

### Determination of dissociation constants between Bax-A488 and BH3-TAMRA

In this FRET experiment, Bax-A488 and BH3-TAMRA are the donor (D) and acceptor (A), respectively. In the absence of the peptide, Bax-A488 experiences no FRET and upon complex formation (DA), the donor (D) Bax-A488 undergoes FRET to BH3-TAMRA. The FRET efficiency within this complex is denoted  $E_{bound}$ . The dissociation constant for the complex is given by:

$$K_d = \frac{[D][A]}{[DA]} \quad (S4)$$

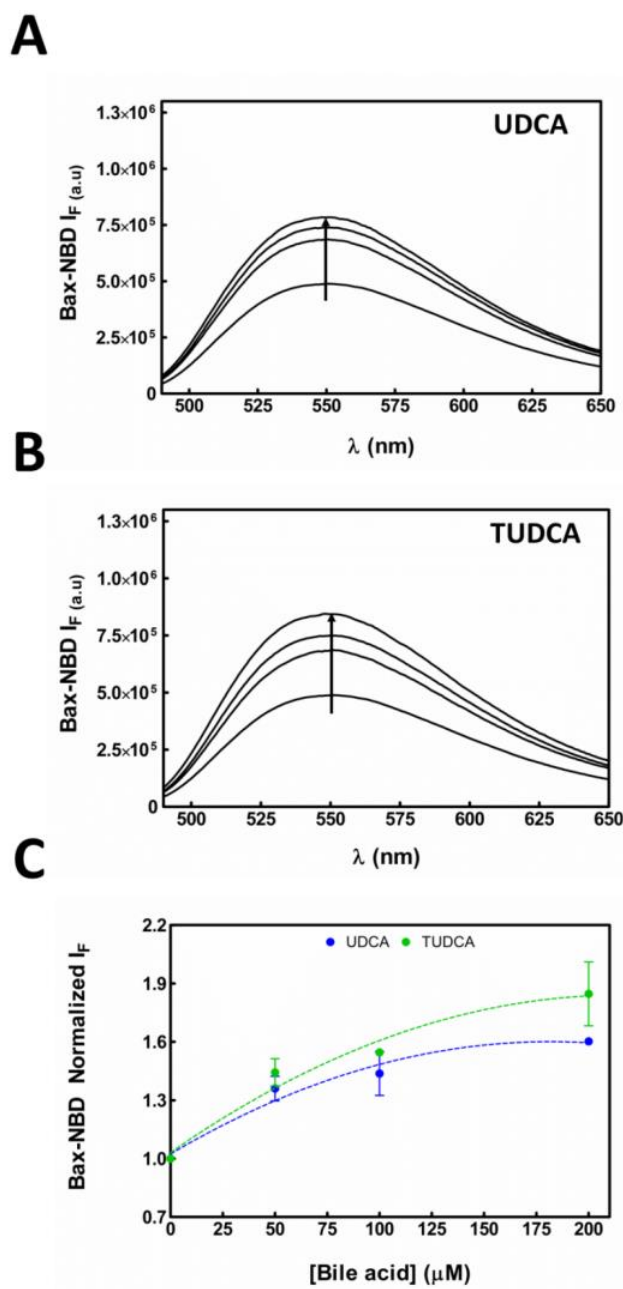
The concentration of the complex formed is then obtained by:

$$[DA] = \frac{([D] + [A] + K_d) - \sqrt{([D] + [A] + K_d)^2 - 4[D][A]}}{2} \quad (S5)$$

Where [D] and [A] are the total concentrations of donor and acceptor in the FRET experiment. Measured FRET efficiency values ( $E$ ) are given by:

$$E = f_{bound} \times E_{bound} \quad (S6)$$

Where,  $f_{bound}$  correspond to the fraction of Bax-A488 that is bound to the acceptor. The parameters  $K_d$  and  $E_{bound}$  were recovered through least-square regression of Eqs. 9 and 10 to the FRET data.

**Figures**

**Figure S1. Bax-NBD interacts with cytoprotective bile acids such as UDCA and TUDCA.** Bax-NBD (100 nM) fluorescence emission spectra were measured in the presence or absence of cytoprotective bile acids UDCA and TUDCA at a concentration range of 0 to 200  $\mu\text{M}$  (A, B) by excitation at 460 nm. Emission spectra integration was performed and normalized for the intensity value in the absence of bile acids (C). Dashed lines are guides to the eye and arrows represent the increase in concentration of bile acids. Results are expressed as mean  $\pm$  SD.

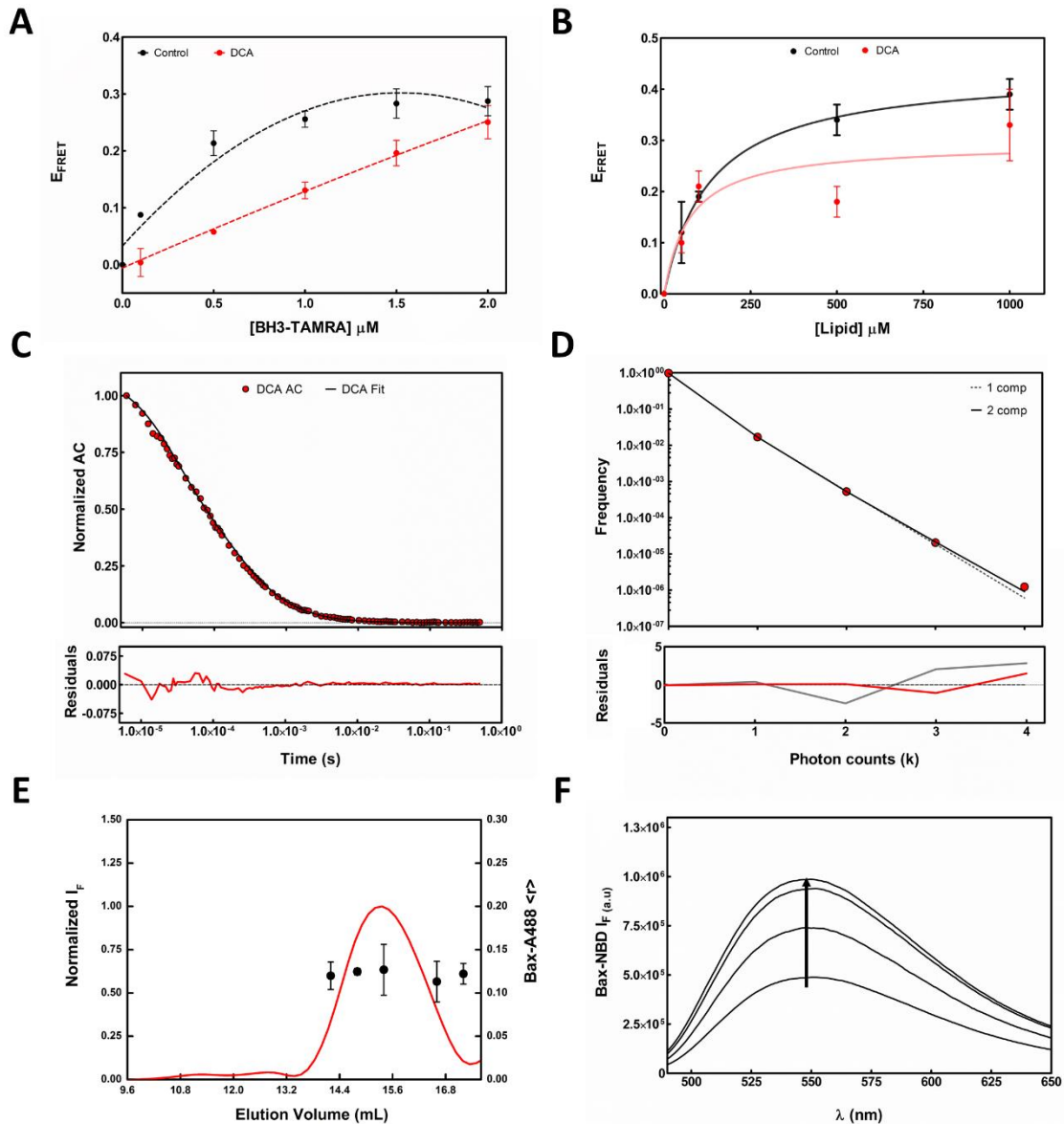


**Figure S2. The impact of TUDCA and UDCA on Bax are not exclusively observed for cytoprotective bile acids.** DCA also inhibits interaction of Bax-A488 with the activating peptide Bid-BH3-TAMRA (A) and promotes a more superficial location for Bax in liposomes mimicking MOM lipid composition (B). The diffusion of soluble Bax in the presence of DCA is also slowed down (C), likely due to the adsorption of a large number of DCA molecules to Bax surface, since Bax-A488 remains monomeric as seen by PCH and SEC (D, E). Evidence for a direct interaction of DCA with Bax is also obtained through monitoring of Bax-NBD fluorescence (F). Arrow represents the increase in concentration of bile acids.

**Tables**

**Table S1.** PCH analysis of Alexa-A488 alone and Bax-A488 in solution in the absence or presence of cytoprotective bile acids. For N and f, the values correspond to the average  $\pm$  SD values recovered after fitting of the model to > 5 sets of PCH data. In each condition,  $\epsilon_{\text{PCH2}}$  is calculated by globally linking this parameter during global analysis of the multiple replicates and also by fixing  $\epsilon_{\text{PCH1}}$  to the value found for the respective histogram in the absence of bile acid. Note that the decrease in brightness from free A488 to Bax-associated A488 is related with the decrease in the fluorophore quantum yield after protein labeling.

Sample	$N_{\text{PCH1}}$	$\epsilon_{\text{PCH1}}$ (cpbm)	$N_{\text{PCH2}}$	$\epsilon_{\text{PCH2}}$ (cpbm)	$f_{\text{PCH1}}$ (%)	$f_{\text{PCH2}}$ (%)
<b>A488</b>	1.748 $\pm$ 0.004	0.162	-	-	100	-
<b>Control</b>	0.31 $\pm$ 0.03	0.069	0.12 $\pm$ 0.02	0.233	72 $\pm$ 5	28 $\pm$ 5
<b>DCA</b>	0.40 $\pm$ 0.04	0.070	0.13 $\pm$ 0.02	0.206	75 $\pm$ 3	25 $\pm$ 3
<b>UDCA</b>	0.33 $\pm$ 0.04	0.068	0.14 $\pm$ 0.03	0.221	71 $\pm$ 5	29 $\pm$ 5
<b>TUDCA</b>	0.35 $\pm$ 0.05	0.071	0.14 $\pm$ 0.04	0.244	72 $\pm$ 8	28 $\pm$ 8

**Table S2.** Dissociation constant ( $K_d$ ) values recovered for Bax-A488/BH3-TAMRA interaction. Values are obtained from the fitting of Eqs S5 and S6 to the FRET data.

	Control	UDCA	TUDCA
$K_d$ ( $\times 10^{-7} \text{ M}^{-1}$ )	2.5 $\pm$ 0.4	11.9 $\pm$ 1.2	8.1 $\pm$ 0.9

**Table S3.** Partition of Bax-A488 to membranes mimicking the MOM in the absence or presence of bile acids. Bax-A488 partition coefficient ( $K_p$ ) and FRET efficiencies estimated for 100% protein bound to the membrane ( $E_L$ ), recovered from fitting of Eq. 4 to the FRET data.

	Control	UDCA	TUDCA	DCA
$K_p$ ( $\times 10^3$ )	9.7	8.1	15.8	3.5
$E_L$	0.44	0.29	0.26	0.29

**Table S4.** Flux  $J$  and  $F_n^0$  obtained by fitting of Eq. 11 to the leakage curves presented in Figure 6 and 8. Results are shown for two different protein-to-lipid ratios (1/200 and 1/100).

Sample	P/L ratio 1/200		P/L ratio 1/100	
	$J$ (nm/min)	$F_n^0$ (%)	$J$ (nm/min)	$F_n^0$ (%)
Control	1.32	36	1.43	50
UDCA	0.65	27	0.88	46
TUDCA	0.72	29	1.14	45
DCA	0.44	29	0.33	35



## **Chapter V**

---

DCA-induced apoptosis and UDCA-mediated cytoprotection are  
independent of Bax in HCT116 cells



## **DCA-INDUCED APOPTOSIS AND UDCA-MEDIATED CYTOPROTECTION ARE INDEPENDENT OF BAX IN HCT116 CELLS**

Tânia Sousa<sup>1,2</sup>, Nuno Bernardes<sup>2</sup>, Ana Coutinho<sup>1,2,3</sup>, Manuel Prieto<sup>1,2</sup>, Fábio Fernandes<sup>1,2</sup>

<sup>1</sup>Centro de Química-Física Molecular and Institute of Nanoscience and Nanotechnology, Instituto Superior Técnico, University of Lisbon, Lisbon, Portugal

<sup>2</sup>iBB-Institute for Bioengineering and Biosciences, Biological Sciences Research Group, Av. Rovisco Pais 1, 1049-001 Lisbon, Portugal

<sup>3</sup>Departamento de Química e Bioquímica, Faculty of Sciences, University of Lisbon, Lisbon, Portugal



## Abstract

The mechanisms by which apoptotic bile acids such as deoxycholic acid (DCA) and cytoprotective bile acids such as ursodeoxycholic acid (UDCA) modulate cell fate are not entirely understood. Previous results suggested that DCA acted through a direct permeabilization of the mitochondrial outer membrane (MOM), with no requirement of cytosolic factors. However, incubation with DCA drives translocation of the apoptotic and pore-forming protein Bax from the cytosol to the mitochondria, which could reflect either a direct modulation of the protein by the bile acid or a cellular response to the stress induced by DCA permeabilization of MOM. On the other hand, results from the previous chapter showed that cytoprotective bile acids inhibit the activity of recombinant Bax, suggesting that Bax could be the molecular target of bile acids such as UDCA.

Characterizing the impact of the interaction of bile acids and Bax on the translocation and pore-forming activity of Bax within a cellular environment is significantly challenging. Due to the non-specific nature of the interaction of Bax with bile acids, it is impossible to predict if the inhibition of Bax by bile acids is important for cell fate or if not yet identified apoptotic/cytoprotective factors could be modulated by bile acids in a more relevant manner. Here, we made use of colon cancer HCT116 Bax/Bak double knockout (DKO) cells to evaluate the role of Bax in bile acid induced cell death. We show that DCA-induced cell death occurs in the absence of Bax. Importantly, cytoprotection by UDCA was also observed in the absence of Bax, suggesting that this bile acid could modulate apoptosis through more complex mechanisms than inhibition of Bax alone.

Bax translocation to the mitochondria was monitored through the expression of Bax-GFP and fluorescence confocal imaging. As expected, incubation with DCA induces translocation of Bax to the mitochondria and pre-treatment of cells with UDCA inhibited this process. Due to plasma membrane impermeability, the intracellular concentration of DCA during these studies is unknown. Permeabilization of cells allow for control of intracellular bile acid concentration and remove ambiguity in data interpretation, as a direct interaction of bile acids with Bax is expected to cause very fast responses in Bax intracellular distribution. Permeabilized HCT116 Bax/Bak DKO cells exposed to DCA, suffered a rapid loss of MMP, and a small decrease in Bax-GFP translocation to the mitochondria. These results suggest that although the apoptotic activity of DCA is not dependent on Bax, the interaction of DCA with Bax by itself can inhibit the translocation of Bax to mitochondria to some extent, and that the increased translocation of Bax during longer treatment of non-permeabilized cells is likely the result of activation of apoptotic pathways due to the cellular stress created by DCA after MOM permeabilization.



## 1. Introduction

Hydrophilic bile acids such as ursodeoxycholic acid (UDCA), have been shown to inhibit apoptosis in both hepatic and nonhepatic cells<sup>1,2</sup>, and UDCA has been extensively employed in therapies of chronic cholestatic liver diseases and intrahepatic cholestasis of pregnancy<sup>3,4</sup>. Interestingly, there is a growing area of research for these molecules as potential therapeutic agents on a wide variety of non-liver diseases, such as neurodegenerative<sup>5-9</sup> and cardiovascular diseases<sup>10,11</sup>.

On the other hand, more hydrophobic bile acids such as deoxycholic acid (DCA) have been shown to induce apoptosis in hepatocytes<sup>12-15</sup>. At submicellar extracellular concentrations (50-100  $\mu$ M), these molecules have been proposed to activate cell death receptors in a ligand independent manner<sup>16</sup>, induce JNK1-mediated activation of p53, EF2-1 and cyclin D1 expression<sup>12,14,17</sup>, induce apoptosis by inhibition of miR-21 in hepatocytes<sup>13</sup>, induce oxidative damage<sup>18</sup>, promote both Bcl-2 associated protein X (Bax) translocation to mitochondria<sup>12</sup> and induce mitochondrial dysfunction<sup>1,18</sup>. Any of these modifications alone are sufficient for caspase activation and initiation of apoptosis<sup>12,15</sup>.

Given the amphipathic nature of bile acids, their presence at physiologically active concentrations (50-100  $\mu$ M)<sup>19,20</sup>, could induce changes in the biophysical properties of mitochondrial membranes. In this regard, it was shown by us and others that while apoptotic bile acids, such as DCA and chenodeoxycholic acid (CDCA), promoted disordering of the lipid membrane on both large unilamellar vesicles<sup>19</sup> (LUVs) and giant plasma membrane vesicles<sup>21</sup> (GPMVs), this effect was not observed for cytoprotective bile acids<sup>19</sup>. Additionally, while cytotoxic bile acids have been shown to promote mitochondrial permeability transition (MPT), cytochrome c release, and changes in mitochondrial outer membrane (MOM) morphology<sup>22,23</sup>, incubations with UDCA and tauroursodeoxycholic acid (TUDCA) had very limited effects on the permeability of isolated mitochondria<sup>24,25</sup>.

Interestingly, UDCA has been shown to inhibit the translocation of Bax to the mitochondria<sup>25,26</sup>. Furthermore, UDCA was shown to be able to inhibit hepatocyte apoptosis by a process that appears to involve direct inhibition of mitochondrial depolarization by preventing MPT, together with modulation of channel-forming activity associated with Bax translocation<sup>26</sup>. UDCA has also been shown to inhibit p53 transactivation, E2F-1 transcriptional activation, and Bcl-2 family expression<sup>27</sup>.

The Bcl-2 family is a protein superfamily that is involved in apoptosis regulation<sup>28-30</sup>. Bax is a pore-forming protein that belongs to the pro-apoptotic multi-domain group of the Bcl-2 proteins. In healthy cells, Bax remains largely on the cytosol in the inactive monomeric form, continuously binding to mitochondria and retrotranslocating back to the cytosol through

interaction with Bcl-xL, an anti-apoptotic member of Bcl-2 family<sup>31,32</sup>. The exact mechanism by which Bax is activated, oligomerize and exert its pore-forming activity is controversial and not yet entirely clear. However, for Bax to be activated, an interaction with a BH3-only protein like truncated Bid (tBid) is needed<sup>33-36</sup>. After this interaction, Bax suffers multiple conformational changes that result in oligomerization and consequently on the formation of pores on mitochondrial membranes. Recent reports show that Bax dimers are the structural unit for pore formation<sup>37-39</sup> and that Bax-induced MOM permeabilization would not be mediated by a unique, well-defined Bax pore structure, but rather by Bax pores of tunable size and stoichiometries that adapt to Bax density at the MOM<sup>40,41</sup>.

Bax is a strong candidate as the molecular target for cytoprotective bile acids, since these molecules effectively inhibit translocation of Bax to the mitochondria. Additionally, as cytoprotective bile acids exhibit low partition to lipid membranes, it is possible that the target of these molecules is Bax in its cytosolic monomeric state. As seen in the previous chapter, the cytoprotective bile acids such as UDCA and TUDCA interact with recombinant full-length Bax, possibly through non-specific adsorption to the protein surface rather than through specific binding sites. These molecules were also shown to be able to inhibit the interaction of the protein with activator molecules such as BH3 peptide and seem to decrease the amount of protein available to interact with lipid membranes. Importantly, the pore-forming activity of Bax was shown to be inhibited by the presence of cytoprotective bile acids. These effects of UDCA and TUDCA are not specific to cytoprotective bile acids, as similar results are obtained for Bax in the presence of DCA. It is possible that for DCA, the direct permeabilization of mitochondrial membranes negates any putative effect on Bax inhibition, which would explain the differences in modulation of cell death for cytoprotective and cytotoxic bile acids.

Given the previous observations, we aimed with this work to verify the relevance of Bax for both bile acid-mediated apoptosis and cytoprotection. The plasma membrane is a formidable permeability barrier for bile acids, and the intracellular concentrations of DCA during incubations with this bile acid are unknown, which adds considerable complexity to the rationalization of results. In this way, to clarify if the changes in Bax translocation observed during incubation with DCA are the result of a direct activation of the protein or are due to downstream signaling events, we employed different methods to control the intracellular concentration of bile acids.

## **2. Materials and methods**

### **2.1 Chemicals and Reagents**

DCA in sodium salt form, NaCl, Trizma® base, bovine serum albumin (BSA), KH<sub>2</sub>PO<sub>4</sub>, Tris(2-carboxyethyl)phosphine hydrochloride (TCEP), Actinomycin D (Act D), and Streptolysin O (SLO, 25.000-50.000 U) were obtained from Sigma-Aldrich (St. Louis MO, USA). UDCA sodium salt was purchased from Santa Cruz Biotechnologies (Santa Cruz, CA), and EDTA from Merck (Darmstadt, Germany).

5(6)-Carboxyfluorescein (CF) and 7-Amino-4-methyl-3-coumarinylacetic acid (AMCA) were obtained from Sigma-Aldrich (St. Louis MO, USA), MitoTracker™ Red CMXRos (CMX), Hoechst 33342 and TO-PRO®-3 stain were purchased from Invitrogen™ and Molecular Probes™, Thermo Fisher Scientific (Eugene, OR), respectively.

### **2.2 Cell culture and transfection chemicals**

HCT116 Bax/Bak DKO cells (kind gift of Dr. Richard J. Youle) were cultured and maintained in McCoy's 5A medium supplemented with 10% heat-inactivated fetal bovine serum and 1% of penicillin-streptomycin (Sigma Chemical Co., St. Louis, MO) at the incubator with controlled temperature (37°C), humidity, and CO<sub>2</sub> levels (5%). For microinjection purposes cells were grown on glass coverslips pre-coated with fibronectin (Thermo Fisher Scientific) at 10 µg/mL for 1 hour at room temperature.

Cells were transfected with the Bax-GFP construct (kind gift of Dr. Richard J. Youle)<sup>42</sup> (hBax-C3-EGFP<sup>42</sup>), using Lipofectamine® 2000 (Invitrogen™, Thermo Fisher Scientific Inc.) according to the manufacturer's instructions. After transfection, cells were grown overnight for confocal imaging.

### **2.3 Microinjection**

Microinjection was carried out with a semi-automatic system based on the combination of InjectMan® 4 and Femtoject® 4i from Eppendorf (Hamburg, Germany). Carboxyfluorescein (CF) was microinjected in HCT116 DKO cells to estimate the dilution factor associated to microinjection of the injection solution. Final intracellular concentration was determined from comparison of CF fluorescence in the cytosol with the fluorescence of the dye in solutions of

different concentrations in 8-well  $\mu$ -Slide from Ibidi (Munich, Germany), using the confocal microscope. Microinjection of bile acids was carried out using a pressure of 1 PSI with an injection time of 0.3 seconds.

HCT116 DKO cells expressing Bax-GFP were microinjected with bile acids at a concentration of 620  $\mu$ M in TEKP buffer (10 mM Tris-HCl, 10 mM  $\text{KH}_2\text{PO}_4$  and 1 mM of EDTA), so that an average intracellular concentration of 50  $\mu$ M was achieved after injection. AMCA was added to the injection solution at 250  $\mu$ M, as a marker for identification of injected cells. In some cases, the microinjection procedure induced morphological alterations in cells, and these were not considered for analysis. Cells where leakage of intracellular content was observed were also excluded for data analysis.

#### **2.4 Streptolysin O permeability assay**

A stock solution of Streptolysin O (SLO, 25.000-50.000 U, Sigma Aldrich) in Milli Q water at a final concentration of 5.000 U/mL was aliquoted and stored at  $-20^\circ\text{C}$ . Aliquots of SLO were reduced in DPBS supplemented with 10 mM TCEP for 30 min at  $37^\circ\text{C}$ . The SLO solution was further diluted to the working concentration in DPBS to a final 250-fold dilution of the stock solution. Successful permeabilization was confirmed using TO-PRO<sup>®</sup>-3 stain, a nuclear counterstain and dead cell indicator that is cell impermeant. HCT116 DKO cells expressing Bax-GFP were permeabilized by incubation with 200 U SLO in the presence or absence of bile acids at 100 or 500  $\mu$ M for 20 min at  $37^\circ\text{C}$ . Co-incubation with 250 nM of MitoTracker<sup>™</sup> Red CMXRos (CMX) to label active mitochondria was also performed. After SLO permeabilization and prior to confocal imaging, the cells were washed with DPBS.

#### **2.5 Confocal and two-photon fluorescence imaging**

All measurements were performed on a Leica TCS SP5 (Leica Microsystems CMS GmbH, Mannheim, Germany) inverted confocal microscope (DMI600). Excitation lines were provided by an Argon laser that was focused into the sample by an apochromatic water immersion objective (63x, NA 1.2; Zeiss, Jena Germany). A 111.4  $\mu$ m diameter pinhole positioned in front of the image plane blocked out-of-focus signals.

Two-photon excitation measurements of Hoechst 33342 were obtained using the same setup coupled to a Ti:sapphire laser (Mai Tai, Spectra-Physics, Darmstadt, Germany) as the

excitation source. The excitation wavelength was set to 780 nm and the fluorescence emission of Hoechst 33342 was collected between 400 and 454nm.

Before microinjection, HCT116 DKO cells expressing Bax-GFP were incubated with 250 nM of CMX, to label mitochondria and consequently follow Bax-GFP translocation from the cytosol to mitochondria after injection with bile acids. Imaging of Bax-GFP was performed through excitation with the 488 nm Argon laser line and emission was collected between 500 and 600 nm, while CMX was excited using 514 nm Argon laser line with detection between 600 and 700 nm. Sequential acquisition of Bax-GFP and CMX was performed before and immediately after microinjection, and data was recorded for 17 min.

Fluorescence confocal measurements for the SLO permeability assays were performed as done for microinjection studies. Imaging was carried out immediately after SLO incubation.

All the quantifications were performed based on the intensity values retrieved from confocal or two-photon images using the image analysis software ImageJ (<https://imagej.nih.gov/ij/index.html>).

### 3. Results

#### ***Bax-GFP is present in both cytosolic and mitochondrial pools***

Previous results (Chapter III and IV) strongly suggested that DCA acted through a direct permeabilization of the mitochondrial membrane, with no requirement of cytosolic factors, while cytoprotective bile acids inhibited the permeabilizing activity of recombinant Bax, suggesting that Bax could be the molecular target of bile acids such as UDCA and TUDCA. In this scenario, Bax would not be strictly necessary for DCA apoptotic activity but would be critical for bile acid-mediated cytoprotection. In order to ascertain if the impact of apoptotic and cytoprotective bile acids is dependent on Bax, we made use of HCT116 DKO cells. Through expression of Bax-GFP in these cells, it is possible to compare the impact of Bax for cellular fate during exposure to apoptotic levels of DCA, both in the presence and absence of pre-treatment with UDCA. GFP-Bax constructs have been shown to rescue cell death after exposure to apoptotic agents in HCT116 Bax DKO cells<sup>43</sup>.

We followed the intracellular distribution of Bax-GFP through confocal microscopy (Figure 1). Bax is mostly found in the cytosol when inactivated and translocates to the mitochondria when activated<sup>31</sup>. In several cell types, Bax is also found in the nucleus<sup>31,44,45</sup>.

For HCT116 DKO cells transfected with Bax-GFP we observed a mixed distribution of protein in the cytosol, nucleus and mitochondria, with higher enrichment in the latter (Fig. 1A, inset). Cells labeled with a fluorescence marker for active mitochondria, MitoTracker™ Red CMXRos (CMX), showed identical staining patterns in the presence or absence of Bax expression (Fig. 1B). The overlay image of both fluorescence intensity channels confirmed that the structures that are seen with higher Bax-GFP content correspond to mitochondria (Fig. 1C).

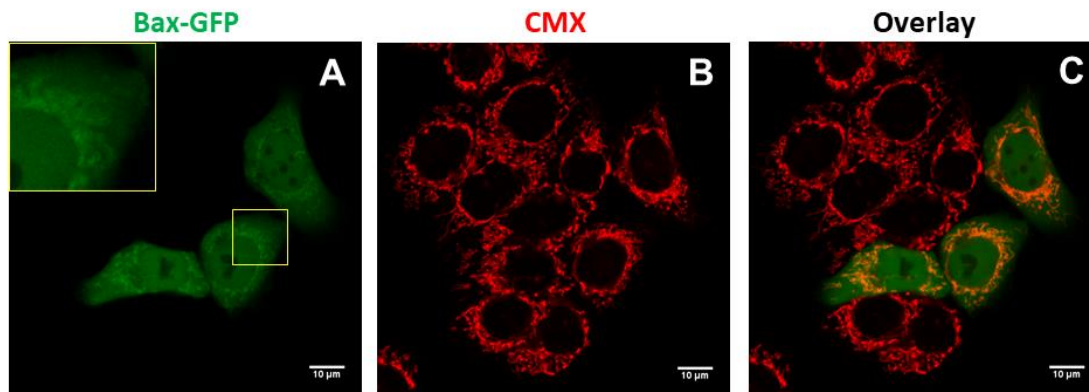


**Figure 1. Bax-GFP shows a mixed subcellular distribution with enrichment in the mitochondria.** Representative confocal microscopy images of the subcellular distribution of Bax-GFP after transfection of HCT116 DKO cells (A). Mitochondria were fluorescently stained with 250 nM CMX for 15min at 37°C (B). Overlay image is shown (C). Inset image shows a clear enrichment of Bax-GFP in mitochondria.

Bax-GFP distribution was monitored through measurement of the fluorescence intensity of Bax-GFP in the mitochondria and the cytosol (Figure 2), and is quantified an intensity ratio:

$$r_{Bax-GFP} = \frac{I_F(Bax - GFP)_{mit}}{I_F(Bax - GFP)_{cyt}} \quad (1)$$

where,  $I_F(Bax - GFP)_{mit}$  and  $I_F(Bax - GFP)_{cyt}$  correspond to the fluorescence intensity of Bax-GFP in mitochondria and in the cytosol, respectively.

Calculation of  $r_{Bax-GFP}$  showed that in mitochondria, the fluorescence signal from Bax-GFP seem to be 2-times higher than in the cytosol and that this value is very reproducible (Fig. 2A). Note that given the fact that the size of mitochondria is very close to the confocal microscopy resolution, the signal measured in this organelle contains contributions of both mitochondria and cytosol and Bax-GFP concentration in the mitochondria is likely higher than

just two times that of the protein in the cytosol. Also, we found that this ratio is independent of the expression levels of Bax-GFP, so that no saturation of the mitochondrial membrane takes place (Fig. 2A). We also observed that the levels of Bax-GFP on mitochondria do not affect mitochondrial membrane potential (MMP), since a higher intensity from Bax-GFP is not associated with a loss in fluorescence intensity from CMX (Fig. 2B), at least at the expression level of our studies.

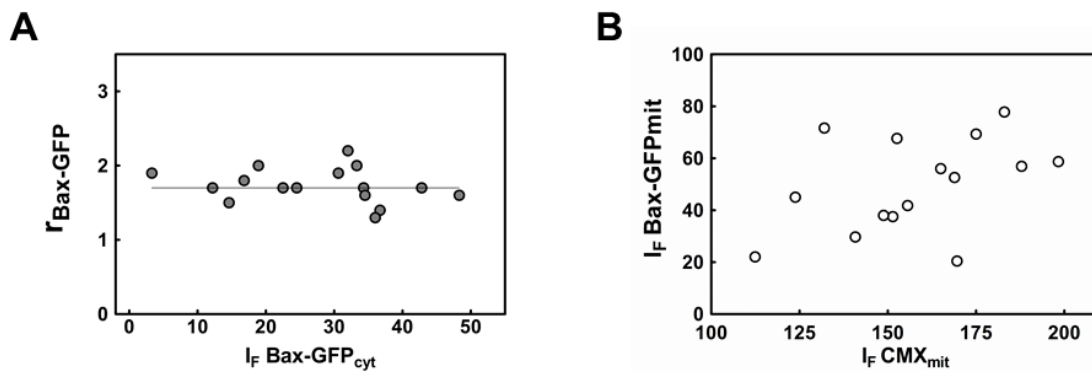


**Figure 2. Quantitative analysis of Bax-GFP and CMX fluorescence signal in different HCT116 DKO organelles shows that Bax-GFP expression is not occurring in mitochondrial saturating levels and that mitochondria integrity is maintained.** Ratio of Bax-GFP signal in mitochondria and cytosol ( $r_{Bax-GFP}$ ) was calculated through Eq.1 (A). Correlation between the fluorescence signals of Bax-GFP and CMX in mitochondria (B). Data points correspond to mean values calculated from 10 mitochondria and 5 regions of interest (ROI) in the cytosol for each cell.  $N > 16$  cells. Line is drawn as a guide.

### ***Bax-GFP translocates to the mitochondria after incubation with Actinomycin D in a concentration dependent manner***

In order to confirm that the Bax-GFP expressed in HCT116 DKO cells is functional, we applied an apoptotic stimulus to induce Bax translocation to mitochondria. Actinomycin D (Act D) is a polypeptide antibiotic that acts as a potent inducer of apoptosis in a variety of cells<sup>46-48</sup>. It binds to DNA and inhibits RNA and protein synthesis<sup>49</sup>. In this way, we incubated HCT116 DKO cells expressing Bax-GFP with different concentrations of Act D for 2h at 37°C (Figure 3), as previously described<sup>31</sup>.

We observed that incubation with Act D leads to an increase in the amount of Bax-GFP that is present on mitochondria, confirming that the apoptotic stimulus resulted in translocation of a fraction of Bax-GFP from the cytosol to mitochondria (Figure 3). This effect is shown to be independent of the levels of expression of Bax-GFP for both 1 and 2  $\mu\text{M}$  of Act D (Fig. 3C, D) and dependent on Act D concentration since a higher concentration of the apoptotic agent results in a higher  $r_{\text{Bax-GFP}}$  (Fig. 3E). These results clearly confirm that Bax-GFP is responsive to an apoptotic stimulus in a concentration dependent manner.

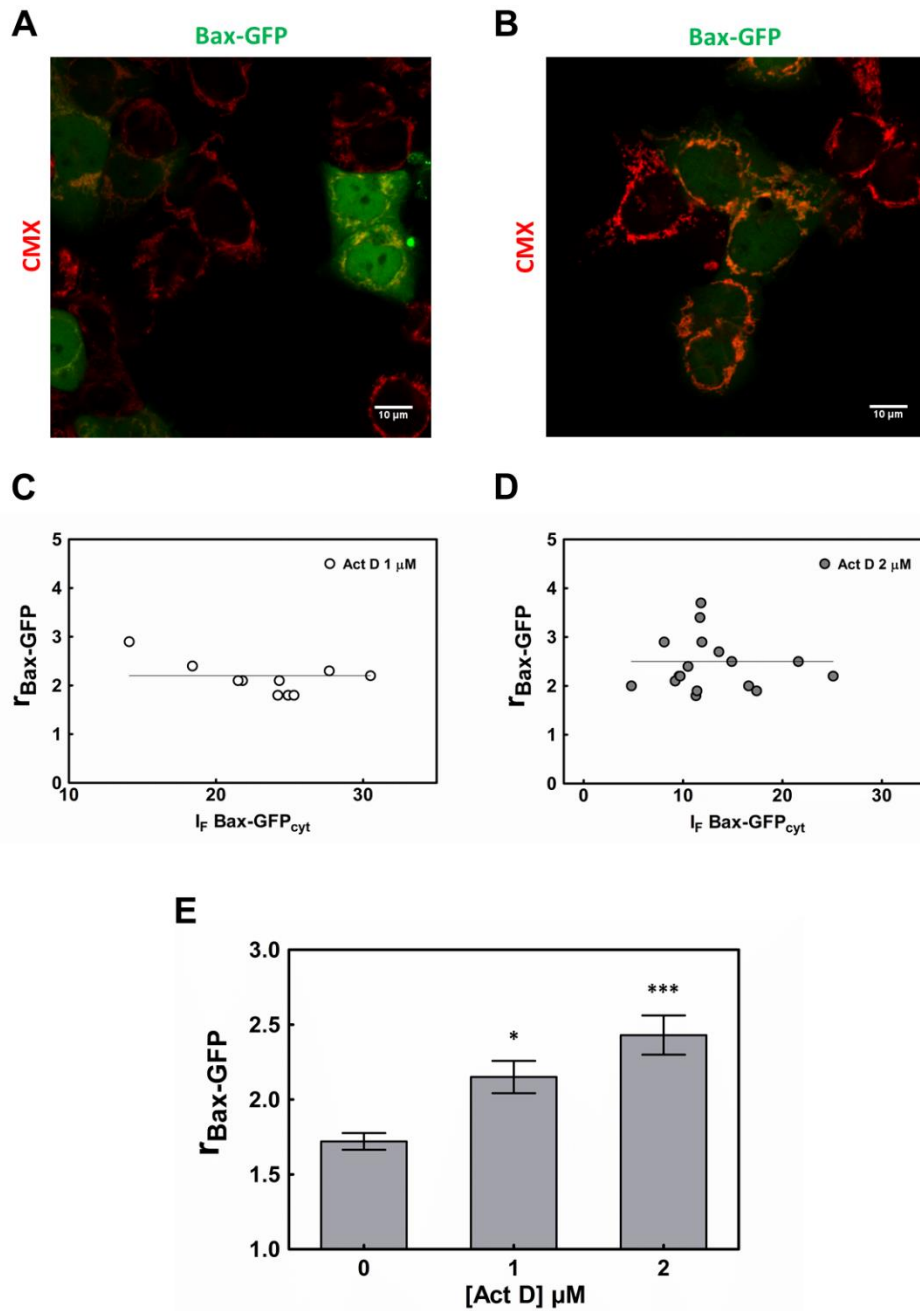


**Figure 3. Bax-GFP partially translocates to the mitochondria after incubation with Actinomycin D in a concentration dependent manner in HCT116 DKO cells.** Representative confocal microscopy images of the subcellular distribution of Bax-GFP after transfection of HCT116 DKO cells and incubation with 1 (A) or 2  $\mu M$  (B) of Act D for 2 hr at 37°C. Independence of Bax-GFP intracellular distribution on Bax-GFP expression levels ( $r_{Bax-GFP}$ ) in the presence of 1 (C) or 2  $\mu M$  (D) of Act D. Average  $r_{Bax-GFP} \pm$  SEM values are represented for the Act D concentrations under study (E). Results are expressed as mean values calculated from 10 mitochondria and 5 regions of interest (ROI) in the cytosol for each cell. N = 10-20 cells. \* P < 0.05, and \*\*\* P < 0.001 from the respective control.

***DCA-induced apoptosis and UDCA-mediated cytoprotection in HCT116 cells are independent of Bax***

Hydrophobic bile acids are known to induce apoptosis both in colon cancer cells and in hepatocytes<sup>50,51</sup>. It was already shown that DCA is able to induce apoptosis in human colon cancer cell line HCT116 in a concentration-dependent manner<sup>50</sup>. Incubation with 500  $\mu$ M DCA was previously shown to result in a fast release of cytochrome c (cyt c) from mitochondria<sup>50-52</sup>.

Onset of apoptosis was evaluated here by monitoring morphological characteristics of nuclei stained with Hoechst 33342, namely through detection of condensed chromatin contiguous to the nuclear membrane as well as nuclear fragmentation (Figure 4). We observed through nuclei staining with 2  $\mu$ M Hoechst 33342 that DCA at 100 and 500  $\mu$ M induces morphological alterations of the nuclei of HCT116 DKO cells in a concentration dependent manner (Fig. 4B, D, H) which are indicators of apoptosis. Importantly, a 6h pre-incubation with UDCA inhibits DCA-induced apoptosis, as previously observed for normal HCT116 cells<sup>50,53</sup> (Fig. 4F, G, H). These results conclusively show that both DCA-induced apoptosis and UDCA-mediated cytoprotection are not dependent on Bax activity. Incubation of HCT116 DKO cells with UDCA at 100  $\mu$ M had no impact on nuclei morphology (Fig 4C, H), while higher concentrations of this bile acid induced moderate levels of chromatin condensation (Fig 4D, H).

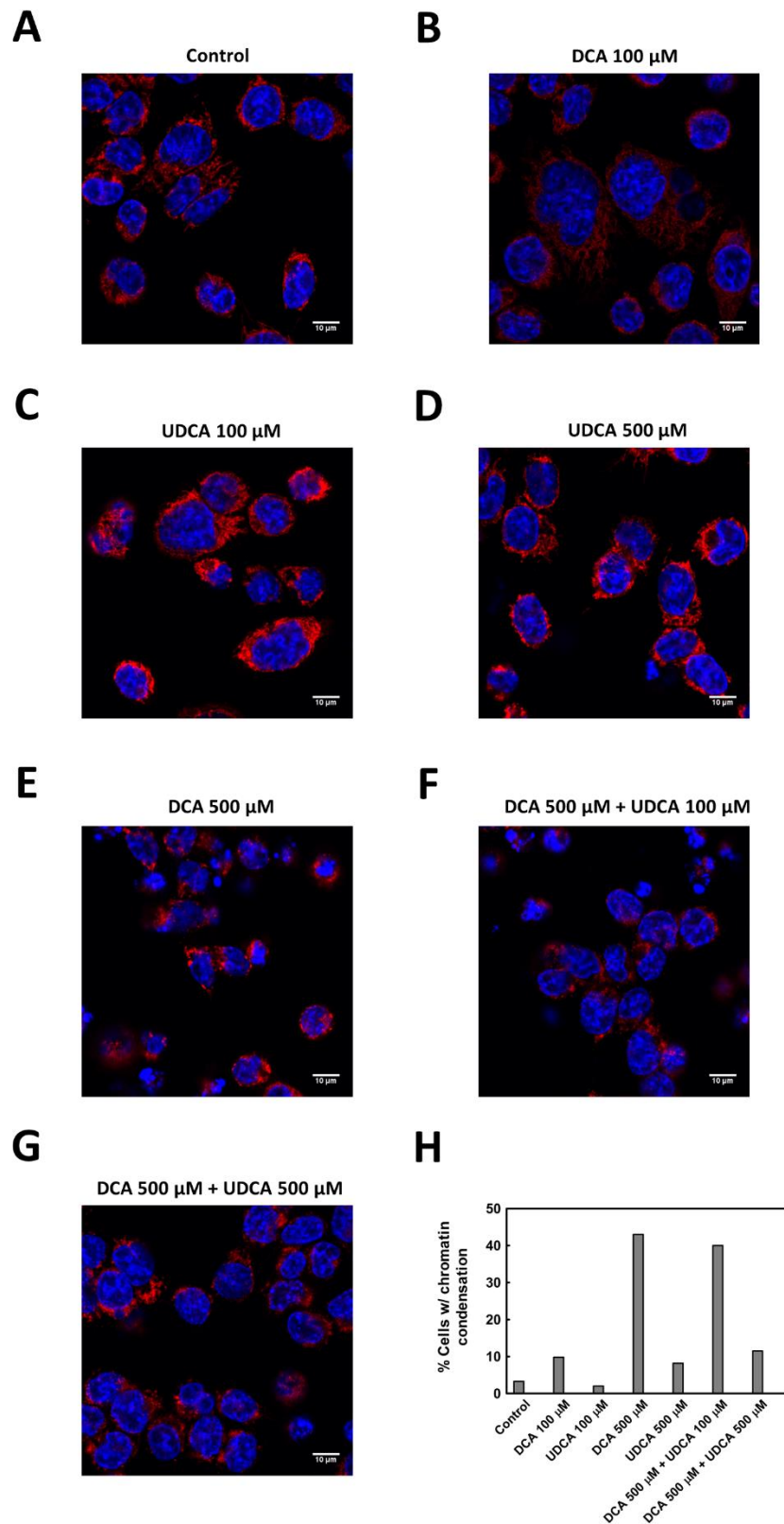


**Figure 4. DCA induces apoptosis in HCT116 DKO cells and both DCA apoptotic activity and UDCA-mediated cytoprotection are independent of the presence of Bax.** Representative confocal microscopy images of Hoechst 33342 staining in HCT116 DKO cells in the absence of bile acids (A). Images obtained after treatment of cells with DCA and UDCA at 100  $\mu$ M (B and C) and at 500  $\mu$ M (E

and D) for 1h at 37°C are also shown. A 6h pretreatment with the cytoprotective bile acid UDCA at 100 (F) and 500  $\mu$ M (G) was also performed prior to the incubation with DCA. The fluorescence signal from CMX (mitochondria) is shown in red and the signal from Hoechst 33342 (chromatin) is shown in blue. (F) Percentage of cells with morphological alterations of chromatin was calculated based on the pattern of Hoechst 33342 staining. N= 60-80 for each condition.

### ***DCA and UDCA modulate Bax-GFP translocation to the mitochondria***

Incubations of HCT116 DKO cells expressing Bax-GFP were carried out with either DCA or UDCA (Fig. 5A) for 1h.  $r_{\text{Bax-GFP}}$  increases in the presence of DCA, reflecting translocation of Bax-GFP to the mitochondria, while UDCA has no impact of Bax distribution (Fig. 5A). Also, Bax translocation to the mitochondria in response to DCA is negated through pre-treatment of HCT116 DKO cells with UDCA (Fig. 5B, C), possibly due to a Bax-independent inhibition of apoptosis as described above.

UDCA-mediated cytoprotection requires in different cell types, particularly long pre-incubations with this bile acid (6-25h)<sup>26,50,53</sup>. For HCT116 cells, previous results showed that a preincubation of UDCA of solely 1h had no inhibitory effect on DCA apoptotic activity, while a 6h incubation suppressed apoptosis entirely<sup>50</sup>. This is likely due to plasma membrane impermeability to the more hydrophilic cytoprotective bile acids, which limit intracellular concentration of these molecules. Due to plasma membrane impermeability, the intracellular concentrations of bile acids during these studies is also unknown, which adds considerable complexity to the rationalization of results. We employed different methods to control the intracellular concentration of bile acids, namely microinjection and transient permeabilization with pore-forming toxins.

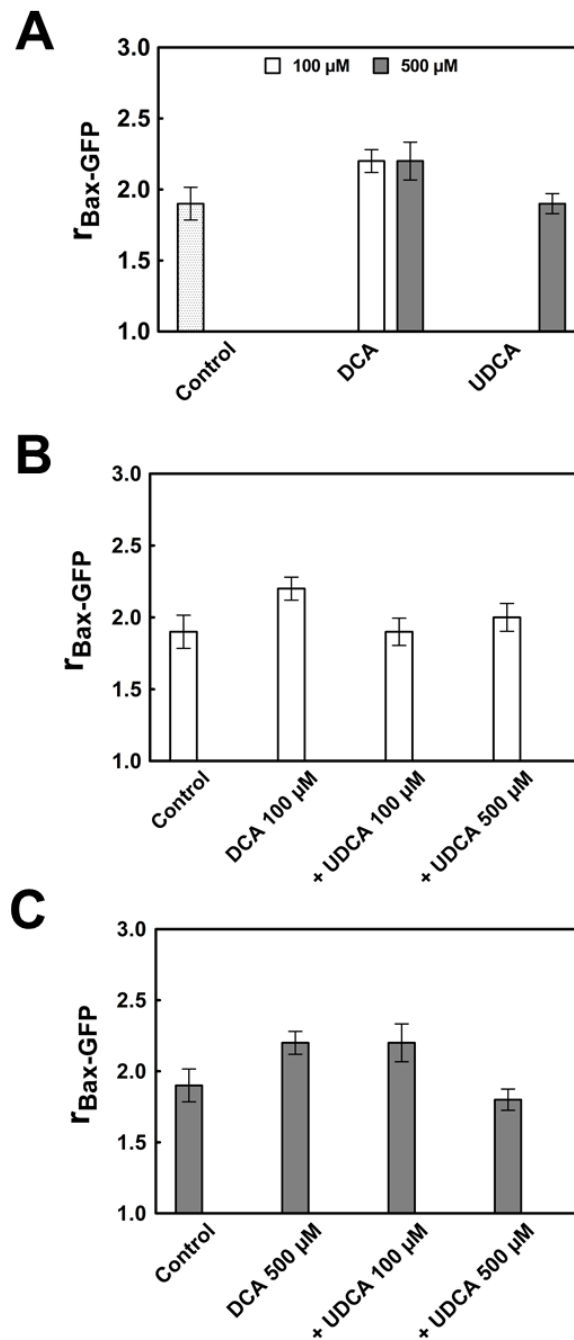


**Figure 5. DCA-induced apoptosis promotes Bax-GFP translocation to mitochondria in HCT116 DKO cells and this effect is inhibited by pre-treatment with UDCA.** Quantitative analysis of the ratio of Bax-GFP fluorescence intensity in mitochondria and cytosol,  $r_{\text{Bax-GFP}}$ , was performed for HCT116 DKO cells after incubation with 100 or 500  $\mu\text{M}$  of either DCA or UDCA, for 1h at 37°C (A). 6h pre-incubations with cytoprotective bile acid UDCA (100 or 500  $\mu\text{M}$ ), were also performed before adding DCA at 100  $\mu\text{M}$  (B) and 500  $\mu\text{M}$  (C) and the respective Bax-GFP ratios were calculated. Results are expressed as mean  $\pm$  SEM values calculated from 10 mitochondria and 5 regions of interest (ROI) in the cytosol for each cell. N = 10-25 cells.

***An intracellular concentration of 50  $\mu\text{M}$  DCA is insufficient for mitochondrial membrane depolarization or Bax translocation***

The first method employed to achieve control of intracellular concentration of bile acids was microinjection. Coupling a microinjection system with the confocal microscope allows for instantaneous observation of the effects of bile acids on Bax translocation or MMP. Microinjection settings were calibrated as described next. Briefly, carboxyfluorescein (CF) was microinjected in HCT116 DKO cells to estimate the dilution factor associated to microinjection of the injection solution. Final intracellular concentration was determined from comparison of the average CF fluorescence in the cytosol of 30 cells after microinjection (Fig. 6F) with the fluorescence of the dye in solutions of different concentrations, using the confocal microscope (Fig. 6A-E).

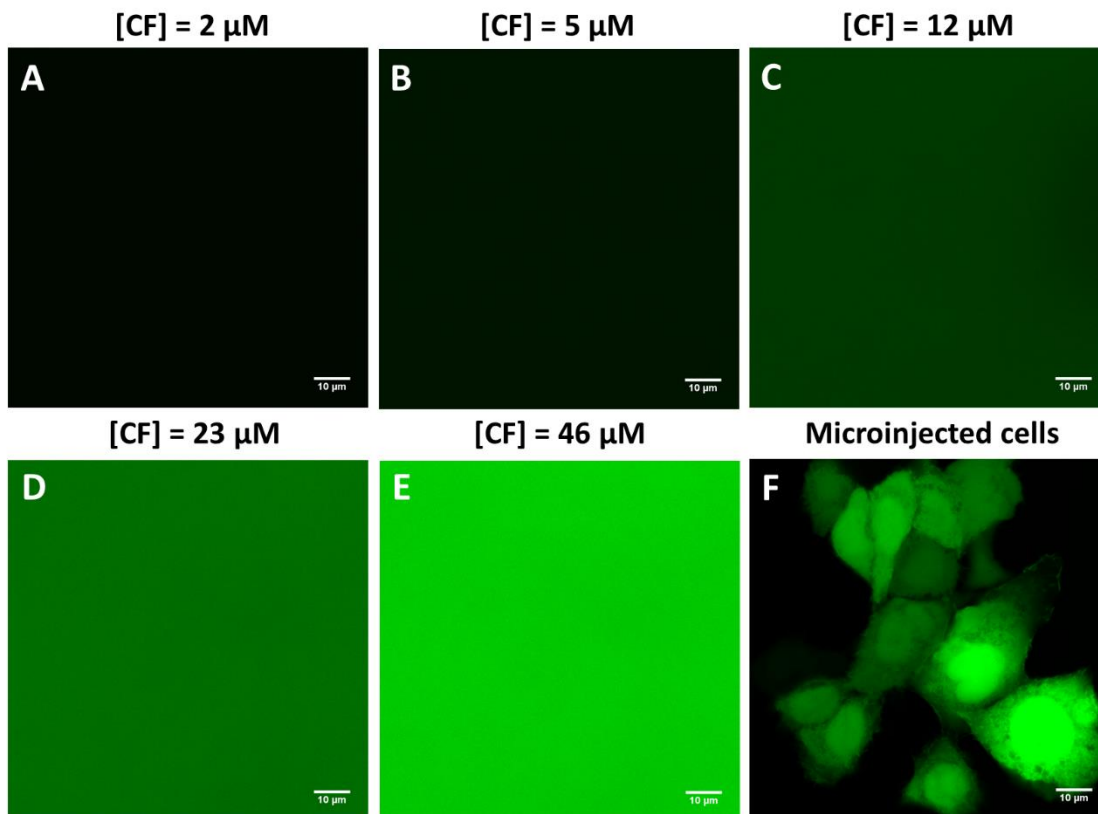


**Figure 6. Calibration of microinjection volume with Carboxyfluorescein (CF).** Confocal microscopy images of CF solutions at different concentrations (A-E). HCT116 DKO cells microinjected with the stock solution of CF (F). The images presented here and in Figure 7 and 8 were obtained after microinjections using a pressure of 1 PSI and 0.3s of microinjection time.

HCT116 DKO cells expressing Bax-GFP and previously stained with 250 nM CMX were microinjected with bile acids to achieve a final intracellular concentration of 50  $\mu\text{M}$ . Due to technical difficulties associated with a high viscosity, microinjection of solutions with a bile acid concentration larger than 620  $\mu\text{M}$  was not carried out and the intracellular concentration that could be achieved through this method was limited to 50  $\mu\text{M}$ , which is in the lower limit of reported physiologically active concentrations for DCA. The fluorophore AMCA was co-injected with bile acids in order to identify injected cells. The impact of microinjecting AMCA alone in Bax translocation was evaluated and found to be none (data not shown). Microinjections of buffer were always performed as a control.

Confocal imaging allowed to follow the fluorescence signal of Bax-GFP, tracking changes in the subcellular distribution of the protein and CMX, the latter as a control for changes in mitochondrial membrane potential. Confocal images were acquired before and immediately after microinjection. Images were then acquired for each cell during 17 minutes to follow changes in Bax-GFP distribution. Examples are shown below for UDCA and DCA at 50  $\mu\text{M}$  (Figure 7 and 8, respectively). A quantitative approach was followed to evaluate changes in Bax-GFP distribution.

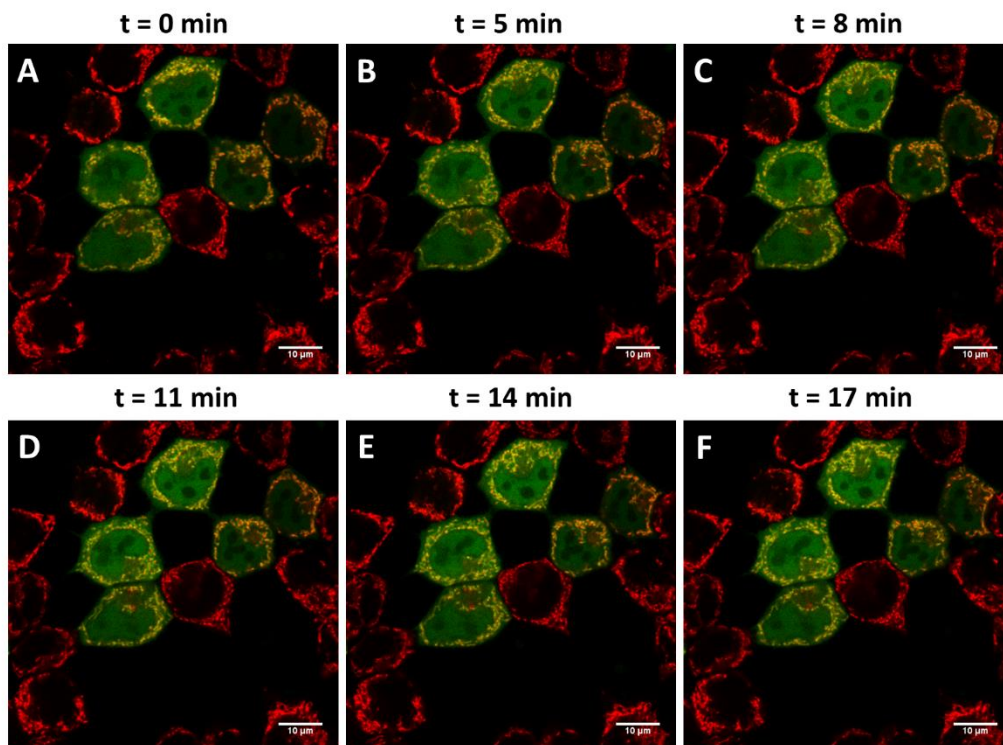


**Figure 7. Fluorescence intensity images of HCT116 DKO cells expressing Bax-GFP and loaded with CMX after microinjection of UDCA.** Representative confocal microscopy images of Bax-GFP in HCT116 DKO cells after microinjection of UDCA to achieve an intracellular bile acid concentration of 50  $\mu\text{M}$ . Sequential acquisition of Bax-GFP and CMX was performed immediately after microinjection.

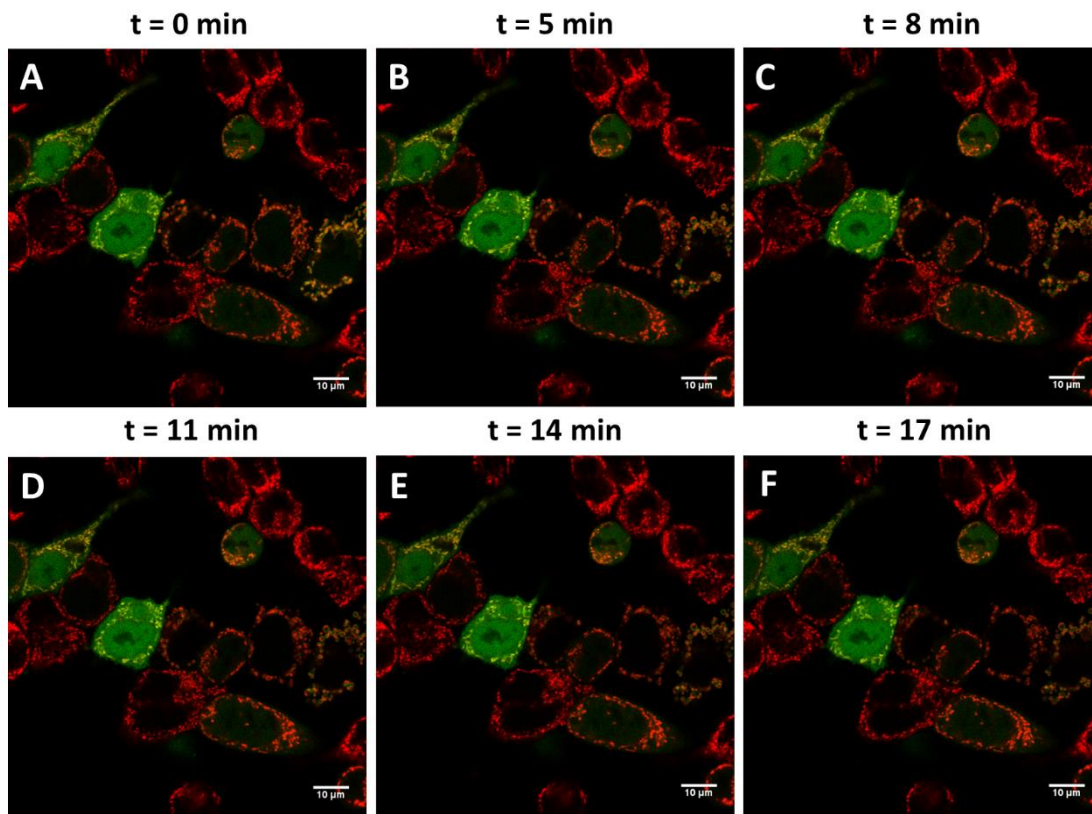


**Figure 8. Fluorescence intensity images of HCT116 DKO cells expressing Bax-GFP and loaded with CMX after microinjection of DCA.** Representative confocal microscopy images of Bax-GFP in HCT116 DKO cells after microinjection of DCA to achieve an intracellular bile acid concentration of 50  $\mu$ M. Sequential acquisition of Bax-GFP and CMX was performed immediately after microinjection.

Quantitative analysis of the fluorescence signal of CMX was performed using ImageJ software through the determination of the average mitochondrial fluorescence intensity of CMX immediately after microinjection ( $CMX_0$ ) and 17 minutes later ( $CMX_F$ ), calculated from 10 mitochondria per cell (Figure 9). For CMX this quantification is given by the ratio of intensities (Eq.2):

$$r_t \text{ CMX(mit)} = \frac{CMX_0}{CMX_F} \quad (2)$$

In the duration of the experiment (17 min), after injection of the cells with buffer, the CMX fluorescence intensity ratio does not change significantly (Figure 9). Also, the intracellular

administration of 50  $\mu\text{M}$  of either DCA or UDCA did not induce a loss of mitochondrial membrane potential (Figure 9).

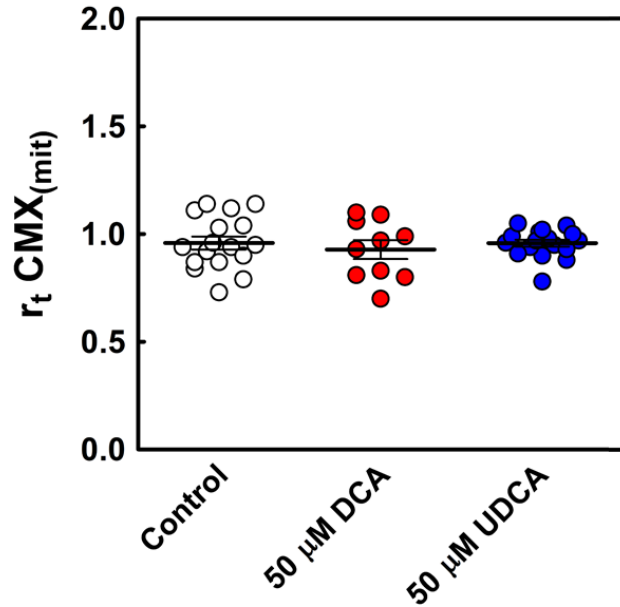


**Figure 9. An Intracellular concentration of 50  $\mu\text{M}$  of DCA does not lead to loss of MMP.**  $r_t \text{CMX}_{(\text{mit})}$  corresponds to the ratio of CMX fluorescence intensity in mitochondria immediately after microinjection and 17 minutes later. Average  $r_t \text{CMX}$  values for mitochondria in a single HCT116 DKO cell are shown as individual data points in the plot. Bars represent mean  $\pm$  SEM values for 10 mitochondria contributions for each cell. N = 10-17 cells per experiment.

Quantitative analysis of changes in Bax-GFP distribution after microinjection was also performed. Differences in  $r_{\text{Bax-GFP}}$  values as calculated according to Eq.1, were evaluated also through ratios, as shown in Eq. 3:

$$R_t \text{ Bax - GFP} = \frac{r_{\text{Bax-GFP}_0}}{r_{\text{Bax-GFP}_F}} \quad (3)$$

where the indices 0 and F refer to the ratios of Bax-GFP fluorescence intensity in the mitochondria and cytosol immediately after (0) and in the end of the experiment (F).

In the duration of the experiment, Bax-GFP does not translocate from the cytosol to the mitochondria both in the absence or presence of 50  $\mu$ M of either DCA or UDCA (Figure 10).

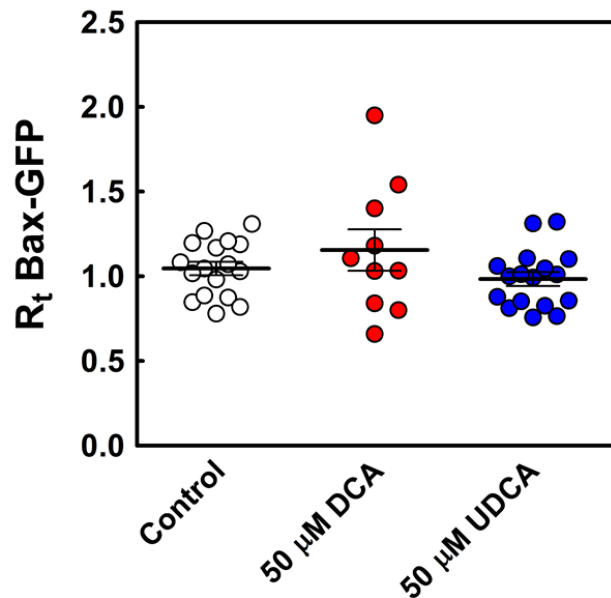


**Figure 10. An intracellular concentration of 50  $\mu$ M of DCA or UDCA has no immediate impact on Bax-GFP distribution.**  $R_t$  Bax-GFP values were determined according to Eq. 3. Average Bax-GFP  $R_t$  values for mitochondria in a single HCT116 DKO cell are shown as individual data points in the plot. Results are expressed as mean  $\pm$  SEM values calculated from 10 mitochondria and 5 regions of interest (ROI) in the cytosol for each cell. N = 10-17cells.

***Permeabilization of HCT116 DKO cells in the presence of 100  $\mu$ M DCA promotes immediate mitochondrial permeabilization without translocation of Bax***

In order to achieve intracellular concentrations of bile acids higher than 50  $\mu$ M, which proved insufficient to trigger apoptosis and mitochondrial membrane depolarization, reversible permeabilization of the plasma membrane was achieved through the use of SLO. SLO is a pore-forming bacterial toxin that allows molecules up to 100 kDa to cross membranes<sup>54-57</sup>. Efficient permeabilization was confirmed through the use of TO-PRO®-3 stain, a nuclear counterstain and dead cell indicator that is cell impermeant. Reversibility of the process occurred in a quick and efficient way, since SLO incubation did not result in any change of cellular morphology or evidence for activation of apoptosis when compared with the control without SLO (Fig. 12A, B). These observations showed us that pore repair through endocytosis, is sufficiently fast to prevent cell death<sup>58,59</sup>.

HCT116 DKO cells expressing Bax-GFP were permeabilized with SLO as described in the Methods section. Cells were also stained with CMX to follow MMP changes. However, permeabilization in the presence of 100  $\mu$ M of DCA leads to the rapid onset of apoptosis, as confirmed through rounding of cells and formation of membrane blebs, which are more easily detected in cells expressing Bax-GFP due to the staining of cytosol (Fig. 11C and inset). Additionally, in the presence of DCA the mitochondrial morphology is changed, and CMX fluorescence intensity in the mitochondria decreases for a fraction of the cells, reflecting a decrease in MMP. Evidence for the onset of apoptosis is again observed both for cells expressing Bax and for cells without the protein (Figure 11), confirming that activation of apoptotic pathways by DCA is not dependent on Bax. For DCA at 500  $\mu$ M, cell morphology is completely altered and we observe an increase in cellular volume, which is an indication of necrosis<sup>60</sup>. CMX staining is also severely diminished, suggesting a dramatic loss of MMP.

On the other hand, UDCA at 100  $\mu$ M does not induce significant morphological alterations on HCT116 DKO cells or a decrease in CMX staining of mitochondria, either in the presence or absence of Bax-GFP (Fig. 11E). At 500  $\mu$ M of UDCA, this bile acid clearly induces apoptosis as evidenced by extensive cell rounding and membrane bleb formation, as well as a clear decrease in CMX staining of mitochondria (Fig. 11F). UDCA-induced apoptosis is also shown to be independent of Bax-GFP expression. These results suggest that the lower apoptotic propensity of UDCA even at higher concentrations<sup>50,53</sup> is in fact at least partially associated with a low permeability of this molecule across the plasma membrane.

Quantification of Bax-GFP intracellular distribution immediately after permeabilization of HCT116 DKO cells was carried out as before through the parameter  $r_{\text{Bax-GFP}}$ . Experiments were performed on cells permeabilized in the presence of buffer alone or in the presence of either DCA or UDCA at 100  $\mu$ M (Figure 12). Also, Bax distribution in cells without permeabilization was evaluated as a control. Results show that the permeabilization procedure alone does not induce changes in Bax-GFP distribution (Figure 12). Surprisingly, 100  $\mu$ M DCA induced a minor but significant decrease in mitochondrial enrichment of Bax. Permeabilization of cells in the presence of 500  $\mu$ M DCA produced even more dramatic changes in the distribution of Bax-GFP, without any evidence for mitochondrial association of Bax (Fig 11D). However, due to the dramatic decrease in mitochondrial staining with CMX with 500  $\mu$ M DCA, a quantification of the  $r_{\text{Bax-GFP}}$  parameter was not carried out.

Permeabilization of HCT116 DKO cells in the presence of 100  $\mu$ M UDCA is ineffective in promoting changes in distribution of Bax-GFP. However, for higher UDCA concentrations (500  $\mu$ M), several cells present a non-uniform distribution of Bax-GFP, with very large aggregates of protein being found. Further work is necessary to identify the nature of these

structures. For 500  $\mu\text{M}$  UDCA, a quantification of the  $r_{\text{Bax-GFP}}$  parameter was also not carried out, again due to the difficulties in mitochondria staining.

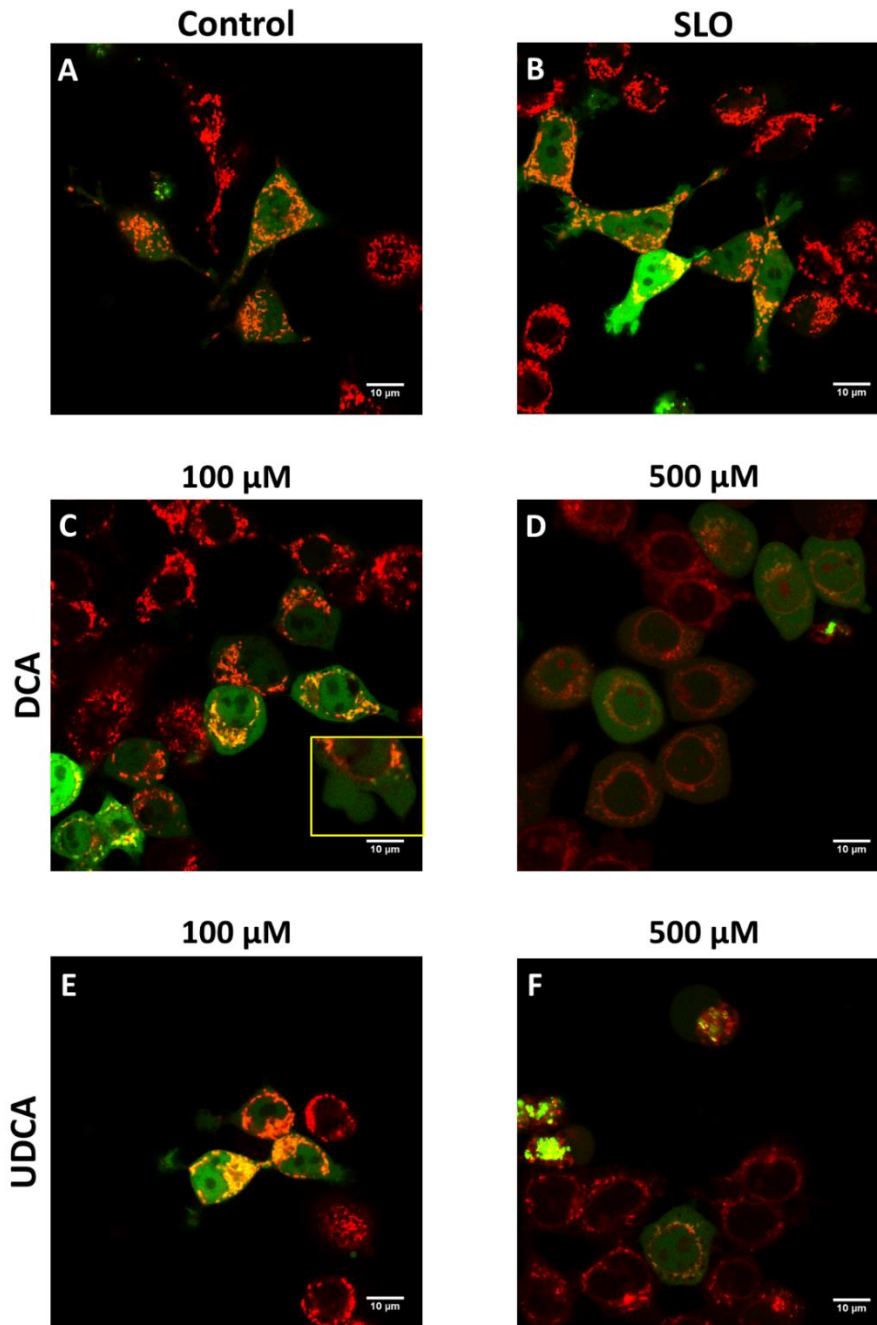


**Figure 11. – Permeabilization of HCT116 DKO cells in the presence of DCA and high UDCA concentrations induce Bax-independent apoptosis and a decrease in mitochondrial enrichment of Bax-GFP.** Representative confocal microscopy images of HCT116 DKO cells expressing Bax-GFP after permeabilization with SLO. Results are shown for non-permeabilized cells (A) and cells permeabilized with SLO (B). Cells were permeabilized in the presence of DCA or UDCA at 100 and 500  $\mu\text{M}$  (C-F). Mitochondria were fluorescently stained with 250 nM CMX.

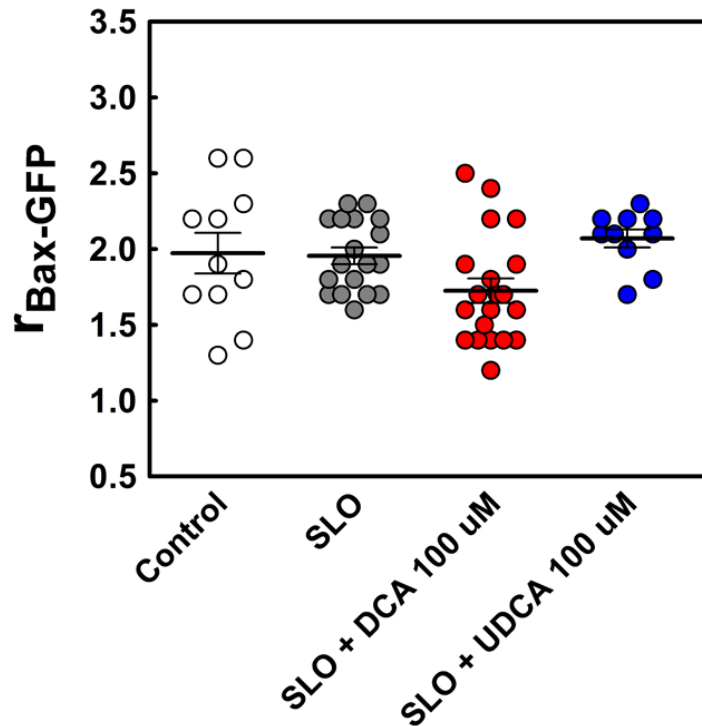


**Figure 12. Permeabilization of HCT116 DKO cells expressing Bax-GFP in the presence of DCA decreases mitochondrial membrane enrichment of the protein.** Intracellular distribution of Bax-GFP was quantified through the parameter  $r_{\text{Bax-GFP}}$ , according to Eq.1. HCT116 DKO cells were permeabilized with SLO as described in the Methods section. Control values correspond to nonpermeabilized cells. Average values of  $r_{\text{Bax-GFP}}$  for each individual permeabilized cell is shown as a data point the plot. Results are expressed as mean  $\pm$  SEM values calculated from 10 mitochondria and 5 regions of interest (ROI) in the cytosol for each cell. N = 10-18 cells.

## 4. Discussion

Bax is one of the most important pore-forming proteins in the MOM and is critical for the regulation of apoptosis. Importantly, it has been shown to translocate from the cytosol to the mitochondria during DCA-induced apoptosis<sup>12</sup>, and pre-incubation of cells with the cytoprotective UDCA lead not only to an inhibition of apoptosis but also to lower translocation of Bax to mitochondria<sup>25,26</sup>. These results suggest that Bax could be the molecular target of either DCA or UDCA during activation of apoptosis or cytoprotection in the cell. In chapter IV,

we showed that these bile acids do indeed interact with recombinant Bax, greatly inhibiting its membrane affinity and permeabilization activity.

Due to the non-specific nature of the interaction of Bax with bile acids, it is impossible to predict if the inhibition of Bax by bile acids is important for cell fate or if a not yet identified apoptotic/cytoprotective factors could be modulated by bile acids in a more relevant manner. This study aimed to test the hypothesis of Bax as the main molecular target of apoptotic/cytoprotective bile acids.

Experiments carried out with HCT116 Bax and Bak double knockout cells, clearly show that neither the apoptotic activity of DCA or the cytoprotective activity of UDCA are abrogated in the absence of Bax or Bak, suggesting that this protein is not the main target of these bile acids. Bax-GFP translocation to the mitochondria is also shown to not be significantly modified during incubation with DCA or UDCA. The intracellular concentration of bile acids in these experiments is unknown as the plasma membrane is a relatively efficient barrier for the diffusion of bile acids, particularly for more hydrophilic bile acids such as UDCA, which exhibit significantly lower affinity for membranes<sup>19,24</sup>. Possibly for this reason, cytoprotective bile acids are only efficient inhibitors of apoptosis after long pre-incubation of cells with these molecules prior to the apoptotic stimulus. In order to control intracellular concentrations of bile acids, HCT116 Bax/Bak DKO cells expressing Bax-GFP were either microinjected with bile acids or reversibly permeabilized with SLO. Fast control of the intracellular concentrations of bile acids also remove ambiguity in data interpretation, as a change in Bax translocation due to interaction with bile acids is then expected to be very rapid, unlike more complex signaling events. The longer incubations with bile acids typically required for activation of apoptosis or cytoprotection can result in the activation of cytotoxic or cytoprotective pathways, masking the real effect of bile acids over Bax translocation.

Unfortunately, microinjection only allowed for a maximum DCA intracellular concentration of 50  $\mu\text{M}$  due to technical issues in the microinjection process, and this concentration proved insufficient to activate rapid onset of apoptosis or trigger fast translocation of Bax.

On the other hand, permeabilization of colon cancer HCT116 DKO cells in the presence of 100-500  $\mu\text{M}$  DCA or high concentrations of UDCA, induced immediate morphological cellular changes as well as a decrease in MMP which are consistent with the onset of apoptosis. These results and the observation that an intracellular concentration of DCA of 50  $\mu\text{M}$  is insufficient for activation of apoptosis, strongly supports a model for DCA-induced apoptosis through which at a threshold concentration of intracellular DCA (superior to 50  $\mu\text{M}$  in HCT116 DKO cells), the DCA at the surface of the MOM is sufficient to trigger a permeability

increase. The fact that DCA was previously shown to permeabilize isolated mitochondria<sup>24,26</sup> but only induce partial permeabilization of liposomes mimicking mitochondrial membranes<sup>24</sup>, suggest that mitochondrial permeabilization by DCA requires activation of a mitochondrial factor, possibly a protein pore, which is shown here to not correspond to Bax for HCT116 cells.

The cytoprotective activity of UDCA is also shown here to not depend on Bax for colon cancer HCT116 cells. This is in agreement with previous reports<sup>50,53</sup> suggesting that the mechanism of action of UDCA in these specific cells is associated with inhibition of the formation of the apoptosome by preventing the association of Apaf-1 and caspase-9<sup>53</sup>. In hepatocytes, extensive evidence suggest that the site of action of UDCA is at the point of cytochrome c release<sup>26,50,53,61</sup>. Colon cancer cells are so called type-1 cells, in which activated initiator caspases (caspase-8 and caspase10) cleave, and activate, effector caspases (caspase-3, caspase-6 and caspase-7), paving the way to the execution phase of apoptosis<sup>62</sup>. On the other hand, hepatocytes are type II cells, for which a sufficient degree of activation of the effector caspases requires the involvement of Bid, Bax and the mitochondrial amplification pathway<sup>62</sup>. In the near future, the methods employed here with cancer colon cells should be tested in hepatocytes, for which the participation of Bax in the apoptotic event is more critical.

It is possible that given the nature of the reported nonspecific interaction of bile acids with Bax (chapter IV), these molecules interact with a multitude of different proteins intracellularly, and that as a result, the subsequent changes in profile of protein activities are extraordinarily complex. In that case, the final outcome regarding triggering of apoptosis or cytoprotection, could be as dependent on cell type as on intracellular bile acid concentration. This would be consistent with the observation of a cytoprotective activity of UDCA during incubation of nonpermeabilized cells with this bile acid, and a significantly apoptotic effect of UDCA when permeabilized cells were exposed to high concentrations of this bile acid.

### ***Acknowledgements/Grant Support***

Authors acknowledge funding by FCT project references RECI/CTM-POL/0342/2012, PTDC/QUI-BIO/119494/2010, PPBI-POCI-01-0145-FEDER-022122 and UID/NAN/50024/2013. T.S was the recipient of a fellowship from FCT (SFRH/BD/92398/2013). F.F acknowledges FCT through Researcher Contract No. IF/00386/2015.

## 5. References

1. Rodrigues, C. M., Fan, G., Ma, X., Kren, B. T. & Steer, C. J. A novel role for ursodeoxycholic acid in inhibiting apoptosis by modulating mitochondrial membrane perturbation. *J. Clin. Invest.* **101**, 2790–9 (1998).
2. Amaral, J. D., Viana, R. J. S., Ramalho, R. M., Steer, C. J. & Rodrigues, C. M. P. Bile acids: regulation of apoptosis by ursodeoxycholic acid. *J. Lipid Res.* **50**, 1721–34 (2009).
3. Paumgartner, G. & Beuers, U. Ursodeoxycholic acid in cholestatic liver disease: mechanisms of action and therapeutic use revisited. *Hepatology* **36**, 525–31 (2002).
4. Beuers, U. Drug insight: Mechanisms and sites of action of ursodeoxycholic acid in cholestasis. *Nat. Clin. Pract. Gastroenterol. Hepatol.* **3**, 318–28 (2006).
5. Ramalho, R. M., Borralho, P. M., Castro, R. E., Solá, S., Steer, C. J. & Rodrigues, C. M. P. Tauroursodeoxycholic acid modulates p53-mediated apoptosis in Alzheimer's disease mutant neuroblastoma cells. *J. Neurochem.* **98**, 1610–8 (2006).
6. Ramalho, R. M., Viana, R. J. S., Low, W. C., Steer, C. J. & Rodrigues, C. M. P. Bile acids and apoptosis modulation: an emerging role in experimental Alzheimer's disease. *Trends Mol. Med.* **14**, 54–62 (2008).
7. Mortiboys, H., Aasly, J. & Bandmann, O. Ursocholic acid rescues mitochondrial function in common forms of familial Parkinson's disease. *Brain* **136**, 3038–3050 (2013).
8. Keene, C. D., Rodrigues, C. M., Eich, T., Linehan-Stieers, C., Abt, a, Kren, B. T., Steer, C. J. & Low, W. C. A bile acid protects against motor and cognitive deficits and reduces striatal degeneration in the 3-nitropropionic acid model of Huntington's disease. *Exp. Neurol.* **171**, 351–60 (2001).
9. Fonseca, I., Gordino, G., Moreira, S., Nunes, M. J., Azevedo, C., Gama, M. J., Rodrigues, E., Rodrigues, C. M. P. & Castro-Caldas, M. Tauroursodeoxycholic Acid Protects Against Mitochondrial Dysfunction and Cell Death via Mitophagy in Human Neuroblastoma Cells. *Mol. Neurobiol.* **54**, 6107–6119 (2017).
10. Dromparis, P., Paulin, R., Stenson, T. H., Haromy, A., Sutendra, G. & Michelakis, E. D. Attenuating endoplasmic reticulum stress as a novel therapeutic strategy in pulmonary hypertension. *Circulation* **127**, 115–125 (2013).

11. Cai, Z., Li, F., Gong, W., Liu, W., Duan, Q., Chen, C., Ni, L., Xia, Y., Cianflone, K., Dong, N. & Wang, D. W. Endoplasmic reticulum stress participates in aortic valve calcification in hypercholesterolemic animals. *Arterioscler. Thromb. Vasc. Biol.* **33**, 2345–2354 (2013).
12. Castro, R. E., Amaral, J. D., Solá, S., Kren, B. T., Steer, C. J. & Rodrigues, C. M. P. Differential regulation of cyclin D1 and cell death by bile acids in primary rat hepatocytes. *Am. J. Physiol. Gastrointest. Liver Physiol.* **293**, G327-34 (2007).
13. Rodrigues, P. M., Afonso, M. B., Simão, A. L., Borralho, P. M., Rodrigues, C. M. P. & Castro, R. E. Inhibition of NF- $\kappa$  B by deoxycholic acid induces miR-21/PDCD4-dependent hepatocellular apoptosis. *Sci. Rep.* **5**, 1–17 (2015).
14. Ferreira, D. M. S., Afonso, M. B., Rodrigues, P. M., Simão, A. L., Pereira, D. M., Borralho, P. M., Rodrigues, C. M. P. & Castro, R. E. c-Jun N-Terminal Kinase 1/c-Jun Activation of the p53/MicroRNA 34a/Sirtuin 1 Pathway Contributes to Apoptosis Induced by Deoxycholic Acid in Rat Liver. *Mol. Cell. Biol.* **34**, 1100–20 (2014).
15. Amaral, J. D., Castro, R. E., Steer, C. J. & Rodrigues, C. M. P. p53 and the regulation of hepatocyte apoptosis: implications for disease pathogenesis. *Trends Mol. Med.* **15**, 531–41 (2009).
16. Faubion, W. A., Guicciardi, M. E., Miyoshi, H., Bronk, S. F., Roberts, P. J., Svingen, P. A., Kaufmann, S. H. & Gores, G. J. Toxic bile salts induce rodent hepatocyte apoptosis via direct activation of Fas. *J. Clin. Invest.* **103**, 137–45 (1999).
17. Webster, C. R. L., Johnston, A. N. & Anwer, M. S. Protein kinase C delta protects against bile acid apoptosis by suppressing proapoptotic JNK and BIM pathways in human and rat hepatocytes. *Am. J. Physiol. Gastrointest. Liver Physiol.* **307**, G1207-1215 (2014).
18. Rodrigues, C. M., Fan, G., Wong, P. Y., Kren, B. T. & Steer, C. J. Ursodeoxycholic acid may inhibit deoxycholic acid-induced apoptosis by modulating mitochondrial transmembrane potential and reactive oxygen species production. *Mol. Med.* **4**, 165–78 (1998).
19. Mello-Vieira, J., Sousa, T., Coutinho, A., Fedorov, A., Lucas, S. D., Moreira, R., Castro, R. E., Rodrigues, C. M. P., Prieto, M. & Fernandes, F. Cytotoxic bile acids, but not cytoprotective species, inhibit the ordering effect of cholesterol in model membranes at physiologically active concentrations. *Biochim. Biophys. Acta* **1828**, 2152–2163 (2013).
20. Benz, C., Angermüller, S., Otto, G., Sauer, P., Stremmel, W. & Stiehl, a. Effect of tauroursodeoxycholic acid on bile acid-induced apoptosis in primary human hepatocytes. *Eur. J. Clin. Invest.* **30**, 203–9 (2000).

21. Zhou, Y., Maxwell, K. N., Sezgin, E., Lu, M., Liang, H., Hancock, J. F., Dial, E. J., Lichtenberger, L. M. & Levental, I. Bile acids modulate signaling by functional perturbation of plasma membrane domains. *J. Biol. Chem.* **288**, 35660–70 (2013).
22. Schulz, S., Schmitt, S., Wimmer, R., Aichler, M., Eisenhofer, S., Lichtmanegger, J., Eberhagen, C., Artmann, R., Tookos, F., Walch, A., Krappmann, D., Brenner, C., Rust, C. & Zischka, H. Progressive stages of mitochondrial destruction caused by cell toxic bile salts. *Biochim. Biophys. Acta* **1828**, 2121–33 (2013).
23. Rolo, A. P., Oliveira, P. J., Moreno, A. J. & Palmeira, C. M. Chenodeoxycholate induction of mitochondrial permeability transition pore is associated with increased membrane fluidity and cytochrome c release: protective role of carvedilol. *Mitochondrion* **2**, 305–11 (2003).
24. Sousa, T., Castro, R. E., Pinto, S. N., Coutinho, A., Lucas, S. D., Moreira, R., Rodrigues, C. M. P., Prieto, M. & Fernandes, F. Deoxycholic acid modulates cell death signaling through changes in mitochondrial membrane properties. *J. Lipid Res.* (2015). doi:10.1194/jlr.M062653
25. Rodrigues, C. M. P., Solá, S., Sharpe, J. C., Moura, J. J. G. & Steer, C. J. Tauroursodeoxycholic acid prevents Bax-induced membrane perturbation and cytochrome C release in isolated mitochondria. *Biochemistry* **42**, 3070–80 (2003).
26. Rodrigues, C. M., Ma, X., Linehan-Stieers, C., Fan, G., Kren, B. T. & Steer, C. J. Ursodeoxycholic acid prevents cytochrome c release in apoptosis by inhibiting mitochondrial membrane depolarization and channel formation. *Cell Death Differ.* **6**, 842–54 (1999).
27. Sola, S., Ma, X., Castro, R. E., Kren, B. T., Steer, C. J. & Rodrigues, C. M. P. Ursodeoxycholic acid modulates E2F-1 and p53 expression through a caspase-independent mechanism in transforming growth factor beta1-induced apoptosis of rat hepatocytes. *J. Biol. Chem.* **278**, 48831–8 (2003).
28. Bleicken, S., Classen, M., Padmavathi, P. V. L., Ishikawa, T., Zeth, K., Steinhoff, H.-J. & Bordignon, E. Molecular details of Bax activation, oligomerization, and membrane insertion. *J. Biol. Chem.* **285**, 6636–47 (2010).
29. Bleicken, S. & Zeth, K. Conformational changes and protein stability of the pro-apoptotic protein Bax. *J. Bioenerg. Biomembr.* **41**, 29–40 (2009).
30. García-Sáez, A. J. The secrets of the Bcl-2 family. *Cell Death Differ.* **19**, 1733–1740 (2012).
31. Edlich, F., Banerjee, S., Suzuki, M., Cleland, M. M., Arnoult, D., Wang, C., Neutzner,

- A., Tjandra, N. & Youle, R. J. Bcl-x(L) retrotranslocates Bax from the mitochondria into the cytosol. *Cell* **145**, 104–16 (2011).
32. Luo, L., Yang, J. & Liu, D. Integration and Oligomerization of Bax Protein in Lipid Bilayers Characterized by Single Molecule Fluorescence Study. *J. Biol. Chem.* **289**, 31708–31718 (2014).
33. Dewson, G. & Kluck, R. M. Mechanisms by which Bak and Bax permeabilise mitochondria during apoptosis. *J. Cell Sci.* **122**, 2801–2808 (2009).
34. Kim, H., Tu, H.-C., Ren, D., Takeuchi, O., Jeffers, J. R., Zambetti, G. P., Hsieh, J. J.-D. & Cheng, E. H.-Y. Stepwise activation of BAX and BAK by tBID, BIM, and PUMA initiates mitochondrial apoptosis. *Mol. Cell* **36**, 487–99 (2009).
35. Lovell, J. F., Billen, L. P., Bindner, S., Shamas-din, A., Fradin, C. & Leber, B. Supplemental Data Membrane Binding by tBid Initiates an Ordered Series of Events Culminating in Membrane Permeabilization by Bax. **135**, 1–12
36. Gonzalvez, F., Pariselli, F., Dupaigne, P., Budihardjo, I., Lutter, M., Antonsson, B., Diolez, P., Manon, S., Martinou, J.-C., Gubern, M., Wang, X., Bernard, S. & Petit, P. X. tBid interaction with cardiolipin primarily orchestrates mitochondrial dysfunctions and subsequently activates Bax and Bak. *Cell Death Differ.* **12**, 614–26 (2005).
37. Subburaj, Y., Cosentino, K., Axmann, M., Pedrueza-Villalmanzo, E., Hermann, E., Bleicken, S., Spatz, J. & García-Sáez, A. J. Bax monomers form dimer units in the membrane that further self-assemble into multiple oligomeric species. *Nat. Commun.* **6**, 8042 (2015).
38. Czabotar, P. E., Westphal, D., Dewson, G., Ma, S., Hockings, C., Fairlie, W. D., Lee, E. F., Yao, S., Robin, A. Y., Smith, B. J., Huang, D. C. S., Kluck, R. M., Adams, J. M. & Colman, P. M. Bax Crystal Structures Reveal How BH3 Domains Activate Bax and Nucleate Its Oligomerization to Induce Apoptosis. *Cell* **152**, 519–531 (2013).
39. Westphal, D., Dewson, G., Czabotar, P. E. & Kluck, R. M. Molecular biology of Bax and Bak activation and action. *Biochim. Biophys. Acta* **1813**, 521–31 (2011).
40. Bleicken, S., Landeta, O., Landajuela, A., Basañez, G. & García-Sáez, A. J. Proapoptotic Bax and Bak proteins form stable protein-permeable pores of tunable size. *J. Biol. Chem.* **288**, 33241–52 (2013).
41. Cosentino, K. & García-Sáez, A. J. Bax and Bak Pores: Are We Closing the Circle? *Trends Cell Biol.* **27**, 266–275 (2017).
42. Nechushtan, A., Smith, C. L., Hsu, Y.-T. & Youle, R. J. Conformation of the Bax C-

- terminus regulates subcellular location and cell death. *EMBO J.* **18**, 2330–2341 (1999).
43. Semaan, S. J. & Nickells, R. W. The apoptotic response in HCT116 BAX<sup>-/-</sup> cancer cells becomes rapidly saturated with increasing expression of a GFP-BAX fusion protein. *BMC Cancer* **10**, 554 (2010).
  44. Nishita, M., Inoue, S., Tsuda, M., Tateda, C. & Miyashita, T. Nuclear translocation and increased expression of bax and disturbance in cell cycle progression without prominent apoptosis induced by hyperthermia. *Exp. Cell Res.* **244**, 357–366 (1998).
  45. Salvador-Gallego, R., Mund, M., Cosentino, K., Schneider, J., Unsay, J., Schraermeyer, U., Engelhardt, J., Ries, J. & Garcia-Saez, J. a. Bax assembly into rings and arcs in apoptotic mitochondria is linked to membrane pores. *EMBO J.* **35**, 389–401 (2016).
  46. Lu, D. F., Wang, Y. S., Li, C., Wei, G. J., Chen, R., Dong, D. M. & Yao, M. Actinomycin D inhibits cell proliferations and promotes apoptosis in osteosarcoma cells. *Int. J. Clin. Exp. Med.* **8**, 1904–1911 (2015).
  47. Kleeff, J., Kornmann, M., Sawhney, H. & Korc, M. Actinomycin D induces apoptosis and inhibits growth of pancreatic cancer cells. *Int. J. Cancer* **86**, 399–407 (2000).
  48. Merkel, O., Wacht, N., Sifft, E., Melchardt, T., Hamacher, F., Kocher, T., Denk, U., Hofbauer, J. P., Egle, A., Scheideler, M., Schleder, M., Steurer, M., Kenner, L. & Greil, R. Actinomycin D induces p53-independent cell death and prolongs survival in high-risk chronic lymphocytic leukemia. *Leukemia* **26**, 2508–2516 (2012).
  49. Liu, X. F., Xiang, L., Zhou, Q., Carralot, J.-P., Prunotto, M., Niederfellner, G. & Pastan, I. Actinomycin D enhances killing of cancer cells by immunotoxin RG7787 through activation of the extrinsic pathway of apoptosis. *Proc. Natl. Acad. Sci.* **113**, 10666–10671 (2016).
  50. Yui, S., Saeki, T., Kanamoto, R. & Iwami, K. Characteristics of apoptosis in HCT116 colon cancer cells induced by deoxycholic acid. *J. Biochem.* **138**, 151–157 (2005).
  51. Powell, A. a, Rue, J. M. L. a, Batta, A. K. & Martinez, J. D. Bile acid hydrophobicity is correlated with induction of apoptosis and/or growth arrest in HCT116 cells. **486**, 481–486 (2001).
  52. YUI, S., KANAMOTO, R., IWAMI, K. & SAEKI, T. Taurocholic Acid Does Not Induce Apoptosis in HCT116 Cells Regardless of Its Intracellular Concentration. *Biosci. Biotechnol. Biochem.* **71**, 800–802 (2007).
  53. Saeki, T., Yui, S., Hirai, T., Fujii, T., Okada, S. & Kanamoto, R. Ursodeoxycholic acid protects colon cancer HCT116 cells from deoxycholic acid-induced apoptosis by inhibiting apoptosome formation. *Nutr. Cancer* **64**, 617–26 (2012).

54. Barry, E. L., Gesek, F. A. & Friedman, P. A. Introduction of antisense oligonucleotides into cells by permeabilization with streptolysin O. *Biotechniques* **15**, 1016–8, 1020 (1993).
55. Liu, S. H., Chu, J. C. & Ng, S. Y. Streptolysin O-permeabilized cell system for studying trans-acting activities of exogenous nuclear proteins. *Nucleic Acids Res.* **21**, 4005–10 (1993).
56. Amidzadeh, Z., Behbahani, A. B., Erfani, N., Sharifzadeh, S., Ranjbaran, R., Moezi, L., Aboualizadeh, F., Okhovat, M. A., Alavi, P. & Azarpira, N. Assessment of different permeabilization methods of minimizing damage to the adherent cells for detection of intracellular RNA by flow cytometry. *Avicenna J. Med. Biotechnol.* **6**, 38–46 (2014).
57. Teng, K. W., Ishitsuka, Y., Ren, P., Youn, Y., Deng, X., Ge, P., Lee, S. H., Belmont, A. S. & Selvin, P. R. Labeling proteins inside living cells using external fluorophores for microscopy. *Elife* **5**, e20378 (2016).
58. Idone, V., Tam, C., Goss, J. W., Toomre, D., Pypaert, M. & Andrews, N. W. Repair of injured plasma membrane by rapid Ca<sup>2+</sup>-dependent endocytosis. *J. Cell Biol.* **180**, 905–14 (2008).
59. Corrotte, M., Fernandes, M. C., Tam, C. & Andrews, N. W. Toxin Pores Endocytosed During Plasma Membrane Repair Traffic into the Lumen of MVBs for Degradation. *Traffic* **13**, 483–494 (2012).
60. Festjens, N., Berghe, T. Vanden & Vandenabeele, P. Necrosis, a well-orchestrated form of cell demise: Signalling cascades, important mediators and concomitant immune response. *Biochim. Biophys. Acta* **1757**, 1371–1387 (2006).
61. Utanohara, S., Tsuji, M., Momma, S., Morio, Y. & Oguchi, K. The effect of ursodeoxycholic acid on glycochenodeoxycholic acid-induced apoptosis in rat hepatocytes. *Toxicology* **214**, 77–86 (2005).
62. Wajant, H. The Fas Signaling Pathway: More Than a Paradigm. *Science (80- )*. **296**, 1635–1636 (2002).



## Chapter VI

---

The mitochondrial affinity of a charge sensor peptide is modified  
by the presence of bile acids



## **THE MITOCHONDRIAL AFFINITY OF A CHARGE SENSOR PEPTIDE IS MODIFIED BY THE PRESENCE OF BILE ACIDS**

Tânia Sousa<sup>1,2</sup>, Samuel Jacob<sup>1,2</sup>, Sandra N. Pinto<sup>1,2</sup>, Ana Coutinho<sup>1,2,3</sup>, Manuel Prieto<sup>1,2</sup>,  
Fábio Fernandes<sup>1,2</sup>

<sup>1</sup>Centro de Química-Física Molecular and Institute of Nanoscience and Nanotechnology, Instituto Superior Técnico, University of Lisbon, Lisbon, Portugal

<sup>2</sup>iBB-Institute for Bioengineering and Biosciences, Biological Sciences Research Group, Av. Rovisco Pais 1, 1049-001 Lisbon, Portugal

<sup>3</sup>Departamento de Química e Bioquímica, Faculty of Sciences, University of Lisbon, Lisbon, Portugal



## Abstract

During apoptosis, anionic lipids play a very important role in signaling cascades. At the level of the plasma membrane, phosphatidylserine (PS) translocates from the inner leaflet of the plasma membrane to the outer leaflet and in mitochondria, cardiolipin (CL), which is normally present in the mitochondrial inner membrane (MIM), translocates to the mitochondrial outer membrane (MOM). Exposure of CL results in the translocation of several proteins to the mitochondria, where they contribute to MOM permeabilization. In this way, membrane surface charge, particularly for mitochondria, is of critical importance for apoptotic signaling.

As shown in previous chapters, cytotoxic bile acids such as DCA, are able to perturb the biophysical properties of model membranes at physiologically active concentrations, and to disturb the structure and permeability of membranes from isolated mitochondria of rat hepatocytes. Additionally, bile acids were shown to modulate the membrane affinity of the apoptotic protein Bax, which is crucial for mitochondrial permeabilization during apoptosis. The aim of this study was to characterize the potential impact of cytotoxic and cytoprotective bile acids on the surface charge of different organelles, which can be a key parameter during apoptotic signaling. For that purpose, we selected the cationic peptide and charge sensor K $\phi$ . We show that DCA increases the partition of K $\phi$ -bimane to model membranes. This effect is related with the insertion of anionic DCA on the lipid bilayer and the increase in surface negative charge of the membrane. The impact of bile acids on the interaction of K $\phi$  with mitochondria was evaluated through expression of the RFP-labeled peptide in HEK293T cells. Surprisingly, as previously observed for Bax, cytoprotective bile acids are shown to inhibit the interaction of K $\phi$ -bimane with mitochondria. These results confirm that in the presence of only non-specific interactions, physiologically active concentrations of either cytotoxic or cytoprotective bile acids are able to change the mitochondrial affinity of charged protein domains. This evidence supports a scenario where a buildup of bile acids in the intracellular environment will lead to complex changes in the subcellular distribution of different proteins of relevance in the apoptotic signaling pathway, possibly contributing in this manner to the activation of apoptotic or cytoprotective molecular machineries.



## 1. Introduction

A wide range of signaling processes occurs at the surface of biomembranes through the reversible association of proteins from the cytosol to the membrane of organelles<sup>1</sup>. Membrane lipids not only confer unique dielectric and permeability properties to the bilayer but also function as second messengers in signal transduction and dictate the partitioning and folding of intrinsic proteins<sup>2</sup>. Membrane surface charges are carried largely by anionic phospholipids and the nature of the lipids composing lipid membranes vary greatly between organelles and cell types<sup>2</sup>.

In the plasma membrane, the lipids that contribute more for the negative charge of its inner leaflet are phosphoinositides (PI), that are highly anionic but represent only 1-2% of total phospholipids in living cells<sup>3</sup>, and phosphatidylserine (PS), that represents 10-20% of plasma membrane phospholipids<sup>4,5</sup>. During apoptosis, the mechanisms responsible for sequestering of PS in the inner leaflet are down-regulated, and PS exposure in the outer leaflet occurs, while PI content decreases. PS exposure is a hallmark of apoptosis and is a recognition signal for phagocytic cells to engage in clearing of dying cells<sup>6,7</sup>.

In mitochondria, the major phospholipids are phosphatidylcholine (PC) and phosphatidylethanolamine (PE), which account together for about 80% of total phospholipids. Cardiolipin (CL), an anionic lipid, is present in the range of 10-20% of total mitochondrial phospholipids<sup>8</sup>, and in healthy cells is almost entirely found in the mitochondrial inner membrane (MIM) rather than the mitochondrial outer membrane (MOM)<sup>9</sup>. For this reason, in normal conditions, the outer leaflet of the MOM is not noticeably electronegative<sup>7</sup>. However, during the early stages of apoptosis, before depolarization of the inner membrane, CL is exposed by translocation to the MOM, where it can interact with important elements of the apoptotic cascade such as cytochrome c (cyt c), Bid, a member of the Bcl-2 family of proteins, and caspase-8<sup>7,9</sup>. The translocation of CL to the MOM leads to a drastic increase in the surface charge of these organelles, and this electrostatic change has been proposed to play a key role in the apoptotic process, by driving the association and retention of different pro-apoptotic proteins with polycationic motifs within the mitochondria<sup>7</sup>. The Bcl-2 family is a protein superfamily that is involved in apoptosis regulation<sup>10-12</sup>. The translocation of CL to the MOM is essential for activation of caspase-8, and upon apoptotic signaling, the activation of caspase-8 results in the cleavage of Bid to a truncated form, tBid<sup>13</sup>. tBid translocates to the MOM and induces the oligomerization of Bax and/or Bak, which leads to MOM permeabilization<sup>14-17</sup>.

In order to investigate changes in the surface charge of organelles during apoptosis, several biosensors have been developed<sup>5,7,18</sup>. They consist of cationic peptides or folded protein domains that transiently associate with anionic phospholipids based on their negative

charges and irrespective of their head group<sup>19-21</sup>. In a recent approach, Grinstein and coworkers used different labeled cationic peptides to quantify surface charge in cells undergoing apoptosis<sup>7,21</sup>. They observed that in untreated cells, several of these peptides localized almost exclusively in the inner leaflet of the plasma membrane, confirming the significant electronegative nature of the plasma membrane<sup>7,21</sup>. Following FAS activation, the cationic peptides showed a remarkable redistribution with punctate plasmalemmal labeling and accumulation in mitochondria, reflecting the accumulation of CL in the MOM<sup>7</sup>. These authors found that reduction of plasmalemmal surface charge is not sufficient to account for the redistribution of the probes to mitochondria, and a concomitant increase in the negativity of the exposed mitochondrial membranes must be invoked<sup>7</sup>. It was also observed that the accumulation of peptides in the mitochondria preceded both cyt c release and MIM permeabilization, confirming that changes in mitochondrial surface charge occurs early in apoptosis.

The cytotoxic bile acids, such as DCA, are known to have higher preference for lipid membranes than the cytoprotective molecules, as a result of their more hydrophobic character<sup>22</sup>. These molecules are also found to partition with higher affinity for membranes with low cholesterol (Chol) content, and to inhibit the ordering effect of Chol at physiologically active concentrations in model membranes<sup>22,23</sup>. Furthermore, it was already shown in hepatocytes that bile acids interact more efficiently with the MOM than with the plasma membrane, while only cytotoxic bile acids were found to affect the structure of the MOM and the permeability of the MIM<sup>24</sup>. In a previous chapter of this thesis, it is also shown that both cytotoxic and cytoprotective bile acids inhibited the interaction of Bax with membranes mimicking the MOM lipid composition, and the studies presented in the previous chapter suggest that this effect could also be observed for the interaction of Bax with mitochondria in colon cancer cells, albeit in very specific conditions. The impact of bile acids on Bax affinity for mitochondrial membranes and liposomes mimicking MOM lipid composition are non-specific and are the result of either the adsorption of a large amount of monomers or pre-micellar aggregates of bile acids to the protein surface, or are the result of adsorption of the bile acids to the membrane surface, changing its structure and surface charge. Since these effects are non-specific in nature, it is almost certain that they will be mirrored for different Bcl-2 proteins or other relevant factors for apoptosis.

In this work, our aim was to characterize the effect of bile acids on the charge of model membrane systems mimicking the inner leaflet of the plasma membrane and the mitochondria outer membrane, and later on HEK293T cells. For that we selected the cationic peptide and charge sensor K $\phi$  (GKKFWKRLRKFLRKLK)<sup>21</sup>. This peptide is an amphipathic helix and binds modestly to isolated mitochondria<sup>7</sup>. This affinity was greatly enhanced in the presence of Bid, and the nature of this interaction is purely electrostatic, as it is highly dependent on ionic

strenght<sup>7</sup>. In this way,  $K_{\phi}$  is an ideal tool to monitor changes in mitochondria and plasma membrane surface charge during incubation with bile acids.

## 2. Materials and methods

### 2.1 Chemicals and Reagents

1,2-dioleoyl-*sn*-glycero-3-phosphocholine (DOPC), 1,2-dioleoyl-*sn*-glycero-3-phosphoethanolamine (DOPE), *L*- $\alpha$ -Phosphatidylinositol sodium salt (PI), 1-palmitoyl-2-oleoyl-*sn*-glycero-3-phosphocholine (POPC); 1-palmitoyl-2-oleoyl-*sn*-glycero-3-phospho-L-serine (POPS); 1,3-bis(*sn*-3'-phosphatidyl)-*sn*-glycerol (cardiolipin, CL), were purchased from Avanti Polar Lipids (Alabaster, AL, USA). Cholesterol (Chol) was obtained from Sigma-Aldrich (St. Louis MO, USA). Stock solutions of all lipids were prepared with Uvasol grade chloroform with the exception of CL that was prepared in chloroform/methanol (2:1). Both solvents were obtained from Sigma-Aldrich. DCA and TUDCA in sodium salt form, Tris(2-carboxyethyl)phosphine hydrochloride (TCEP), NaCl, Actinomycin D (Act D), Streptolysin O (SLO, 25.000-50.000 U) and Trizma®, were purchased from Sigma-Aldrich (St. Louis MO, USA). UDCA sodium salt was purchased from Santa Cruz Biotechnologies (Santa Cruz, CA),  $K_{\phi}$ -bimane was purchased from Anaspec (Fremont, USA). [6-amino-9-(2-methoxycarbonylphenyl)xanthen-3-ylidene]azanium (Rho-123) was purchased from Invitrogen™, Thermo Fisher Scientific (Eugene, OR).

### 2.2 Lipid vesicle preparation

Large unilamellar vesicles (LUVs) for partition studies were prepared by extrusion of multilamellar vesicles as previously described<sup>25</sup>. Required volumes of lipid stock solutions were mixed in chloroform and dried under a flow of dry nitrogen gas (N<sub>2</sub>). Last traces of solvent were removed overnight under vacuum. Multilamellar vesicles were obtained through hydration in 10 mM Tris-HCl, 150 mM NaCl at pH 7.4, prepared in Milli-Q water, followed by freeze-thaw cycles. LUVs were produced by extrusion through polycarbonate filters with a pore size of 100 nm (Whatman, USA) on a mini-extruder (Avanti Polar Lipids). LUVs were kept at room temperature and in the dark until being used, at most for 48 h after being prepared. Chol concentration was determined gravimetrically.

### 2.3 Zeta-Potential measurements

Zeta potential measurements were performed in a Malvern Zetasizer Nano ZS apparatus (Malvern, UK), equipped with a He-Ne laser ( $\lambda = 632.8$  nm), at 25 °C. Folded capillary cells DTS 1061 (Malvern, UK) were used. LUV samples at 400  $\mu$ M were in Tris-HCl 10 mM, NaCl 150 mM, pH 7.4. Samples were then dispensed into the zeta cells and allowed to equilibrate at 25 °C for 5 minutes. Values of viscosity and refractive index were set to 0.8872 cP and 1.330, respectively<sup>52</sup>. The zeta potential measurements were thus performed in monomodal mode, assuming a monodisperse sample size distribution. At least three measurements of minimum 30 runs were performed. Data analysis was carried out using the Zetasizer software (Malvern, UK).

### 2.4 Steady-state fluorescence spectroscopy

Fluorescence measurements of K $\phi$ -bimane were carried out, at room temperature, with SLM-Aminco 8100 Series 2 spectrofluorimeter (Rhocester, NY) with double excitation and emission monochromators (MC-400), in right-angle geometry. The light source was a 450-W Xe arc lamp and the reference a Rhodamine B quantum counter solution. Quartz cuvettes (0.5x0.5 cm) from Hellma Analytics were used.

K $\phi$ -bimane fluorescence intensity was followed by excitation at 396 nm and collection between 415 and 650 nm. When needed, fluorescence intensities were corrected for the inner filter effects as described elsewhere<sup>26</sup>. K $\phi$ -bimane steady-state anisotropy,  $\langle r \rangle$ , was measured with excitation at 396 nm and emission at 480 nm and is defined as<sup>27</sup>:

$$\langle r \rangle = \frac{I_{VV} - GI_{VH}}{I_{VV} + 2GI_{VH}} \quad (1)$$

where  $I_{VV}$  and  $I_{VH}$  are the steady-state vertical and horizontal components of fluorescence emission, respectively, with excitation accomplished with vertically polarized light. The  $G$  factor is calculated by considering the components with excitation horizontal to the emission axis,  $I_{HV}$  and  $I_{HH}$ <sup>27</sup>:

$$G = \frac{I_{HV}}{I_{HH}} \quad (2)$$

For the polarization of excitation and emission light, Glan-Thompson polarizers were used. Blank subtraction was taken into account in all the anisotropy components as well as in the other fluorescence measurements.

Membrane-water partition coefficient ( $K_p$ ) values for partition allow a quantified evaluation of the affinity of a particular molecule for lipid membranes. The increase of the fluorescence steady-state anisotropy  $\langle r \rangle$  of the peptide after insertion in liposomes, allows for measurement of  $K_p$ 's of K $\phi$ -bimane to lipid membranes according to Eq. 3<sup>28</sup>:

$$r = \frac{r_w[(\gamma_L[L])^{-1} - 1] + r_L K_p \varepsilon_L \phi_L / (\varepsilon_w \phi_w)}{(\gamma_L[L])^{-1} - 1 + K_p \varepsilon_L \phi_L / (\varepsilon_w \phi_w)} \quad (3)$$

where  $[L]$  is the concentration of accessible lipid, and  $\gamma_L$  is the lipid molar volume.  $r_i$  are steady-state anisotropies,  $\varepsilon_i$  are the extinction coefficients, and  $\phi_i$  are the quantum yield of K $\phi$ -bimane in phase  $i$ . The indices  $L$  and  $W$  correspond to the lipid and aqueous phases<sup>28</sup>. A  $\gamma_L = 0.76 \text{ dm}^3 \text{ mol}^{-1}$  was used during fitting<sup>29</sup>.  $r_L$  and  $K_p$  were optimized using the least-square method on GraphPad Prism 5 (GraphPad Software, CA, USA).

## 2.5 Cell culture and transfection chemicals

HEK293T cells were cultured and maintained in DMEM with 10% FBS and 1% of penicillin-streptomycin (Sigma Chemical Co., St. Louis, MO) at the incubator with controlled temperature (37°C), humidity, and CO<sub>2</sub> levels (5%). For microscopy experiments, cells were added to  $\mu$ -Slide 8-well glass bottom ibidi chambers (Munich, Germany) pre-coated with fibronectin (Thermo Fisher Scientific) at 10  $\mu\text{g}/\text{mL}$ . Cells in  $\mu$ -slides were transfected with the K $\phi$ -RFP construct using Lipofectamine® 2000 (Invitrogen™, Thermo Fisher Scientific Inc.), according to the manufacturer's instructions. K $\phi$ -mRFP was a gift from Sergio Grinstein (Addgene plasmid # 17276)<sup>21</sup>. Cells were grown overnight for fluorescence confocal imaging.

## **2.6 Streptolysin O permeability assay**

A stock solution of Streptolysin O (SLO, 25.000-50.000 U, Sigma Aldrich) in Milli Q water at a final concentration of 5.000 U/mL was aliquoted and stored at -20°C. Aliquots of SLO were reduced in DPBS supplemented with 10 mM TCEP for 30 min at 37°C. The SLO solution was further diluted to the working concentration in DPBS to a final 250-fold dilution of the stock solution. HEK293T cells expressing K $\phi$ -RFP were reversibly permeabilized by incubation with 200U SLO in the presence or absence of bile acids at 100 or 500  $\mu$ M for 20 min at 37°C. Successful permeabilization was confirmed using TO-PRO<sup>®</sup>-3 stain, a nuclear counterstain and dead cell indicator that is cell impermeant. Co-incubation with 1  $\mu$ M of Rho123 to label active mitochondria was also performed. After SLO reversible permeabilization and prior to confocal imaging, the cells were washed with DPBS.

## **2.7 Confocal fluorescence imaging**

All measurements were performed on a Leica TCS SP5 (Leica Microsystems CMS GmbH, Mannheim, Germany) inverted confocal microscope (DMI600). Excitation lines were provided by an Argon laser that was focused into the sample by an apochromatic water immersion objective (63x, NA 1.2; Zeiss, Jena Germany). A 111.4  $\mu$ m diameter pinhole positioned in front of the image plane blocked out-of-focus signals.

For the SLO permeability assays, imaging of K $\phi$ -RFP was performed through excitation with the 514 nm Argon laser line and emission was collected between 600 and 700 nm, while Rhodamine 123 (Rho-123) was excited using the 476 nm Argon laser line with detection between 480 and 530 nm. Imaging was carried out immediately after SLO permeabilization.

For quantification of the fluorescent intensity signal from both fluorophores, K $\phi$ -RFP and Rho-123, spectral imaging was performed in combination with linear unmixing<sup>30</sup>, since the RFP and Rho-123 emission spectra are partially overlapping. Briefly, fluorescence from cells expressing K $\phi$ -RFP with Rho-123 was acquired at different wavelengths for excitation at 476 and 514 nm, and images were computationally processed by a linear unmixing algorithm using the distinct reference spectrum of RFP and Rho-123, which were obtained independently. This procedure was carried out using homemade software created in a MATLAB environment (MathWorks, Natick, MA). All other quantifications were performed using the image analysis software ImageJ (<https://imagej.nih.gov/ij/index.html>).

### 3. Results

#### ***Impact of bile acids on the surface charge of liposomes mimicking plasma membrane and MOM composition***

The adsorption and intercalation of DCA in lipid membranes has been shown to induce considerable changes in membrane structure and dynamics<sup>22,24</sup>. Although the  $pK_a$  of DCA increases to 7.5 after insertion into POPC membranes<sup>31</sup>, it is still expected that a large fraction of membrane-bound DCA molecules remain charged at physiological pH. In these conditions, the interaction of bile acids at physiologically active concentrations with mitochondria and the plasma membrane would undoubtedly induce a considerable increase in the electronegativity of these organelles, possibly contributing to the recruitment of apoptotic factors and the onset of apoptosis. To test this hypothesis, we begin by evaluating the change in surface charge of different liposome formulations mimicking either the inner leaflet of the plasma membrane (cytosolic surface) and the MOM.

Fig.1A shows the  $\zeta$ -potential of liposomes composed of POPC and POPS. These are the most common classes of phospholipids at the inner leaflet of the plasma membrane. As expected,  $\zeta$ -potential progressively decreased upon increasing the anionic phospholipid content of the lipid mixtures, reflecting an increase in their anionic net surface charge density.

To mimic the lipid composition of the inner leaflet of the plasma membrane, POPC:POPS:Chol mixtures were used (50:30:20% and 40:30:30%) (Fig. 1B), reflecting the approximate lipid content of these lipid classes in the inner leaflet<sup>32</sup>. Two different cholesterol concentrations are used, since the exact fraction of cholesterol in the inner leaflet is still the matter of controversy. Moreover, this is expected to vary significantly between different cell types. As expected, cholesterol content has very little impact on the surface charge of liposomes, which is mainly defined by the fraction of PS.

In order to mimic the mitochondrial outer membrane (MOM), a DOPC:DOPE:PI:Chol (51:26.6:12.8:9.6%) lipid mixture was used<sup>8</sup>. Not surprisingly, the surface of these liposomes is considerably less negatively charged than the membranes mimicking the cytosolic surface of the plasma membrane. This difference in surface charge between the MOM and the plasma membrane intracellular surface is also observed when measuring the subcellular distribution of peptide charge sensors in different cells<sup>7,21</sup>.

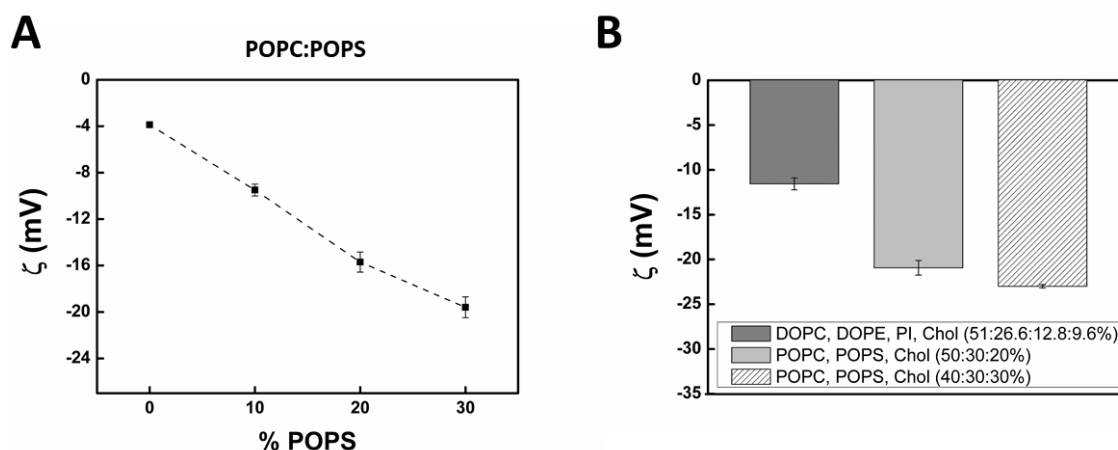


**Figure 1. Characterization of net surface charge density of LUVs with different lipid compositions by Zeta ( $\zeta$ ) potential.** (A)  $\zeta$ -potential of liposomes with different POPS content in POPC:POPS LUVs and (B) for LUVs mimicking the inner leaflet of the plasma membrane (POPC:POPS:Chol 50:30:20% and 40:30:30%), and LUVs mimicking MOM (DOPC:DOPE:PI:Chol 51:26.6:12.8:9.6 %). Total lipid concentration was 400  $\mu$ M. Error bars represent SD of at least three different measurements.

In the presence of DCA at 100 and 500  $\mu$ M, the  $\zeta$ -potential of POPC:POPS mixtures decrease significantly ( $\Delta\zeta = 4-8$  mV) (Figure 2), reflecting the association of negatively charged DCA molecules to the membrane. Interestingly, DCA is found to increase the anionic nature of liposomes even for liposomes with a very high anionic lipid content, showing that the presence of anionic phospholipids do not impair association of the negatively charged bile acid to a significant extent.

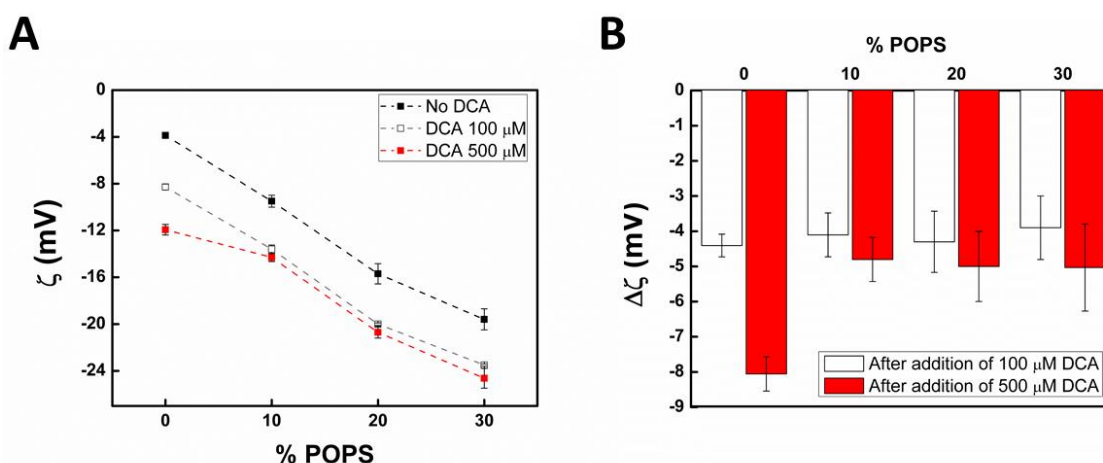


**Figure 2. Insertion of DCA in POPC:POPS liposomes leads to a higher anionic surface charge.** (A)  $\zeta$ -potential of liposomes with different POPS content in POPC:POPS LUVs in the absence and presence of 100 or 500  $\mu$ M of DCA. (B) Variation of zeta potential ( $\Delta\zeta$ ) after the addition of 100 or 500

$\mu\text{M}$  DCA to liposomes of different POPS content. Total lipid concentration was  $400 \mu\text{M}$ . Error bars represent SD of at least three different measurements.

For liposomes mimicking the MOM or the inner leaflet of the plasma membrane, the impact of DCA on  $\zeta$ -potential values is also evident ( $\Delta\zeta = 3\text{-}8 \text{ mV}$ ) (Figure 3). Here, the smallest  $\Delta\zeta$  in the presence of DCA is observed for the lipid mixture with 30% cholesterol. Importantly, the mixture mimicking the MOM lipid composition exhibits  $\Delta\zeta$  values considerably larger than the ones measured for the mixtures with higher cholesterol content, mimicking the inner leaflet of the plasma membrane. In fact, high cholesterol concentrations were previously shown to inhibit the interaction of bile acids with lipid membranes<sup>22,31,33</sup>. In this way, the interaction of bile acids at physiologically active concentrations with both the inner leaflet of the plasma membrane or the MOM is certain to produce significant changes in the surface charge of these organelles. Notably, the liposomes mimicking MOM lipid composition and with a lower cholesterol content show a larger uptake of negatively charged DCA in the presence of  $500 \mu\text{M}$  of the bile acid, in support of previous reports that showed considerable uptake of fluorescent-labeled deoxycholic acid in the mitochondria of different cell types, while the plasma membrane was relatively depleted of this molecule<sup>24</sup>.

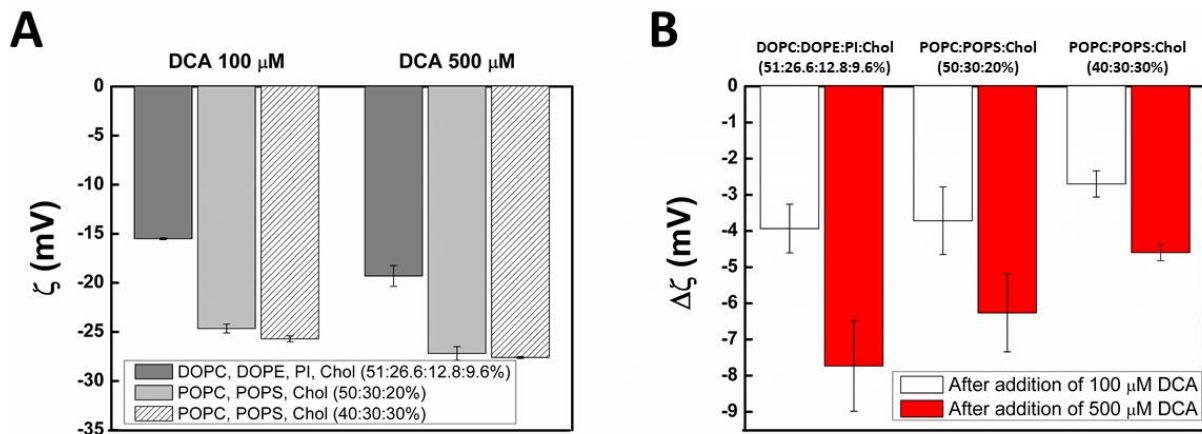


**Figure 3. Insertion of DCA in liposomes mimicking the cytosolic surface of the plasma membrane or the MOM leads to a higher anionic surface charge.** (A)  $\zeta$ -potential for LUVs mimicking the inner leaflet of the plasma membrane (POPC:POPS:Chol 50:30:20%) and (POPC:POPS:Chol 40:30:30%), and LUVs mimicking MOM (DOPC:DOPE:PI:Chol 51:26.6:12.8:9.6%), in the absence and presence of 100 and 500  $\mu\text{M}$ . (B) Variation of zeta potential ( $\Delta\zeta$ ) after the addition of 100 and 500  $\mu\text{M}$  DCA when compared with the absence of this component, for the different lipid mixtures. Total lipid concentration was  $400 \mu\text{M}$ . Error bars represented average values of at least three different measurements.

These results confirm that cytotoxic bile acids such as DCA, which exhibit considerable partition to cellular membranes, particularly to the mitochondria due to its low cholesterol content, have the potential to trigger an increase in the surface charge of these organelles. In order to evaluate if such changes could trigger significant shifts in the recruitment of cationic protein domains to the mitochondria, experiments were carried out with the cationic peptide  $K\phi$  labeled with the fluorescent probe bimane.  $K\phi$  has been successfully used to identify the changes in MOM surface charge that occur during the early stages of apoptosis<sup>7</sup>.

### ***Characterization of $K\phi$ -bimane as an accurate sensor for membrane charge***

In order to evaluate the usefulness of  $K\phi$  as a membrane surface charge sensor, a detailed characterization of the dependence of  $K\phi$ -bimane membrane-water partition coefficient ( $K_p$ ) with lipid composition was carried out. The peptide was found to be stable in solution with no signs of aggregation (results not shown), so that a partition model that considers a single peptide specie can be used. The increase of the fluorescence steady-state anisotropy  $\langle r \rangle$  of the peptide after insertion in liposomes, allows for measurement of  $K_p$ 's of  $K\phi$ -bimane to lipid membranes according to Eq. 3<sup>28</sup>. The fluorescence intensity of  $K\phi$ -bimane is also found to change upon association to lipid membranes as a result of a higher quantum yield of bimane in the membrane environment. However, since fluorescence anisotropies are independent of fluorophore concentration, measurements of  $\langle r \rangle$  are less prone to errors arising from concentration uncertainty and are generally more robust for determination of  $K_p$ .

The effect of charge screening on the membrane affinity of  $K\phi$ -bimane was evaluated through determination of the  $K_p$  for LUVs composed of POPC:POPS:Chol (55:15:30%), in the absence or presence of 150 mM of NaCl (Figure 4). Since  $K\phi$  is believed to bound mostly through electrostatic interactions, charge screening is expected to inhibit the interaction of  $K\phi$ -bimane with membranes. This is indeed the case, with considerably less binding of  $K\phi$ -bimane to the liposomes in the presence of 150mM NaCl, and the  $K_p$  increases almost 4-fold when

salt is removed from the buffer (see legend of Figure 4). In further experiments, NaCl concentration was kept at 150 mM.

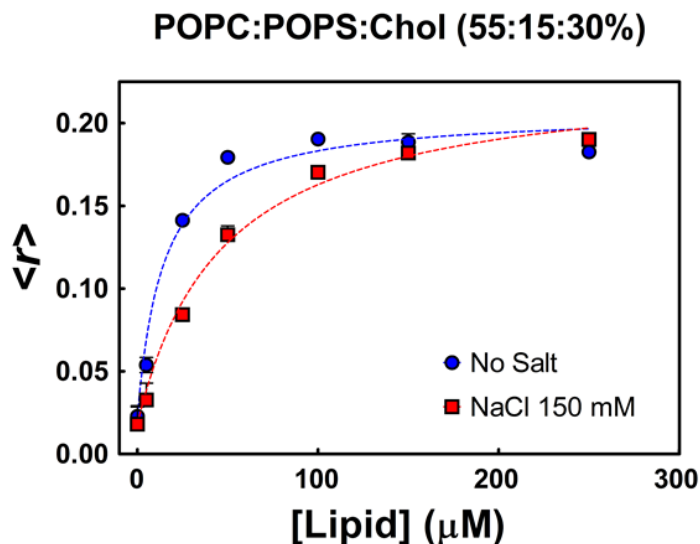


**Figure 4. Charge screening decreases the affinity of  $K\phi$ -bimane towards POPC:POPS:Chol membranes.** Fluorescence steady-state anisotropy of  $K\phi$ -bimane over different lipid concentrations for LUVs composed of POPC:POPS:Chol 55:15:30% in 10 mM Tris-HCl, pH 7.4 buffer with or without 150 mM NaCl. Lines are the fitted partition curves according to Eq. 3, with  $K_p([\text{NaCl}] = 150 \text{ mM}) = 3.2 \pm 0.5 \times 10^3$  and  $K_p([\text{NaCl}] = 0 \text{ mM}) = 8.2 \pm 2.2 \times 10^3$ . Note that lipid concentrations represent only the accessible lipid to the peptide (outer leaflet) and not the total lipid concentration.  $K\phi$ -bimane concentration was 2  $\mu\text{M}$ . Error bars represent SD values from at least two independent measurements.

Using the ternary mixture POPC:POPS:Chol representing the three classes of lipids most relevant for this study (zwitterionic lipids, anionic lipids and cholesterol), the impact of increasing anionic lipid content on the affinity of  $K\phi$ -bimane for membranes was evaluated (Figure 5). Cholesterol content was kept fix at 30% and only PC:PS content differed between the different lipid compositions. As expected, the peptide is found to have a higher affinity for membranes with a higher PS content. The increase in  $K_p$  is very pronounced from 15 to 22.5% of POPS, with a more than 2-fold increase in  $K_p$  for a 50% increase in anionic lipid content

(Table S1), showing that the peptide is very sensitive to small changes in the surface charge of anionic lipids.

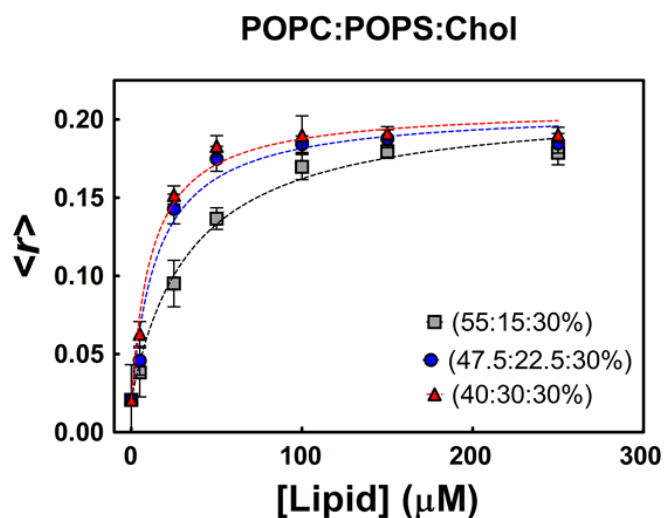


**Figure 5. Partition of K $\phi$ -bimane to membranes increases with higher anionic lipid content.** Fluorescence steady-state anisotropy of K $\phi$ -bimane over different lipid concentrations for LUVs composed of POPC:Chol:POPS and varying concentrations of POPS (15, 22.5 and 30%). Lines are the fitted partition curves according to Eq.3. Note that lipid concentrations represent only the accessible lipid to the peptide and not the total lipid concentration.  $K_p$  values are shown on Table S1. K $\phi$ -bimane concentration was 2  $\mu\text{M}$ . Error bars represent SD values from at least two independent measurements.

Since the cholesterol content of the plasma membrane and the MOM differ substantially, it is also useful to evaluate the impact of different cholesterol concentrations on the partition of K $\phi$ -bimane when the surface charge is kept constant. Partition experiments were again carried out using the ternary lipid mixture POPC:POPS:Chol. However, this time the content of PS was kept fixed and only the fractions of PC and Chol were varied, using three different cholesterol concentrations (10, 20 and 30%). Two sets of experiments were carried out, one for 15 and another for 30% PS (Figure 6). Although there is a small decrease in K $\phi$ -bimane affinity for membranes with high cholesterol content, differences are relatively small and are

completely overshadowed by the differences observed for liposomes with different anionic lipid content (Table S1).

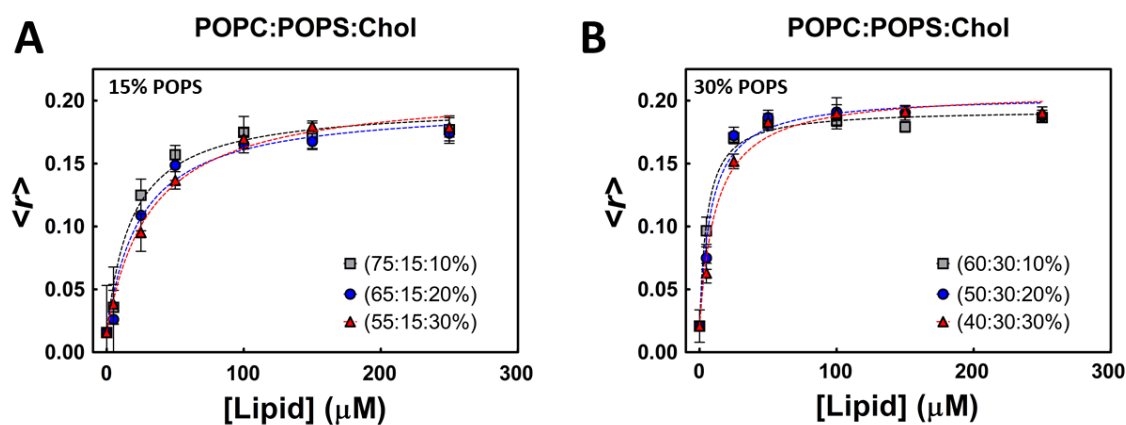


**Figure 6. Anionic lipid content is vastly more relevant for  $K\phi$ -bimane partition than cholesterol content.** Fluorescence steady-state anisotropy of  $K\phi$ -bimane over different lipid concentrations for LUVs composed of POPC, 15% POPS and 10, 20 and 30% Chol (A) and POPC, 30% POPS and 10, 20 and 30% Chol (B). Lines are the fitted partition curves according to Eq.3. Note that lipid concentrations represent only the accessible lipid to the peptide and not the total lipid concentration.  $K_p$  values are shown on Table S1.  $K\phi$ -bimane concentration was 2  $\mu\text{M}$ . Error bars represent SD values from at least two independent measurements.

### ***Impact of DCA on the recruitment of $K\phi$ -bimane to membranes mimicking the plasma membrane and to the MOM***

Having established the dominance of electrostatic effects on the interaction of  $K\phi$ -bimane with lipid membranes, we proceeded to use  $K\phi$ -bimane as a model for a cationic protein domain, in order to evaluate the impact of bile acids at physiologically active concentrations on the recruitment of cationic proteins to the plasma membrane and to the MOM.

Notably, the anisotropy values of  $K\phi$ -bimane in the absence of lipid (Figure 7) are identical with or without 100  $\mu\text{M}$  DCA, suggesting that interaction of the peptide with DCA in solution is moderate at most. However, at 500  $\mu\text{M}$  DCA, the anisotropy of  $K\phi$ -bimane increases dramatically, reflecting the interaction of the peptide with pre-micellar aggregates of DCA, which decreases the rotational dynamics of the peptide. In fact bile acids are known to aggregate in small numbers in a stepwise fashion below their reported CMC of around 3mM, mainly as a response to the hydrophobic effect<sup>34</sup>. It is likely that at 500  $\mu\text{M}$  DCA, the peptide

contributes to the nucleation of DCA aggregation into relatively large mixed peptide-bile acid complexes in solution, as seen for Bax in Chapter IV. These results suggest that while the effects of 100  $\mu\text{M}$  DCA on the partition of K $\phi$ -bimane are likely mostly related with the interaction of the bile acid with lipid membranes (which increases their anionic character as seen through  $\zeta$ -potential measurements), the formation of mixed peptide-DCA complexes in solution cannot be totally excluded, as evidence exist for their formation at higher bile acid concentrations. Nevertheless, given the large affinity of DCA for lipid membranes, it is certain that the concentration of DCA free for protein interaction in solution is much smaller in the presence of liposomes. An increase in fluorescence anisotropy could also be induced by a dramatic decrease in fluorescence lifetime values. However, since fluorescence intensities are not changed in the presence of high DCA concentrations (results not shown), this possibility can be safely excluded.

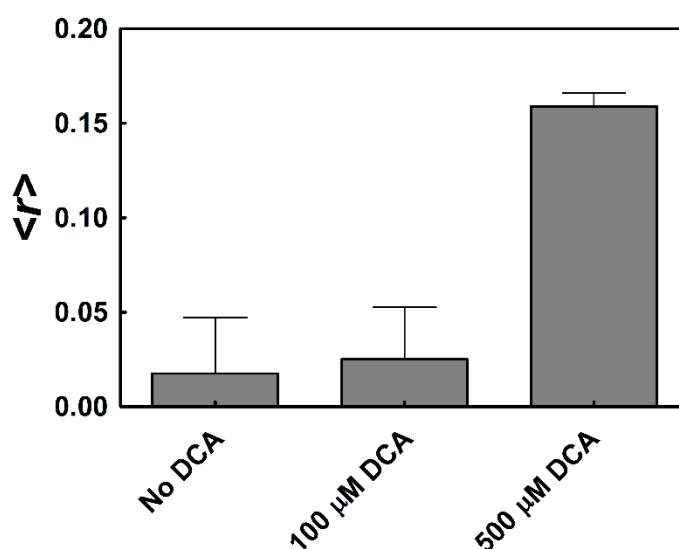


**Figure 7. At high concentration of DCA, the anisotropy of K $\phi$ -bimane increases, reflecting the interaction of the peptide with pre-micellar aggregates of DCA, which decreases the rotational dynamics of the peptide.** Fluorescence steady-state anisotropy of K $\phi$ -bimane in the absence of lipid and DCA or in the presence of 100 or 500  $\mu\text{M}$  DCA was measured with excitation at 396 nm and emission at 480 nm with excitation and calculated according to Eq. 1. K $\phi$ -bimane concentration was 2  $\mu\text{M}$ . Error bars represent SD values from at least two independent experiments with 8 measurements each.

The same liposome formulations used before to mimic the plasma membrane and the MOM were again used to measure the impact of DCA on the partition of  $K_{\phi}$ -bimane (Figure 8). The same experiment was also carried out for a mixture of POPC:Chol, in the absence of anionic lipids. In the latter case, the impact of DCA on the affinity of  $K_{\phi}$ -bimane is dramatic, increasing the  $K_p$  by  $\sim 68$  fold (Table S2). For all lipid compositions, DCA is found to increase the partition of  $K_{\phi}$ -bimane.

Comparing the effect of DCA in the biomimetic lipid mixtures in study, we observed that the increase in  $K_{\phi}$ -bimane partition coefficient is more pronounced for membranes mimicking the MOM, likely due to the fact that these membranes have a lower Chol content, and as such accumulate a larger amount of DCA.

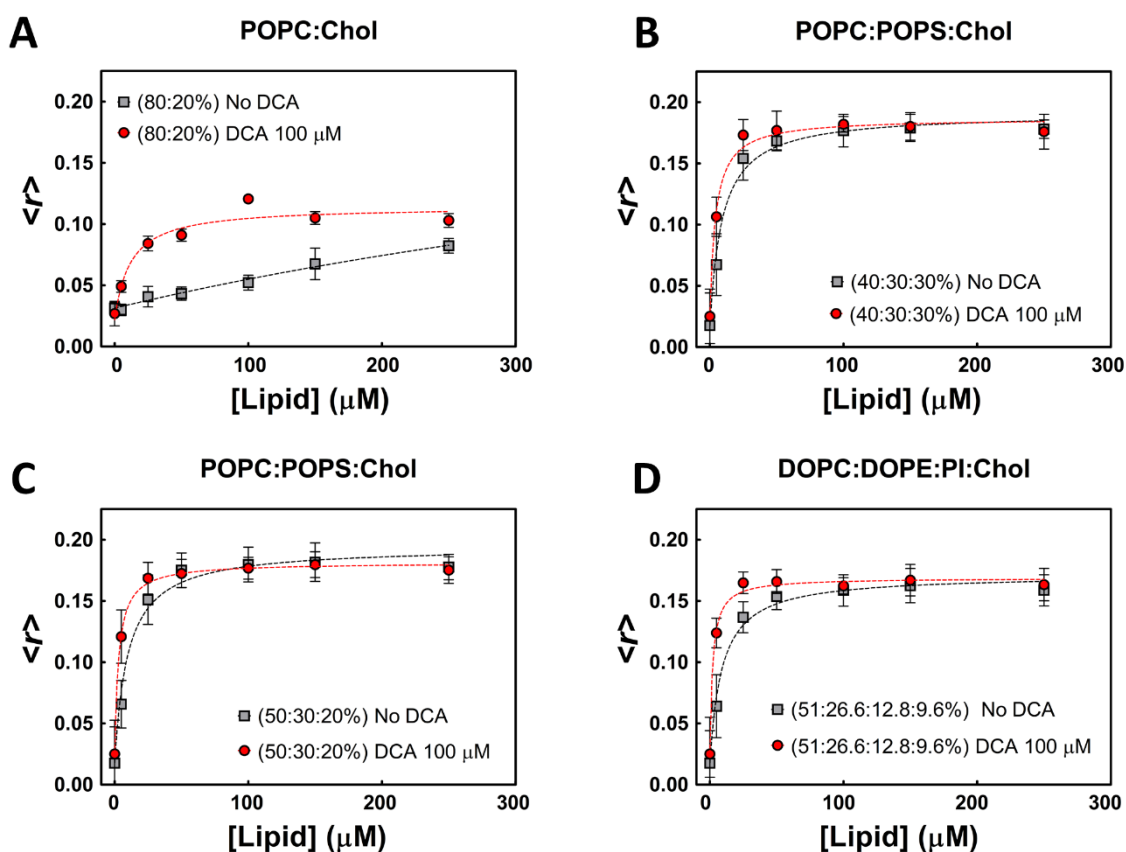


**Figure 8. DCA increases the partition of  $K_{\phi}$ -bimane for membranes.** Fluorescence steady-state anisotropy of  $K_{\phi}$ -bimane over different lipid concentrations for LUVs composed of (A) POPC:Chol 80:20%, (B) POPC:POPS:Chol 40:30:30%, (C) POPC:POPS:Chol 50:30:20%, and (D) DOPC:DOPE:PI:Chol 51:26.6:12.8:9.6% in the absence or presence of 100  $\mu\text{M}$  DCA. Lines are the fitted partition curves according to Eq.3. Note that lipid concentrations represent only the accessible lipid to the peptide and not the total lipid concentration.  $K_p$  values are shown on Table S2.  $K_{\phi}$ -bimane concentration was 2  $\mu\text{M}$ . Error bars represent SD values from at least two independent measurements.

***UDCA and TUDCA at cytoprotective concentrations have limited impact on the recruitment of K $\phi$ -bimane to membranes***

While DCA induces apoptosis in many cells types, more hydrophilic bile acids, such as UDCA or TUDCA, have a cytoprotective effect on different cell types following long incubations with the bile acids preceding an apoptotic stimulus. This difference in physiological activity is possibly related to a lower partition of the more hydrophilic bile acids to lipid membranes<sup>22,24</sup>. The impact of UDCA and TUDCA on the surface charge of membrane model systems was also evaluated for the ternary mixture POPC:POPS:Chol, through the use of K $\phi$ -bimane (Figure 9). TUDCA and UDCA at 100  $\mu$ M are shown to have no impact on the K<sub>p</sub> of K $\phi$ -bimane (Fig. 9 A, B, Table S2). These bile acids had also no impact on the partition of K $\phi$ -bimane to a lipid mixture mimicking the MOM (results not shown). These results confirm that at this concentration, these cytoprotective bile acids are not able to modulate the surface charge of lipid membranes. However, when using 500  $\mu$ M of UDCA, some aggregation of UDCA and the peptide is also evident through a significant increase in  $\langle r \rangle$  of K $\phi$ -bimane in buffer (Fig. 9C). It is important to note that after exposure of permeabilized colon cancer cells to this concentration of UDCA, a rapid onset of signs of apoptosis was observed (chapter V). It is likely that the toxicity of UDCA at the aggregating pre-micellar concentration of 500  $\mu$ M, is the result of either an increase in the accumulation of this bile acid in the MOM membrane with an impact on permeability or surface charge, or of the interaction of premicellar aggregates with relevant protein apoptotic factors. Surprisingly, 500  $\mu$ M of TUDCA had no effect on the fluorescence anisotropy of K $\phi$ -bimane (Fig. 9D), suggesting limited or no interaction of the peptide with this bile acid in solution, even at relatively high concentrations.

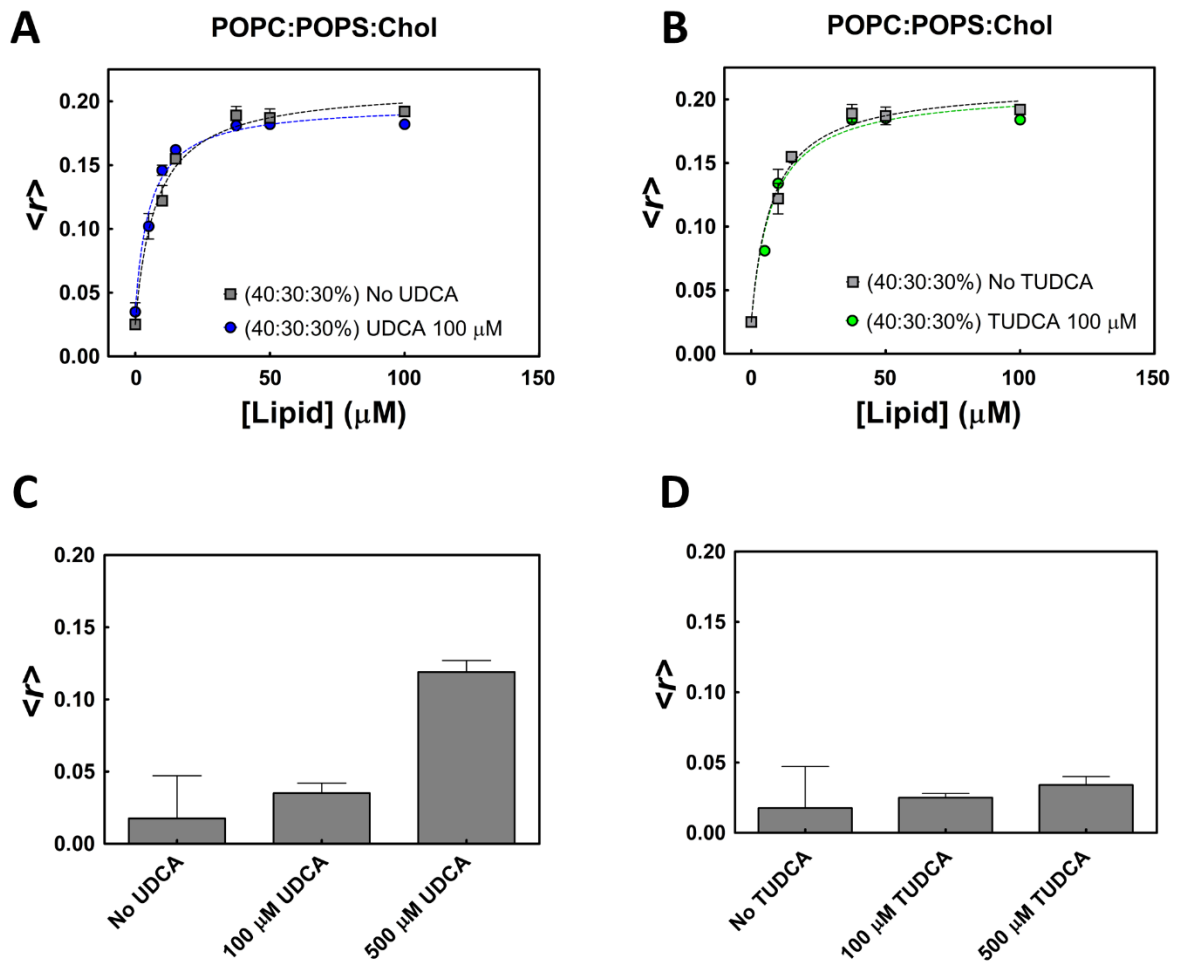


**Figure 9. UDCA and TUDCA have limited impact on the recruitment of K $\phi$ -bimane to membranes at cytoprotective concentrations.** Fluorescence steady-state anisotropy of K $\phi$ -bimane over different lipid concentrations for LUVs composed of POPC:POPS:Chol 40:30:30 %, in the absence or presence of 100  $\mu\text{M}$  UDCA (A) and TUDCA (B). Lines are the fitted partition curves according to Eq. 3. Note that lipid concentrations represent only the accessible lipid to the peptide and not the total lipid concentration. K $\phi$  values are shown on Table S2. K $\phi$ -bimane concentration was 2  $\mu\text{M}$ . Error bars represent SD values from at least two independent measurements. Fluorescence steady-state anisotropy values of K $\phi$ -bimane in buffer in the presence of 100 and 500  $\mu\text{M}$  of UDCA (C) and TUDCA (D) are also shown.  $\langle r^2 \rangle$  was measured with excitation at 396 nm and emission at 480 nm with excitation and calculated according to Eq. 1. Error bars represent SD values from at least two independent experiments with 8 measurements each.

**Impact of bile acids on  $K\phi$ -RFP distribution in live HEK293T cells**

Expression of  $K\phi$ -RFP has been used as a tool to monitor changes in the surface charge of different organelles during phagocytosis and apoptosis<sup>7,21</sup>. Here, we made use of HEK293T cells expressing  $K\phi$ -RFP to monitor changes in surface charge of MOM and the inner leaflet of the plasma membrane after exposure of the intracellular environment to physiologically active concentrations of both apoptotic and cytoprotective bile acids. Active mitochondria were stained with the cationic dye Rho-123<sup>35</sup>. Note that spectral unmixing of RFP and Rho-123 signals was required due to a partial overlap between their fluorescence emission spectra (for more detail see Materials and Methods section). As expected,  $K\phi$ -RFP is largely found in the plasma membrane, with a small percentage of fluorescent signal coming from intracellular organelles (Figure 10). This observation is in agreement with what was previously observed in HeLa cells<sup>7</sup> and with the more electronegative character of the inner leaflet of the plasma membrane when compared with the surface of other organelles.

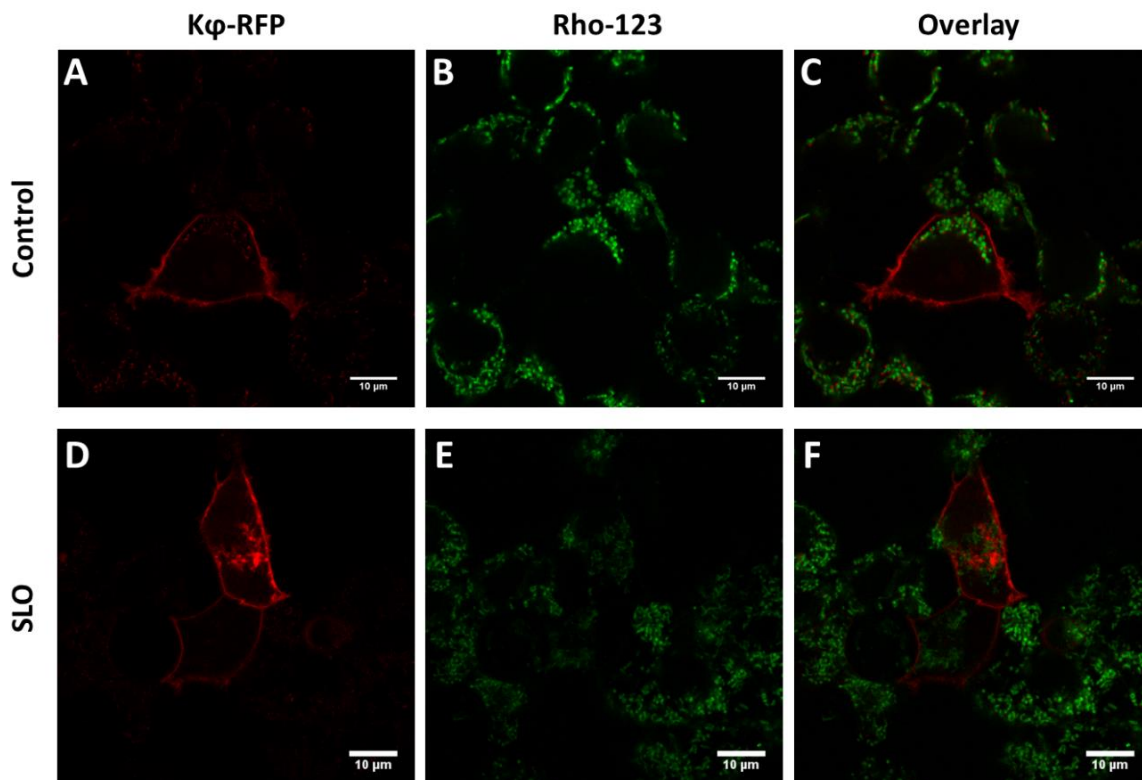


**Figure 10.  $K\phi$ -RFP is mainly found in plasma membrane rather than in intracellular organelles and SLO treatment does not result in any evidence of apoptosis activation.** Representative confocal microscopy images of the subcellular distribution of  $K\phi$ -RFP in HEK293T cells without (A-C) or with permeabilization with SLO (D-F),  $K\phi$ -RFP signal is shown in red (A, D). Mitochondria were

fluorescently stained with 1  $\mu$ M of Rho-123, whose signal is shown in green (B, E). Overlay images are also shown (C, F).

Since HEK293T cells do not possess specific transporters for bile acids, intracellular accumulation of bile acids is certain to be a slow process, particularly for the more hydrophilic UDCA and TUDCA. Rapid change in the intracellular concentration of bile acids on live HEK293T cells, was achieved through fast, specific and reversible permeabilization of the plasma membrane by the pore forming toxin SLO. Permeabilization of HEK293T cells by SLO was carried out as described in the Materials and Methods section. Successful permeabilization was confirmed using TO-PRO<sup>®</sup>-3 stain, a nuclear counterstain and dead cell indicator that is cell impermeant (results now shown). Permeabilization of HEK293T cells with SLO did not induce morphological changes in cells consistent with onset of apoptosis or a decrease in Rho-123 consistent with mitochondrial depolarization (Figure 10). The subcellular distribution of K $\phi$ -RFP after permeabilization with 100  $\mu$ M of DCA, UDCA and TUDCA is shown in Figure 11.

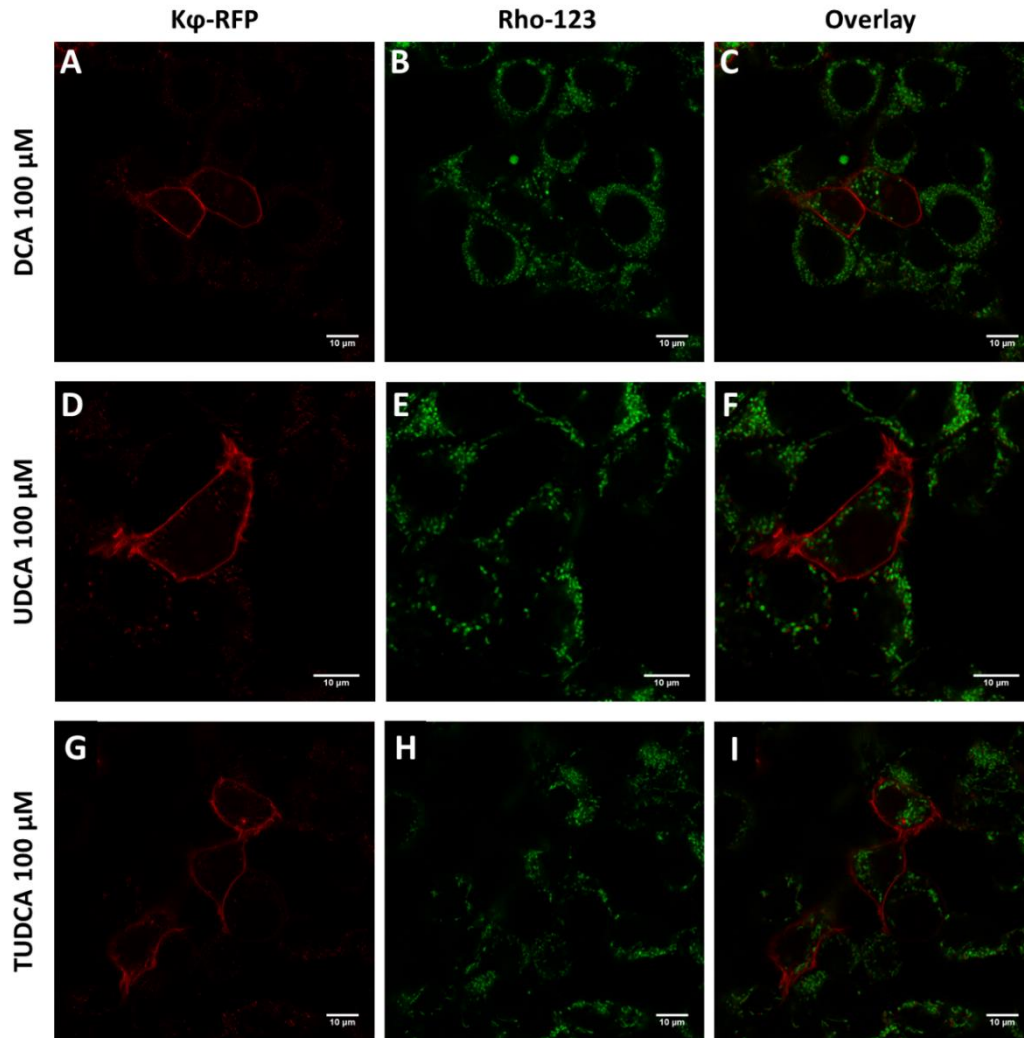


**Figure 11. Subcellular distribution of K $\phi$ -RFP after permeabilization of HEK293T cells with 100  $\mu$ M of DCA, UDCA and TUDCA** Representative confocal microscopy images of the subcellular distribution of K $\phi$ -RFP in HEK293T cells after permeabilization with SLO, in the presence of DCA (A-C), UDCA (D-F) and TUDCA (G-I) at 100  $\mu$ M. K $\phi$ -RFP signal is shown in red and mitochondria were fluorescently stained with 1 $\mu$ M of Rho-123, whose signal is shown in green. Overlay images are also shown (C, F, I).

In order to quantify the fraction of K $\phi$ -RFP associated with the MOM, a quantitative approach was followed. The fraction of fluorescence intensity of K $\phi$ -RFP arising from the plasma membrane and mitochondria were both calculated using digital masks. A mask for the plasma membrane was manually defined in ImageJ using the fluorescence of K $\phi$ -RFP itself as a reference. This is a simple procedure as the plasma membrane structure is clearly defined by a strong signal from K $\phi$ -RFP. A mask for the mitochondria pixels is defined making use of the Rho-123 signal. The results of this quantitative analysis is shown on Figure 12.

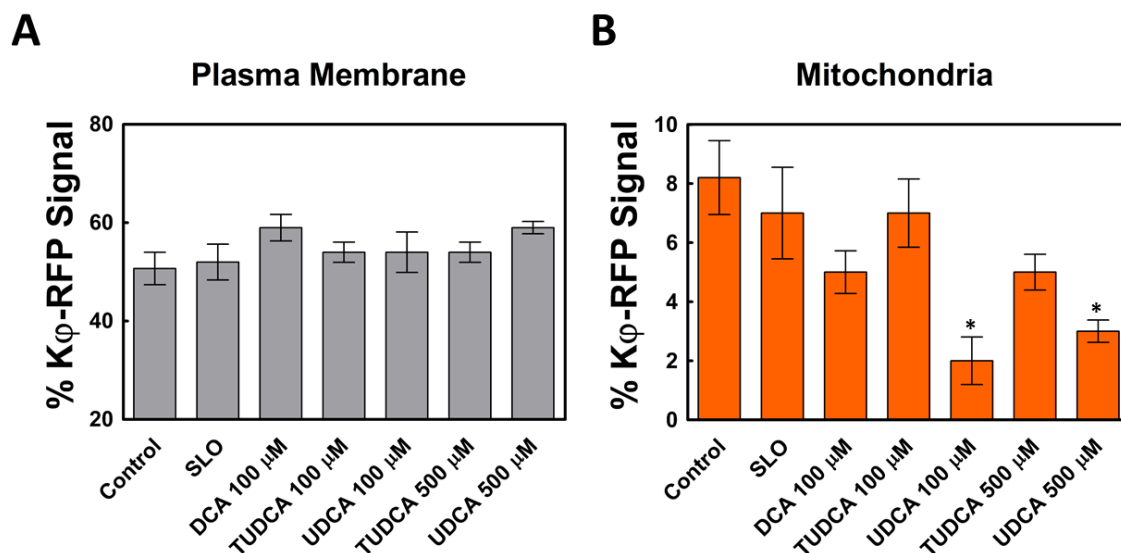


**Figure 12. Bile acids inhibit the association of K $\phi$ -RFP with the mitochondria.** Fraction of K $\phi$ -RFP in the plasma membrane (A) and in the mitochondria (B) of HEK293T cells. Measurements were carried out in the absence of permeabilization (Control) or for permeabilization with SLO in the absence of bile acids (SLO). Measurements with permeabilized HEK293T cells were also carried out in the presence of DCA (100  $\mu$ M), UDCA (100 and 500  $\mu$ M), and TUDCA (100 and 500  $\mu$ M). Values are mean  $\pm$  SEM values. \*P < 0.05 from the permeabilization control with SLO.

Surprisingly, results show that at 100  $\mu$ M intracellular concentration, both DCA and UDCA induce a decrease in the fraction of K $\phi$ -RFP associated with the mitochondria, while TUDCA had no impact on the distribution of K $\phi$ -RFP. The decrease is particularly evident for UDCA. At this concentration, DCA also induced a moderate increase in the concentration of K $\phi$ -RFP at the plasma membrane.

Similar experiments were also carried out in the presence of 500  $\mu$ M UDCA and TUDCA (Figure 13). Quantification of the subcellular distribution of K $\phi$ -RFP after permeabilization in the presence of 500 DCA was not possible because of extensive depolarization of mitochondria (Fig. 13B). For UDCA and TUDCA at 500  $\mu$ M, once more an inhibition of K $\phi$ -RFP association with the mitochondria is observed (Fig.12B).

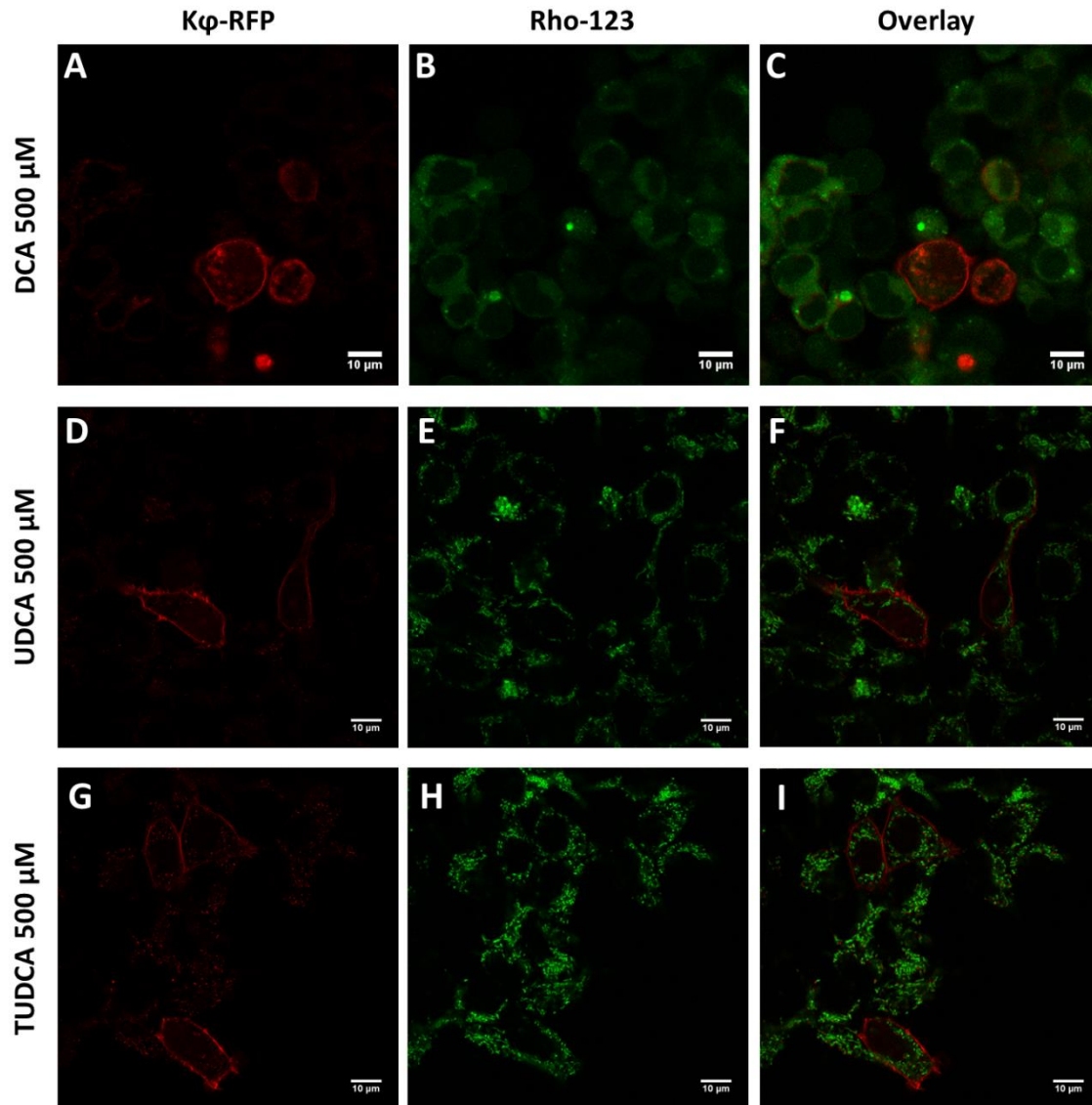


**Figure 13. Subcellular distribution of K $\phi$ -RFP after permeabilization of HEK293T cells with 500  $\mu$ M of DCA, UDCA and TUDCA.** Representative confocal microscopy analysis of the subcellular distribution of K $\phi$ -RFP in HEK293T cells after permeabilization with SLO, in the presence of DCA (A-C), UDCA (D-F) and TUDCA (G-I) at 500  $\mu$ M. K $\phi$ -RFP signal is shown in red and mitochondria were fluorescently stained with 1 $\mu$ M of Rho-123 whose signal is shown in green. Overlay images for the three bile acids are also shown (C, F, I). Incubation with SLO plus bile acids and Rho-123 was performed for 20min at 37°C.

## 4. Discussion

Membrane surface charge, particularly for mitochondria, is of critical importance for apoptotic signaling. In fact, exposure of highly anionic CL in the cytosolic leaflet of the MOM has been shown to precede mitochondrial permeabilization during apoptosis<sup>7</sup>. This is likely to be a critical trigger for recruitment of several pro-apoptotic factors, including caspase-8, Bid and Bax. While hydrophobic and cytotoxic bile acids such as DCA are known to interact strongly with different cellular membranes, including the MOM<sup>23,24</sup>, little is known regarding the impact of this association with different organelles on their respective surface charge. In fact, although association of DCA with lipid membranes shifts the pKa of this molecule to pH values in the physiological range<sup>31</sup>, a significant fraction (~50%) of lipid bound DCA remains negatively charged.

Through  $\zeta$ -potential of liposomes mimicking the plasma membrane and MOM compositions, we confirmed that in both cases, the insertion of DCA in the lipid bilayer induced a significant increase in negative charges on the surface of these membranes. Likely due to a greater affinity of DCA for membranes with lower cholesterol concentrations, the impact of the bile acid on the surface charge of liposomes mimicking the MOM was greater. Considering this evidence, we proposed to clarify if the exposure of mitochondria and the plasma membrane to either cytotoxic or cytoprotective bile acids induced a significant change in the affinity of cationic peptide domains to these organelles, using for that effect  $K\phi$ <sup>7,21</sup>, a peptide sensor for membrane surface charge.

A detailed characterization of the lipid binding properties of a fluorescent labeled  $K\phi$  was carried out, and we showed that  $K\phi$  is a reliable membrane surface charge sensor that shows higher partition to membranes with low cholesterol and high anionic lipid content. DCA is shown to greatly increase the affinity of  $K\phi$  to model membranes, while cytoprotective bile acids have a limited potential for modulation of  $K\phi$  affinity for artificial biomimetic lipid membranes. Interestingly, at high concentrations of either DCA or UDCA,  $K\phi$  is found to complex in solution with pre-micellar aggregates of bile acids. In fact, a similar result was obtained for recombinant Bax, which interacted extensively with different bile acids in solution, and in the presence of bile acids exhibited lower affinity for interaction with binding partners such as Bid, as well as lower membrane affinity and permeabilization activity (chapter IV).

When studies were carried out in permeabilized HEK293T cells, bile acids, including the hydrophilic and cytoprotective UDCA, were shown to inhibit the interaction of  $K\phi$ -RFP with mitochondrial membranes, but had little impact on the fraction of  $K\phi$ -RFP associated with the

plasma membrane. Possibly, given the lower affinity of the peptide for the MOM, this interaction is more sensitive to moderate changes in membrane or protein electrostatic properties. Further studies will be required to interpret this result with more certainty, but considering the previous observations regarding translocation of Bax to the mitochondria (chapter V), it seems plausible that a significantly large intracellular concentration of bile acids has the potential to modulate the affinity of cationic peptides or protein domains for cellular organelles in a general and non-specific manner, not necessarily through changes of membrane structure (as even the hydrophilic UDCA inhibited the interaction of K $\phi$  with mitochondria), but also through modulation of the properties of soluble proteins/peptides themselves.

This evidence supports a scenario where a buildup of bile acids in the intracellular environment will lead to an extremely complex change in the subcellular distribution of different proteins of relevance in the apoptotic signaling pathway, possibly contributing in this manner to the activation of apoptotic or cytoprotective molecular machineries.

### **Acknowledgements/Grant Support**

Authors acknowledge funding by FCT project references PTDC/QUI-BIO/119494/2010, PPBI-POCI-01-0145-FEDER-022122 and UID/NAN/50024/2013. T.S was the recipient of a fellowship from FCT (SFRH/BD/92398/2013). F.F acknowledges FCT through Researcher Contract No. IF/00386/2015.

## **5. References**

1. Platre, M. P. & Jaillais, Y. Anionic lipids and the maintenance of membrane electrostatics in eukaryotes. *Plant Signal. Behav.* **12**, 1–5 (2017).
2. Leventis, P. a. & Grinstein, S. The Distribution and Function of Phosphatidylserine in Cellular Membranes. *Annu. Rev. Biophys.* **39**, 407–427 (2010).
3. Balla, T. Phosphoinositides: Tiny Lipids With Giant Impact on Cell Regulation. *Physiol. Rev.* **93**, 1019–1137 (2013).
4. Lemmon, M. A. Membrane recognition by phospholipid-binding domains. *Nat. Rev. Mol. Cell Biol.* **9**, 99–111 (2008).
5. Yeung, T., Gilbert, G. E., Shi, J., Silvius, J., Kapus, A. & Grinstein, S. Membrane

- phosphatidylserine regulates surface charge and protein localization. *Science* (80-. ). **319**, 210–213 (2008).
6. Callahan, M. K., Popernack, P. M., Tsutsui, S., Truong, L., Schlegel, R. A. & Henderson, A. J. Phosphatidylserine on HIV envelope is a cofactor for infection of monocytic cells. *J. Immunol.* **170**, 4840–5 (2003).
  7. Heit, B., Yeung, T. & Grinstein, S. Changes in mitochondrial surface charge mediate recruitment of signaling molecules during apoptosis. *Am. J. Physiol. Physiol.* **300**, C33–C41 (2011).
  8. Daum, G. & Graz, T. U. Lipids of mitochondria. *Biochim. Biophys. Acta* **822**, 1–42 (1985).
  9. Schug, Z. T. & Gottlieb, E. Cardiolipin acts as a mitochondrial signalling platform to launch apoptosis. *Biochim. Biophys. Acta* **1788**, 2022–31 (2009).
  10. Bleicken, S., Classen, M., Padmavathi, P. V. L., Ishikawa, T., Zeth, K., Steinhoff, H.-J. & Bordignon, E. Molecular details of Bax activation, oligomerization, and membrane insertion. *J. Biol. Chem.* **285**, 6636–47 (2010).
  11. Bleicken, S. & Zeth, K. Conformational changes and protein stability of the pro-apoptotic protein Bax. *J. Bioenerg. Biomembr.* **41**, 29–40 (2009).
  12. García-Sáez, A. J. The secrets of the Bcl-2 family. *Cell Death Differ.* **19**, 1733–1740 (2012).
  13. Gross, A., Yin, X. M., Wang, K., Wei, M. C., Jockel, J., Milliman, C., Erdjument-Bromage, H., Tempst, P. & Korsmeyer, S. J. Caspase cleaved BID targets mitochondria and is required for cytochrome c release, while BCL-XL prevents this release but not tumor necrosis factor-R1/Fas death. *J. Biol. Chem.* **274**, 1156–63 (1999).
  14. Dewson, G. & Kluck, R. M. Mechanisms by which Bak and Bax permeabilise mitochondria during apoptosis. *J. Cell Sci.* **122**, 2801–2808 (2009).
  15. Kim, H., Tu, H.-C., Ren, D., Takeuchi, O., Jeffers, J. R., Zambetti, G. P., Hsieh, J. J.-D. & Cheng, E. H.-Y. Stepwise activation of BAX and BAK by tBID, BIM, and PUMA initiates mitochondrial apoptosis. *Mol. Cell* **36**, 487–99 (2009).
  16. Lovell, J. F., Billen, L. P., Bindner, S., Shamas-din, A., Fradin, C. & Leber, B. Supplemental Data Membrane Binding by tBid Initiates an Ordered Series of Events Culminating in Membrane Permeabilization by Bax. **135**, 1–12
  17. Gonzalez, F., Pariselli, F., Dupaigne, P., Budihardjo, I., Lutter, M., Antonsson, B., Diolez, P., Manon, S., Martinou, J.-C., Goubern, M., Wang, X., Bernard, S. & Petit, P.

- X. tBid interaction with cardiolipin primarily orchestrates mitochondrial dysfunctions and subsequently activates Bax and Bak. *Cell Death Differ.* **12**, 614–26 (2005).
18. Grinstein, S. Imaging signal transduction during phagocytosis: phospholipids, surface charge, and electrostatic interactions. *AJP Cell Physiol.* **299**, C876–C881 (2010).
19. Moravcevic, K., Mendrola, J. M., Schmitz, K. R., Wang, Y.-H., Slochower, D., Janmey, P. A. & Lemmon, M. A. Kinase Associated-1 Domains Drive MARK/PAR1 Kinases to Membrane Targets by Binding Acidic Phospholipids. *Cell* **143**, 966–977 (2010).
20. Heo, W. Do, Inoue, T., Park, W. S., Kim, M. L., Park, B. O., Wandless, T. J. & Meyer, T. PI(3,4,5)P3 and PI(4,5)P2 lipids target proteins with polybasic clusters to the plasma membrane. *Science* **314**, 1458–61 (2006).
21. Yeung, T., Terebiznik, M., Yu, L., Silvius, J., Abidi, W. M., Philips, M., Levine, T., Kapus, A. & Grinstein, S. Receptor Activation Alters Inner Surface Potential During Phagocytosis. *Science (80- )*. **313**, 347–351 (2006).
22. Mello-Vieira, J., Sousa, T., Coutinho, A., Fedorov, A., Lucas, S. D., Moreira, R., Castro, R. E., Rodrigues, C. M. P., Prieto, M. & Fernandes, F. Cytotoxic bile acids, but not cytoprotective species, inhibit the ordering effect of cholesterol in model membranes at physiologically active concentrations. *Biochim. Biophys. Acta* **1828**, 2152–2163 (2013).
23. Zhou, Y., Maxwell, K. N., Sezgin, E., Lu, M., Liang, H., Hancock, J. F., Dial, E. J., Lichtenberger, L. M. & Levental, I. Bile acids modulate signaling by functional perturbation of plasma membrane domains. *J. Biol. Chem.* **288**, 35660–70 (2013).
24. Sousa, T., Castro, R. E., Pinto, S. N., Coutinho, A., Lucas, S. D., Moreira, R., Rodrigues, C. M. P., Prieto, M. & Fernandes, F. Deoxycholic acid modulates cell death signaling through changes in mitochondrial membrane properties. *J. Lipid Res.* (2015). doi:10.1194/jlr.M062653
25. Sarmiento, M. J., Coutinho, A., Fedorov, A., Prieto, M. & Fernandes, F. Ca(2+) induces PI(4,5)P2 clusters on lipid bilayers at physiological PI(4,5)P2 and Ca(2+) concentrations. *Biochim. Biophys. Acta* **1838**, 822–830 (2014).
26. Puchalski, M. M. M., Morra, M. J. J. & von Wandruszka, R. Assessment of inner filter effect corrections in fluorimetry. *Fresenius. J. Anal. Chem.* **340**, 341–344 (1991).
27. Lakowicz, J. R. *Principles of Fluorescence Spectroscopy*. (2006).
28. Santos, N., Prieto, M. & Castanho, M. A. R. B. Quantifying molecular partition into model systems of biomembranes: an emphasis on optical spectroscopic methods. *Biochim. Biophys. Acta* **1612**, 123–135 (2003).

29. Pandit, S. A., Chiu, S.-W., Jakobsson, E., Grama, A. & Scott, H. L. Cholesterol surrogates: a comparison of cholesterol and 16:0 ceramide in POPC bilayers. *Biophys. J.* **92**, 920–7 (2007).
30. Zimmermann, T., Rietdorf, J. & Pepperkok, R. Spectral imaging and its applications in live cell microscopy. *FEBS Lett.* **546**, 87–92 (2003).
31. Coreta-Gomes, F. M., Martins, P. T., Velázquez-Campoy, A., Vaz, W. L. C., Geraldés, C. F. G. C. & Moreno, M. J. Interaction of bile salts with model membranes mimicking the gastrointestinal epithelium: a study by isothermal titration calorimetry. *Langmuir* 150804122127008 (2015). doi:10.1021/acs.langmuir.5b01810
32. Ingólfsson, H. I., Melo, M. N., van Eerden, F. J., Arnarez, C., Lopez, C. A., Wassenaar, T. A., Periole, X., de Vries, A. H., Tieleman, D. P. & Marrink, S. J. Lipid Organization of the Plasma Membrane. *J. Am. Chem. Soc.* **136**, 14554–14559 (2014).
33. Heuman, D. M., Bajaj, R. S. & Lin, Q. Adsorption of mixtures of bile salt taurine conjugates to lecithin-cholesterol membranes: implications for bile salt toxicity and cytoprotection. *J. Lipid Res.* **37**, 562–73 (1996).
34. Roda, A., Hofmann, A. & Mysels, K. The influence of bile-salt structure on self association in aqueous solutions. *J. Biol. Chem.* **258**, 6362–6370 (1983).
35. Kim, M., Cooper, D. D., Hayes, S. F. & Spangrude, G. J. Rhodamine-123 staining in hematopoietic stem cells of young mice indicates mitochondrial activation rather than dye efflux. *Blood* **91**, 4106–17 (1998).



## **THE MITOCHONDRIAL AFFINITY OF A CHARGE SENSOR PEPTIDE IS MODIFIED BY THE PRESENCE OF BILE ACIDS**

Tânia Sousa<sup>1,2</sup>, Samuel Jacob<sup>1,2</sup>, Sandra N. Pinto<sup>1,2</sup>, Ana Coutinho<sup>1,2,3</sup>, Manuel Prieto<sup>1,2</sup>,  
Fábio Fernandes<sup>1,2</sup>

<sup>1</sup>Centro de Química-Física Molecular and Institute of Nanoscience and Nanotechnology, Instituto Superior Técnico, University of Lisbon, Lisbon, Portugal

<sup>2</sup>iBB-Institute for Bioengineering and Biosciences, Biological Sciences Research Group, Av. Rovisco Pais 1, 1049-001 Lisbon, Portugal

<sup>3</sup>Departamento de Química e Bioquímica, Faculty of Sciences, University of Lisbon, Lisbon, Portugal

***Supplementary Material***

**Table S1.**  $K_p$  Partition coefficient ( $K_p$ ) values, with associated error, extracted from fluorescence steady-state anisotropy values for LUVs composed of POPS, POPS and Chol at different percentages in 10 mM Tris-HCl, pH 7.4 buffer with 150 mM NaCl or with no salt.  $K_p$  values were calculated considering only the accessible lipid to the peptide and not the total lipid concentration.

Figure	Lipid composition (mol %)			$K_p <r> \pm$ Error ( $\times 10^3$ )
	POPC	POPS	Chol	
5	55	15	30	$4.4 \pm 0.7$
	47.5	22.5	30	$11.4 \pm 3.1$
	40	30	30	$17.5 \pm 3.5$
6A	75	15	10	$11.5 \pm 2.1$
	65	15	20	$7.4 \pm 1.5$
	55	15	30	$4.0 \pm 0.8$
6B	60	30	10	$39.6 \pm 6.4$
	50	30	20	$25.5 \pm 6.4$
	40	30	30	$15.6 \pm 3.2$

**Table S2.**  $K_p$  partition coefficient ( $K_p$ ) values, with associated error, extracted from either fluorescence steady-state anisotropy, for LUVs composed of POPC, Chol (80:20%), POPC, POPS, Chol (50:30:20%), POPC, POPS, Chol (40:30:30%) and DOPC, DOPE, PI, Chol (51:26.6:12.8:9.6%), in the absence or presence of 100  $\mu\text{M}$  or 500  $\mu\text{M}$  of Biles acids.  $K_p$  values were calculated considering only the accessible lipid to the peptide and not the total lipid concentration and are based on the curves presented in figures 8 and 9.

Bile acid	Sample [ ] ( $\mu\text{M}$ )	Lipid composition (mol:mol:mol%)				
		POPC:Chol (80:20%)	POPC:POPS:Chol (50:30:20%)	POPC:POPS:Chol (40:30:30%)	DOPC:DOPE:PI:Chol (51:26.6:12.8:9.6%)	
None	-	0.6 $\pm$ 0.4	21.9 $\pm$ 4.4	22.4 $\pm$ 4.1	24.5 $\pm$ 4.1	
	100	41.0 $\pm$ 16.0	84.0 $\pm$ 7.1	55.2 $\pm$ 9.7	128.9 $\pm$ 21.2	
DCA	500	-	21.9 $\pm$ 8.1	-	-	
	100	-	-	27.7 $\pm$ 4.9	-	
UDCA	500	-	-	64.5 $\pm$ 12.4	-	
	100	-	-	17.1 $\pm$ 3.6	-	
TUDCA	500	-	-	40.0 $\pm$ 6.6	-	



# Chapter VII

---

Conclusions and future perspectives



---

## Conclusions

Apoptosis itself and all the signaling pathways and molecules involved in such a highly regulated process of programmed cell death have been a hot topic in cell biology and biophysics due to being vital for a wide variety of biological processes, providing a defense mechanism by which damaged, and potentially dangerous cells can be eliminated for the benefit of the organism as a whole. Cellular membranes play a central role in apoptosis. These structures are responsible for maintaining concentration gradients of ions and proteins across the membrane of different organelles, which when perturbed, act as triggers for apoptosis. Controlling apoptosis could be the key for the cure of a variety of diseases that affect world population at an increasing rate, such as cancer and neurodegenerative diseases.

Several molecules were shown along the years to be relevant for the modulation of the apoptotic process. Bile acids have been shown to interfere with the apoptotic machinery, contributing to the development of a large number of digestive tract diseases, including colon cancer and cholestasis. Such molecules have been studied for decades due to their special and opposite effects. As explained in chapter I, bile acids are particularly interesting molecules since they present similar, chemical structures that show different physical-chemical properties and even more diverse biological features. While molecules such as DCA are reported to induce apoptosis, molecules such as UDCA and TUDCA have cytoprotective properties. Although these opposite effects are strongly associated with bile acid hydrophobicity, the exact mechanism by which they trigger these effects remains elusive. In this context, our main goal was to combine spectroscopy and microscopy approaches to understand the effect of apoptotic and cytoprotective bile acids on cell membranes and also on the activity of apoptotic Bax protein. More specifically, we wanted to identify the possible targets of bile acids effects and elucidate the specific mechanisms behind their effects through the use of membrane model systems, isolated mitochondria, human cell lines and rat hepatocytes, following a bottom-up approach.

First, we started by a detailed characterization of the impact of bile acids on the membrane properties of the most likely targets for modulation of cell death by bile acids, the plasma membrane and the mitochondrial membranes of hepatocytes (chapter III). Here we showed that DCA increases the plasma membrane fluidity of hepatocytes only to a minor extent, and that this effect is not correlated with the incidence of apoptosis. Additionally, plasma membrane fluidity recovers to normal values overtime suggesting that the transient nature of these changes is likely due to the presence of cellular compensatory mechanisms to maintain membrane integrity. Colocalization experiments in living cells confirmed the presence of bile acids within mitochondrial membranes. Experiments with active isolated mitochondria,

revealed that physiologically active concentrations of DCA changes mitochondrial outer membrane order in a concentration- and time-dependent manner, and that these changes preceded the MPT. Importantly, these effects are not observed on liposomes mimicking MOM lipid composition, suggesting that DCA apoptotic activity depends on features of mitochondrial membranes which are absent from protein-free mimetic liposomes, such as the double membrane structure, lipid asymmetry or the mitochondrial protein environment. In contrast, the mechanism of action of cytoprotective bile acids is likely not associated with changes in cellular membrane structure.

The next step was carried out in response to the conclusions described above. Given that the permeabilization of isolated mitochondria by apoptotic bile acids depend on features of mitochondrial membranes other than lipid composition, the work focused on a particularly important protein for mitochondria permeabilization, the pore-forming Bax protein. It has already been shown that both UDCA and TUDCA are able to inhibit the translocation of Bax to the mitochondria. Bax plays a key role in apoptosis, which is achieved through translocation of the protein to the mitochondria from the cytosol after an apoptotic stimulus and formation of pores in mitochondrial membranes. Given the reported impact of cytoprotective bile acids on Bax mitochondrial translocation, this protein is a strong candidate as the crucial target for cytoprotective bile acids. This study aimed to characterize the impact of physiologically active concentrations of UDCA and TUDCA on recombinant Bax oligomerization, membrane affinity and activity (chapter IV). We showed that both UDCA and TUDCA interact with soluble recombinant Bax, being able inhibit the interaction of Bax with activator molecules such as the Bid-BH3 peptide and decrease the affinity of Bax for liposomes mimicking outer mitochondrial membrane composition. Importantly, UDCA and TUDCA were shown to dramatically inhibit Bax-induced permeabilization of model membranes. These effects are not specific to cytoprotective bile acids, as incubation of recombinant Bax with the apoptotic bile acid DCA produces similar results. The findings presented here clearly show that at physiologically active submicellar concentrations, bile acids have the ability to inhibit Bax pore-forming activity and suggested that the cytoprotective activity of UDCA and TUDCA could be the result of this process. On the other hand, for toxic bile acids, these cytoprotective effects are negated due to the intrinsic mitochondrial permeabilization properties of these molecules.

Chapter V emerged in order to clarify the impact of bile acids on Bax properties in a cellular environment. Characterizing the impact of the interaction of bile acids and Bax on the translocation and pore-forming activity of Bax within a cellular environment is significantly challenging. Due to the non-specific nature of the interaction of Bax with bile acids, it is impossible to predict if the inhibition of Bax by bile acids is important for cell fate or if not yet identified apoptotic/cytoprotective factors could be modulated by bile acids in a more relevant

manner. Here, we made use of colon cancer HCT116 Bax/Bak double knockout (DKO) cells to evaluate the role of Bax in bile acid induced cell death. We show that DCA-induced cell death occurs in the absence of Bax. Importantly, cytoprotection by UDCA was also observed in the absence of Bax, suggesting that this bile acid could modulate apoptosis through more complex mechanisms than inhibition of Bax alone.

Bax translocation to the mitochondria was monitored through the expression of Bax-GFP and fluorescence confocal imaging. As expected, incubation with DCA induces translocation of Bax to the mitochondria and pre-treatment of cells with UDCA inhibited this process. Due to plasma membrane impermeability, the intracellular concentration of DCA during these studies is unknown. Permeabilization of cells allow for control of intracellular bile acid concentration and remove ambiguity in data interpretation. In this way, permeabilized HCT116 Bax/Bak DKO cells exposed to DCA, suffered a rapid loss of MMP, and a small decrease in Bax-GFP translocation to the mitochondria. These results suggest that although the apoptotic activity of DCA is not dependent on Bax, the interaction of DCA with Bax by itself can inhibit the translocation of Bax to mitochondria to some extent, and that the increased translocation of Bax during longer treatment of non-permeabilized cells is likely the result of activation of apoptotic pathways due to the cellular stress created by DCA after MOM permeabilization.

As a final approach and since changes in mitochondrial surface charge mediate recruitment of signaling molecules during apoptosis, we also evaluated the impact of bile acid treatment on the surface charge of mitochondria and the plasma membrane (chapter VI). We confirmed that in liposomes of different lipid compositions and mimicking different organelles, the insertion of DCA in the lipid bilayer induced a significant increase in the negative charges on the surface of these membranes. The interaction of a cationic peptide and charge sensor, K $\phi$ , with liposomes mimicking the inner leaflet of the plasma membrane and the mitochondria outer membrane, was characterized, as well as its distribution between the two organelles in HEK293T cells. Surprisingly, different bile acids, and particularly the hydrophilic and cytoprotective UDCA, were shown to inhibit the interaction of K $\phi$ -RFP with mitochondrial membranes but had little impact on the fraction of K $\phi$ -RFP associated with the plasma membrane. These results suggest that a significantly large intracellular concentration of bile acids has the potential to modulate the affinity of cationic peptides or protein domains for cellular organelles in a general and non-specific manner, not necessarily through changes of membrane structure (as even the hydrophilic UDCA inhibited the interaction of K $\phi$  with mitochondria), but also through modulation of the properties of soluble proteins/peptides themselves.

Altogether, these results suggest that while the mechanism of action of cytotoxic bile acids is expected to be dictated mostly by permeabilization of mitochondrial outer membrane,

the events associated with cytoprotection by bile acids are likely to be more complex. In fact, while at cytoprotective concentrations, bile acids such as UDCA or TUDCA, have the potential to modulate the pore-forming activity of Bax, possibly regulating the threshold for activation of apoptosis, similar effects were also observed for the apoptotic DCA. A buildup of bile acids in the intracellular environment will lead to an extremely complex change in the subcellular distribution of different proteins of relevance in the apoptotic signaling pathway, with unforeseen consequences for activation/deactivation of cytoprotection/apoptotic pathways. Moreover, the non-specific nature of the mechanism of action by cytoprotective bile acids is supported by the fact that UDCA cytoprotection to DCA-induced apoptosis in colon cancer cells, is shown to occur even in the absence of Bax.

## Future perspectives

With the extensive work developed in this thesis we were able to unveil additional information regarding the mechanism behind the modulation of apoptosis by bile acids. Nevertheless, certain studies remain to be completed in order to obtain further insights on the theme of this thesis. Importantly, the observations regarding the role of Bax in bile acid-mediated cytoprotection in colon cancer cells should be confirmed with hepatocytes, where Bax plays a more central role in apoptosis.

Additionally, the observation of a small decrease in Bax translocation to the mitochondria upon to the increase in intracellular concentration of DCA, will have to be characterized in greater detail, namely regarding the dependence on bile acid concentration of this process and its kinetics. Through monitoring of variations in Bax levels on individual mitochondria overtime after exposure to bile acids, important information should be recovered regarding the occurrence of Bax translocation before or after changes in mitochondrial surface charge and permeabilization changes, as well as regarding the synchronous nature of these changes for a given cell. Additionally, making use of Fluorescence recovery after photobleaching (FRAP) or Fluorescence loss in photobleaching (FLIP), it should also be possible to obtain information on the presence of different pools of Bax, with different mitochondria association properties. These experiments could be carried out both in hepatocytes and HCT116 cells.

One important factor for mitochondrial permeabilization which was not analyzed here was Bax oligomerization in the mitochondria, as this is the basis of permeabilization of the MOM during apoptosis, and translocation of monomers by itself is not sufficient to activate an increased permeability. This could be followed within individual mitochondria through

Fluorescence Anisotropy Imaging (FAIM), and information regarding the existence of a correlation between the onset of Bax oligomerization and individual mitochondria permeabilization would provide additional valuable information.

Obtaining information regarding the translocation to the mitochondria in response to bile acids for different proteins of relevance within the intrinsic pathway of apoptosis, such as Bid, would also contribute to obtain a clearer view of the general impact of bile acids on the apoptotic machinery and to confirm that there is no activation/deactivation of a specific apoptotic factor during exposure of cells to apoptotic and cytoprotective bile acids.

The additional information provided by this long list of studies would undoubtedly enrich not only our understanding of the role of bile acids for modulation of apoptosis at the molecular level, but also our comprehension of the intricacies of the apoptotic process itself. Such insight would be highly valuable for the understanding of different diseases and would assist in the search of new therapeutical approaches.

